Airborne and spaceborne LiDAR data as a measurement tool for peatland topography, peat fire burn depth, and forest above ground biomass in Central Kalimantan, Indonesia

Uwe Ballhorn

Munich 2012

Dissertation der Fakultät für Biologie
der Ludwig-Maximilian-Universität München

Airborne and spaceborne LiDAR data as a measurement tool for peatland topography, peat fire burn depth, and forest above ground biomass in Central Kalimantan, Indonesia

vorgelegt von

Uwe Ballhorn

München, 6. Februar 2012

1. Gutachter: Prof. Dr. Florian Siegert, LMU München

2. Gutachter: PD Dr. Martin Heß, LMU München

Tag der mündlichen Prüfung: 30. Juli 2012

ACKNOWLEDGMENTS

First I would like to thank Prof. Dr. Florian Siegert for giving me the opportunity to conduct my PhD thesis and to learn more about the different technologies and methodologies involved in remote sensing. His broad knowledge and deep insights were an important resource and helped me to understand the ecological interrelations of tropical peatlands. He also opened my eyes for the different and difficult problems in the conservation of these fascinating ecosystems. Thank you for inspiring and guiding me while giving me the freedom to follow my own scientific interests and for creating an environment where I could learn and grow.

Further I would like to thank PD Dr. Martin Heß very much for being the second referee of my PhD thesis and for showing interest in my topic.

The friendly atmosphere at Remote Sensing Solutions (RSS) GmbH has been much appreciated and has positively contributed to my work. For that I say thank you to all my dear former and present colleagues for the positive work environment. Thanks to Peter, Claudius, Juilson, Jonas, Vanessa, Karin, Iris, Keith, Sandra, Julia, Christian, Marie, Tanja, Sebastian, Maike, Florian, Jasmin, and Olaf for all those interesting discussions, thoughts, and time we spent together. Special thanks to Claudius. Without you I would not be sitting here finishing by PhD thesis. All the best to you. Many thanks to Peter for always helping me out with computer-problems and being such a relaxed comrade, and to Juilson for being so helpful in the processing of the LiDAR data. Having the possibility to work in a team of environmental scientists helped me to gain a great deal of experience and knowledge.

I was involved in several very interesting international projects where I was able to meet with other scientists in the scope of cooperation, course trainings, ground surveys, and academic conferences. In this context I would like to express my thanks to Suwido Limin (University of Palangka Raya, Indonesia), Sampang Gaman, Agung Restu Susantu, Yuda Prawira, Dr. Lilik Budi Prasetyo (Bogor Agricultural University, Indonesia), Prof. Dr. Olavi Luukkanen (University of Helsinki, Finland), Dr. Eshetu Yirdaw (University of Helsinki, Finland), Prof. Dr. Damrong Pipatwattanakul (Kasetsart University, Thailand), Gernot Rücker (Zebris, Germany), Mike Mason

(Climate Care, United Kingdom), Dr. Karl Heinz Steinmann, Prof. Dr. Jack Rieley (The University of Nottingham, United Kingdom), Dr. Viktor Böhm (Kalteng Consultants, Germany), and Dr. Barnaby Clark.

There are also lots of other people, too numerous to mention in name, that have contributed towards my PhD studies and to my time here in Munich in many different and wonderful ways, and to whom I would like to say thank you. I wish everyone who I have befriended all the best.

Very special thanks go to my family, relatives, and friends. My friends, especially Katja, Kati, Joshi, Pat, Sebastian, Lisa, and Robert, thank you for the continued understanding, support, and encouragement. Also thanks to all the musicians, skateboarders, and artists who constantly remind me that there is a different view on life than just science.

Last but certainly not least, very special thanks go to my family for giving me their love, care, and support. Thank you very much Anneliese, Jens, Angelika, and Helene.

This thesis is dedicated to my mother for her continuous unconditional support and love during my whole life. Thank you very very much.

ABSTRACT

It is estimated that in 2008, worldwide deforestation and forest degradation emissions contributed about 6-17% of the total anthropogenic carbon dioxide (CO_2) emissions. In Indonesia deforestation and forest degradation are almost exclusively caused by human economic activities such as shifting cultivation, illegal logging, and the establishment of industrial timber estates and large-scale oil palm plantations. Green House Gas (GHG) emissions are particularly evident in the costal lowlands of Sumatra and Kalimantan, where peat fires and peat decomposition, due to peatland drainage, result in the release of huge amounts of CO_2. Current estimates indicate that the total area of undeveloped tropical peatland is in the range of 30-45 million hectares (ha) (approximately 10-12% of the global peatland resource); about 16.8-27.0 million ha are found in Indonesia, which makes them one of the largest near-surface pools of terrestrial organic carbon. With Indonesia's ranking as one of the world's biggest emitters of carbon and with a peat carbon store of about 57 ±11 giga tons (Gt), it has enormous potential to negatively influence the global climate if its peatlands are burned and drained at rates currently observed. One important measure of the United Nations Framework Convention on Climate Change (UNFCCC) to curb GHG emissions from this sector is the program on Reducing Emissions from Deforestation and forest Degradation in developing countries (REDD+) which involves the private sector of industrialized countries in the protection of the remaining tropical forests to compensate the exceeding of their GHG emission quota. The quantification of tropical forest carbon stocks is a key challenge in creating a basic methodology for REDD+ projects. Since most peatlands in Indonesia are highly inaccessible, very few field measurements have been made to date. One way to overcome this problem is the use of Light Detection and Ranging (LiDAR) data. LiDAR is based on the transmission of laser pulses toward the ground surface and the recording of the return signal. Airborne LiDAR systems, compared to other remote sensing technologies, have been shown to yield the most accurate estimates for land topography, forest structural properties, and forest Above Ground Biomass (AGB). The main goal of this thesis was the assessment of the potential and accuracy of airborne and spaceborne LiDAR data in measuring peatland topography, peat fire burn depth, peat fire carbon emissions, and forest AGB in Central Kalimantan, Indonesia. The focus of our investigation was on a peat dominated

landscape in Central Kalimantan where almost all peat swamp forest ecosystems have been severely impacted by extensive logging and drainage for more than two decades. The application of airborne LiDAR data succeeded in deriving estimates on peat loss after single and multiple fire events. Based on this estimates peat fire carbon emissions could be extrapolated to the sub district, district, and national level. The findings of these analyses resulted in a deeper understanding of the dimension and impact of these peat fires on the global carbon cycle and their ecological dynamics. It was estimated that within a 2.79 million ha study area in Central Kalimantan (approximately 13% of the Indonesian peatland area) 49.15 ±26.81 mega tons (Mt) of carbon were released from peat fires during the 2006 El Niño episode. This represents 10–33% of all carbon emissions from transport for the European Community in the year 2006. It was also possible to derive large scale AGB estimates and show its spatial variability for peat swamp and lowland diperocarp forests through correlating field estimates with airborne LiDAR point cloud metrics. In combination with satellite data (optical and/or RADAR) airborne LiDAR is a cost effective approach which could then be used as input to future REDD+ projects. Further the results demonstrated the usefulness and robustness of ICESat/GLAS data (spaceborn LiDAR) as a sampling tool to extract information on peatlands, which can be used as a proxy for peat volume and consequently carbon storage, state and structure of peat swamp forests, and peat swamp forest AGB for large inaccessible areas at low costs where no systematic sampling has been conducted yet.

ZUSAMMENFASSUNG

Schätzungen nach stammen 6-17% des totalen 2008 anthropogen verursachten Kohlendioxidausstoßes aus der weltweiten Abholzung und Degradierung von Wäldern. In Indonesien lassen sich die Ursachen für Abholzung und Degradierung der Wälder fast ausschließlich auf wirtschaftliche Aktivitäten wie Wanderfeldbau, illegaler Holzeinschlag und das Anlegen industrieller Holz- und großflächiger Palmölplantagen zurückführen. Hohe Treibhausgasemissionen sind besonders in den küstennahen Tiefländern von Sumatra und Kalimantan zu beobachten, wo Torffeuer und die Zersetzung von Torf, bedingt durch die Entwässerung dieser Torfgebiete, zur Emission riesiger Mengen an Kohlenstoffdioxid (CO_2) führen. Nach aktuellem Kenntnisstand liegt die gesamte Fläche an unerschlossenen tropischen Torfgebieten im Bereich von 30-45 Millionen Hektar (ha) (annähernd 10-12% der globalen Torfreserven). Davon kommen etwa 16,8-27,0 Millionen ha in Indonesien vor, welches diese zu einem der größten oberflächennahen Vorkommen an terrestrischen organischen Kohlenstoff macht. Da Indonesien zu den weltweit größten Emittenten von Kohlenstoff zählt und einen Torfkohlenstoffspeicher von etwa 57 ±11 Gigatonnen (Gt) aufweist, ist das Potential zur negativen Beeinflussung des globalen Klimas gewaltig, wenn die dortigen Torgebiete weiterhin in dem Tempo verbrannt und entwässert werden wie es derzeitig beobachtet wird. Eine wichtige Maßnahme des United Nations Framework Convention on Climate Change (UNFCCC) zur Reduzierung der Treibhausgasemissionen dieses Sektors ist das Programm „Reducing Emissions from Deforestation and forest Degradation in developing countries (REDD+)“. Mit Hilfe dieses Programmes wird der Privatsektor industrieller Länder in den Schutz der verbleibenden tropischer Wälder involviert, um die Überschreitung festgelegter Treibhausgasemissionen dieser Länder zu kompensieren. Bei der Entwicklung einer grundlegenden Methode für REDD+ Projekte ist die Quantifizierung des im tropischen Wald gespeicherten Kohlenstoffs die nahezu größte Herausforderung. Da die meisten Torfgebiete in Indonesien sehr unzugänglich sind, wurden bisher nur wenige Feldinventuren durchgeführt. Ein Weg, dieses Problem zu bewältigen, wäre die Nutzung von Light Detection and Ranging (LiDAR) Daten. LiDAR basiert auf der Aussendung von Laserpulsen in Richtung der Bodenoberfläche und der Aufzeichnung des Rücksignals. Es zeigte sich, dass flugzeuggetragene LiDAR Systeme, verglichen mit anderen

Fernerkundungstechnologien, die genausten Abschätzungen für Landtopographie, Waldstrukturparameter und oberirdischer Waldbiomasse liefern. Das Hauptziel dieser Doktorarbeit war die Beurteilung des Potentials und der Genauigkeit von flugzeug- und satellitengetragener LiDAR Systeme zur Messung von Torfgebietstopographie, Tiefe von Torfbränden, Torffeuerkohlenstoffemissionen und oberirdischer Waldbiomasse in Zentral Kalimantan, Indonesien. Der Fokus der Untersuchung lag auf einer torfdominierten Landschaft in Zentral Kalimantan, in welcher fast alle Torfsumpfwaldökosysteme über mehr als zwei Jahrzehnte durch extensiven Holzeinschlag und Entwässerung beeinflusst wurden. Durch die Auswertung von Daten eines luftgetragenem LiDAR Systems wurden Torfverluste nach einzelnen und mehreren Feuerereignissen erfolgreich abgeschätzt. Basierend auf diesen Abschätzungen konnten Torffeuerkohlenstoffemissionen auf den subdistrikt, distrikt und nationalen Level extrapoliert werden. Die Ergebnisse dieser Analysen resultierten in einem tieferen Verständnis der Dimension und Bedeutung dieser Torffeuer für den globalen Kohlenstoffkreislauf und ihrer ökologischen Dynamik. Für ein 2,79 Millionen ha großes Studiengebiet in Zentral Kalimantan (etwa 13% der indonesischen Torfgebietsfläche) wurde geschätzt, dass 49,15 ±26,81 Megatonnen (Mt) an Kohlenstoff durch Torffeuer während des El Niño Phänomens des Jahres 2006 emittiert wurden. Dies repräsentiert 10-33% aller Kohlenstoffemissionen des Transportsektors der Europäischen Gemeinschaft für das Jahr 2006. Durch die Korrelation von Forstinventurparametern und den luftgetragenen LiDAR Punktwolkenmetriken war auch das großräumige Herleiten und Aufzeigen der räumlichen Variabilität der oberirdischen Biomasse von Torfsumpfwäldern und Tieflanddipterocarpaceenwäldern möglich. In Kombination mit Satellitendaten (optisch und/oder RADAR) sind luftgetragene LiDAR Systeme ein kostengünstiger Ansatz, der dann als Beitrag für zukünftige REDD+ Projekte dienen könnte. Weiterhin demonstrierten die Ergebnisse die Nützlichkeit und Robustheit von ICESat/GLAS Daten (satellitengetragenes LiDAR System) bei der Entnahme von kostengünstigen Stichproben in diesen Torfgebieten. Die Informationen aus jenen Stichproben könnten dann Hinweise auf Torfvolumen und folglich auch auf Kohlenstoffspeicher, Zustand, Struktur und oberirdische Biomasse von Torfsumpfwäldern für große unzugängliche Gegenden ohne vorhandene systematische Inventur, liefern.

STATEMENT AND DECLARATION OF HONOR

This PhD thesis has been supervised by Prof. Dr. Florian Siegert according to §6 promotion regulations. I herewith declare that this dissertation has not been submitted (as a whole or in part) to any other commission and that I did not try to pass any other doctoral examinations without success.

I herewith assure that this dissertation was written exclusively by me without the help of any illegal additives.

_____

Date

_____ _____

Uwe Ballhorn Prof. Dr. Florian Siegert

PUBLICATIONS ORIGINATING FROM THIS THESIS

CHAPTER II

Ballhorn U, Siegert F, Mason M, Limin S (2009) Derivation of burn scar depths and estimation of carbon emissions with LiDAR in Indonesian peatlands. *Proceedings of the National Academy of Sciences of the United States of America*, **106**, 21213-21218.

CHAPTER III

Ballhorn U, Jubanski J, Siegert F Pre-fire surface 3D modeling of tropical peatland burn scars based on airborne LiDAR in Central Kalimantan, Indonesia. Manuscript in preparation for *Global Change Biology*.

CHAPTER IV

Ballhorn U, Jubanski J, Siegert F (2011) ICESat/GLAS Data as a Measurement Tool for Peatland Topography and Peat Swamp Forest Biomass in Kalimantan, Indonesia. *Remote Sensing*, **3**, 1957-1982.

CHAPTER V

Kronseder K, **Ballhorn U**, Böhm V, Siegert F Above ground biomass estimation across forest types at different degradation levels in Central Kalimantan using LiDAR data. *International Journal of Applied Earth Observations and Geoinformation*, **18**, 37-48.

CHAPTER VI

Jubanski J, **Ballhorn U**, Kronseder K, Siegert F Deriving forest above ground biomass in Central Kalimantan (Indonesia) using airborne LiDAR. Manuscript in preparation for *Nature Climate Change*.

CONTRIBUTION OF THE AUTHORS

CHAPTER II

Planning of the study, processing of the LiDAR data, derivation of the peat burn depths, the calculation of the peat fire carbon emission, and the writing of the publication was conducted by Uwe Ballhorn. Prof. Dr. Florian Siegert participated in planning the study and also revised the manuscript on several occasions before submission. Mike Mason gave critical comments and thus improved the manuscript. Suwido Limin helped planning the field trip in Central Kalimantan (Indonesia) and conducted the in situ peat fire depth measurements.

CHAPTER III

Planning of the study, derivation of the peat loss, relating peat loss to other environmental factors, the calculation of the carbon emissions, and the writing of the publication was conducted by Uwe Ballhorn. Dr. Juilson Jubanski processed the LiDAR data, modeled the pre-fire peat surface, and revised the manuscript on several occasions. Prof. Dr. Florian Siegert participated in planning the study and also revised the manuscript on several occasions.

CHAPTER IV

Uwe Ballhorn planned the study, processed the different LiDAR data sets, established the correlations between the different datasets, conducted the field inventory work in Central Kalimantan (Indonesia), and wrote the publication. Dr. Juilson Jubanski helped to process the ICESat/GLAS data sets and revised the manuscript on several occasions. Prof. Dr. Florian Siegert participated in planning the study and also revised the manuscript on several occasions before submission.

CHAPTER V

Karin Kronseder planned the study, processed the LiDAR data sets, conducted the field inventory work in Central Kalimantan (Indonesia), established the correlations between the different datasets, and wrote the publication. Uwe Ballhorn helped in planning the study, processing the LiDAR data sets, establishing correlations between the different datasets, and revising the manuscript. Uwe Ballhorn also

conducted field inventory work in Central Kalimantan. Dr. Viktor Böhm gave critical comments and thus improved the manuscript. Prof. Dr. Florian Siegert participated in planning the study and also revised the manuscript on several occasions before submission.

CHAPTER VI

Dr. Juilson Jubanski planned the study, processed the LiDAR data sets, established the correlations between the different datasets, and wrote the publication. Uwe Ballhorn helped in planning the study, processing the LiDAR data sets, establishing correlations between the different datasets, and wrote the manuscript. Uwe Ballhorn and Karin Kronseder conducted field inventory work in Central Kalimantan (Indonesia). Prof. Dr. Florian Siegert participated in planning the study and also revised the manuscript on several occasions before submission.

I hereby confirm the above statements

_____

Date

_____ _____

Uwe Ballhorn Prof. Dr. Florian Siegert

TABLE OF CONTENTS

LIST OF FIGURES

LIST OF TABLES

xxx

ABBREVIATIONS

1DD	One – Degree Daily data set
3D	Three Dimensional
a.s.l.	above sea level
ADB	Asian Development Bank
AGB	Above Ground Biomass
ALOS	Advanced Land Observation Satellite
ANOVA	ANalysis Of VAriance
AR	Afforestation and Reforestation
ATSR	Along-Track Scanning Radiometer
AVHRR	Advanced Very High Resolution Radiometer
C/A code	Coarse/Acquisition code
CC	Canopy Cover
CDM	Clean Development Mechanism
CH	Centroid of the LiDAR point cloud height histogram
CH_4	Methane
CHM	Canopy Height Model
CIMTROP	Centre for International co-operation in Management of TROpical Peatland
CL	Centroid of the LiDAR point cloud height histogram
CO	Carbon monoxide
CO_2	Carbon dioxide
CSM	Canopy Surface Model
DBH	Diameter at Breast Height
DGPS	Differential Global Positioning System
DTM	Digital Terrain Model
E	Sinusoidal electric wave
EGM96	Earth Gravitational Model 1996
ENVI/IDL	Environment for Visualizing Images / Interactive Data Language
ERS-2	European Remote Sensing Satellite 2
ERTS	Earth Resource Technology Satellite
ESRI	Environmental Systems Research Institute

ETM	Enhanced Thematic Mapper
ETM+	Enhanced Thematic Mapper Plus
FAO	Food and Agriculture Organization
FIRMS	Fire Information for Resource Management System
FORRSA	FOrest Restoration and Rehabilitation in Southeast Asia
GHG	Green House Gas
GIS	Geographic Information System
GLAS	Geoscience Laser Altimeter System
GmbH	Gesellschaft mit beschränkter Haftung
GPCP	Global Precipitation Climatology Project
GPS	Global Positioning System
Gt	Giga tons
ha	hectare
ICESat	Ice, Cloud, and land Elevation Satellite
IDW	Inverse Distance Weighted
IMU	Inertial Measurement Unit
IPCC	Intergovernmental Panel on Climate Change
JI	Joint Implementation
JPL	Jet Propulsion Laboratory
KEYTROP	KEYs for securing TROpical Peat carbon
KNMI	Koninklijk Nederlands Meterologisch Instituut
LDF	Lowland Dipterocarp Forest
LiDAR	Light Detection and Ranging
LM	LiDAR Metrics
LVIS	Laser Vegetation Imaging Sensor
M	Sinusoidal magnetic wave
Mha	Million hectares
MODIS	MODerate resolution Imaging Spetroradiometer
MRP	Mega Rice Project
MSS	MultiSpectral Scanner
Mt	Mega tons
MTMF	Mixture Tuned Matched Filtering
NASA	National Aeronautics and Space Administration
NIMA	National Imagery and Mapping Agency

NOAA	National Oceanic and Atmospheric Administration
OUTROP	Orang Utan TROpical Peatland project
PAD	Precise Altitude Data
PALSAR	Phased Array type L-band Synthetic Aperture Radar
POD	Precise Orbit Data
PSF	Peat swamp Forest
pt	points
QMCH	Quadratic Mean Canopy profile Height
R^2	coefficient of determination
R^2_{adj}	adjusted coefficient of determination
R^2_{corr}	corrected coefficient of determination
RADAR	RAdio Detection And Ranging
RBV	Return Beam Vidicon
REDD	Reducing Emissions from Deforestation and forest Degradation in developing countries
REDD+	Reducing Emissions from Deforestation and forest Degradation in developing countries Plus
RGB	Red Green Blue
RMSE	Root Mean Square Error
SAR	Synthetic Aperture Radar
SEE	Standard Error of the Estimate
SEM	Standard Error of the Mean
SLC	Scan Line Corrector
SLICER	Scanning LiDAR Imager of Canopies by Echo Recovery
SMA	Spectral Mixture Analysis
SP	Sample Plot
SRTM	Shuttle Radar Topography Mission
TM	Thematic Mapper
TOPEX	TOPography Experiment
UNFCCC	United Nations Framework Convention on Climate Change
US	United States (of America)
VCF	Vegetation Continuous Fields
WGS84	World Geodetic System 1984
yr	year

CHAPTER I:
Introduction

1 The tropical peatlands of Indonesia

1.1 Characteristics

Peatlands store huge amounts of carbon as peat consists of dead, incompletely decomposed plant material that has accumulated over thousands of years in waterlogged environments that lack oxygen. Tropical peatlands are found in mainland East Asia, Southeast Asia, the Caribbean, Central America, South America, and Southern Africa (Rieley & Page, 2005). Current estimates indicate that the total area of undeveloped tropical peatland is in the range of 30-45 million hectare (ha) (approximately 10-12% of the global peatland resource); about 16.8-27.0 million ha are found in Indonesia (Immirzi *et al.*, 1992; Rieley *et al.*, 1996; Page & Banks, 2007), which makes them one of the largest near-surface pools of terrestrial organic carbon (Sorensen, 1993; Page & Rieley, 1998; IPCC, 2007). The tropical peatlands of Indonesia are typically located at low altitudes in alluvial floodplains where peat swamp forests form smooth convex shaped peat domes up to 20m thick (Figure I-1) and cover at least 9% of the Indonesian land surface (Anderson, 1983; Rieley *et al.*, 1996; Riely & Page, 2005) (Figure I-2). Peat domes can be more than 100km wide incorporating entire water catchments between rivers (Rieley & Page, 2005). In Indonesia the beginning of the peatland formation ranges from the Late Pleistocene through to the early Holocene (Siefferman *et al.*, 1988; Staub & Esterle, 1994; Neuzil, 1997). Some of the sub-coastal peatlands on Borneo, for example, started to accumulate as early as 22,000-23,000 years ago (Page *et al.*, 2004). In the absence of human intervention the current average peat accumulation rate for Indonesian peatlands has been estimated to be 1-2 mm per year (yr) (Sorensen, 1993), which is substantially higher than the rates of 0.2-0.8mm/yr reported for boreal and subarctic peatlands (Gorham, 1991) and of 0.2-1.0mm/yr for temperate peatlands (Aaby & Tauber, 1975).

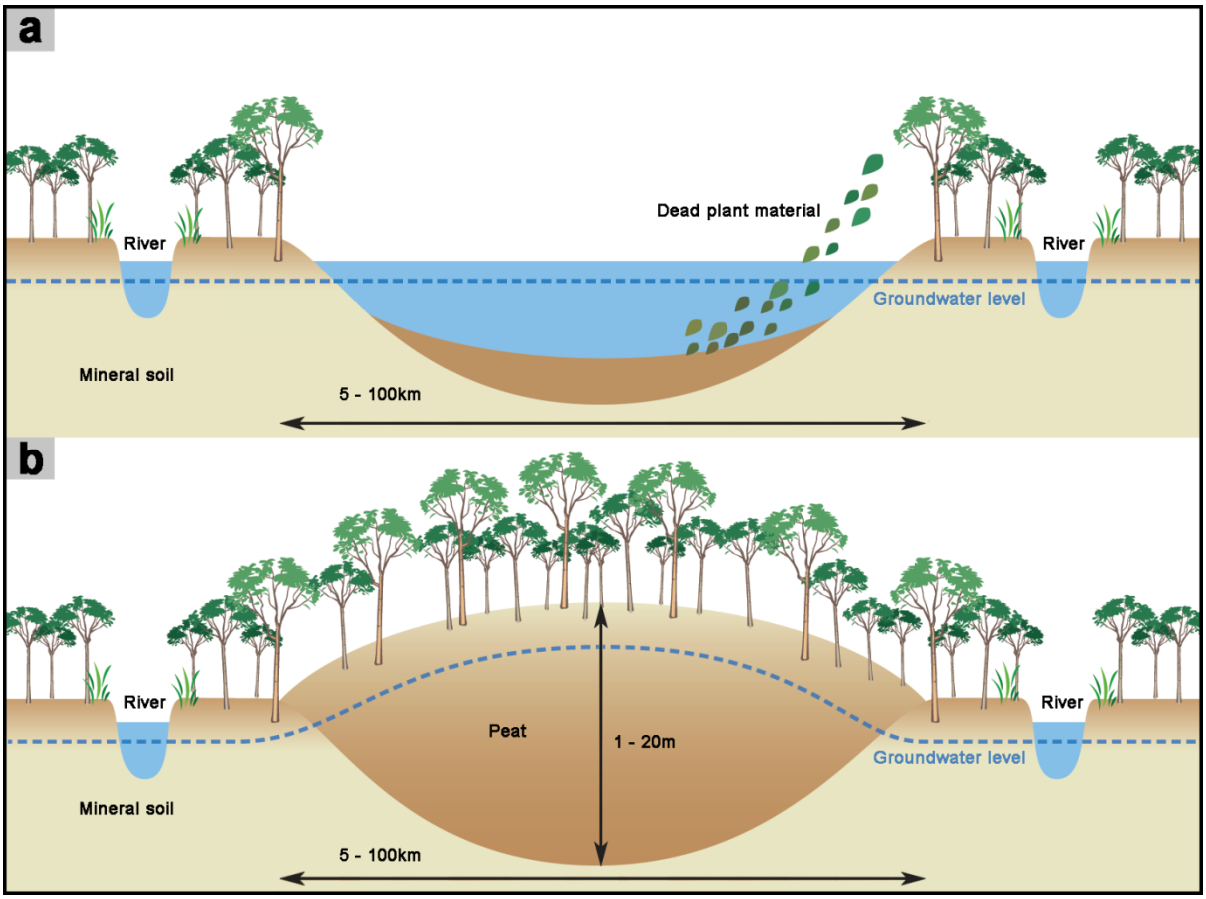

Figure I-1: Schematic cross-section through a typical tropical peat dome in Indonesia (WWF, 2009; modified). (a) Formation of a peat dome. A peat dome develops where large amounts of dead, incompletely decomposed plant material accumulates over thousands of years in waterlogged environments that lack oxygen. The yearly peat accumulation rate is only a few millimeters. (b) Full-grown peat dome. Full-grown peat domes mostly have a convex shaped surface which can be up to 20m thick and be more than 100km wide, covering entire water catchments between rivers. Usually they are covered by different peat swamp forest types reflecting the variations in water- and nutrient-availability.

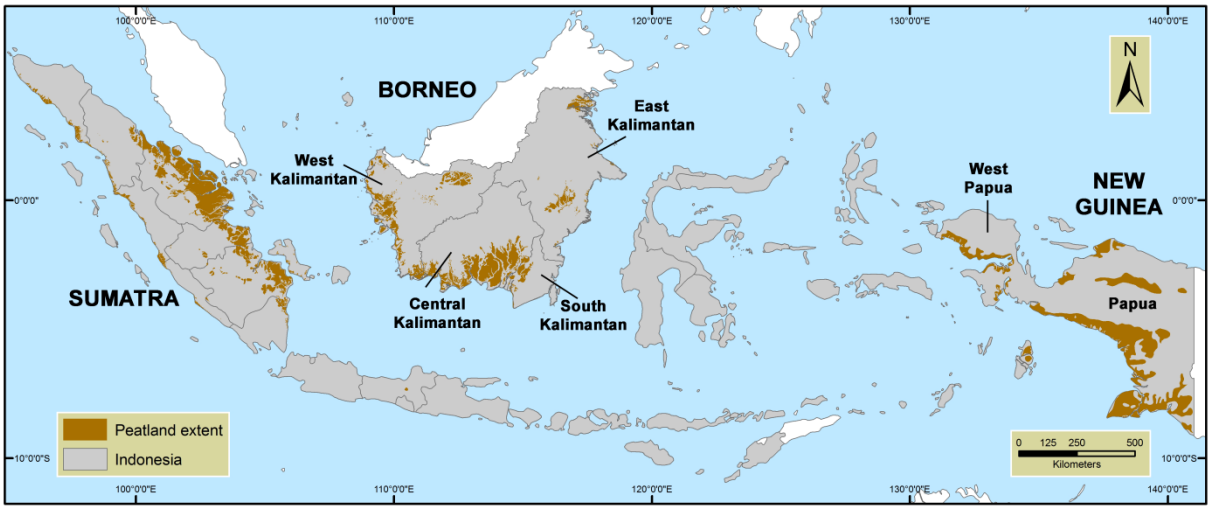

Figure I-2: Peatland extent within Indonesia (peatland data from Wetlands International 2003; 2004; 2005). Most of the peatlands in Indonesia are located at low altitudes in coastal and sub-coastal areas on the islands of Sumatra, Borneo (Kalimantan), and New Guinea (West Papua and Papua).

Peatlands in Indonesia are naturally covered by forests discriminated in different sub-forest types reflecting the variations in water- and nutrient-availability (Anderson, 1964; Shepherd *et al.*, 1997; Page *et al.*, 1999). These differences may range from a mixed swamp community with up to 240 tree species per ha on shallow peat around the margins of the peat dome to a less diverse, low canopy, small pole forest, usually associated with the wettest, deepest peat, in which tree species number can decline to 30–55 species per ha (Rieley & Page, 2005). Additionally there is a significant local and regional variation in species composition and vegetation types of peat swamp forest across Southeast Asia (Rieley & Ahmad-Shah, 1996). Peat that forms under the influence of fluctuating levels of river flood water is called topogenous, while that which is subjected to rainfall only is called ombrogenous (Rieley & Page, 2005). Topogenous peat can be found along flood zones and banks of rivers, but most of the peat in the lowlands of Southeast Asia is ombrogenous where it extends over catchments and watersheds (Rieley & Page, 2005). As ombrogenous peat is purely rainwater fed, the water is nutrient poor and very acidic (pH 3.0-4.5) (Rieley & Page, 2005). Further Indonesian peatlands feature a characteristic micro-topography consisting of hummocks and hollows (Rieley & Page, 2005). Hummocks are up to 0.5m in height and are usually formed around tree bases and comprise large proportions of both living and dead tree roots (Rieley & Page, 2005). These hummocks are interspersed with hollows of similar depth which form an

interconnected network that carries water from the interior peat dome to its periphery (Rieley & Page, 2005).

Natural tropical peat swamp forest ecosystems have a wealth of ecological and hydrological functions such as water retention, flood reduction, protection against seawater intrusion, support of high levels of endemism, and finally as a retreat for endangered species such as the Bornean orangutan (*Pongo pygmaeus*) (Rieley & Page, 2005). Compared to the adjacent terrestrial rain forest ecosystems the diversity associated with ombrotrophic lowland tropical peatlands is usually lower, but many peatland species are specialist, which are not found in other habitats (Rieley & Page, 2005).

1.2 Degradation and the impact on the global climate

Between 1990 and 2005 about 13 million ha of tropical forest were deforested annually and with 0.98% South and Southeast Asia had one of the highest annual deforestation rates for the time period of 2000 to 2005 (FAO, 2006). Between the years 2002 and 2005, with 1.7%, this rate was ever higher for Borneo (Langner *et al.*, 2007). Deforestation and forest degradation in Indonesia are almost exclusively caused by human economic activities such as shifting cultivation, illegal logging, and the establishment of industrial timber estates and large-scale oil palm plantations (Rieley & Page, 2005; Hansen *et al.*, 2009). During extended drought caused by the periodic El Niño phenomenon vast areas of the Indonesia forest have been destroyed by fire (Langner & Siegert, 2009). Fire serves as the principal tool for land clearing and its impacts and severity increases in degraded forests (Siegert *et al.*, 2001). It is estimated that in 2008, worldwide deforestation and forest degradation emissions contributed about 6% to 17% of the total anthropogenic carbon dioxide (CO_2) emissions (Van der Werf *et al.*, 2009).

In Indonesia increased Green House Gas (GHG) emissions are particularly evident in the coastal lowlands of Sumatra and Kalimantan, where peat fires and peat decomposition, due to peatland drainage, results in the release of huge amounts of CO_2 (Page *et al.*, 2002; Ballhorn *et al.*, 2009; Hooijer *et al.*, 2010). The ability of peatlands to sequester and store these huge amounts of carbon is threatened by persistent anthropogenic impacts (Rieley & Page, 2005; Jaenicke *et al.* 2008; Hooijer

et al., 2010). Especially drainage and forest clearance disturb their hydrological stability (Page & Rieley, 1998) and make these otherwise waterlogged ecosystems susceptible to fire (Langner *et al.* 2007) (Figures I-3 and I-4).

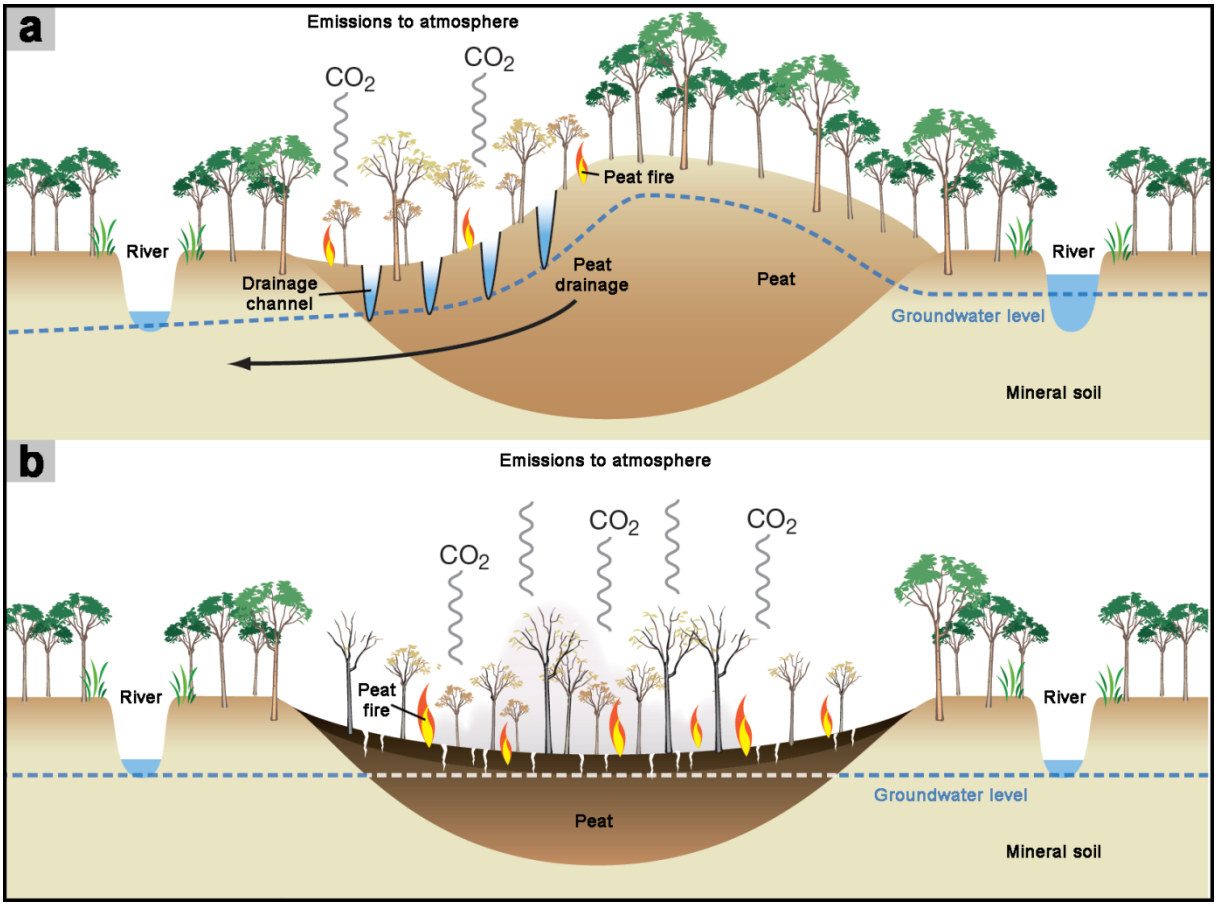

Figure I-3: Degradation of a tropical peat dome (WWF, 2009; modified). (a) Beginning of the degradation process. Construction of a network of drainage channels to control and lower the groundwater level for plantations and/or agricultural development, to facilitate the access to the peat swamp forest, and to extract timber. This leads to emissions of mainly CO_2, due to micro-biotical decomposition and peat fires. (b) If no restoration measures are undertaken (e.g. blocking the drainage channels) these emissions will continue until no peat is left.

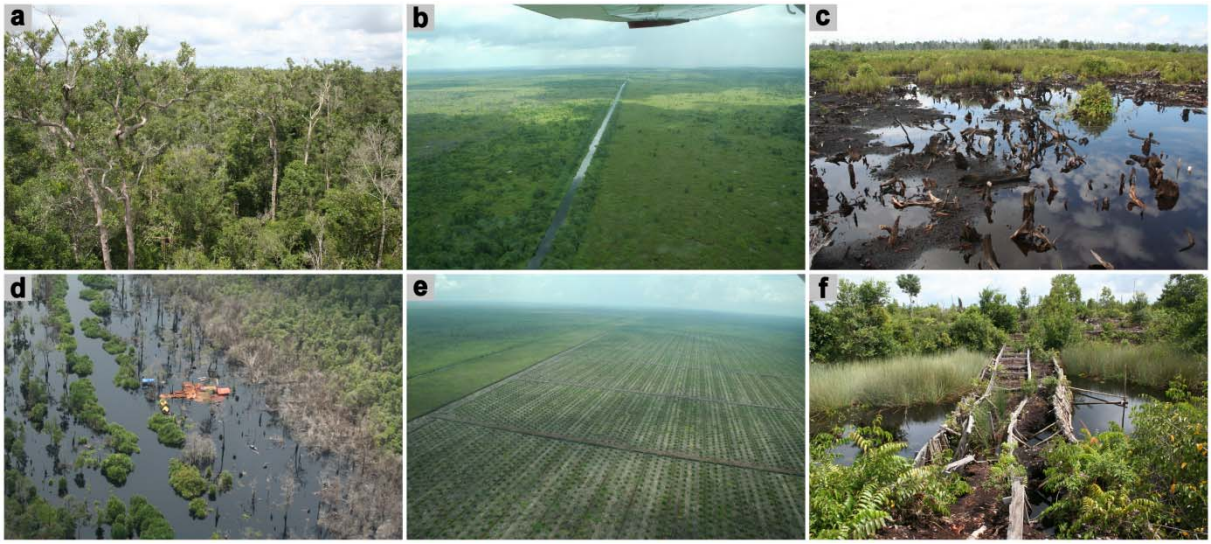

Figure I-4: Examples of peatlands in Central Kalimantan, Indonesia. (a) Undisturbed peat swamp forest. (b) Drainage channel. (c) Burned peatland. (d) Illegal logging. (e) Large-scale oil palm plantation on peatland. (f) Dam constructed for drainage channel blocking.

After peatland drainage there are four largely irreversible processes that lead to a drop in peat surface level, called subsidence (Rieley & Page, 2005): (a) Consolidation is the compression of saturated peat due to increased 'overburden' (no peat matter is lost; increase of bulk density); (b) Shrinkage is the gradual volume reduction of peat in the unsaturated zone due to loss of water from pores (no peat matter is lost; increase of bulk density); (c) Oxidation is the gradual volume reduction of peat in the unsaturated zone due to micro-biotical decomposition of organic matter; and (d) Fire which results in the complete loss of peat organic matter from the burned zone (CO_2, to a lesser degree carbon monoxide (CO), methane (CH_4), and other volatile compounds). Nearly all peatland fires are started by farmers to clear land and on a larger scale by private companies as a cheap tool to clear forest before establishing oil palm and pulp wood plantations (ADB/BAPPENAS, 1999; Bompard & Guizol, 1999; Bowen *et al.*, 2000; Siegert *et al.*, 2001). Peat fires cause both severe deterioration in air quality and health problems by releasing huge volumes of aerosols and noxious gases (ADB/BAPPENAS, 1999; Bowen *et al.*, 2000). Globally peat fires have the potential to accelerate global warming by releasing huge amounts of CO_2 which has increased interest in tropical peatlands in the context of global warming (Page *et al.*, 2002; Rieley & Page, 2005; Hooijer *et al.*, 2006; Ballhorn *et al.*, 2009; Hooijer *et al.*, 2010). Particularly acute is this problem on tropical peatlands in Indonesia, where severe peat fires occurred almost every second year during El Niño

induced droughts in 1997/98, 2002, 2004, 2006, and 2009, which is a new phenomenon and has not been observed in this frequency and spatial extent before (Ballhorn *et al.*, 2009). These recurrent peat fires release huge amounts of CO_2 to the atmosphere (Page *et al.*, 2002; Ballhorn *et al.*, 2009; Langner & Siegert, 2009). For example during the 1997/98 El Niño-induced drought peatland fires in Indonesia alone may have released 13-40% of the mean global carbon emissions from fossil fuels (Page *et al.*, 2002). This important source of carbon emissions is currently not yet included in the Intergovernmental Panel on Climate Change estimates (IPCC, 2007) or in most regional and global carbon cycling models. Additionally drained and deforested peatland areas release huge amounts of carbon due to micro-biotical decomposition (Hooijer *et al.*, 2006; Hooijer *et al.*, 2009; Hooijer *et al.*, 2010). Due to the increased demand for palm oil, triggered by the biofuel boom, this situation will be seriously aggravated since peatlands are the only remaining uninhabited near coastal land resource in Indonesia.

One important measure of the United Nations Framework Convention on Climate Change (UNFCCC) to curb GHG emissions from this sector is the program on Reducing Emissions from Deforestation and forest Degradation in developing countries (REDD+) which involves the private sector of industrialized countries in the protection of the remaining tropical forests to compensate the exceeding of GHG emission quota. To estimate GHG emissions from deforestation and forest degradation information on both the area of forest loss and/or degradation and the corresponding carbon stock of the land that is cleared and/or degraded is needed which remains a big challenge in tropical forests (Gibbs *et al.*2007). Especially GHG emission from forest degradation is difficult to monitor, particularly considering that degraded and regrowing forests are predicted to include increasingly large portions of the tropics (Gibbs *et al.*, 2007).

2 Market based mechanisms for forest conservation

Forests provide a multitude of ecosystem goods and services of fundamental significance, among which are: food and timber, regulation of climate and hydrology, formation of soils, and recreational, aesthetic, and spiritual enjoyment of nature (World Resources Institute, 2005). Regulating the global climate is one of the most important ecosystem service provided by forests today. Most decisions to convert

forests to other land uses are based on market incentives without considering these ecosystem services, as conventional market systems undervalue these services in everyday decision-making (Holling, 1996; Chomitz *et al.*, 1999). Policy instruments, incentives, or a change in undesirable behaviors are necessary to correct for this market failure (Portela *et al.*, 2008). Some of the most common policy mechanisms to correct for this market failure are regulatory, or command-and-control, instruments (e.g. establishment of protected areas, environmental treaties) (Portela *et al.*, 2008). Although still common, in recent years a shift has taken place toward more participatory mechanisms, economic incentives, and market-based instruments (Portela *et al.*, 2008). There are also other approaches to change the behavior of people from deforestation to forest conservation relying on education and local participation, but it has to be kept in mind that these kinds of initiatives fail to address the key issue of market failure (Portela *et al.*, 2008).

Market-based approaches to forest conservation encourage a particular behavior by changing the incentives for individual agents (Portela *et al.*, 2008). Further they differ from command-and-control approaches in that they allow more flexibility in the way policy targets are met (Portela *et al.*, 2008). Currently two market opportunities exist: the regulatory carbon markets and the voluntary carbon markets. Regulatory markets were established to meet emissions targets as mandated by international and national authorities (Portela *et al.*, 2008). Voluntary carbon markets on the other hand help governments, organizations, companies, and individuals to reduce carbon emissions outside the regulatory mandates (Portela *et al.*, 2008). Currently opportunities for forest carbon projects exist in forest conservation, restoration, and sustainable forest management and the most common are afforestation and reforestation (AR) projects (Portela *et al.*, 2008). The regulatory carbon market is dominated by the Kyoto Protocol of the UNFCCC (Portela *et al.*, 2008). The Kyoto Protocol's flexible mechanisms, the Clean Development Mechanism (CDM) and the Joint Implementation (JI) framework, allow market-based forestry activities in order to help mitigate climate change (Portela *et al.*, 2008). Only credits for carbon sequestration through AR are allowed through CDM forestry carbon projects and project development is considerable restricted (Portela *et al.*, 2008). Under the CDM no other forest carbon activities, such as avoided deforestation, are allowed, which limits the opportunities for forest conservation severely (Portela *et al.*, 2008). The

voluntary carbon markets on the other hand offer a large majority of forestry carbon offsets with multiple benefits (Portela *et al.*, 2008). And although most voluntary carbon markets also impose standards and verification guidelines the stringent compliance with CDM rules and paperwork is not required (Portela *et al.*, 2008). There is a significant difference in market value between regulatory and voluntary carbon projects as regulatory projects receive higher prices than similar voluntary projects (Portela *et al.*, 2008).

What holds the greatest promise in protecting tropical forests and their services is the allowance of emissions credits based on the commitment of developing countries to reduce deforestation and forest degradation. Policy instruments that could provide an incentive to Reduce Emissions from Deforestation and Degradation in developing countries (REDD+) are being seriously explored by the UNFCCC. Including REDD+ in the next global climate agreement (post-2012) would give developing countries significant financial and technical support to protect forests and their services (Portela *et al.*, 2008). The development of reference scenarios and the accurate measurements of forest carbon stocks and emissions (monitoring, reporting, and verification) pose technical and scientific challenges in implementing REDD+ projects. The scientific community believes that especially monitoring and estimating forest degradation in a cost-effective way is very difficult. Up to now it is not possible to directly measure forest carbon stocks across a landscape, so that tools and models have to be developed that can scale up or extrapolate destructive harvest data points to larger scales based on proxies measured in the field or from remote sensing instruments (Brown *et al.*, 1989; 1993; Waring *et al.*, 1995; Brown 1997; Chave *et al* 2005; Gibbs *et al.*, 2007; Saatchi *et al* 2007). REDD+ projects pose a promising solution in protecting the last remaining undisturbed tropical peatlands in Indonesia.

3 The use of remote sensing data to monitor Indonesian peatlands

3.1 Introduction to remote sensing

Lillesand *et al.* (2008) define remote sensing as "*the science and art of obtaining information about an object, area, or phenomenon through the analysis of data acquired by a device that is not in contact with the object, area, or phenomenon*

under investigation". Many forms, including variations in force distribution, acoustic wave distributions, or electromagnetic energy, can be used to collect data remotely (Lillesand *et al.*, 2008). Figure I-5 gives an overview of the processes and elements involved in electromagnetic remote sensing.

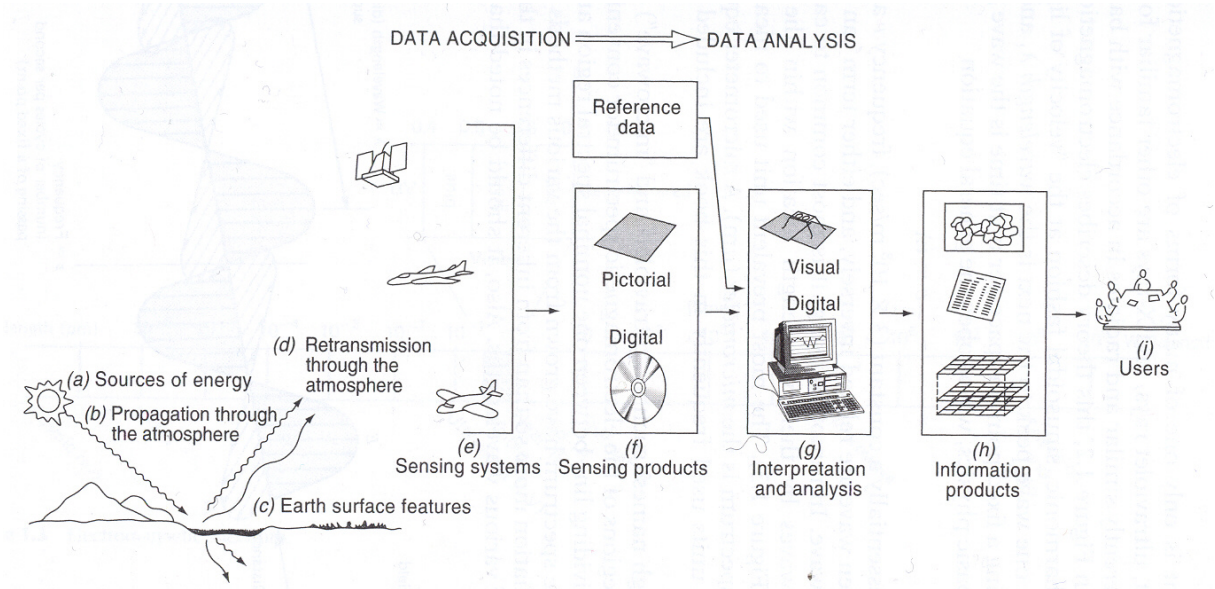

Figure I-5: Electromagnetic remote sensing (Lillesand *et al.*, 2008).

Electromagnetic remote sensing can be split up into two basic processes; data acquisition and data analysis (Lillesand *et al.*, 2008). It can be said that in the data acquisition process sensors are used to record variations in the way earth surface features reflect and emit electromagnetic energy (Lillesand *et al.*, 2008). Visible light, radio waves, heat, ultraviolet rays, and X-rays are forms of electromagnetic energy and radiate in accordance with the basic wave theory. This theory describes electromagnetic energy as traveling in a harmonic, sinusoidal fashion at the velocity of light (Lillesand *et al.*, 2008). Components of electromagnetic energy include a sinusoidal electric wave (E) and a similar magnetic wave (M) at right angles, both being perpendicular to the direction of propagation (Lillesand *et al.*, 2008) (Figure I-6).

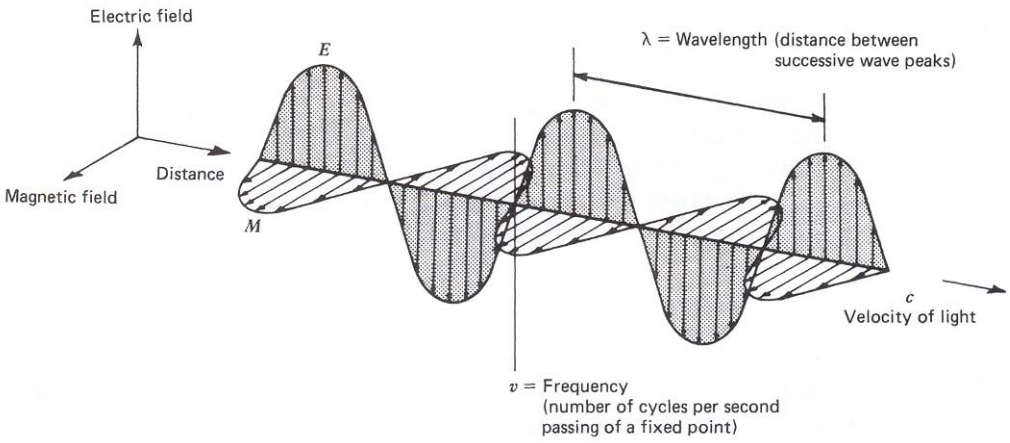

Figure I-6: Electromagnetic wave (Lillesand *et al.*, 2008).

As we know from basic physics, waves obey the following general equation (Lillesand *et al.*, 2008):

$$c = v\lambda \qquad \text{(eq. I-1)}$$

Where:

c = velocity of light; essentially a constant ($3*10^8$ m/sec)

v = wave frequency; number of wave peaks passing a fixed point in space

λ = wavelength; distance from one wave peak to the next

With frequency and wavelength related inversely and c being constant, both frequency and wavelength can be used to characterize a wave. It is common in remote sensing to categorize electromagnetic waves by their wavelength location within the electromagnetic spectrum (Lillesand *et al.*, 2008). Figure I-7 displays this electromagnetic spectrum.

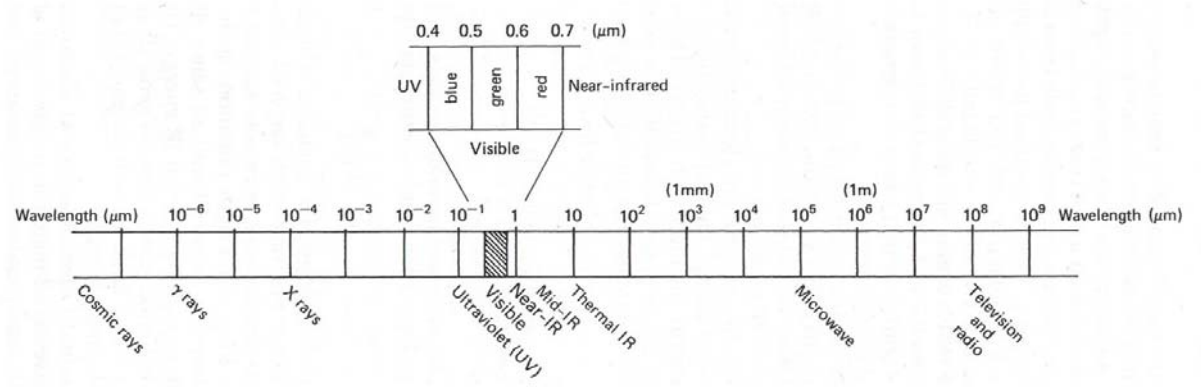

Figure I-7: Electromagnetic spectrum.

Remote sensing sensors can be on airborne or spaceborne platforms (Figure I-5) and each kind of sensor produces images with specific characteristics that allow different applications. These characteristics involve the kind of sensor, image resolution, kind of orbit, size of the scene, and others. The sensors can be summarized as the active and the passive ones. The first one makes use, for example, of the emission of microwaves and registers the difference between the signal emitted by the system and the signal received from the terrestrial surface. The second one registers the electromagnetic reflectance of the earth's surface. The pieces of information are usually stored in grids composed of units called pixels (Lillesand *et al.*, 2008). These pixels represent the average values of reflectance by objects in a fixed area according to the kind of sensor that is being used (Lillesand *et al.*, 2008). To characterize the different sensors, four types of resolution are of importance: (a) The spatial resolution is the limit on how small an object on the earth's surface can still be separated from its surroundings (Lillesand *et al.*, 2008). Spatial resolution is an indication on how well spatial detail can be recorded (Lillesand *et al.*, 2008). (b) Sensors are able to collect information in different parts of the electromagnetic spectrum and store them independently in units called bands (Lillesand *et al.*, 2008). The number, wavelength region, and width of these spectral bands are defined as the spectral resolution (Lillesand *et al.*, 2008). (c) The amount of information collected by a pixel is dependent on the photon count sensitivity of the sensor (Lillesand *et al.*, 2008). Radiometric resolution could be described as the capability to differentiate intensity or brightness classes (Lillesand *et al.*, 2008). (d) Temporal resolution is defined as the repeat frequency of revisiting the same ground segment and is dependent on the registration platform, the ground resolution, and the orbit parameter (Lillesand *et al.*, 2008).

For the remotely sensed images to be integrated in a Geographic Information System (GIS) or to be able to represent reality correctly, keeping proportion relations between what you see in reality and what you see in the image, they need to be put in reality (Longley *et al.*, 2005). This process is called georeferencing and it involves the registration of the image to a reference coordinate system (Longley *et al.*, 2005). Georeferencing begins by defining ground control points with accurate geographic coordinates. These points may be extracted from an image, an aerial photo already corrected from maps, or points captivated in the field through the Global Positioning

System (GPS) (Longley *et al.*, 2005). The process of defining the reference points is interactive (Longley *et al.*, 2005). This way a point in reference is defined and is found in the image to be georeferenced one by one (Longley *et al.*, 2005).

Also of importance are processes of image rectification and restoration. They have the objective to correct distorted image data in order to produce a more faithful representation of the original scene (Lillesand *et al.*, 2008). Typical processes include the correction of geometric distortions, the radiometric calibration of the data, and the elimination of noise present in the data (Lillesand *et al.*, 2008). A special form of rectification that corrects for terrain displacement is called orthorectification (Lillesand *et al.*, 2008).

In the following sections only the sensors used in this thesis are described.

3.2 LiDAR data

Light Detection and Ranging (LiDAR) is an active remote sensing technique which is based on the transmission of laser pulses toward the ground surface and the recording of the return signal. By analyzing the time delay for each pulse back to the sensor, the heights of all reflecting objects can be measured in the range of a few centimeters. LiDAR systems are usually classified using three characteristics: (a) the type of recording the return signal, (b) footprint size, and (c) sampling rate and scanning pattern (Dubayah & Drake, 2000). Two recording types can be differentiated, the discrete-return and the full-waveform system (Figure I-8). For discrete-return systems, pulse detection is conducted in real-time on the returned signal, so that the system detector splits a continuous waveform into several time stamped pulses giving the position of the individual targets (Mallet & Bretar, 2009). These laser scanning systems are called multi-echo or multi-pulse and typically collect first and last pulses but some are able to differentiate up to six individual returns from one pulse. The footprints of these systems are small reaching sizes of 0.2 to 0.9m. Full-waveform systems on the other hand record the amount of energy for a series of equal time intervals and give more control to the user as their processing methods increase pulse detection reliability, accuracy, and resolution. A certain amplitude against time waveform is obtained for each time interval. To understand these waveform pre-processing is necessary which is usually the

decomposition of these waveforms into a sum of echoes generating a three dimensional (3D) point cloud. Most commercial LiDAR systems nowadays are small-footprint systems (0.2 to 3.0m), depending on flying height and beam divergence, and a high repetition frequency. In this thesis data from an airborne and a spaceborne LiDAR system was analyzed.

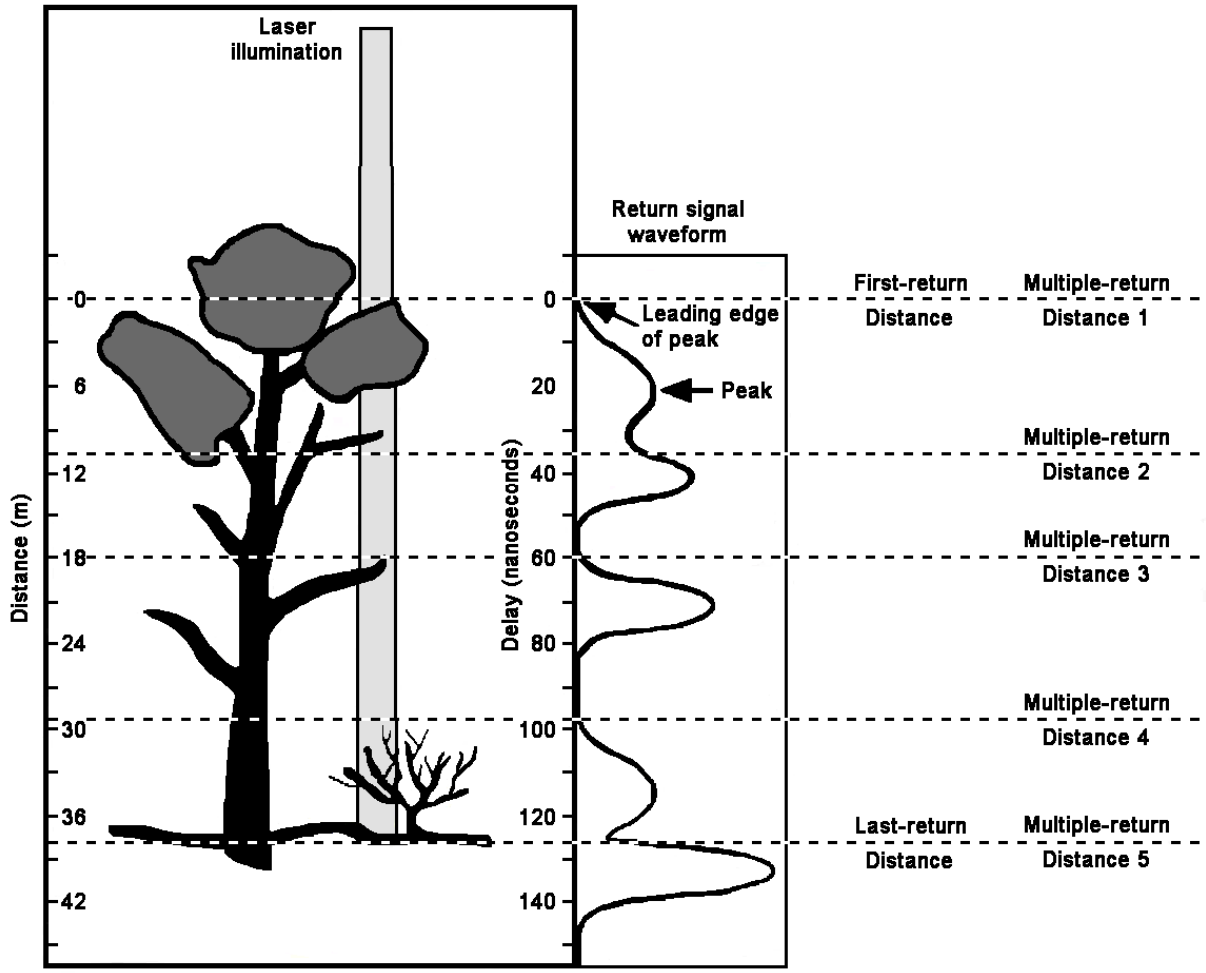

Figure I-8: Conceptual differences between full-waveform and discrete-return LiDAR systems (Lefsky *et al.*, 2002b; modified). In the left the intersection of a laser illumination area, or footprint, through a simplified tree crown is shown. In the center the hypothetical return signal collected by a full-waveform recording device is depicted. In the right three different discrete-return LiDAR sensors are indicated. First-return LiDAR devices only record the position of the first object hit by the laser beam. Last-return LiDAR devices on the other had record the position of the last object hit by the laser beam and are especially useful for topographic mapping. Multiple-return LiDAR sensors record the positions of a smaller number of objects in the path of the illumination.

Airborne LiDAR data was acquired during a flight campaign conducted between 5 and 10 August 2007. A Riegl LMS-Q560 Airborne Laser Scanner was mounted to a

Bell 206 helicopter. Small-footprint full-waveform LiDAR data was collected from a flight altitude of 500m above ground over a scan angle of ±30° (swath width ±500m). The laser sensor had a pulse rate of up to 100,000 pulses per second with a footprint of 0.25m and a wavelength of 1.5µm (near infrared). Due to the accurate time stamping (10^9 samples per second), the three dimensional coordinates of the laser beam reflections (x, y, and z), the intensity, and the pulse width can be extracted by a waveform decomposition, which fits a series of Gaussian pulses to the waveform. This resulted in an average of 1.4 echoes per square meter. The Riegl LMS-Q560 Airborne Laser Scanner system allows height measurements of ±0.02m. Single beam measurements have an absolute horizontal accuracy of ±0.50m and vertical accuracy of ±0.15m Root Mean Square Error (*RMSE*).

The Ice, Cloud, and land Elevation Satellite (ICESat) has been orbiting the earth since 12 January 2003 at an altitude of 600km with a 94° inclination and during most of its operating life it has been programmed for a 91-day orbital repeat cycle and was decommissioned from operation on 14 August 2010. The Geoscience Laser Altimeter System (GLAS) onboard ICESat was a full waveform sensor using a 1,064nm laser operating at 40Hz. This resulted in a nominal footprint of about 65m diameter on the earth's surface with each pulse separated by 172m postings (Schutz *et al.*, 2005). There were three lasers onboard ICESat of which the first one failed about 38 days into the mission (29 March 2003). The original temporally continuous measurements were replaced by three 33 day operating periods per year, so that the life of the second and third laser could be extended (Sun *et al.*, 2008). The laser footprint on the earth's surface actually was in the form of an ellipse and its size varied over time as a function of power output from the laser (Harding & Carajabal, 2005). As the GLAS sensor recorded the returned energy over time these waveforms represented the vertical distribution of the terrain and vegetation within each footprint. GLAS data have been demonstrated to accurately estimate forest height (Lefsky *et al.*, 2007; Rosette *et al.*, 2008; Lefsky, 2010) and AGB (Harding & Carajabal, 2005; Boudreau *et al.*, 2008). In this study we used the ICESat/GLAS data from release version 31. According to The National Snow and Ice Data Center ICESat/GLAS this release version had an average horizontal geolocation error for all laser campaigns of 0.78 ±5.09m (The National Snow and Ice Data Center, 2011b).

3.4 Optical satellite data

Optical data from different Landsat satellites, the Advanced Very High Resolution Radiometer (AVHRR) on board the National Oceanic and Atmospheric Administration (NOAA) satellite, the Along-Track Scanning Radiometer (ATSR) on board the European Remote Sensing Satellite 2 (ERS-2), and the MODerate resolution Imaging Spetroradiometer (MODIS) on board the Terra and Aqua satellites were analyzed in this thesis.

The beginning of the Landsat program was a conceptual study of the feasibility of a series of Earth Resource Technology Satellites (ERTSs) by the National Aeronautics and Space Administration (NASA) and the United States (US) Department of the Interior (Lillesand *et al.*, 2008). This study resulted in a planned sequence of six satellites called ERTS-A, -B, -C, -D, -E, and -F (after launch there were to become ERTS-1, -2, -3, -4, -5, and -6) (Lillesand *et al.*, 2008). ERTS-1 was launched on July 23, 1972, and represented the first unmanned satellite specifically designed to acquire data about earth resources on a systematic, repetitive, medium resolution, and multispectral basis (Lillesand *et al.*, 2008). The collected data was open to everyone and all nations of the world were invited to take part in evaluating ERTS-1 data (Lillesand *et al.*, 2008). NASA officially renamed the ERTS program as the Landsat program prior to the launch of ERTS-B on January 22, 1975 (ERTS-1 was retroactively named Landsat-1) (Lillesand *et al.*, 2008). Up until now six Landsat satellites have been launched successfully, namely Landsat-1 to -5 and Landsat-7 (Landsat-6 suffered a launch failure) (Lillesand *et al.*, 2008). Five different types of sensors have been included in various combinations on these missions. These are the Return Beam Vidicon (RBV), the MultiSpectral Scanner (MSS), the Thematic Mapper (TM), the Enhanced Thematic Mapper (ETM), and the Enhanced Thematic Mapper Plus (ETM+). A summary of the Landsat program with the different sensors is given in Tables I-1 and I-2. A problem occurred on May 31, 2003, with Landsat-7 as an instrument malfunctioned (Lillesand *et al.*, 2008). The cause was a failure of the Scan Line Corrector (SLC) and without an operating SLC the ETM+ line of sight now traces a zig-zag pattern along the satellite ground track with a resulting duplication of imaged area that increases toward the scene edge (Lillesand *et al.*, 2008).

Table I-1: Characteristics of Landsat-1 to -7 missions (Lillesand *et al.*, 2008).

Satellite	Launched	Decommissioned	RBV bands	MSS bands	TM bands	Orbit
Landsat-1	July 23, 1972	January 6, 1978	1-3 (simultaneous images)	4-7	None	18 days/900km
Landsat-2	January 22, 1975	February 25, 1982	1-3 (simultaneous images)	4-7	None	18 days/900km
Landsat-3	March 5, 1978	March 31, 1983	A-D (one-band side-by-side images)	4-8[a]	None	18 days/900km
Landsat-4	July 16, 1982[b]	June 15, 2001	None	1-4	1-7	16 days/705km
Landsat-5	March 1, 1984[c]	-	None	1-4	1-7	16 days/705km
Landsat-6	October 5, 1993	Failure upon launch	None	None	1-7 plus panchromatic band (ETM)	16 days/705km
Landsat-7	April 15, 1999[d]	-	None	None	1-7 plus panchromatic band (ETM+)	16 days/705km

[a]Band 8 (10.4-12.6 µm) failed shortly after launch.
[b]TM data transmission failed in August 1993.
[c]MSS powered off in August 1995; solar array drive problems began in November 2005.
[d]Scan Line Corrector (SLC) malfunctioned on May 31, 2003.

Table I-2: Sensors used on Landsat-1 to -7 missions (Lillesand *et al.*, 2008).

Sensor	Mission	Sensitivity (µm)	Resolution (m)
RBV	1, 2	0.475-0.575	80
		0.580-0.680	80
		0.690-0.830	80
	3	0.505-0.750	30
MSS	1-5	0.5-0.6	79/82[a]
		0.6-0.7	79/82[a]
		0.7-0.8	79/82[a]
		0.8-1.1	79/82[a]
	3	10.4-12.6[b]	240
TM	4, 5	0.45-0.52	30
		0.52-0.60	30
		0.63-0.69	30
		0.76-0.90	30
		1.55-1.75	30
		10.4-12.5	120
		2.08-2.35	30
ETM[c]	6	Above TM bands	30 (120 thermal band)
		plus 0.50-0.90	15
ETM+	7	Above TM bands	30 (60 thermal band)
		plus 0.50-0.90	15

[a]79m for Landsat-1 to -3 and 82m for Landsat-4 and -5.
[b]Failed shortly after launch (band 8 of Landsat-3).
[c]Landsat-6 launch failed.

Active fire occurrence was analyzed from day-light independent thermal IR bands (3-4µm) incorporated in the AVHRR, ATSR, and MODIS sensors (Cochrane, 2003; Siegert *et al.*, 2004; Davies *et al.*, 2009).

3.5 RADAR satellite data

RAdio Detection And Ranging (RADAR) was developed to detect the presence of objects, to determine their distance, and sometimes their angular position by using radio waves (Lillesand *et al.*, 2008). Short burst or pulses of microwaves energy are

transmitted in the direction of interest and the strength and origin of the reflections received are recorded (Lillesand *et al.*, 2008). As these systems supply their own source of energy, they are active remote sensing systems and are therefore day-light independent. Additionally they are able to penetrate clouds and haze so that they are of special interest to the tropics as these regions are often covered by clouds. Data from the Shuttle Radar Topography Mission (SRTM) was used in this thesis.

The SRTM, a joint mission conducted by the NASA and the National Imagery and Mapping Agency (NIMA), was flown from 11 to 22 February 2000 and collected single-pass radar interferometry data covering 119.51 million km^2 of the earth's surface including over 99.9% of the land area between 60°N and 56°S latitude (Lillesand *et al.*, 2008). The C-band InSAR acquired data in 225km swaths and was provided by the Jet Propulsion Laboratory (JPL). For Southeast Asia digital elevation models with a pixel spacing of three arcseconds (about 90m) were produced. The absolute horizontal and vertical accuracy of the data are better than 20 and 16m respectively (Lillesand *et al.*, 2008).

4 Approach and specific objectives

Since most peatlands in Indonesia are highly inaccessible, very few field measurements have been made to date. One way to overcome this problem may be the use of airborne LiDAR data. The resulting 3D LiDAR point clouds (x, y, and z coordinates) are differentiated into ground points, points reflected from the terrain, and non-ground points mainly reflected from the vegetation in forested regions. The ground points are then used to generate Digital Terrain Models (DTMs). Aerial LiDAR systems (discrete-return and full-waveform), compared to other remote sensing technologies, have been shown to yield the most accurate estimates for land topography, forest structural properties, and forest Above Ground Biomass (AGB). On the other hand systems operated from airplanes have limitations due to large data volumes and high costs (Ranson *et al.*, 2007). The GLAS onboard the ICESat mission is the first spaceborne LIDAR system capable of providing global data sets of the earth's topography (Schutz *et al.*, 2005). ICESat/GLAS data have been demonstrated to accurately estimate forest structural properties especially well in topographically even areas with uniform forest cover (Harding & Carajabal, 2005; Lefsky *et al.*, 2007; Baccini *et al.*, 2008; Boudreau *et al.*, 2008, Rosette *et al.*, 2008;

Sun *et al.*, 2008; Goetz *et al.*, 2010; Lefsky, 2010; Dolan *et al.*, 2011). In areas of moderate to high relief the results show lower reliability (Harding & Carajabal, 2005). Peatlands have an especially smooth topography. The inland peat swamps of Central Kalimantan (Indonesia), for example, have an elevation rise of only about 1m per km (Page *et al.*, 1999; Rieley & Page, 2005). Therefore ICESat/GLAS data might be an adequate tool to measure the topography of the peat soil and the forest AGB.

The main goal of this thesis was *the assessment of the potential and accuracy of airborne and spaceborne LiDAR data in measuring peatland topography, peat fire burn depth, peat fire carbon emissions, and forest AGB in Central Kalimantan, Indonesia*.

We focused our investigation on a peat dominated landscape in Central Kalimantan, Indonesia (Figure I-9). Almost all peat swamp forest ecosystems within Central Kalimantan have been severely impacted by extensive logging and drainage for more than two decades (Rieley & Page, 2005). The area also covers the former Mega Rice Project (MRP), an ill-fated transmigrasi resettlement project initiated in 1995 by the Indonesian government, which resulted in the serious degradation of more than one million ha of peat swamp forest (Rieley & Page, 2005).

To reach this main goal following specific objectives were formulated:

(1) *Assessment of the potential and accuracy of airborne LiDAR data to measure peat burn depth for single and multiple fire events.*
(2) *Estimation of carbon emissions from peat fires for single and multiple fire events at different spatial scales from the sub district level to the national level based on the peat depth calculations.*
(3) *Assessment of the potential and accuracy of spaceborne LiDAR data to measure peatland topography.*
(4) *Collection of forest in-situ data at various degradation levels.*
(5) *Assessment of the potential and accuracy of airborne and spaceborne LiDAR data to calculate forest AGB through correlation with the collected forest in situ data.*

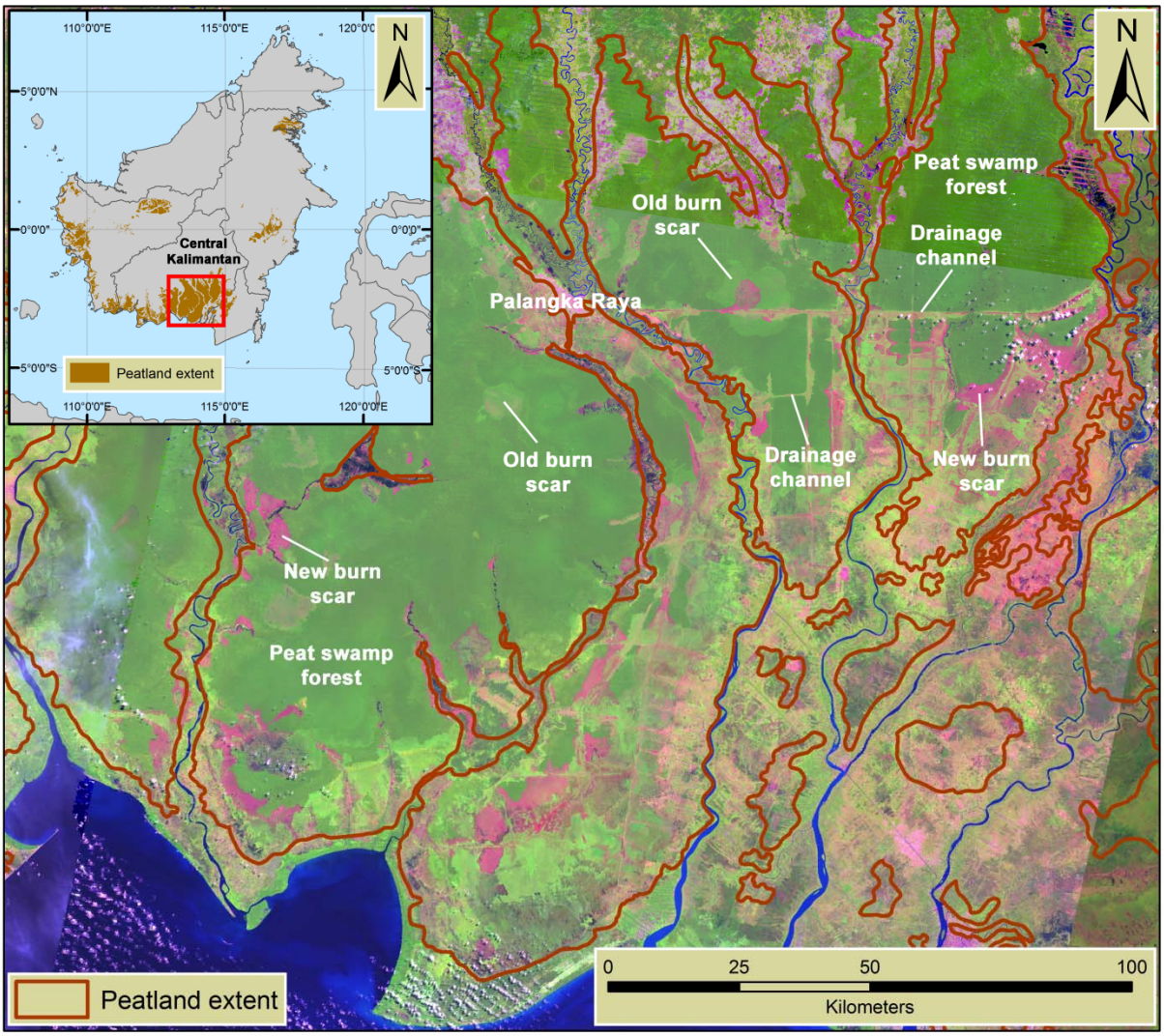

Figure I-9: Overview of the study area in Central Kalimantan, Indonesia. Peatland extent is superimposed on Landsat ETM+ imagery (bands 5, 4, 3). Buildings and new burn scars appear in red, old burn scars in light green, and peat swamp forest in dark green. Also visible is the drainage channel network. The red rectangle in the upper left depicts the location of the study area within Central Kalimantan.

5 Structure of the thesis

This thesis is structured in seven sections (CHAPTER I-VII). In Chapter I a short introduction to Indonesian peatlands, the environmental problems surrounding these ecosystems, possible mechanisms in protecting their ecosystems services, an overview of the used remote sensing sensors, the main goal, the specific objectives, and the structure of the thesis are given. CHAPTER II-VI are the main sections and relate to the specific objectives outlined above. In CHAPTER II, using an airborne LIDAR data set acquired in Central Kalimantan, in 2007, one year after the severe peatland fires of 2006, the average peat burn scar depth was determined. Based on this result and the burned area determined from Landsat imagery the emitted carbon, within a 2.79 million hectare study area, was estimated. Further the approximate carbon emissions through peatland fires for Indonesia in 2006 based on active fire recording of the MODIS, a correction factor for the MODIS burned area determined from a correlation with Landsat-derived burned areas, peatland maps of Indonesia, and the derived peat burn depth were calculated. In CHAPTER III, based on the same airborne LiDAR set analyzed in CHAPTER II, peat loss not only after single but also multiple fire events were calculated through 3D modelling of a pre-fire peat surface. These peat loss calculations were then set in relation to water table measurements, burn frequency, the year of the fire occurrence, and the duration of the dry season to assess the influence of these factors. Additionally based on object oriented fire scar classifications (derived from Landsat data) between the years 1990-2009 and the calculated peat loss the carbon emitted within the Kapuas district (1,489,325ha; Central Kalimantan) was estimated. In CHAPTER IV the applicability of quality filtered ICESat/GLAS data to measure peatland topography as a proxy for peat volume and to estimate peat swamp forest AGB in a thoroughly investigated study site in Central Kalimantan was assessed. Mean SRTM elevation and three 3D peatland elevation models derived from SRTM data were correlated to the corresponding ICESat/GLAS elevation. Based on the correlation of in-situ peat swamp forest AGB and airborne LiDAR data an ICESat/GLAS AGB prediction model was developed. In CHAPTER V the applicability of airborne LiDAR data, based on the same airborne LiDAR set analyzed in CHAPTER II, to estimate AGB of two different tropical rainforest types (lowland dipterocarp and peat swamp forest) in Central Kalimantan was tested by developing multiple regression models at plot

level. In order to sample a high number of field plots the angle count method was applied which allows fast sampling and more laborious fixed-area plots (three nests of circular shape) were used as a control. AGB-prediction models were established for each forest type using statistical values of the LiDAR point clouds and the forest inventory plots. These regression models were then applied to six LiDAR tracks (altogether with a size of 5,241ha) covering unlogged, logged and burned lowland dipterocarp and peat swamp forest. In CHAPTER VI AGB was estimated for different tropical forests (lowland dipterocarp and peat swamp forest) in Central Kalimantan through correlating airborne LiDAR data (the same airborne LiDAR set analyzed in CHAPTER II) to forest inventory data. Two metrics, the Quadratic Mean Canopy profile Height (QMCH) and the Centroid Height (CH), derived from the LiDAR height histograms were correlated to AGB values from a forest inventory. A possible improvement of the regression models through the use of the LiDAR point densities as weight was tested. A rigorous covariance propagation analysis was carried out to find the LiDAR point density with the best cost-benefit relation. Further a Landsat based classification approach, in which each land cover class was linked to a single biomass value determined from a regional biomass database, was compared to LiDAR derived AGB estimates. Finally, CHAPTER VII synthesizes the six preceding sections and provides directions for future research.

CHAPTERS II-VI were written as stand-alone manuscripts to be published in international peer-reviewed journals. Each chapter is therefore structured into subsections introduction, materials and methods, results, discussion and conclusions, thereby resulting in a limited amount of recurring material:

CHAPTER II: **Ballhorn U**, Siegert F, Mason M, Limin S (2009) Derivation of burn scar depths and estimation of carbon emissions with LiDAR in Indonesian peatlands. *Proceedings of the National Academy of Sciences of the United States of America*, **106**, 21213-21218.

CHAPTER III: **Ballhorn U**, Jubanski J, Siegert F Pre-fire surface 3D modeling of tropical peatland burn scars based on airborne LiDAR in Central Kalimantan, Indonesia. Manuscript in preparation for *Global Change Biology*.

CHAPTER IV: **Ballhorn U**, Jubanski J, Siegert F (2011) ICESat/GLAS Data as a Measurement Tool for Peatland Topography and Peat Swamp Forest Biomass in Kalimantan, Indonesia. *Remote Sensing*, **3**, 1957-1982.

CHAPTER V: Kronseder K, **Ballhorn U**, Böhm V, Siegert F Above ground biomass estimation across forest types at different degradation levels in Central Kalimantan using LiDAR data. *International Journal of Applied Earth Observations and Geoinformation*, in print.

CHAPTER VI: Jubanski J, **Ballhorn U**, Kronseder K, Siegert F Deriving forest above ground biomass in Central Kalimantan (Indonesia) using airborne LiDAR data. Manuscript in preparation for *Nature Climate Change*.

CHAPTER II:
Derivation of burn scar depths and estimation of carbon emissions with LiDAR in Indonesian peatlands

Proceedings of the National Academy of Sciences of the United States of America, **106**, 21213-21218

Uwe Ballhorn[a,b], Florian Siegert[a,b], Mike Mason[c], Suwido Limin[d]

[a]Biology Department II, GeoBio Center, Ludwig-Maximilians-University, Grosshaderner Strasse 2, D-82152 Planegg-Martinsried, Germany

[b]Remote Sensing Solutions GmbH, Isarstrasse 3, D-82065 Baierbrunn, Germany

[c]J.P. Morgan ClimateCare, Magdalen Road 112, OX4 1RQ Oxford, United Kingdom

[d]Centre for International Co-operation in Management of Tropical Peatland, Faculty of Agriculture, University of Palangka Raya, Palangka Raya 73112, Indonesia

doi: 10.1073/pnas.0906457106
Received for review 10th June 2009
Approved 14th October 2009

Abstract

During the 1997/98 El Niño-induced drought peatland fires in Indonesia may have released 13–40% of the mean annual global carbon emissions from fossil fuels. One major unknown in current peatland emission estimations is how much peat is combusted by fire. Using a light detection and ranging data set acquired in Central Kalimantan, Borneo, in 2007, one year after the severe peatland fires of 2006, we determined an average burn scar depth of 0.33 ±0.18m. Based on this result and the burned area determined from satellite imagery, we estimate that within the 2.79 million hectare study area 49.15 ±26.81 mega tons of carbon were released during the 2006 El Niño episode. This represents 10–33% of all carbon emissions from transport for the European Community in the year 2006. These emissions, originating from a comparatively small area (approximately 13% of the Indonesian peatland area), underline the importance of peat fires in the context of green house gas emissions and global warming. In the past decade severe peat fires occurred during El Niño-induced droughts in 1997, 2002, 2004, 2006, and 2009. Currently, this important source of carbon emissions is not included in IPCC carbon accounting or in regional and global carbon emission models. Precise spatial measurements of peat combusted and potential avoided emissions in tropical peat swamp forests will also be required for future emission trading schemes in the framework of Reduced Emissions from Deforestation and Degradation in developing countries.

Keywords: climate change; fires; Indonesia; tropical peat; remote sensing

1 Introduction

Current estimates indicate that the total area of undeveloped tropical peatland is in the range of 30–45 million ha (approximately 10–12% of the global peatland resource); about 16.8–27.0 million ha are found in Indonesia (Immirzi *et al.*, 1992; Rieley *et al.*, 1996; Page & Banks, 2007), which makes them one of the largest near-surface pools of terrestrial organic carbon (Sorensen, 1993; Page & Rieley, 1998; IPCC, 2007). Typically, tropical peat is located at low altitudes where peat swamp forest forms peat domes up to 20m thick that usually have a convex shaped surface (Anderson, 1983; Rieley *et al.*, 1996; Rieley & Page, 2005). Some of the sub-coastal peatlands on Borneo started to accumulate as early as 22,000–23,000 years ago (Page *et al.*, 2004). Their ability to sequester and store huge amounts of carbon is threatened by persistent anthropogenic impacts (Rieley & Page, 2005; Hooijer *et al.*, 2006; Jaenicke *et al.*, 2008). Drainage and forest clearance in particular disturb their hydrological stability (Page & Rieley, 1998) and make them susceptible to fire (Langner *et al.*, 2007). Nearly all peatland fires are of anthropogenic origin, as they are started by farmers to clear land and on a much larger scale by private companies as the cheapest tool to clear forest before establishing oil palm and pulp wood plantations (ADB/BAPPENAS, 1999; Bompard & Guizol, 1999; Bowen *et al.*, 2000; Siegert *et al.*, 2001). Peat fires cause both severe deterioration in air quality and health problems in the region by releasing huge volumes of aerosols and noxious gases (ADB/BAPPENAS, 1999; Bowen *et al.*, 2000). Globally peat fires have the potential to accelerate global warming by releasing huge amounts of carbon dioxide (Page *et al.*, 2002; Hooijer *et al.*, 2006).

To quantify the role of peatland fires in the release of carbon, it is important to know how much of the peat layer is consumed by a fire. Since most peatlands in Indonesia are highly inaccessible, very few field measurements have been made to date, as this would require either knowing the fire affected area in advance or igniting peatland on a larger scale intentionally. Due to these constraints, previous peat fire carbon emission estimates were based on a very limited number of spatially non-representative field samples (Page *et al.*, 2002). To overcome these problems and to obtain spatial measurements on burn depth across large fire scars, we used light detection and ranging (LiDAR) aerial remote sensing. LiDAR is based on the transmission of laser pulses toward the ground surface and the recording of the

return signal. By analyzing the time delay for each pulse back to the sensor, relative and absolute surface heights can be determined with an accuracy of several centimeters. We focused our investigation on 2.79 million ha of a peat dominated landscape in Central Kalimantan, Borneo, where in 2006 severe wildfires destroyed large tracts of peat swamp forest (Figure II-1*a*). Our main objectives were to (*a*) assess the potential and accuracy of LIDAR 3D height measurements to measure the peat volume combusted by fire in peat swamp forests, (*b*) develop an operational methodology to do this, (*c*) provide accurate information on the depth of specific burn scars within the study area that originated in the 2006 El Niño fire event and compare these to previous estimates, and (*d*) to estimate carbon emissions from peat fires for the 2006 fire season within the study area.

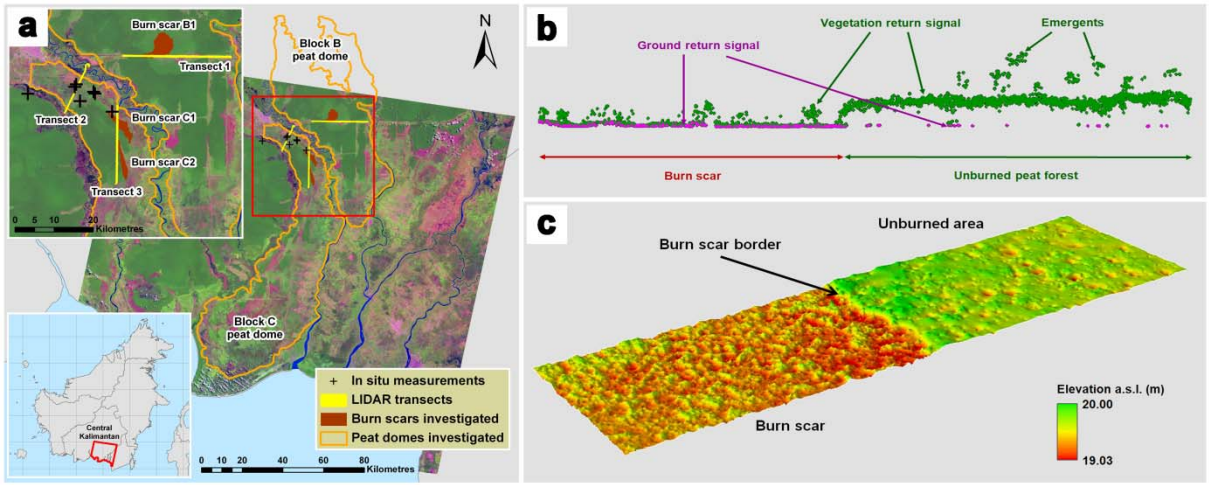

Figure II-1: (*a*) Study area in Central Kalimantan, Borneo, Indonesia Landsat ETM+ 7 image 118–62, August 5, 2007, (gap filled) covering the study area; burn scars are visible in shades of red and pink (RGB: ETM+ 7 bands 5, 4, 3); the LiDAR transects are indicated in yellow, investigated burn scars in dark brown, peat domes of Block B and Block C in orange and in situ peat fire depth measurements as black crosses. (*b*) Three hundred meter LiDAR cross-section through a burn scar within a peat swamp forest; vegetation return signals are indicated in green and ground return signals are indicated in magenta; in peat forests about 1.0 ±0.5% and in burn scars about 6.4 ±2.1% of the return signal were classified as ground. (*c*) Interpolated DTM derived from the LiDAR ground return signals; note the height difference between the burn scar (*Left*) and the unburned forest floor (*Right*).

2 Results

Land cover and previous fire history was analyzed using a time series of 11 Landsat images acquired between 1997 and 2007. The extent of peatland in Indonesia was

determined from maps prepared by Wetlands International (Wetlands International, 2003, 2004, 2006) (see *Materials and Methods*). We analyzed peat fire occurrence in Borneo based on a fire hotspot database, spanning from January 1, 1997, to August 31, 2009, (Langner & Siegert, 2009). As there is not a single sensor system which covers the full time period, a separate analysis for 2 investigation periods was carried out: (*a*) from 1997 to 2000 using fire hotspots from the Advanced Very High Resolution Radiometer (AVHRR) on board the National Oceanic and Atmospheric Administration (NOAA) satellite and from the Along-Track Scanning Radiometer (ATSR) on board the European Remote Sensing Satellite 2 (ERS-2), and (*b*) and from 2001 to 2009 using fire hotspots from the MODerate resolution Imaging Spectroradiometer (MODIS) on board the Terra and Aqua satellites (Davies *et al.*, 2009; Langner & Siegert, 2009). This fire hotspot time series showed that the peat fires in 2006 were the most severe after the well known 1997–1998 fire disaster. In 2002 and 2004, and January–September, 2009, fewer, yet more extensive, peat fires were observed in Borneo, especially in the Indonesian part of Borneo (Kalimantan), resulting in 5 years of significantly increased fire activity within one decade (Figure II-2) (Langner & Siegert, 2009) (see *Materials and Methods*). This is very unusual in this wet swamp ecosystem and was not observed to this extent before 1997 (Field *et al.*, 2009). The El Niño episode of 2006 caused a drier and longer dry season than usual. During these drought conditions the average groundwater table sank from a normal value of -0.16m to -1.61m near burn scar C1 and -1.68m near burn scar C2 (Figure II-1*a*) (*Materials and Methods*). In total 256,783ha of pristine and logged-over peat swamp forests, as well as degraded forests and forests regrowing after previous fires (almost 10% of the study area), were seriously affected by fire in 2006 (Table II-1) (*Materials and Methods*).

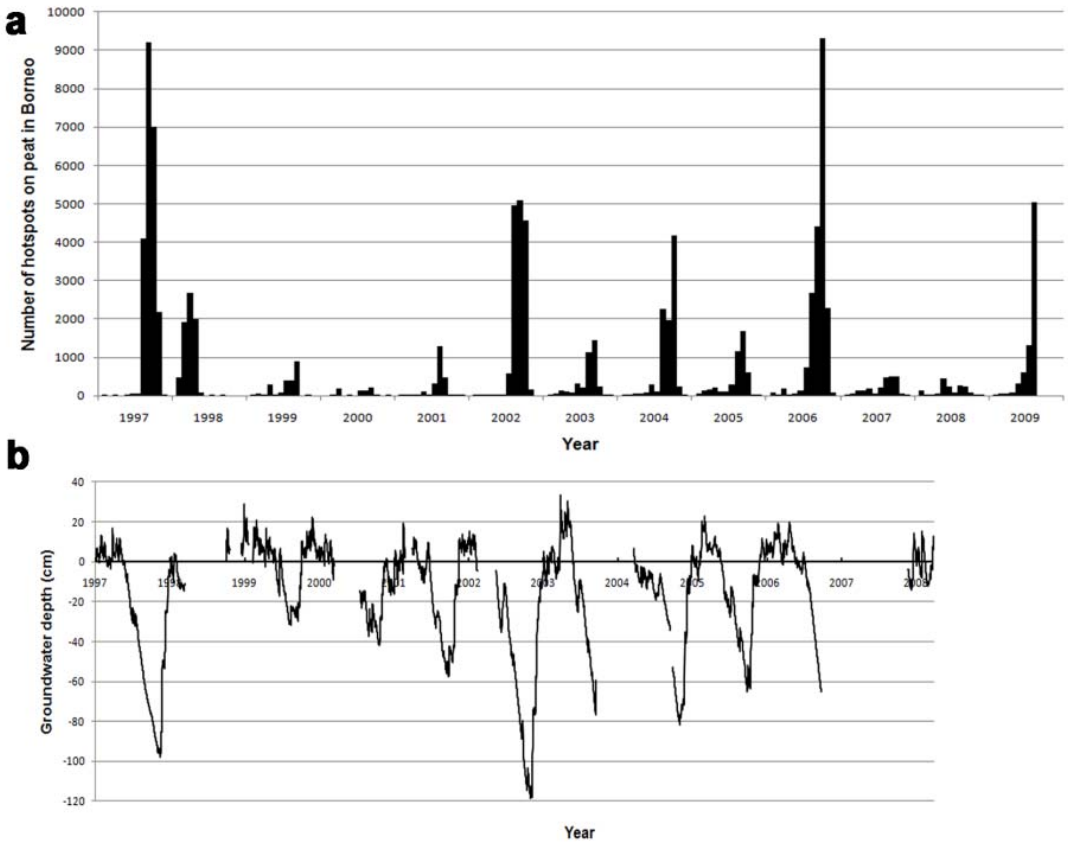

Figure II-2: Fire occurrence (hotspots) on peat in Borneo and groundwater depth (cm) measured in a peat swamp forest. (*a*) Fire occurrence (hotspots) on peat in Borneo from January 1, 1997 to August 31, 2009. Fire hotspots before the year 2001 were derived from the NOAA AVHRR and ATSR data and after 2001 from the MODIS on board the Terra and Aqua satellites; 2006 had the highest number of fires occurrences since 1997–1998 which resulted in exceptionally high carbon emissions compared to the other years. (*b*) Groundwater depth (cm) measured in a largely undisturbed peat swamp forest in the Sebangau National Park situated in Central Kalimantan. Low groundwater depth correlates with a high occurrence of fire (hotspots). The data gaps are due to a failure of the data logger.

For the purpose of this study, 3 transects were analyzed: transect 1 had a length of 27,900m and an average width of 600m, transect 2 had a length of 15,340m and an average width of 460m, and transect 3 had a length of 20,700m and an average width of 580m (Figure II-1*a*). The LiDAR transects covered 3 major individual burn scars (B1, C1, C2) and several small ones (Figure II-1*a*). These transects covered burned and adjacent unburned peatlands, the elevation difference between burned and unburned areas is clearly visible (Figure II-1*c*). Burn scar B1 had a size of 2,632ha, C1 a size of 1,209ha, and C2 a size of 864ha (Figure II-1*a*; Table II-1). The exact time of fire occurrence was determined using daily MODIS hotspot data.

Seventy-eight percent of the investigated burn scar borders are located in peat swamp forests previously not affected by fire but which showed a disturbed canopy due to many years of legal and illegal logging operation. Sixteen percent of the investigated burn scar borders burned during the 1997 El Niño and were covered by dense regrowing forest approximately 10–15m tall. In 2007, one year after the fire, all fire scars were sparsely covered with regrowing tree saplings, ferns, and vines. Often, unburned wood debris and toppled over tree trunks were scattered on the ground. On fire scars, the LiDAR signal is often reflected directly from the peat soil surface, while in peat swamp forests most of the signal is echoed from leaves and branches and not from the ground. Nevertheless, logged over peat swamp forests are much less dense and shorter than typical tropical lowland rainforests.

The 3D LiDAR point clouds (x, y, and z coordinates) were differentiated into ground points, points reflected from the terrain, and non-ground points reflected from the vegetation (Figure II-1*b*). To generate a digital terrain model (DTM), it was necessary to eliminate all vegetation points while at the same time preserving the ground points. A statistical analysis of the signals reflected from the peat soil surface showed that in unburned peat forests about 1.0 ±0.5% of the points were reflected from the ground surface and in burn scars about 6.4 ±2.1% of the points were reflected (Figure II-1*b*) (see *Materials and Methods*). This adds up to about 112 ±80 ground return signals per ha (0.011 per square m) in unburned peat forests and to about 1298 ±212 ground return signals per ha (0.13 per square m) in burn scars. The inland peat swamps of Central Kalimantan are flat with a rise of only about 1m per km (Figure II-3*b*) (Page *et al.*, 1999; Rieley & Page, 2005). Due to the smooth topography across distances of up to 40km, it is justified to interpolate this low number of ground echoes. The typical ground surface microtopography in peat swamp forests, a mosaic of hummocks and hollows, could not be resolved by the LiDAR frequency applied in this study.

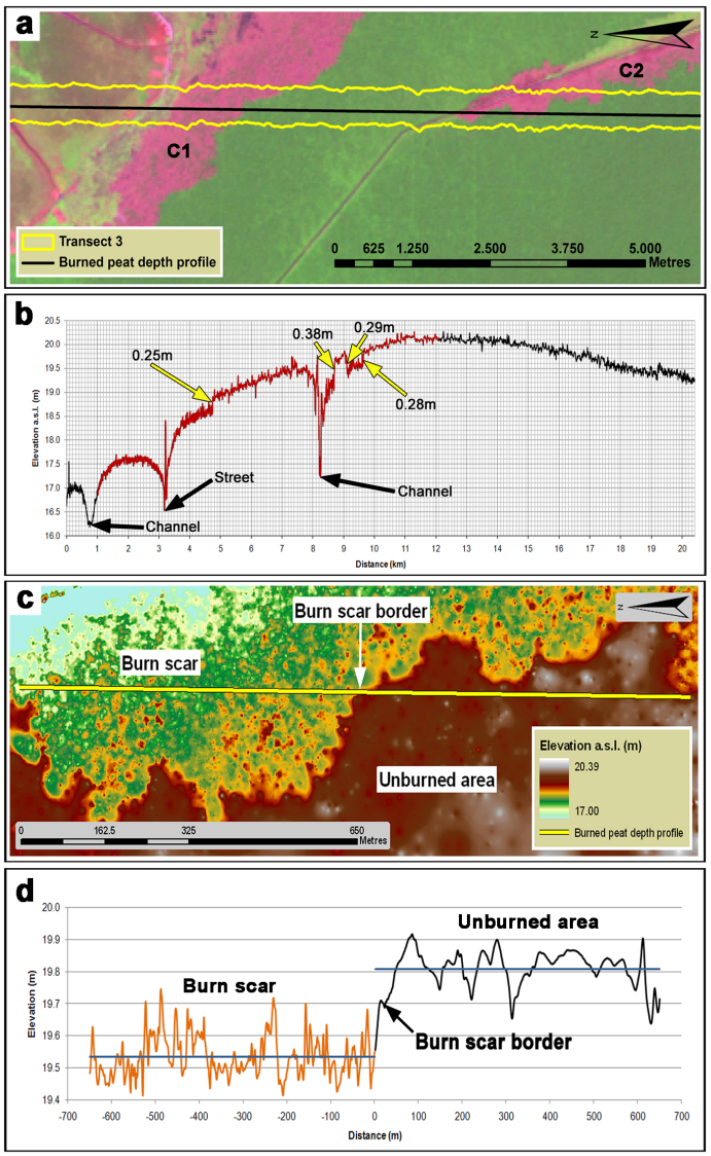

Figure II-3: Analysis of LiDAR Transect 3. (*a*) Subset from LiDAR Transect 3 (yellow outlines) covering two of the investigated burn scars (C1 and C2); the location of a burned peat depth profile is indicated by a black line. (*b*) Transect across a peat dome, note the curvature of the peat dome. The range covered by the subset shown in (b) is colored red. (*c*) DTM left burn scar and right unburned area; note the fire spread into the forest forming bud-like structures. (*d*) Burn scar depth was calculated by subtracting the mean of the burned peat depth profile of the burned area from the mean of the burned peat depth profile of the unburned area. The inclination due to the convex shape of the peat surface was excluded mathematically.

The elevation difference between unburned und burned peat was measured using height profiles of one meter width extracted from interpolated continuous DTM (Figure II-1*c* and Figure II-3) (see *Materials and Methods*). The height difference between burned and adjacent unburned peat swamp forest was calculated at 79 locations. However, not all reflected signals may have come from the true soil

surface, since fires often consume only part of the above ground biomass, leaving large quantities of wood debris and tree trunks scattered in the area (Figure II-4). To make sure that we did not include return signals from tree trunks and branches lying on top of the peat surface, we investigated the resulting burned depth if only 30% or 10% of the lowest values of the DTM were included in the calculation. The average standard deviation in all unburned height profiles was 0.037m and 0.036m for all burned profiles for the 10% lowest values. The average burn scar depth among all investigated burn scar borders was 0.30 ±0.15m based on 100% ground point values, 0.33 ±0.17m based on the 30% lowest values, and 0.33 ±0.18m based on the 10% lowest values. For all further calculations we used the 10% value because this was a reasonable tradeoff between a low standard deviation and a sufficiently high number of ground points for the determination of the burned depth. A low standard deviation indicates that possible returns from wood debris and regrowing vegetation are excluded.

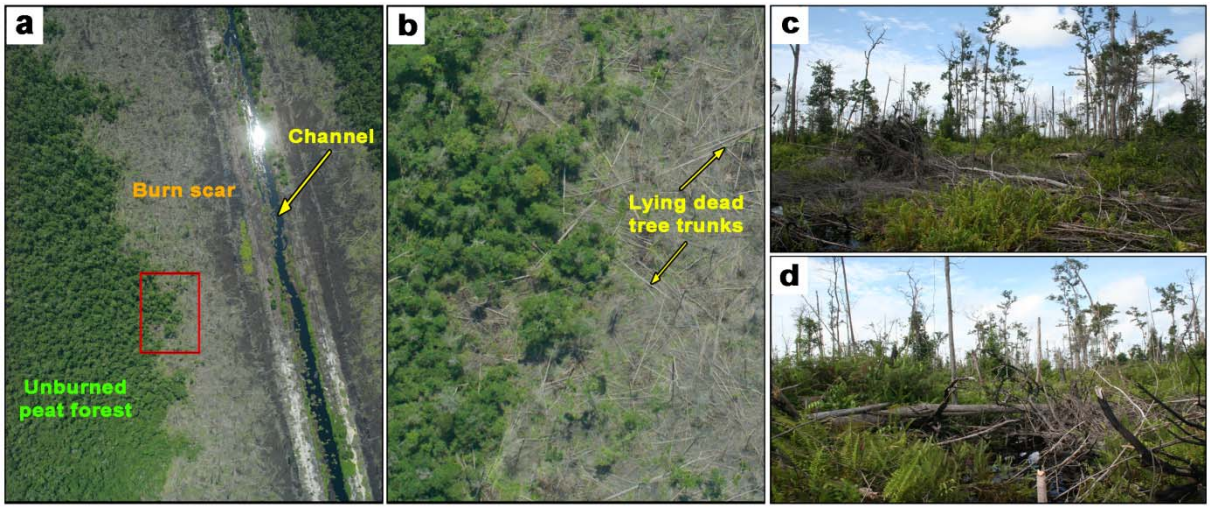

Figure II-4: Aerial and in situ photos of a part of the investigated burn scar C2. (*a*) Aerial photo of a part of the investigated burn scar C2 taken from a helicopter; visible is the burn scar, the unburned peat forest, and a drainage channel; the red rectangle indicates the location of (*b*). (*b*) Subset of (*a*) toppled over trees and dead tree trunks are scattered across the burn scar. (*c* and *d*) Photos taken on the ground within the investigated burn scar C2.

The height profiles across fire scars often showed a constant burned depth across large distances, although in some locations we observed depressions several meters wide and more than a meter deep. Because these measurements were made one year after the fires, it cannot be excluded that some of the peat loss is due to

bacterial oxidation and/or compaction. Since 2007 was an unusually wet year (La Niña following El Niño), we expect that the groundwater table was higher than in dry years, which would limit bacterial decomposition (Figure II-2, few fires). It was shown that bacterial decomposition causes up to 2cm of peat loss per year, which is a small fraction of the measured depth of fire scars (Wösten *et al.*, 1997).

Field data on burned depth collected during the 2006 El Niño fire event by the Centre for International Co-operation in Management of Tropical Peatland (CIMTROP) (Figure II-1*a*) confirmed the LiDAR measurements. Iron rods placed in front of the fire front showed that on average 0.30 ±0.13m (n = 40) of peat was combusted by fire (see *Materials and Methods*).

The amount of carbon released to the atmosphere was estimated by combining the average burned depth with published figures on peat carbon content. We assumed a smooth surface for the prefire peat dome across distances up to several kilometers, which justifies using an average burned depth of 0.33m to calculate the peat volume loss. The 3 burn scars (B1, C1, and C2) with a total area of 4,705ha were selected (Figure II-1*a*; Table II-1). Peat carbon content was calculated by applying a dry peat bulk density of 0.1 gram per cubic centimeter (g cm^{-3}) and a peat carbon content of 58% (Neuzil, 1997). Most of the carbon lost will be emitted as carbon dioxide, with additional emissions of carbon monoxide and methane (Muraleedharan *et al.*, 2000). We calculated carbon emissions of 0.50 ±0.27 mega tons (Mt) for burn scar B1, 0.23 ±0.13Mt for burn scar C1, and 0.17 ±0.09Mt for burn scar C2 (Table II-1). Based on a digital map of the study area showing burned peat forest from the year 2007, peat fires released 49.15 ±26.81Mt of carbon (Table II-1) (see *Materials and Methods*). This is equal to about 10-33% of all carbon emissions from transport (civil aviation, road transportation, railways, navigation, and other transportation) for the European Community in the year 2006 (http://unfccc.int/di/DetailedByParty/Event.do;jsessionid_4B56CEF8097A1587450FBB5AC8451F87.diprod02?event_go).

Table II-1: Different peat fire carbon emissions in Indonesia from the 2006 El Niño fire season.

	Specific burn scars in the study area			Study area	Indonesia
	Block B peat dome	Block C peat dome			
	B1	C1	C2		
Peatland area	283,800ha*	361,400ha*		1,651,805ha†	21,892,399ha†
Mean peat thickness	4.90 ±1.15m*	3.65 ±0.92m*		4.65 ±1.05m‡	4.5 ±0.85m*
Peat Volume	13.86 ±3.26 10^9m^3*	13.17 ±3.32 10^9m^3*		76.81 ±17.34 10^9m^3§	985.16 ±186.09 10^9m^3§
Carbon storage	0.80 ±0.19Gt*	0.76 ±0.19Gt*		4.45 ±1.01Gt‖	57.14 ±10.79Gt‖
Fire damaged peatland	2,632ha	1,209ha	864ha	256,783ha#	1,331,367haΔ
Per cent peatland damaged	0.9%	0.3%	0.2%	15.5%	6.1%
Peat volume loss	8.69 ±4.74 10^6m^3Ω	3.99 ±2.18 10^6m^3Ω	2.85 ±1.55 10^6m^3Ω	847.38 ±462.21 10^6m^3Ω	4.39 ±2.40 10^9 m^3Ω
Peat carbon loss	0.50 ±0.27Mt‖	0.23 ±0.13Mt‖	0.17 ±0.09Mt‖	49.15 ±26.81Mt‖	0.25 ±0.14Gt‖

* (Jaenicke *et al.*, 2008).
† (Wetlands International, 2003; 2004; 2006).
‡Average peat thickness of the three peat domes in Central Kalimantan (Block B, Block C, and Sebangau) modeled by Jaenicke *et al.* (2008).
§derived by multiplying peatland area and mean peat thickness.
‖Based on a peat bulk density of 0.1g cm^{-3} and a peat carbon content of 58% (0.58) (Neuzil, 1997).
¶Derived from visually digitizing the burn scars based on the Landsat ETM+ 7 image (118-62, 05 August 2007, gap filled) (see *Materials and Methods*).
#Derived from the object oriented classification of the Landsat ETM+ 7 image (118-62, 05 August 2007, gap filled) (see *Materials and Methods*).
ΔDerived from MODIS hotspot data of the year 2006 converted to fire affected areas minus a correction factor of 30% (see *Materials and Methods*).
ΩDerived from a burned peat depth of 0.33 ±0.18m based on this LiDAR study.

3 Discussion

The results presented here demonstrate that LiDAR has the ability to collect sufficiently accurate and spatially representative measurements of the burn scar depths in peat over large areas in very inaccessible terrain. The determined average burn depth of 33cm correlated well with field measurements recorded in the same year at locations near the LiDAR transects. The LiDAR measurements also showed that the surface of the peat dome is very smooth over many kilometers. This allowed us to reconstruct the prefire peat surface and thus to calculate the peat volume combusted by a fire. The relatively invariable burned depth and the low standard deviation of 0.18m across several kilometers indicate restrictions in fire behavior and impact. Fires never burned considerably deeper than 0.5m although extreme burned depths of up to 1.1m sometimes were observed. However, these extremes were small in scale and originated most probably from places where ignited tree trunks and roots facilitated oxygen supply and thus allowed the fire to propagate deeper into the peat layer. The consistent burned depth relates to the groundwater table in the peat layer, leading to a higher moisture content of the substrate with increasing depth. Additional factors may be important in regulating burned depth, for example, as fire progresses deeper a build-up of char and ash makes the peat less flammable and impedes the flow of oxygen. Usup *et al.* (2004) observed that the ignition temperature of peat in deep layers is higher than that of surface peat and that a change in fire behavior occurs between 0.20–0.40m below the surface in Central Kalimantan's peatlands. This LiDAR study also suggests that peat fires that burn

several meters below the surface (Goldammer, 1993), like fires observed in coal deposits, are extremely unlikely.

The available transects covered only fire scars in which peat fires burned into previously undisturbed peat swamp forest (78%, disturbed only by logging) or in 10-year-old regrowing peat swamp forest (16%). Evidence from aerial and field surveys suggest that fires in peat swamp forests burn deeper than fires on deforested peatland or peatland that has been previously affected by fire. Toppled over trees and exposed root systems in burned peat swamp forests are indicators of such fires. Deforested peatland is often covered by dense pockets of ferns and sedges through which the fire propagates quickly with little impact on the deeper peat layer. In addition, LiDAR measurements acquired in wet years are needed to be able to correlate burned depth to groundwater depth and land cover type.

During the last decade the global carbon dioxide concentration growth rate was 1.9ppm per year on average, resulting mainly from the emission of 7.2 giga tons (Gt) carbon per year due to the use of fossil fuel and approximately 1.6Gt carbon per year due to land use change (IPCC, 2007). With Indonesia's ranking as one of the world's biggest emitters of carbon (Hooijer *et al.*, 2006) and with a peat carbon store of about 57 ±11Gt (Wetlands International, 2003, 2004, 2006; Jaenicke *et al.*, 2008), it has an enormous potential to negatively influence the global climate if its peatlands are burned and drained at rates currently observed (Table II-1). To estimate Indonesia's contributions to global carbon emissions through peatland fires, we calculated the approximate emissions for Indonesia in 2006 based on (*a*) active fire recordings of the MODIS (Davies *et al.*, 2009), (*b*) a correction factor for the MODIS burned area determined from a correlation with Landsat-derived burned areas, (*c*) peatland maps of Indonesia (Wetlands International, 2003, 2004, 2006), and (*d*) the burned depth measurements described here. We are well aware that there is considerable uncertainty in this estimate due to a range of factors (e.g., MODIS burned area, extent of the peatland, burned depth in relation to water table, moisture conditions, emission factors), but this calculation may provide a reasonable estimate of the order of magnitude of this event. Peat fires in 2006 released about 0.25 ±0.14Gt (Table II-1) of carbon which is equal to 7–24% of all global emissions by land use change in that year (IPCC, 2007). Van der Werf *et al.* (2008) estimated that in 2006 0.30 ±0.12Gt of carbon were released by fires in Indonesia and Papua New Guinea,

however, this estimate also includes non-peat fires and above ground biomass burning.

In the past decade, severe peat fires have occurred almost every second year during El Niño induced droughts in 1997, 2002, 2004, 2006, and 2009 (Figure II-2). This is a new phenomenon and has not been observed in this frequency and spatial extent before. Undisturbed tropical peat swamp forests are, as the name suggests, just too wet to burn. Currently, this important source of carbon emissions is not yet included in the IPCC estimate for land cover change (IPCC, 2007) or in most regional and global carbon cycling models.

As most studies on land conversion and climate change consider only above ground biomass in forests this study shows that in the future, emissions from below ground biomass combustion should be included in the emission estimates. The carbon content of the peat layers depends on its thickness and can be up to 19 times higher than that of a pristine peat swamp forest growing on top of the peat (Jaenicke *et al.*, 2008). In addition, deforested and drained peatlands release considerable amounts of carbon due to bacterial oxidation (Hooijer *et al.*, 2009). These emissions are persistent for many years and add to the estimates given here.

The increased demand for palm oil, triggered by the biofuel boom, will seriously aggravate the situation since peatlands are the only remaining uninhabited near coastal land resource in Indonesia. The Clean Development Mechanism (CDM) and the proposed Reduced Emissions from Deforestation and Degradation in developing countries (REDD) schemes represent promising financial incentives to preserve the remaining tropical peat swamp forests and their huge underground carbon stock.

4 Materials and methods

4.1 Satellite data processing and classification

The 2.79 million ha study area is located in Central Kalimantan, Borneo, and covers a part of the former Mega Rice Project (MRP). The MRP, a failed transmigrasi resettlement project in Central Kalimantan, was initiated in 1995 by the Indonesian government and resulted in serious degradation of more than one million ha of peat swamp forest (Figure II-1*a*). The area was selected because (*a*) it contains one of the largest remaining undisturbed peat swamp forest ecosystems in Indonesia, (*b*) it is

under high pressure through the plantation business, and (*c*) severe peat fires were recorded there in 2006.

To obtain the fire history within the study area Landsat TM and ETM+ images (118–62) acquired between 1991–2007 were visually analyzed. The impact of fire and regrowth conditions in the 2006 fire scars was investigated on the ground in selected sites and in 86 aerial photos that were recorded using a Bell 206 helicopter between August 5–10, 2007, with a Hasselblad H3D-22 digital camera (50 millimeter (mm) lens) from an altitude of ±500m. All images were coregistered and projected to the World Geodetic System (WGS) 1984 Universal Transverse Mercator (UTM) zone 49 south.

Burned areas from the year 2006 were mapped at a 1:50.000 scale (minimum mapping unit 5ha) using an object oriented classification on the basis of a Landsat ETM+ 7 image (118–62, August 5, 2007, gap filled). Data from the MODIS was used to unambiguously discriminate burned areas from sparsely vegetated soils, which eventually have a similar spectral response as fire scars. The MODIS system detects active burning fires, so called hotspots, at a spatial resolution of 1km in tropical regions (Langner *et al.*, 2007; Davies *et al.*, 2009; Langner & Siegert, 2009). The classification accuracy was determined through visual on screen validation. The overall accuracy for the discrimination of burned and unburned vegetation was 89% with a kappa coefficient of 0.845.

The 3 investigated burn scars B1 (located in the Block B peat dome of the former MRP), C1 and C2 (located in the Block C peat dome of the former MRP) were visually digitized at a scale of 1:25,000 (minimal mapping unit 1ha) on the basis of the Landsat ETM+ 7 image (118–62, August 5, 2007, gap filled).

We analyzed MODIS data recorded by Fire Information for Resource Management System (FIRMS) (Davies *et al.*, 2009; http://maps.geog.umd.edu/firms/) to estimate the burned peat area for Indonesia. Previous studies showed that there is a reasonable correlation between burned areas deduced from MODIS hotspots and those derived from high resolution Landsat imagery, especially in peatlands, although a fire may cover the whole area of the sensor element (1 square km) or only a small fraction of it (Langner *et al.*, 2007; Miettinen *et al.*, 2007; Langner & Siegert, 2009). When using hotspots to determine burned areas, several constrictions have to be

kept in mind: (*a*) fires are only detected once or twice a day and thus rapidly spreading fires escape recording, (*b*) smoke from the fire often impedes the detection of hotspots, and (*c*) ground fires in tropical forests generally produce too little heat to be detected from space. (*a*) is irrelevant for peat fires, while (*b*) and (*c*) are relevant for peat fires. To convert hotspot data to fire affected areas, it was assumed that the area of each hotspot (1 square km) was completely affected by fire. Areas in which several hotspots were recorded were considered to have burned only once. A direct comparison of the burned area derived from MODIS hotspots with the object oriented classification result from Landsat within the study area showed that MODIS overestimated the burned area by 30% (Langner *et al.*, 2007; Miettinen *et al.*, 2007; Langner & Siegert, 2009) (Table II-1). When estimating the burned peat area for Indonesia, we discounted this factor.

The extent of peatland in Indonesia was determined from maps prepared by Wetlands International (Wetlands International, 2003, 2004, 2006). According to these maps, Indonesia has 21,892,399ha of peatland comprising approximately 11% of its land mass (Table II-1).

4.2 Light Detection and Ranging (LiDAR) data processing, filtering and Digital Terrain Model (DTM) generation

LiDAR is an active remote sensing technique which is based on the transmission of laser pulses toward the ground surface and the recording of the return signal. By analyzing the time delay for each pulse back to the sensor, the heights of all reflecting objects can be measured in the range of a few centimeters. The aircraft was equipped with an airborne global positioning system (GPS) to record the position of the sensor and an inertial measurement unit (IMU) to measure the angular orientation of the sensor with respect to the ground. To calculate absolute height values, the LiDAR system was calibrated with a ground based differential GPS. To further assure and verify the accuracy of the LiDAR data, a calibrated alignment process for the GPS position of the sensor and the orientation parameters was applied.

Small-footprint full waveform LiDAR data were collected using a Riegl LMS-Q560 Airborne Laser Scanner from an altitude of ±500m, over a scan angle of ±30° (swath

width ±500m). The laser pulse repetition rate was 66,000–100,000 pulses per second with a footprint of 0.25m and a wavelength of 1.5µm. Any echo, caused by multiple targets hit by a single laser shot, was received, digitized, time-stamped, compressed, and stored on the data recorder. Due to the accurate time stamping for each sample (109 samples per seconds), the 3D coordinates of the laser beam reflections, the intensity and the pulse width can be extracted by a waveform decomposition, which fits a series of Gaussian pulses to the waveform. To avoid noise and outliers only echoes with an intensity higher than 9 were used in this study. This resulted in an average of 1.4 echoes per square meter. Basically each reflection can be detected by the waveform decomposition and thus eliminates the dead zone effect. Conventional LiDAR systems (recording at most five reflections) can have a dead zone of up to 3m which makes these systems effectively blind after a reflection and thus impedes the discrimination of small height differences. The position and orientation of the system was measured in-flight using GPS and an IMU, with a stationary GPS located at the nearby airport of Palangka Raya for differential correction. The Riegl LMS-Q560 Airborne Laser Scanner system allows height measurements of ±0.02m. Single beam measurements have an absolute horizontal accuracy of ±0.50m and vertical accuracy of ±0.15m root mean square (*RMS*) error. Between 05–10 August 13,626ha of LiDAR measurements were recorded using a Bell 206 helicopter, of which 3,750ha were investigated in this study.

We applied a terrain-adaptive bare earth extraction algorithm to discriminate ground points from non-ground points reflected by the vegetation which is a utility integrated with Cloud Peaks software's LASEdit version 1.15.1 tool Surface Magic 2 (Figure II-1*b*). This algorithm provides unsupervised classification of non-ground features and adapts to the terrain condition. Furthermore, the ground points were visually searched to eliminate outliers. Off nadir locations with viewing angles larger than 20° showed little difference in the detected number of ground points.

Finally, the ground points were interpolated using a GIS inverse distance weighted (IDW) interpolation model (Figure II-1*c*). For the interpolation we used a cell size of 1 m, a variable search radius of 20 points, power 2 and no barriers. There was almost no difference between the interpolated DTM and the original ground point cloud. In transect 1 and 2 48% of the original ground return signals were below the interpolated DTM and 52% above with an average difference of -0.02 ±0.02m and

0.02 ±0.02m respectively. In transect 3 47% of the ground return signals were below the interpolated DTM and 53% above with an average difference of -0.01 ±0.02m and 0.01 ±0.01m respectively. We used the DTM instead of the original 3D point clouds because it facilitated all further data handling and analysis.

4.3 Burn scar depth analysis and in situ measurements

Height profiles (burned peat depth profiles) of one meter width were extracted from the DTMs stretching along the full length of the transects with a spacing of 25m to each other. All together, 41 profiles were analyzed: 15 for transect 1, each with 27,850m length, 13 for transect 2, each with 10,745m length, and 13 for transect 3, each with 20,400m length. The DTM profiles, the corresponding remote sensing images (aerial photos and Landsat images), and the digital burn scar map were exactly aligned to identify the boundary between burned and unburned peat (Figure II-3). 79 locations were assessed in detail to determine burned depth. The profiles were clipped to cover a distance of 1,000m within the burned area and 1,000m within the unburned area (Figure II-3*c* and *d*). If the extent of the burned and/or unburned area was smaller than 1,000m we clipped the maximum distance possible on both sides. Linear regression models were used to eliminate the inclination resulting from the convex shaped peat surface. To statistically analyze the reliability of the determined ground points and the interpolated DTMs we investigated the resulting burned depth if only the 30% or 10% of the lowest values from profiles were considered for the burned peat depth calculation. The average standard deviation in all unburned height profiles was 0.063m (100% ground point values), 0.040m (30% lowest values), and 0.037m (10% lowest values). The average standard deviations in all burned height profiles was 0.093m (100% ground point values), 0.043m (30% lowest values), and 0.036m (10% lowest values). Moreover, we statistically tested whether the mean of the unburned and burned surfaces differed significantly. If the values of the both height profiles were distributed normally a parametric T-Test was applied, if not a non-parametric Mann Whitney U-Test was applied. The level of significance (p) for 94 T-tests and 143 Mann Whitney U-tests with a confidence interval of 95% was calculated. All levels of significance were smaller than 0.001. It can be concluded that the differences in the means of the unburned and burned surfaces are highly significant and not random. In Transect 3 we additionally

compared burned depths derived from DTM profiles to 3D point clouds. The average difference of the burned depth was 0.01m based on 100% ground point values, -0.01m based on the 30% lowest values, and -0.01m based on the 10% lowest values.

In situ data of peat fire depth was collected in 2006 by the CIMTROP of the University of Palangka Raya. With the exception of the plots along the Sebangau River (10 measurements), all these measurements were situated on burn scars within Block C of the former MRP (Figure II-1*a*). This was done by inserting 40 iron rods in front of the fire. The surface of the peat layer before and after the fire was measured. The water table in the peat dome of Block C during the peat fires in 2006 that formed the burn scars C1and C2 was measured at 3 locations (2 in a burn scar from the year 2002 and 1 in an unburned peat forest). No water table measurements were available for Block B.

Acknowledgments

The authors would like to thank D. Davies (University of Maryland) who provided the MODIS hotspot data. Special thanks to J. Jauhianinen (KEYTROP project, Finland) and H. Takahashi for supplying groundwater data and V. Böhm (Kalteng Consultants, Germany) for conducting the LiDAR flight campaign. We also thank Wetlands International, Indonesia, for providing the peatland distribution maps. We gratefully acknowledge JP MORGAN for financial support.

CHAPTER III:
Pre-fire surface 3D modeling of tropical peatland burn scars based on airborne LiDAR in Central Kalimantan, Indonesia

Manuscript in preparation for *Global Change Biology*

Uwe Ballhorn[a,b], Juilson Jubanski[b], Florian Siegert[a,b]

[a]Biology Department II, GeoBio Center, Ludwig-Maximilians-University, Grosshaderner Strasse 2, D-82152 Planegg-Martinsried, Germany

[b]Remote Sensing Solutions GmbH, Isarstrasse 3, D-82065 Baierbrunn, Germany

Abstract

Indonesian peatlands store about 57 ±11 giga tons (Gt) of carbon and have enormous potential to negatively influence the global climate if they are drained and burned at rates currently observed. Since most peatlands in Indonesia are highly inaccessible very few field measurements on peat loss after fire exist. Peat loss after single and multiple fire events within a study area in Central Kalimantan (Indonesia) were estimated through 3D modeling of a pre-fire peat surface based on airborne Light Detection and Ranging (LiDAR) data. Since there were no historical burn depth field measurements and only mono-temporal LiDAR data available it was not possible to distinguish between peat subsidence caused by fire and peat subsidence caused by other processes within the investigated fire scars and to determine the difference of these subsidence processes between differing land covers. The results showed that after the first fire event peat loss with 0.37 ±0.22m was the highest, the second with 0.30 ±0.17m was less and the third with 0.11 ±0.25m was the lowest, so that no linear relationship was observed. Additionally the results indicated that there is a relation between the duration of the dry season and the mean peat loss. Based on object oriented fire scar classifications (derived from Landsat data) between the years 1990-2009 it was estimated that 61.361 mega tons (Mt) of peat carbon were emitted within the Kapuas district (1,489,325ha), Central Kalimantan (Indonesia). This is equal to about 25% of all carbon emissions from transport for the European Community in the year 2009. The presented approach could be used as an input to future Reduced Emissions from Deforestation and Degradation in developing countries (REDD+) projects which represent promising financial incentives to preserve the remaining tropical peat swamp forests.

Keywords: climate change; tropical peat; fires; Indonesia; remote sensing; carbon; LiDAR; 3D surface modeling; REDD+; green house gas emissions

1 Introduction

It is estimated that the total area of tropical peatland is in the range of 30-45 million hectares (ha), approximately 10-12% of the global peatland resource, and about 16.8-27.0 million ha are found in Indonesia (Immirzi *et al.*, 1992; Rieley *et al.*, 1996; Page & Banks, 2007; Page *et al.*, 2010). Tropical peatlands act as sinks and store huge amounts of carbon as peat consist of dead, incompletely decomposed plant material that has accumulated over thousands of years in waterlogged environments that lack oxygen, which makes them one of the largest near-surface pools of terrestrial organic carbon (Sorensen, 1993; Page & Rieley, 1998; IPCC, 2007). Typically tropical peatlands are located at low altitudes in alluvial floodplains where peat swamp forests form smooth convex shaped peat domes up to 20m thick (Anderson, 1983; Rieley *et al.*, 1996; Rieley & Page, 2005). Indonesian peatlands feature a characteristic micro-topography consisting of hummocks and hollows (Rieley & Page, 2005). Hummocks are up to 0.5m in height and are usually formed around tree bases and comprise of large proportion of both living and dead tree roots (Rieley & Page, 2005). These hummocks are interspersed with hollows of similar depth which form an interconnected network that carries water from the interior peat dome to its periphery (Rieley & Page, 2005). The ability of tropical peatlands to sequester and store these huge amounts of carbon is threatened by persistent anthropogenic impacts (Rieley & Page, 2005; Jaenicke *et al.*, 2008; Hooijer *et al.*, 2010). Especially drainage and forest clearance disturb their hydrological stability (Page & Rieley, 1998) and make these otherwise waterlogged ecosystems susceptible to fire (Langner *et al.*, 2007). After peatland drainage there are four largely irreversible processes that lead to a drop in peat surface level, called subsidence (Rieley & Page, 2005): (a) Consolidation is the compression of saturated peat due to increased ‘overburden’ (no peat matter is lost; increase of bulk density); (b) Shrinkage is the gradual volume reduction of peat in the unsaturated zone due to a loss of water from pores (no peat matter is lost; increase of bulk density); (c) Oxidation is the gradual volume reduction of peat in the unsaturated zone due to decomposition of organic matter; and (d) Fire which results in the complete loss of peat organic matter from the burned zone (carbon dioxide (CO_2) to a lesser degree carbon monoxide (CO), methane (CH_4), and other volatile organic compounds). Nearly all peatland fires are started by farmers to clear land and on a larger scale by

private companies as a cheap tool to clear forest before establishing oil palm and pulp wood plantations (ADB/BAPPENAS, 1999; Bompard & Guizol, 1999; Bowen *et al.*, 2000; Siegert *et al.*, 2001). Particularly acute is this problem on tropical peatlands in Indonesia, where recurrent peatland fires release huge amounts of carbon to the atmosphere (Page *et al.*, 2002; Ballhorn *et al.*, 2009; Langner & Siegert, 2009). This has increased interest in tropical peatlands in the context of global warming (Page *et al.*, 2002; Rieley & Page, 2005; Ballhorn *et al.*, 2009; Hooijer *et al.*, 2010).

It is important to know how much of the peat layer is consumed by a fire in order to quantify the role of peatland fires in the release of carbon. Most peatlands in Indonesia are highly inaccessible so that very few field measurements have been made to date, as this would require either knowing the fire affected area in advance or igniting peatland on a larger scale intentionally. Ballhorn *et al.* (2009) used airborne Light Detection and Ranging (LiDAR) data to overcome these problems and to obtain spatial measurements on peat burn depth across large fire scars in a study site in Central Kalimantan, Indonesia. LiDAR is based on the transmission of laser pulses towards the ground surface and the recording of the return signal. By analyzing the time delay for each pulse reflected back to the sensor, surface elevation can be determined with an accuracy of a few centimeters. The resulting three dimensional (3D) LiDAR point clouds are then differentiated into ground points and non-ground points mainly reflected from vegetation in forested areas. Finally the ground points are used to interpolate Digital Terrain Models (DTMs). Airborne LiDAR systems, of all remote sensing technologies, have shown to yield the most accurate estimates for land topography. Ballhorn *et al.* (2009) determined an average peat burn scar depth of 0.33 ±0.18m. Based on this result and the burned area determined from satellite imagery, they estimated that within the 2.79 million hectare study area 49.15 ±26.81 mega tons (Mt) of carbon were released during the 2006 El Niño episode which represents 10-33% of all carbon emissions from transport for the European Community for that year (Ballhorn *et al.* 2009). The increased demand for palm oil, triggered by the biofuel boom, seriously aggravates the situation since peatlands are the only remaining uninhabited near coastal land resource in Indonesia.

In the present study the same LiDAR data set used by Ballhorn *et al.* (2009) was processed. Ballhorn *et al.* (2009) calculated peat burn depth for single fire events

through determining the elevation difference of LiDAR derived DTMs at the border between burned and adjacent unburned peatlands. Other subsidence processes caused by consolidation, shrinkage, or decomposition played only a minor role, because the LiDAR data set was acquired shortly after the fire event. Here a different and advanced approach to estimate peat loss after not only single but also multiple fire events is introduced. Based on 3D modeling a pre-fire peat surface is reconstructed from which peat loss is then derived. In 1997, drainage channels were created which lead to the occurrence of huge fires and it is likely that the whole peatland area has undergone significant subsidence (Rieley & Page, 2005). Without repetitive field measurements, initiated before 1997, it is impossible to quantify the rates of the various subsidence processes (Figure III-1). The subsidence rate is a function of the original peat type (degree of maturation, mineral content), mechanical compaction, fire history, and most importantly water table level (Rieley & Page, 2005), as there is a clear relationship between the subsidence rate and water table level (Hooijer *et al.*, 2011). The pre-fire peat surface was modelled using anchor points to the left and right of each of the recorded fire scars, either in undisturbed reference areas or in areas which had burned once, twice and so forth (Figure III-1). The peat loss after single and multiple fire events was calculated by comparing the LiDAR derived DTM with the modelled pre-fire peat surface (Figure III-1). As mentioned above, it is likely that the whole hydrological system of the peat dome was affected by the extensive drainage network that caused overall peat dome subsidence. Most published studies analysing GHG emissions from drained tropical peatlands in Indonesia use gas chamber measurements and do not report on the corresponding subsidence rate of the peat surface (Hooijer *et al.*, 2006; 2009; 2010; Jauhiainen *et al.*, 2001; 2004; 2005; 2011). One exception is a publication by Wösten *et al.* (1997) showing that the average subsidence rate for a peatland area in Malaysia was 2cm of peat loss per year and 60% of the total subsidence originates from oxidation and 40% from shrinkage. Since in our study no historical burn depth field measurements and only mono-temporal LiDAR data was available it was impossible to distinguish between subsidence caused by fire and other subsidence processes (especially subsidence due to peat decomposition) within the investigated fire scars or to determine the difference of these subsidence processes between differing land covers (e.g. peat swamp forest, secondary forest, bushland, and fire scars). Due to this only peat loss after fire with the possibility of including other

subsidence processes could be estimated. As our results for single fire events agreed well with previous published results (Ballhorn *et al.*, 2009; Van der Werf *et al.*, 2010) and are in line with observations made during various field visits we believe that the approach presented here is a possible solution to determine the impact of single and multiple fire events on a peat dome with this limited data availability.

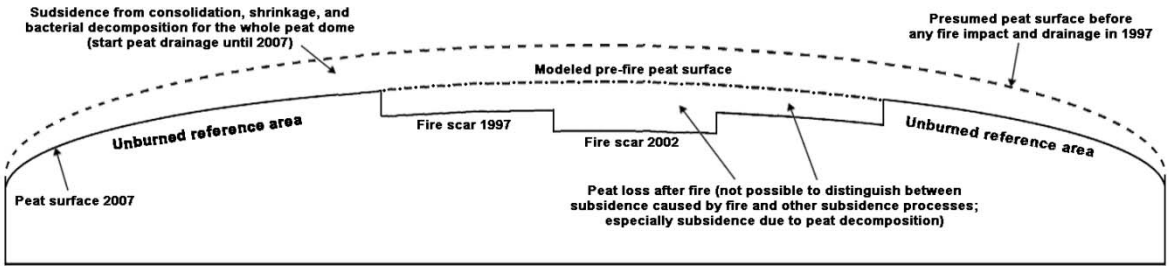

Figure III-1: Schematic overview of the main processes that lead to peat subsidence. The dashed line indicates the peat surface at the time when the peat dome was undisturbed and covered by pristine peat swamp forest. The solid line indicates the peat surface measured by LiDAR in 2007 (the LiDAR derived DTM). It is likely that the whole hydrological system of this peat dome was affected by the extensive drainage network that caused overall subsidence of it. The scale of subsidence is unknown due to the lack of historical field measurements. Also shown is the estimation of the pre-fire peat surface (dashed line with points), that was modeled based on reference areas.

Additionally the calculated peat loss was set in relation to in-situ water table measurements, burn frequency, the year of the fire occurrence, and the duration of the dry season to assess the influence of these factors.

To indicate the area of total fire impact further a historical analysis of peat fire occurrence and extent in the Kapuas district (1.49 million ha), also located in Central Kalimantan, was conducted. This was accomplished using a time series of Landsat images from 1990-2009. Based on the LiDAR peat loss calculations and the historical peat burn scar classification the peat volume lost and the corresponding carbon emitted within the Kapuas district were estimated.

2 Materials and methods

2.1 Study area

The island of Borneo lies in a region of constant rainfall and high temperatures throughout the year which are ideal conditions for plant growth. The major part of Borneo lies within Indonesia and is known as Kalimantan. 5.7 million ha or 27.8% of Indonesia's peatland resources are found in Kalimantan (Wetlands International, 2004). Peat depth varies from very shallow (less than 0.5m) to very deep peat with up to 12m (Wetlands International, 2004). The 62 investigated burn scars and the Kapuas district are located within Central Kalimantan (Figure III-2). All peat swamp forest ecosystems within Central Kalimantan have been severely impacted by extensive logging and drainage for more than two decades (Rieley & Page, 2005). The area also covers the former Mage Rice Project (MRP), an ill-fated transmigrasi resettlement project initiated in 1995 by the Indonesian government, which resulted in the serious degradation of more than one million ha of peat swamp forest (Rieley & Page, 2005).

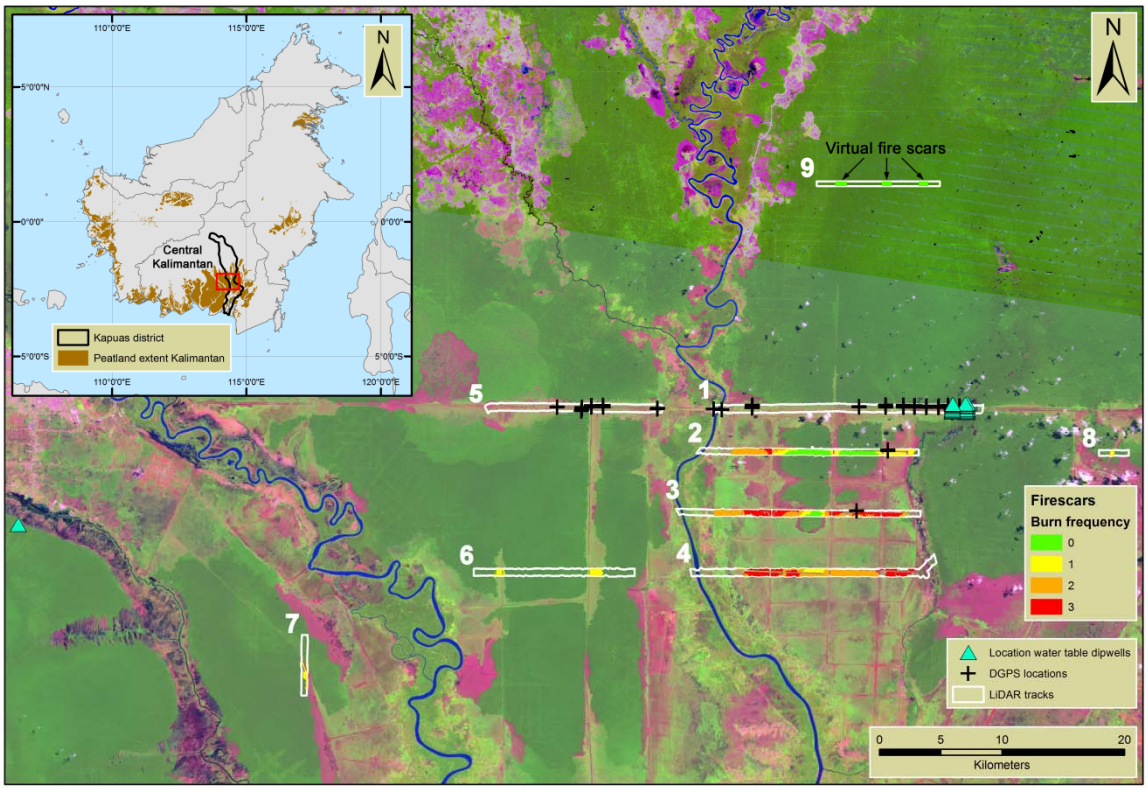

Figure III-2: Location of the LiDAR tracks (white outlines), 62 investigated peat fire scars, water table (turquoise triangles), and Differential Global Positioning System (DGPS) measurements (black crosses) superimposed on Landsat imagery (ETM+ 118-61, 2009-05-22 and ETM+ 118-62, 2007-08-05, bands 5-4-3, and both scenes gap filled). For validation purposes additionally 3 areas (virtual fires scars) within unburned pristine peat swamp forest were delineated. The Kapuas district (black outlines) within Central Kalimantan (Indonesia), the peatland extent (brown) within Kalimantan (derived from maps prepared by Wetlands International (2004), and the extent of the study area within Kalimantan (extent of the big figure, red rectangle) are shown in the smaller upper left figure.

2.2 Data

2.2.1 Airborne LiDAR data and digital photos

Airborne LiDAR data and digital photos were acquired during a flight campaign conducted between the 5th to 10th August 2007 (Ballhorn *et al.*, 2009). A Riegl LMS-Q560 Airborne Laser Scanner was mounted to a Bell 206 helicopter. This system allows height measurements of ±0.02m. Single beam measurements have an absolute horizontal accuracy of ±0.50m and a vertical accuracy of ±0.15m Root Mean Square Error (*RMSE*). The small-footprint full-waveform LiDAR data was collected from a flight altitude of ±500m above ground over a scan angle of ±30 degrees (swath width ±500m). This survey has an average of 1.4 points per square meter

(pt/m^2). 6,852ha of LiDAR data, composed of 9 tracks, were used in this study (Figure III-2). The aerial photos were recorded with a Hasselblad H3D-22 digital camera (focal distance of 50mm).

2.2.2 Landsat data

The dates of investigation were chosen according to the fire activity and Landsat imagery availability. The study is based on 49 high resolution Landsat images (39 Landsat ETM+, 10 Landsat-5 TM) acquired from 1991-2010. Scenes acquired during or shortly after the fire events (mostly during August to October) detect burn scars with higher confidence due to the fast regrowth of vegetation. Often images acquired directly after the fire season were too obstructed by clouds and therefore not available, so that images acquired before the next fire season of the following year were also analyzed. To determine the lengths of the individual fire seasons between 1997-2009 MODIS collection 5 hotspot data was used to identify suitable image acquisition dates.

2.2.3 MODIS hotspot, DGPS, water table, and rainfall data

The latest MODIS Collection 5 hotspot data for the study area was provided by the University of Maryland's Fire Information for Resource Management System (FIRMS) as ESRI point shapefiles for the time period from 1997 to 2009 (http://maps.geog.umd.edu/firms/). Each hotspot/active fire detection represents the center of a 1km^2 pixel flagged as containing at least one active fire (Davies *et al.*, 2009).

To assess the accuracy of the LiDAR derived DTMs points were measured with a Trimble 5700 Differential Global Positioning System (DGPS) device from May to August 2010. The locations of the 201 DGPS measurements overlapping the LiDAR tracks are shown in Figure III-2. For every DGPS measurement digital photos were taken in the field.

Water table data (cm below peat surface) for the years 1997 to 2007 were measured in dipwells at different locations (Figure III-2).

To assess rainfall patterns in the study area the Global Precipitation Climatology Project (GPCP) One – Degree Daily (1DD) data sets for the years 1997 to 2007 were downloaded from the KNMI (Koninklijk Nederlands Meterologisch Instituut) Climate Explorer Website (http://climexp.knmi.nl/start.cgi?someone@somewhere). The GPCP 1DD data set provides daily, global 1x1 degree gridded fields of precipitation (mm/day) for October 1996 to the present from currently available observational data (Huffman *et al.*, 2001).

2.3 Data analysis

2.3.1 LiDAR data filtering and interpolation of DTMs

The filtering of the LiDAR point clouds consisted in the separation between ground and off-ground points, since within the study area all off-ground points consisted of vegetation. The used filtering methodology was the hierarchic robust filtering. This algorithm is based on linear prediction with individual accuracies for each measurement and works iteratively (Pfeifer *et al.*, 2001). After the filtering process every track was examined further in small subsets to validate the results and manually delete outliers. The method used to generate the DTMs (1m resolution) was the linear adaptable prediction interpolation (Assmus, 1975; Wild, 1983; Kraus, 1998), which corresponds to the statistical estimation method kriging (Kraus, 1998). Both filtering and the interpolation were carried out with the Inpho software package (DTMaster and SCOP++).

In order to assure the accuracy of the LiDAR derived DTMs, 66 DGPS field measurements overlapping the LiDAR tracks were compared to the corresponding LiDAR derived DTMs.

2.3.2 Visual delineation of fire scars within the LiDAR tracks

First all historic fires and their spatial extent and distribution along the LiDAR tracks were visually digitized in a Geographical Information System (GIS). This historical fire scar analysis was based on Landsat satellite imagery acquired between 1990 and 2007. The results of the historical fire analysis are burned area maps for the investigated years indicating the extent of the burned areas along the LiDAR tracks.

In LiDAR track 9 no fires occurred in the past, but to validate the accuracy of the modeling method additionally three areas (virtual fire scars) were delineated within unburned peat swamp forest sites (Figure III-2).

2.3.3 LiDAR based pre-fire peat surface modeling

In order to mathematically define the pre-fire peat surface, a Bézier surface was calculated based on the LiDAR points within reference areas (Figure III-1). Bézier surfaces are popular and commonly used in practical works (Salomon, 2006). These surfaces are visually intuitive and mathematically convenient, since they permit one to define complex surfaces with a relatively small number of parameters. A Bézier surface is able to resume millions of LiDAR measurements in a small set of significant parameters that mathematically describe the surface, in this specific case, a peat dome. The Bézier surface is obtained by applying a Cartesian product to the Bézier equations of a Bézier curve, using the Bernstein binomial coefficients $B_{m,i}(x)$ and $B_{n,j}(y)$ (Salomon, 2006):

$$P(x,y) = \sum_{i=0}^{m}\sum_{j=0}^{n} B_{m.i}(x)P_{i,j}B_{n,j}(y) \qquad \text{(eq. III-1)}$$

Peat domes are relatively simple surfaces and have an especially smooth topography. The inland peat swamps of Central Kalimantan, for example, have an elevation rise of only about 1m per km (Page *et al.*, 1999; Rieley & Page, 2005). For this reason, we assumed that just one set of parameters is enough to define the peat surface. Usually, the polynomial order of a Bézier surface is defined by the number of points within the surface. In the case of modeling the pre-fire peat surface, an alternative approach is necessary, because it is mathematically and computationally impossible to solve polynomials with orders of up to millions. Engels (1986) presented a least squares method for estimation of Bézier curves and surfaces which overcomes this issue, and this approach was adapted to this study. Every LiDAR point P with height (z) is defined by an equation:

$$z = P(x,y) \qquad \text{(eq. III-2)}$$

Where $P(x,y)$ is the eq. III-1. Defining (x,y) as constants and z as variable, the Bernstein coefficients $B_{m,i}(x)$ and $B_{n,j}(y)$ become constant and just the polynomial

parameters $P_{i,j}$ must be determined. Denoting Z the vector with all z coordinates of the LiDAR points, W the weight matrix containing the inverse of the variances of the heights (obtained from the LiDAR precision) and A the matrix of the derivatives of the mathematical model (eq. III-1), the least squares solution becomes:

$$P_{ij} = (A^t W A)^{-1}(A^t W Z) \qquad \text{(eq. III-3)}$$

The interpolated surface is obtained by applying the adjusted parameters $P_{i,j}$ in eq. III-1, for all DTM points, generating a smooth raster that represents the pre-fire surface model (Figure III-5c).

For every of the LiDAR tracks 5 to 9 (in LiDAR track 9 three virtual fire scars for validation purpose where delineated) a pre-fire peat surface based on unburned reference areas was modeled (Figure III-2). For LiDAR tracks 1-4 on the other hand one pre-fire peat surface also covering the gaps between the four LiDAR tracks was modeled (Figure III-2). First profiles for the four LiDAR tracks based on the LiDAR derived DTMs were assessed to evaluate the limits of the peat dome. This data was used as constrains in the Bézier surface adjustment. Next based on the determined historical fire occurrence (see section *Visual delineation of fire scars*) a set of reference areas that best geometrically cover the study area were determined. From a strictly geometric point of view, the areas which burned twice were the best choice. The proposed solution is to reconstruct the peat dome based on these areas (‘degraded peat model’), and then, using the peat swamp forest islands as reference, to correct this model, reconstructing the pre-fire peat surface in this way. This was achieved by determining the differences between the ‘degraded peat model’ and the LiDAR ground points within the forest islands and performing an adjustment with a small degree polynomial surface.

Since subsidence is higher near channels (where peat is washed away and undergoes compaction and shrinkage more intensively), we excluded a 50m wide strip to both sides of drainage channels from the modeling process. Another reason to exclude these stripes was that in some areas there are significant mounds of excavated peat and sand material (berms) along the channels which are remnants from channel construction. The distance of 50m was decided on the basis of a careful analysis of the LiDAR track data, the fire scars, and the number of fire occurrences. The LiDAR derived DTM with 1m horizontal resolution provided detailed information on small scale topography near channels, such as berms (Figure III-3).

2.3.4 Peat loss calculation

We then calculated the peat loss for fire scars that burned once, twice, and three times (Figure III-2). This was done by generating 50 randomly distributed sample plots (10x10m) per ha inside the boundaries of these fire scars (Figure III-3). Here also no plots were generated within 50m distance to channels (see section *LiDAR based pre-fire peat surface modeling* and Figure III-3). For each of the sample plots the minimum, maximum, mean and the standard deviation of the normalized surface (z values of the modeled pre-fire peat surface were subtracted from the LiDAR derived DTMs) were extracted. This normalized surface constitutes the estimated peat loss at the specific locations. The final peat loss estimations after the different fire events were calculated by averaging plots with the same number of fire events. The peat loss for fire scars that burned more than three times was not calculated due to the geo-statistically (size and spatial distribution) not sufficient occurrence of them (Figure III-2).

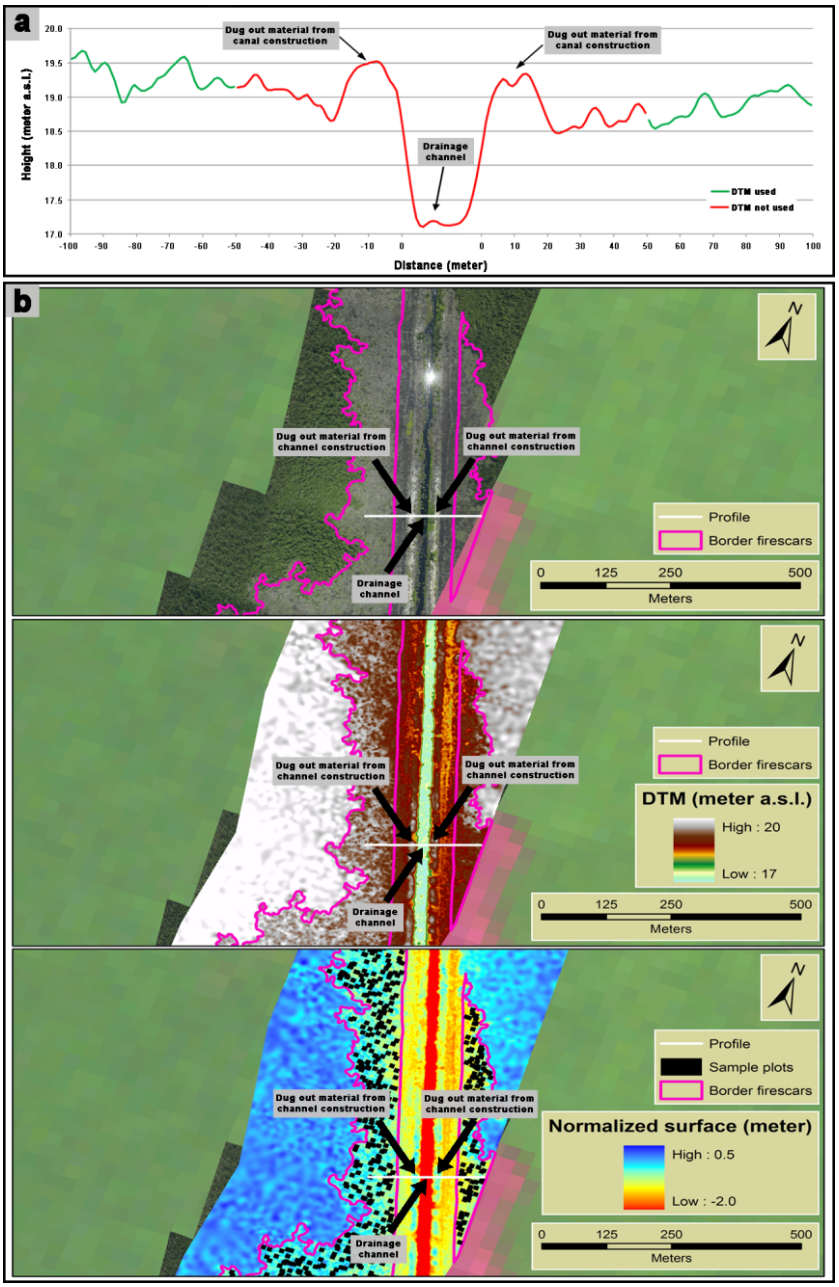

Figure III-3: Example of two fire scars along a channel in LiDAR track 7 (Figure III-2) that burned once. (a) Height profile through a drainage channel and the surrounding area based on a LiDAR derived DTM (white lines in b). Visible is excavated material left over from channel construction. (b) Aerial photos (upper image), the LiDAR derived DTM (middle image), and the normalized LiDAR derived DTM (on basis of the modeled pre-fire peat surface, lower image) superimposed on a Landsat image (ETM+ 118-62, 2007-08-05, bands 5-4-3, and gap filled). For the modeling of the pre-fire peat surface and the distribution of the 10x10m sample plots (black rectangles in the lower image) for the peat loss calculation a 50m wide impact zone on both sides of the channel was chosen were no data was used.

2.3.5 Relation of peat loss to burn frequency, water table measurements, and duration of dry season

The calculated peat loss was set in relation to water table measurements, burn frequency, the year of the fire occurrence, and the duration of the dry season to assess the influence of these factors.

A MODIS hotspot analysis was carried out to derive the dates of the different fire events within all fire scars. With these dates it was possible to relate peat loss after the different fire events to water table measurements.

Next a boxplot analysis war carried out to compare the peat loss of sample plots that never burned, burned once, twice, and three times.

Finally the peat loss of sample plots that burned once but in different years (1997, 2002, and 2006) were compared with boxplots. The duration of the dry season for these specific years (1997, 2002, and 2006) was also determined. The duration of the dry season for a specific year was defined as the longest continuity of days were the sum of the rainfall (mm/day) of the 30 previous days was less than 200mm. The rainfall in the study area was determined with the GPCP 1DD product (see Section *DGPS, water table, and rainfall data*).

2.3.6 Object-oriented historical fire scar classification within the Kapuas district

A Landsat object-oriented fire scar classification for the years 1990, 1997, 2001, 2002, 2004, 2005, 2006, and 2009 within the Kapuas district (Figure III-2) was carried out. The software used was eCognition Developer 8. To classify burned areas a method was developed based on the normalized burn ratio (Tansey *et al.*, 2008), an additional ratio based on Landsat bands 4 and 6, and on a Spectral Mixture Analysis (SMA) (Adams *et al.*, 1986; Tompkins *et al.*, 1997; Rashed *et al.*, 2003). A special type of SMA, the Mixture Tuned Matched Filtering (MTMF) was applied using ENVI/IDL (Boardman, 1998; Williams & Hunt, 2002). Each classification result was manually post-processed to eliminate misclassifications.

2.3.7 Estimation of peat volume loss and carbon emitted within the Kapuas district

The extent of peatlands within the Kapuas district was identified through a digital map prepared by Wetlands International (Wetlands International, 2004). With the help of the historical burned area maps (see section *Object-oriented historical fire scar classification within the Kapuas district)* the extent and the fire occurrence on peatlands was determined. The peat volume loss was estimated by multiplying the burned area extent with the obtained peat loss which is related to the fire occurrence at the respective location.

The amount of carbon emitted was estimated by combining the peat volume loss with published figures on peat carbon content. Peat carbon content was calculated by applying a dry peat bulk density of 0.1 gram per cubic centimeter (g/cm^3) and a peat carbon content of 58% (Neuzil, 1997).

3 Results

3.1 LiDAR derived DTMs

In order to assure the quality of the LiDAR derived DTMs, 66 of the originally 201 DGPS elevation measurements overlapping the LIDAR tracks (see section *DGPS, water table, and rainfall data* and Figure III-2) were correlated to the corresponding elevation of the interpolated LiDAR DTMs using an in house developed software. Only DGPS measurements lying within bushland or forest and outside the 50m buffer zone along the channels were used for comparison. Also DGPS measurements where the LiDAR point density was lower than $0.1pt/m^2$ and within new fire scars from 2009 were eliminated. With a coefficient of determination (R^2) of 0.94 and a *RMSE* of 0.33m good regression results were observed between the elevations of both data sets (Figure III-4a). In Figure III-4b it is noticeable that in areas with higher LiDAR point densities (as occurs in bushlands) the *RMSE* goes as low as 0.20m (with a very high R^2 value of 0.98). Whereas in areas of lower LiDAR point densities (as occurs in forested areas) lesser correlation is obtained (R^2 = 0.80, *RMSE* = 0.42m) (Figure III-4c).

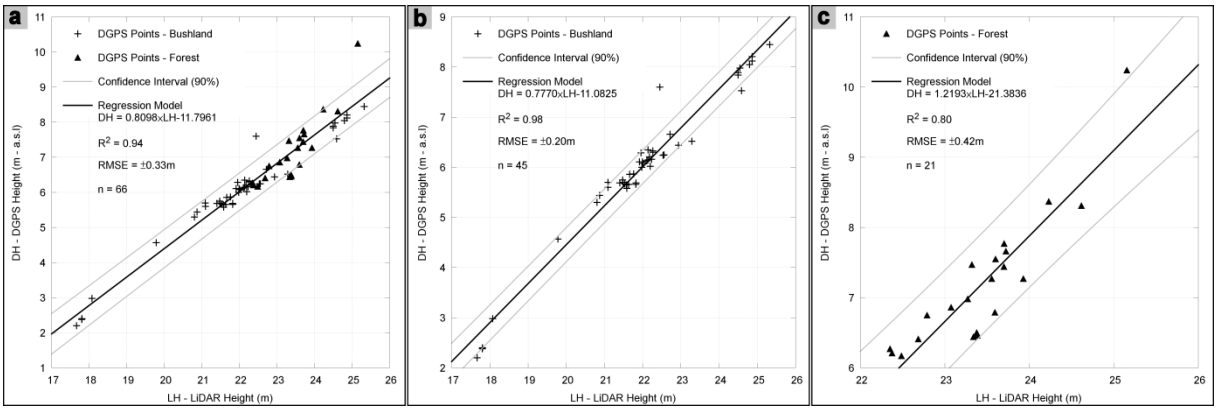

Figure III-4: Correlation of the LiDAR derived DTM heights and the DGPS heights collected in the field. (a) Regression model with all points. (b) Regression using just bushland points. (c) Regression using just forest points.

3.2 Modeled pre-fire peat surfaces

To validate the accuracy of the modeling method the elevation within the 10x10m sample plots of a modeled surface was compared to the LiDAR derived DTM elevation of three areas (virtual fire scars) within LiDAR track 9 located in unburned peat swamp forest (Figure III-2). There were very small mean elevation differences of -0.01-0.02 ±0.07-0.08m observed between the modeled surface and the LiDAR derived DTM (Table III-1).

Table III-1: Elevation differences between three modeled surfaces and the corresponding LiDAR derived DTM located in unburned peat swamp forest within LiDAR track 9 (virtual fire scars, Figure III-2).

Virtual fire scar nr.	Number of sample plots	Area virtual fire scars (ha)	Minimum (m)	Maximum (m)	Mean (m)	Standard deviation (m)
1	1,754	35	-0.22	0.21	-0.01	0.07
2	1.510	30	-0.28	0.23	-0.01	0.07
3	1,452	29	-0.24	0.26	0.02	0.08
Total	**4,716**	**94**	**-0.28**	**0.26**	**0.00**	**0.07**

Next for every of the LiDAR tracks 5 to 8 a pre-fire peat surface based on unburned reference areas was modeled (Figure III-2). For LiDAR tracks 1-4 on the other hand one pre-fire peat surface also covering the gaps between the four LiDAR tracks was modeled (Figure III-2). Figure III-5 illustrates the results of the pre-fire peat surface modeling process for LiDAR tracks 1-4. Figure III-5a exemplarily shows profiles along each of the 4 LiDAR tracks displaying the elevations of the LiDAR derived DTMs and the pre-fire peat surface. Also shown is the burn frequency along these profiles. In areas where it never burned the elevations of the pre-fire peat surface and of the

LiDAR derived DTM fall together (e.g. middle part of profile 2 in Figure III-5) and in areas where it burned, dependent on burn frequency, the difference between these two elevations is visible. In the west of the DTM profile 1 it is visible that the peat dome got heavily degraded, so that a reliable pre-fire peat surface was difficult to reconstruct. As a consequence no peat loss analysis of fire scars located in this area was carried out. Profiles 2-4 show the dome curvature reconstruction and that the peat dome begins on the west (by the Kapuas River) at an elevation of about 17.4m and ends on the east at the Mentangai River. In order to assure a higher reliability of the modeling outcome some reference areas have been set at these edges forcing the pre-fire peat surface to cross elevation at 17.4m in the west and the Mentangai River in the east. Figure III-5b displays the LiDAR derived DTMs and Figure III-5c the final pre-fire peat surface for these four LiDAR tracks.

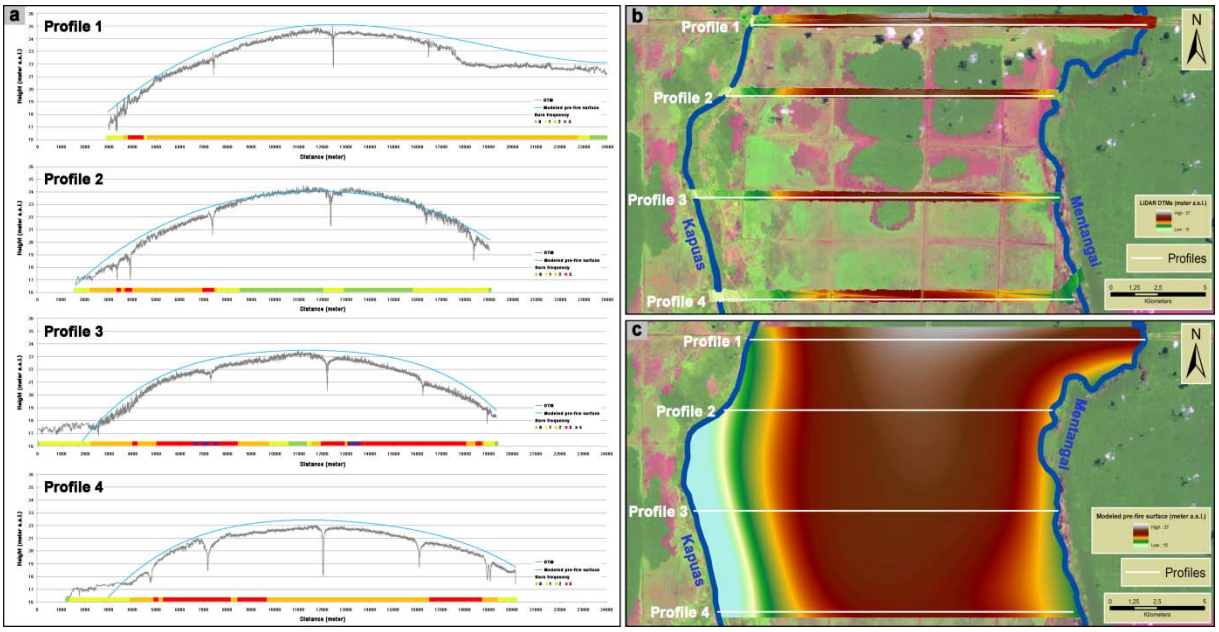

Figure III-5: Results of the pre-fire peat surface modeling for LiDAR tracks 1-4 (Figure III-2.). (a) Elevation Profiles 1-4 for LiDAR tracks 1-4. Shown are the elevations of the LiDAR derived DTMs (grey lines) and the modeled pre-fire peat surface (blue lines). Also shown is the burn frequency (red = high burn frequency, green = not burned) along these profiles. The white lines in b and c show the location of these profiles. (b) The LiDAR derived DTMs for LiDAR tracks 1-4 superimposed on a Landsat image (ETM+ 118-62, 2007-08-05, bands 5-4-3, and gap filled). (c) Final pre-fire peat surface based on LiDAR tracks 1-4 superimposed on a Landsat image (ETM+ 118-62, 2007-08-05, bands 5-4-3, and gap filled).

3.3 Peat loss

Figure III-6 shows a fire scar which burned once and twice. Cleary visible are the different depths for areas that never burned, burned once or twice of the LiDAR derived DTM in relation to the modeled pre-fire peat surface (Figure III-6a).

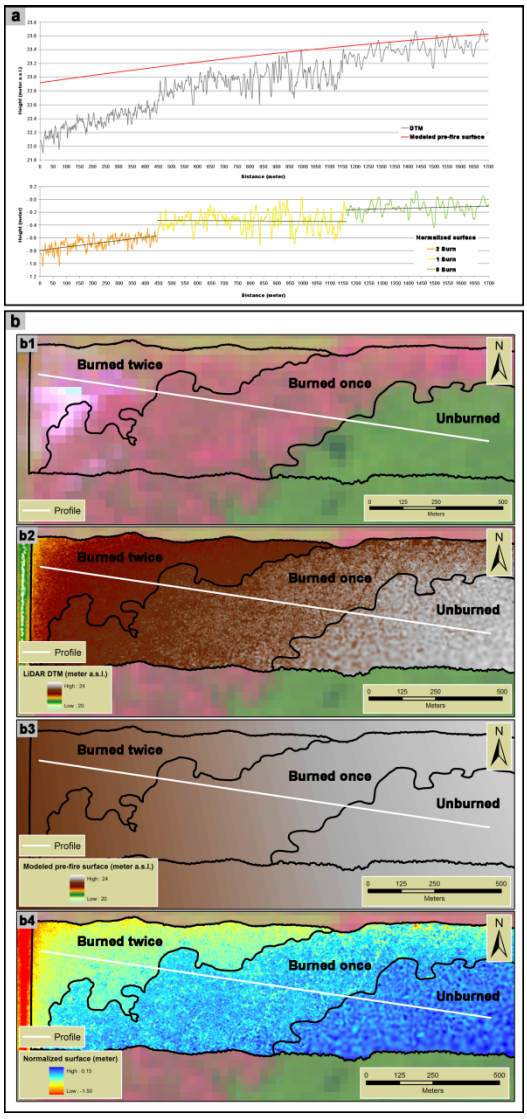

Figure III-6: Example of an area where it never burned, burned once and twice. (a) Upper profile displaying the elevation of the LiDAR derived DTM (black line) and the modeled pre-fire peat surface (red line). Lower profile illustrates the normalized surface (z values of the modeled pre-fire peat surface were subtracted from the LiDAR derived DTM) which constitutes the estimated peat loss depth. The black lines indicate the trend of the normalized surface for the areas where it never burned (green line), burned once (yellow line) and twice (orange line). The white lines in b show the location of the profiles. (b) Extent of an area which never burned, burned once and twice (b1), the LiDAR derived DTM (b2), the modeled pre-fire peat surface (b3), and the normalized surface (b4) superimposed on a Landsat image (ETM+ 118-62, 2007-08-05, bands 5-4-3, and gap filled).

All together 98,971 sample plots (10x10m) within 62 areas (see section *Visual delineation of fire scars within the LiDAR tracks*) were assessed. The average size of these areas was 32ha. 4 areas never burned, 17 areas burned once, 20 areas burned twice, and 21 areas burned three times. Table III-2 summaries the results of the peat loss calculations. The peat loss after every fire event is estimated by calculating the difference of the mean z value of the normalized surface to a previous fire event. Also given are the summed up peat losses for the different number of fires. Results show that peat loss after the first fire with a mean 0.37 ±0.22m is the highest, after the second fire with a mean of 0.30 ±0.17m is lower and after the third fire with a mean of 0.11 ±0.25m is the lowest.

Table III-2: Results of the peat loss calculations. Minimum, maximum, range, mean, and standard deviation of the normalized surface (z values of the modeled pre-fire peat surface were subtracted from the LiDAR derived DTM) based on the 10x10m sample plots for the different burn frequencies (0 = never burned, 1 = burned once, 2 = burned twice, and 3 = burned three times). Also given is the average peat loss after a fire event (estimates by calculating the difference of the mean z values of the normalized surface to a previous fire event) and the summed up peat losses.

Burn frequency	Number of fire scars	Number of sample plots	Area (ha)	Minimum (m)	Maximum (m)	Mean (m)	Standard deviation (m)	Peat loss (m)	
								Per fire event	Fire events summed
0	4	15,242	305	-0.91	0.76	0.02	0.19	0.00	0.00
1	17	20,848	419	-1.57	0.51	-0.34	0.22	0.37	0.37
2	20	34,741	695	-1.62	1.13	-0.65	0.17	0.30	0.67
3	21	28,140	563	-1.91	0.06	-0.76	0.25	0.11	0.78
Sum	**62**	**98,971**	**1,981**						

The accuracy of the pre-fire peat surface model for the LiDAR tracks 1-4 was also assessed by comparing elevations within the 10x10m sample plots of the modeled surface with the corresponding elevations of the LiDAR derived DTM elevation for the four areas that did not burn. The overall mean difference was with 0.02 ±0.19m very low (Table III-2).

3.4 Relation of peat loss to burn frequency, water table measurements, and duration of dry season

When correlating peat loss to water table measurements at the different dates of the fire events (see section *Relation of peat loss to burn frequency, water table*

measurements, and duration of dry season) all R^2 values were lower than 0.29, so that no statistical significant correlation could be identified.

Looking at the boxplots for the different burn frequencies (Figure III-7a) it is obvious that for every successive fire event the mean peat loss is less deep as the mean depth of the prior fire event (Figure III-7a). The range between both the maximum and minimum peat loss and the first and third quartile of the peat loss differ considerably from each other for the different fire events.

Only considering areas that burned once it is noticeable that for the year 1997 (0.57 ±0.09m) compared to the years 2002 (0.35 ±0.17m) and 2006 (0.33 ±0.23m) the mean peat loss is by far the deepest (Figure III-7b). The years 2002 and 2006 have similar average peat losses. Additionally plotting the duration of the dry season (as defined in section *Relation of peat loss to burn frequency, water table measurements, and duration of dry season*) into Figure III-7b shows that the year 1997 with 184 days had the longest dry season compared to 132 days for the year 2002 and 128 days for the year 2006. As in the case of the average peat loss here also the years 2002 and 2006 had similar long dry seasons.

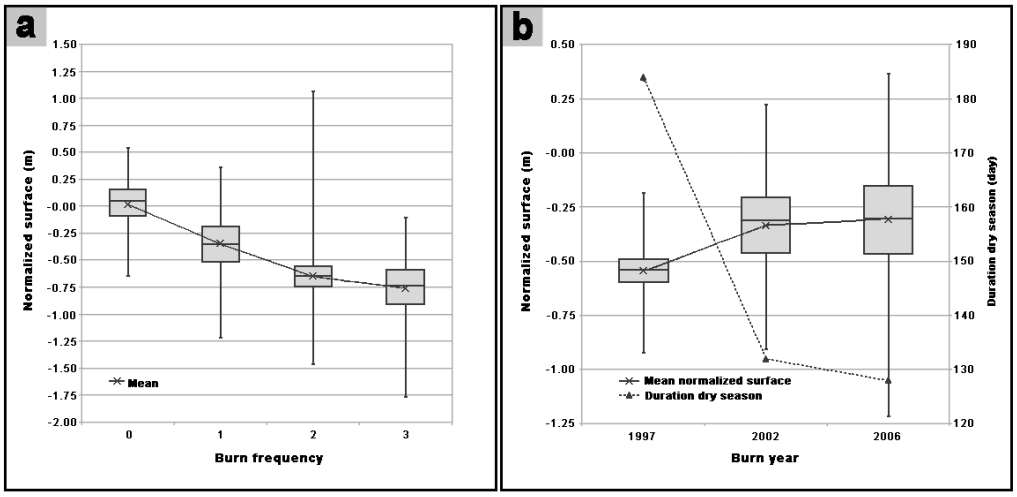

Figure III-7: Results of the boxplot analyses. (a) Boxplot analysis for burn frequencies (0 = never burned, 1 = burned once, 2 = burned twice, and 3 = burned three times). The normalized surface (z values of the modeled pre-fire peat surface were subtracted from the LiDAR derived DTM) is equal to the peat loss. A non linear trend is visible where the mean peat loss of a successive fire event is less deep than of the previous fire event. (b) Boxplot analysis of the burn year for sample plots that only burned once. Here the year 1997 had the highest peat loss (as in a the normalized surface is equal to the peat loss). Also shown is the duration of the dry season for these three years. The duration of the dry season for the year 1997 was the longest.

3.5 Historical fire scar classification, estimation of the peat volume loss, and carbon emitted within the Kapuas district

Figure III-8 displays an overview of the historical fire scar classification (between the years 1990-2009) on peatlands within the Kapuas district. It is clearly visible that by far most of the fire occurrences are near water drainage channels (Figure III-8). Fire scars that burned up to seven times were observed. Table III-3 gives the peatland area affected according to the different burn frequencies.

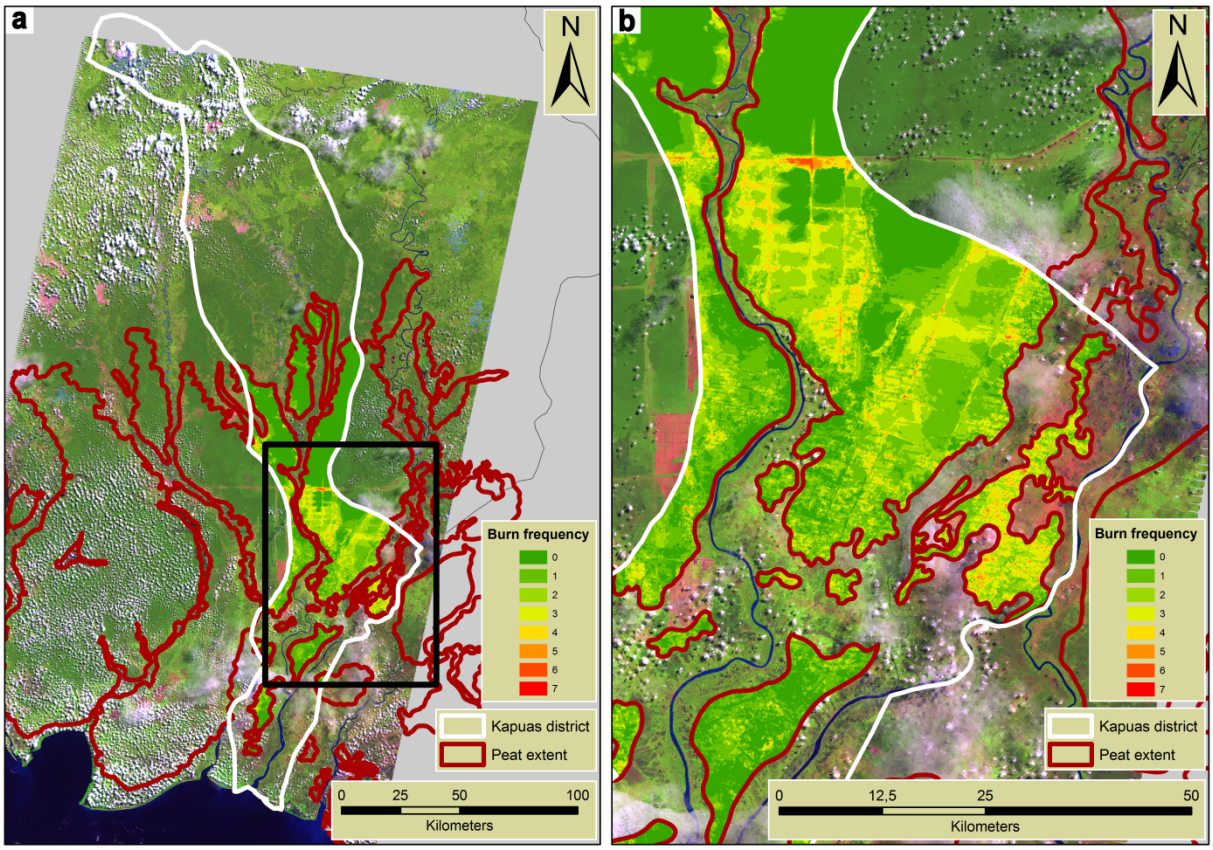

Figure III-8: Historical fire scar classification results for the years 1990 to 2009 on peatlands within the Kapuas district. (a) Historical fire scar classification results (with areas of up to seven fire events), the boundaries of the Kapuas district, and the peatland extent (derived from maps prepared by Wetlands International (2004) superimposed on Landsat imagery (ETM+ 118-61+62, 2009-05-22, bands 5-4-3, and both scenes gap filled). The black rectangle indicates the extent of b. (b) Enlarged detail from the central area of the Kapuas district also displaying the results of the historical fire scar classification. It is clearly visible that most of the fire occurrences are near the water drainage channels.

Based on the results of the peat loss calculations (see section *Peat loss*) and the historical fire scar classification the peat volume loss and the carbon emitted were estimated for the Kapuas district. As already mentioned above only peat loss of fire

scars burned up to three times were assessed, so that any additional fire was assumed to have the same peat loss as the third fire (0.11m). Based on these calculations about 61.361 mega tons (Mt) of carbon were emitted from fire scars within the Kapuas district between the years 1990 and 2009.

Table III-3: Results of the historical fire scar classification, estimation of the peat loss volume, and carbon emitted within the peatlands of the Kapuas district between the years 1990 and 2009.

Burn frequency	Area affected (ha)	Peat loss summed (m)	Peat loss volume (m^3)	Carbon released (Mt)
0	202,853	0.00	0	0.000
1	80,933	0.37	299,451,170	17.368
2	63,212	0.67	423,517,298	24.564
3	31,686	0.78	247,153,764	14.335
4	7,801	0.89	69,429,475	4.027
5	1,542	1.00	15,419,831	0.894
6	249	1.11	2,766,456	0.160
7	17	1.22	206,202	0.012
Sum	**388,293**		**1,057,944,196**	**61.361**

4 Discussion and conclusions

In 1997 an enormous system of drainage channels was created within the study area so that it is likely that the whole peatland has undergone significant other subsidence processes than those caused by fire (Rieley & Page, 2005). The subsidence rate is a function of the original peat type (degree of maturation, mineral content), mechanical compaction, fire history, and most importantly water table level (Rieley & Page, 2005), as there is a clear relationship between the subsidence rate and the water table level (Hooijer *et al.*, 2011). Most published figures on GHG emissions from drained tropical peatlands in Indonesia use gas chamber measurements and do not report on the corresponding subsidence rate of the peat surface (Hooijer *et al.*, 2006; 2009; 2010; Jauhiainen *et al.*, 2001; 2004; 2005; 2011). One exception is a study by Wösten *et al.* (1997) which shows that the average subsidence rate for a peatland area in Malysia was 2cm of peat per year and 60% of the total subsidence originates from oxidation and 40% from shrinkage. For our study no historical burn depth field measurements, initiated before 1997, and only mono-temporal LiDAR data was available. Due to these constraints (no historical in-situ measurements and no literature values on the various subsidence rates) we are aware that it is impossible to distinguish between subsidence caused by fire and other subsidence processes within the investigated fire scars or to determine the difference of these subsidence processes between differing land covers (e.g. peat swamp forest, secondary forest,

bushland, and fire scars). Because of this only peat loss after fire with the possibility of including other subsidence processes could be estimated. Our results for peat loss after single fire events agreed well with previous published peat fire depth calculations (Ballhorn *et al.*, 2009; Van der Werf *et al.*, 2010) and are in line with observations made during various field visits. One explanation for this good accordance is that other subsidence processes than fire have a similar impact outside and inside the fire scar so that the here measured peat loss might mostly originate from fire. In future the uncertainties described above could be better estimated and reduced once multi-temporal LiDAR data will be available (currently a new LiDAR campaign is conducted within the investigated area). By comparing the 2007 and the new LiDAR data sets, the results of this study could be re-evaluated and subsidence rates across the peatland and within different land covers or in proximity to channels could be spatially estimated in more detail. In our opinion however the approach presented here is a possible solution to determine the impact of single and multiple fire events on a peat dome with this limited data availability.

An accuracy assessment of the LiDAR derived DTMs through 66 DGPS elevation measurements resulted in overall good regression results (R^2 = 0.94, *RMSE* = 0.33m, Figure III-4a). It is also noticeable that in areas with higher LiDAR point densities (as occurs in bushlands) a R^2 value of 0.98 (*RMSE* = 0.20m) whereas in areas of lower point densities (as occurs in forested areas) a lesser R^2 value of 0.80 (*RMSE* = 0.42m) was obtained (Figs. 4b and 4c). The LiDAR derived DTMs stem from a large number of filtered LiDAR ground return signals (several million) and the DGPS measurements are point measurements. A statistical analysis of the LiDAR signals reflected from the peat surface showed that in unburned peat forests about 1% of the points were reflected from the ground surface and in burn scars about 6% of the points were reflected. Nevertheless, peat swamp forests are much less dense than tropical lowland rainforests, so that more LiDAR signals are returned from the ground. As there are far too few LiDAR ground returns it is impossible to correctly map the typical micro-topography of hummocks and hollows as observed in Indonesian peatlands (Rieley & Page, 2005). The observed texture in the LiDAR derived DTMs is related to large scale undulations of the terrain and the random representation of signals from hummocks and hollows (Figures III-5b and III-6b2). The results from the accuracy assessment above prove the quality of the LiDAR

derived DTMs and that the elevation differences of the two data sets are related to the natural micro-topography and not to the quality of the LiDAR filtering process. However it is justified to interpolate this low number of ground echoes, as the peatlands of Central Kalimantan are flat with a rise of only about 1m per km (Page *et al.*, 1999; Rieley & Page, 2005) and have a smooth topography across distances of up to 40km. It should be added that a 4 year gap between the different acquisition dates of the two data sets can also lead to differences in elevation due to related subsidence processes.

The small mean elevation differences of -0.01-0.02 ±0.07-0.19m between the modeled pre-fire surface and the LiDAR derived DTMs in unburned areas (Tables III-1 and III-2) demonstrated that the applied modeling approach accurately estimated pre-fire peat surface elevation.

The peat loss calculations showed that after the first fire event the mean peat loss with 0.37 ±0.22m was the highest, after the second fire with 0.30 ±0.17m was less high, and after the third fire with 0.11 ±0.25m was the lowest (Table III-1 and Figure III-7a), so that no linear relationship was observed. These results agree with evidence from aerial and field surveys suggesting that fires in peat swamp forests burn deeper into the peat layer than fires on areas previously affected by fire. Dense pockets of ferns and sedges through which fire propagates quickly, with little impact on the deeper peat layer, often cover these deforested peatlands.

Due to the geo-statistically (size and spatial distribution) not sufficient occurrence of areas that burned more than three times no peat loss calculations were carried out for these areas (Figure III-2). For future research it would be of interest how high the mean peat loss after the third fire event would be. Does the mean peat loss stabilize at a certain level or does it become less and less after every successive fire event? How important is the fuel loads on top of the peatland for the mean peat loss? In future these research questions could be answered in more detail once the multi-temporal LiDAR data will be available.

The results for the mean peat loss for the first fire event (0.37 ±0.22m) is higher compared to studies on peat burn depth by Ballhorn *et al.* (2009) (0.33 ±0.18m) and Van der Werf *et al.* (2010) (0.30 ±0.08m). Also field data on burn depth collected during the 2006 El Niño fire event, through placing iron rods in front of the fire front,

by the Centre for International Co-operation in Management of Tropical Peatlands (CIMTROP) showed a lower mean peat burn depth (0.30 ±0.13m, n = 40). Comparing the mean peat loss separately for these years (1997 = 0.57 ±0.09m; 2002 = 0.35 ±0.17m; 2006 = 0.33 ±0.23m) it is obvious that the year 1997 had by far the highest peat loss (Figure III-7b). Additionally comparing the duration of the dry season for these three years the year 1997 with 184 days also had the longest dry season. This results indicate that there is a relation between the duration of the dry season and the mean peat loss.

When correlating peat loss after different fire events to water table measurements all R^2 values were lower than 0.29. This shows that no statistical significant correlation could be identified here. One explanation for this unexpected weak correlation could be that the in-situ water table measurements were collected at sites far away from the investigated fire scars, so that they might not be a good enough representation of the hydrological conditions at the fire scars during the specific fire events. To investigate the relation between peat loss and water table level more accurately in future it would be necessary to collect water table measurements near burning peat fires.

Based on the historical fire scar classification and the peat loss identified 61.361Mt of carbon were emitted within the Kapuas district (1,489,325ha) between the years 1990-2009. This is equal to about 25% of all carbon emissions from transport (civil aviation, road transportation, railways, navigation, and other transportation) for the European Community in the year 2009 (http://unfccc.int/di/DetailedByParty/Event.do;jsessionid_4B56CEF8097A1587450FBB5AC8451F87.diprod02?event_go). This high number once more demonstrates the possible impact of tropical peat fires on the global climate and the necessity to accurately determine peat loss after fires to get better estimates on carbon emissions. Currently, this important source of carbon emissions is not yet included in the IPCC estimate for land cover change (IPCC, 2007) or in most regional and global carbon cycling models.

The results of our study demonstrates the usefulness and robustness of LiDAR data to be used as input to model pre-fire peat surfaces from which it is then possible to calculate peat loss after not only single but also multiple fire events. This is a significant advance to the method used by Ballhorn *et al.* (2009), as they only

investigated fire scars which burned once. Additionally only peat fires within previously undisturbed peat swamp forest (78%, disturbed only by logging) or 10-year-old regrowing peat swamp forest (16%) were analyzed. When combining the determined peat loss with fire scar classifications from other remote sensing sources (optical and/or RADAR satellite imagery) this approach will help to better estimate the amount and spatial distribution of disturbed peatland carbon emission. Additional this method could be used as an input tool to future Reduced Emissions from Deforestation and Degradation in developing countries (REDD+) projects which represent promising financial incentives to preserve the remaining tropical peat swamp forests.

Acknowledgements

The authors would like to thank H. Takahashi and the Central Kalimantan Peat Project (CKPP) project for the water table data, D. Davis (University of Maryland) who provided the MODIS hotspot data, and Koninklijk Nederlands Meterologisch Instituut (KNMI) for supplying the Global Precipitation Climatology Project (GPCP) One –Degree Daily (1DD) data sets. Special thanks to Suwido Limin and his team from the Centre for International Co-operation in Management of Tropical Peatland (CIMTROP) in Palagka Raya for the peat burn depth measurements in the field. We also thank Wetlands International, Indonesia, for providing the peatland distribution maps. The LiDAR data set was acquired by Kalteng Consultans.

CHAPTER IV:
ICESat/GLAS data as a measurement tool for peatland topography and peat swamp forest biomass in Kalimantan, Indonesia

Remote Sensing, **3**, 1957-1982

Uwe Ballhorn[a,b], Juilson Jubanski[b], Florian Siegert[a,b]

[a]Biology Department II, GeoBio Center, Ludwig-Maximilians-University, Grosshaderner Strasse 2, D-82152 Planegg-Martinsried, Germany

[b]Remote Sensing Solutions GmbH, Isarstrasse 3, D-82065 Baierbrunn, Germany

doi: 10.3390/rs3091957
Received 21st July 2011; in revised form 22nd August 2011
Accepted 26th August 2011

Abstract

Indonesian peatlands are one of the largest near-surface pools of terrestrial organic carbon. Persistent logging, drainage and recurrent fires lead to huge emission of carbon each year. Since tropical peatlands are highly inaccessible, few measurements on peat depth and forest biomass are available. We assessed the applicability of quality filtered ICESat/GLAS (a spaceborne LiDAR system) data to measure peatland topography as a proxy for peat volume and to estimate peat swamp forest Above Ground Biomass (AGB) in a thoroughly investigated study site in Central Kalimantan, Indonesia. Mean Shuttle Radar Topography Mission (SRTM) elevation was correlated to the corresponding ICESat/GLAS elevation. The best results were obtained from the waveform centroid (R^2 = 0.92; n = 4,186). ICESat/GLAS terrain elevation was correlated to three 3D peatland elevation models derived from SRTM data (R^2 = 0.90; overall difference = −1.0m, ±3.2m; n = 4,045). Based on the correlation of *in situ* peat swamp forest AGB and airborne LiDAR data (R^2 = 0.75, n = 36) an ICESat/GLAS AGB prediction model was developed (R^2 = 0.61, n = 35). These results demonstrate that ICESat/GLAS data can be used to measure peat topography and to collect large numbers of forest biomass samples in remote and highly inaccessible peatland forests.

Keywords: ICESat/GLAS; LiDAR; SRTM; tropical peatlands; carbon; above ground biomass; peat swamp forest; Indonesia

1 Introduction

Peatlands store huge amounts of carbon as peat consists of dead, incompletely decomposed plant material that has accumulated over thousands of years in waterlogged environments that lack oxygen. In the tropics, peatland is usually covered by forests and current estimates indicate that the total area of tropical peatland is in the range of 30–45 million ha (approximately 10–12% of the total global peatland resource); about 16.8–27.0 million ha are found in Indonesia (Page *et al.*, 2010). This is one of the largest near-surface pools of terrestrial organic carbon (Sorensen, 1993; Page & Rieley, 1998; IPCC, 2007; Page *et al.*, 2010). Peat swamp forests have a wealth of ecological and hydrological functions such as water retention, flood reduction, protection against seawater intrusion, support of high levels of endemism, and finally as a retreat for endangered species such as the Bornean Orangutan (*Pongo pygmaeus*). Tropical peat typically accumulates in alluvial floodplains where peat swamp forests, over thousands of years, formed convex shaped peat domes up to 20m thick (Anderson, 1983; Rieley *et al.*, 1996; Page *et al.*, 2004; Rieley & Page, 2005). Persistent anthropogenic impacts by logging and drainage diminish their ability to sequester carbon and conversion to plantations and recurrent uncontrolled fire release huge amounts of carbon dioxide each year (Rieley & Page, 2005; Jaenicke *et al.*, 2008; Hooijer *et al.*, 2010). In particular drainage and forest clearance disturb the hydrological stability (Page & Rieley, 1998) and make these otherwise waterlogged ecosystems susceptible to fire (Langner *et al.*, 2007). Usually peatland fires are started by farmers to clear land and on a larger scale by private companies as a cheap tool to clear forest before establishing oil palm and pulp wood plantations (ADB, 1999; Bompard & Guizol 1999; Bowen *et al.*, 2000; Siegert *et al.*, 2001). Fire is particularly acute in Indonesia, where recurrent fires release large amounts of carbon dioxide to the atmosphere (Page *et al.*, 2002; Ballhorn *et al.*, 2009; Langner & Siegert, 2009). This has increased interest in tropical peatlands in the context of global warming (Page *et al.*, 2002; Rieley & Page, 2005; Ballhorn *et al.*, 2009; Hooijer *et al.*, 2010).

To measure the carbon content it is necessary to determine the carbon density of the peat and the peat volume. Peat thickness is usually measured by using manually operated peat corers at intervals of 500–2,000m. Since most peatlands in Indonesia are highly inaccessible, very few field measurements have been made to date. To

overcome these constraints, Jaenicke *et al.* (2008) applied 3D modeling based on the combined analysis of earth observation data and *in situ* peat thickness measurements. They demonstrated that Shuttle Radar Topography Mission (SRTM) data can be used to determine the extent and topography of the dome shaped surface and correlation was obtained between the convex peat dome surface and the depth of the underlying mineral ground, which was determined by manually operated peat corers in the field. These results were then used to calculate the peat volume and carbon store. The main problem of this approach was the determination of the vegetation height growing on peat domes as the SRTM C-band sensor does not penetrate dense and tall vegetation cover straight to the soil surface.

One way to overcome this problem may be the use of aerial Light Detection and Ranging (LiDAR). LiDAR is based on the transmission of laser pulses toward the ground surface and the recording of the return signal. By analyzing the time delay for each pulse reflected back to the sensor, surface elevation can be determined with an accuracy of a few centimeters. The resulting three dimensional LiDAR point clouds (x, y, and z coordinates) are differentiated into ground points, points reflected from the terrain, and non-ground points mainly reflected from the vegetation in forested regions. The ground points are then used to generate Digital Terrain Models (DTMs). Aerial LiDAR systems (discrete return and full waveform), compared to other remote sensing technologies, have been shown to yield the most accurate estimates for land topography, forest structural properties, and forest Above Ground Biomass (AGB). On the other hand systems operated from airplanes have limitations due to large data volumes and high costs (Ranson *et al.*, 2007).

The GeoScience Laser Altimeter System (GLAS) onboard NASA's Ice, Cloud, and land Elevation Satellite (ICESat) mission is the first spaceborne LiDAR system capable of providing global datasets of the earth's topography (Schutz *et al.*, 2005). ICESat/GLAS data have been demonstrated to accurately estimate forest structural properties especially well in topographically even areas with uniform forest cover (Harding & Carajabal, 2005; Lefsky *et al.*, 2007; Baccini *et al.*, 2008; Boudreau *et al.*, 2008, Rosette *et al.*, 2008; Sun *et al.*, 2008; Goetz *et al.*, 2010; Lefsky, 2010; Dolan *et al.*, 2011). In areas of moderate to high relief the results show lower reliability (Harding & Carajabal, 2005).

Peatlands have an especially smooth topography. The inland peat swamps of Central Kalimantan (Indonesia), for example, have an elevation rise of only about 1m per km (Page *et al.*, 1999; Rieley & Page, 2005). Therefore ICESat/GLAS data might be an adequate tool to measure the topography of the peat soil and the forest AGB. On the other hand, based on the authors' airborne LiDAR data estimates (see section IV-2.3.1), the canopy coverage can be higher than 95%, depending on the peat swamp forest subtype and previous logging impacts.

In order to assess the applicability of ICESat/GLAS, the following questions were proposed: (1) Is ICESat/GLAS capable of penetrating the dense peat swamp forest cover and to measure the peat surface topography? (2) How accurate is the SRTM digital elevation model in comparison to ICESat/GLAS measurements on peatlands? (3) How accurate are 3D peatland elevation models derived from SRTM data? (4) How accurate are ICESat/GLAS measurements of peat swamp forest canopy heights compared to airborne LiDAR measurements? (5) Is it possible to derive a peat swamp forest AGB prediction model from ICESat/GLAS data based on airborne LiDAR and forest inventory data?

2 Methodology

2.1 Study area

Borneo is the third largest island in the world and the largest land mass in the Sundaic area. The island lies in a region (between latitudes 7°N and 4°S) of constant rainfall and high temperatures throughout the year which are ideal conditions for plant growth. Forest types include mangrove forests, peat swamp and freshwater swamp forests, the most extensive extent of heath forests (*kerangas*) in Southeast Asia, lowland dipterocarp forests, ironwood (*ulin*) forests, forests on limestone and ultrabasic soils, hill dipterocarp forests and various montane formations (MacKinnon *et al.*, 1996). The major part of Borneo (539,460km^2 or 73%) lies within Indonesian territory and is known as Kalimantan; the rest of the island consists of the states of Sarawak and Sabah (together forming East Malaysia) and the independent sultanate of Brunei Darussalam (Figure IV-1(A)).

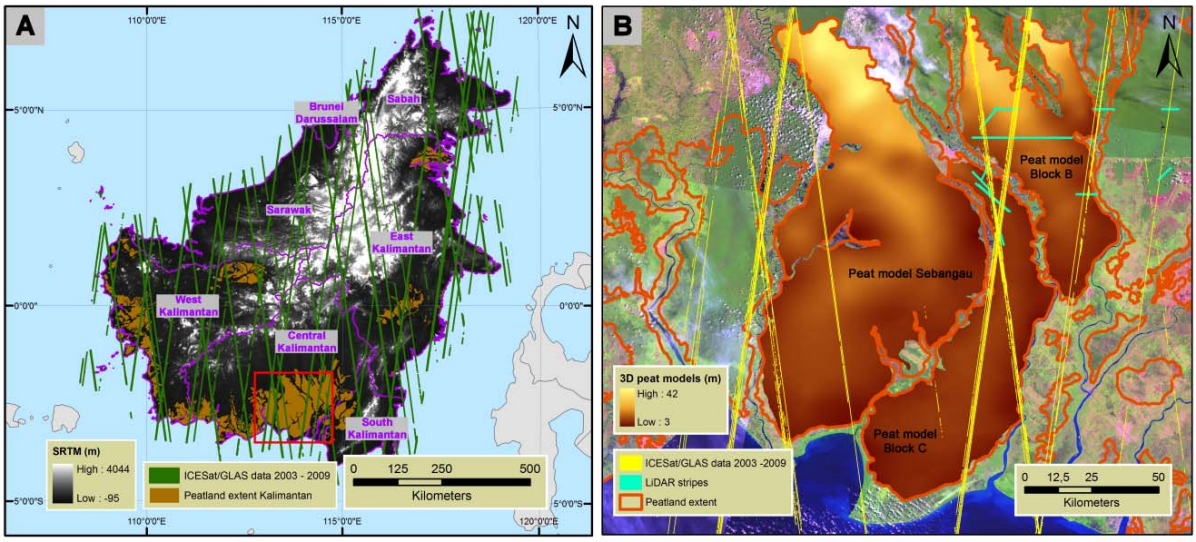

Figure IV-1: Overview of the study area: **(A)**: The island of Borneo and the peatland extent within Kalimantan, Indonesia, derived from maps prepared by Wetland International (2004). Shown are the ICESat/GLAS transects from the years 2003 to 2009, which were used in this study (shots with incorrect elevation flags were filtered out), superimposed on Shuttle Radar Topography Mission (SRTM) data; **(B)**: Location of the investigated 3D peat models and the LiDAR stripes intersecting ICESat/GLAS data within Central Kalimantan superimposed on Landsat TM and ETM+ data (bands 5, 4, 3). Peatland extent (orange outline) and the examined ICESat/GLAS data from the years 2003 to 2009 are also indicated. The red rectangle in (A) shows the location and extent of (B).

The focus of this study is the peatlands of Central Kalimantan. Their extent within Kalimantan was determined from maps prepared by Wetlands International (2004) and the authors' Landsat satellite image interpretations (Figure IV-1(A)). 5.7 million ha or 27.8% of Indonesia's peatland resources are found in Kalimantan (Wetlands International, 2004). Peat depth varies from very shallow (less than 0.5m) to very deep peat with up to 12m (Wetlands International, 2004). 42% were classified as very deep peat (Wetlands International, 2004). The three 3D peatland elevation models and airborne LiDAR data were available from other research projects (Figure IV-1(B)) (Jaenicke *et al.*, 2008; Ballhorn *et al.*, 2009). A detailed description of the methodology on how these 3D peatland elevation models were extracted from SRTM data is given by Jaenicke *et al.* (2008). Within Central Kalimantan all peat swamp forest ecosystems have been severely impacted by extensive logging and drainage for more than two decades (Moeliono *et al.*, 2009). The area also covers the former Mega Rice Project (MRP), an ill-fated transmigrasi resettlement project, initiated in 1995 by the Indonesian government.

2.2 Data

2.2.1 ICESat/GLAS data

The Ice, Cloud, and land Elevation Satellite (ICESat) has been orbiting the earth since 12 January 2003 at an altitude of 600km with a 94° inclination and during most of its operating life it has been programmed for a 91-day orbital repeat cycle and was decommissioned from operation on 14 August 2010. The GeoScience Laser Altimeter System (GLAS) onboard ICESat was a full waveform sensor using a 1,064nm laser operating at 40Hz. This resulted in a nominal footprint of about 65m diameter on the earth's surface with each pulse separated by 172m postings (Schutz *et al.*, 2005). There were three lasers onboard ICESat of which the first one failed about 38 days into the mission (29 March 2003). The original temporally continuous measurements were replaced by three 33 day operating periods per year, so that the life of the second and third laser could be extended (Sun *et al.*, 2008). The laser footprint on the earth's surface actually was in the form of an ellipse and its size varied over time as a function of power output from the laser (Harding & Carajabal, 2005). As the GLAS sensor recorded the returned energy over time these waveforms represented the vertical distribution of the terrain and vegetation within each footprint. GLAS data have been demonstrated to accurately estimate forest height (Lefsky *et al.*, 2007; Rosette *et al.*, 2008; Lefsky, 2010) and AGB (Harding & Carajabal, 2005; Boudreau *et al.*, 2008). In this study we used the ICESat/GLAS data product GLA14 Global Land Surface Altimetry Data release version 31 for all acquisition dates from February 2003 to October 2009 for the island of Borneo (Figure IV-1(A,B)). This data product can be downloaded at The National Snow and Ice Data Center (The National Snow and Ice Data Center, 2011a). According to The National Snow and Ice Data Center ICESat/GLAS data release version 31 had an average horizontal geolocation error for all laser campaigns of 0.78m (±5.09m) The National Snow and Ice Data Center, 2011b). For the comparison of the ICESat/GLAS data and SRTM data only ICESat/GLAS data acquired from February 2003 to October 2003 was used, as these are the nearest acquisition dates to the SRTM data (11–22 February 2000), so that potential vegetation cover change could be minimized (see section IV-2.2.4). To compare ICESat/GLAS data to the airborne LiDAR data and the 3D peatland elevation models all ICESat/GLAS acquisitions from February 2003 to October 2009 were utilized.

The elevations from the GLA 14 product were obtained by combining Precise Orbit Data (POD) (Rim & Schutz, 2002), Precise Altitude Data (PAD) (Bae & Schutz, 2002), and range data. To determine the range data the time stamps between the centroid of the transmitted pulse and the corresponding reference point, mostly the centroid, of the return waveform were compared. Latitude, longitude and footprint elevation were computed (Schutz, 2002), after all instrumental, atmospherical, and tidal corrections are applied (Brenner *et al.*, 2003). The positions of these reference points were then stored as range offsets. The waveforms received by the GLAS sensor were characterized by a single Gaussian peak over oceans, sea ice, and ice sheets, and by multiple peaks over irregular surfaces such as land covered by vegetation. Over vegetated land the GLA14 product extracted information from these complex waveforms by fitting up to six Gaussian distributions to the waveform (Harding & Carajabal, 2005). From these Gaussian distributions different waveform peaks were derived that describe different features of the vertical vegetation structure and the underlying topography (Harding & Carajabal, 2005). For tree-covered areas a bimodal GLAS waveform was typical, where topographic relief within a footprint was small compared to vegetation height, which can be used to estimate biophysical parameters. Reflections from the underlying ground, where hit through canopy gaps, and plant surfaces were separated vertically. The height where half of the return energy is above and half below correspond to the centroid of the waveform (Ranson *et al.*, 2004a; 2004b). The distance between the signal beginning and the centroid of the ground return corresponds to the maximum canopy height and can be used as an estimate of AGB (Lefsky *et al.*, 2005). Sometimes the last Gaussian peak is not a good representation of the ground surface, for example when the last peak has a lower amplitude than another peak close to it (Boudreau *et al.*, 2008; Rosette *et al.*, 2008). In this case the higher amplitude peak represents ground surface height (Boudreau *et al.*, 2008; Rosette *et al.*, 2008). The distance between signal begin and signal end corresponds to the total waveform length and also provides information on vegetation height although it is combined with effect of topographic slope (Lefsky *et al.*, 2005). A simplified overview of the different ICESat/GLAS elevations and height metrics is given in Figure IV-2. The interpretation of waveforms is significantly more difficult for areas where within-footprint topographic relief is a substantial fraction of the vegetation height, so that the canopy and ground reflections are mixed.

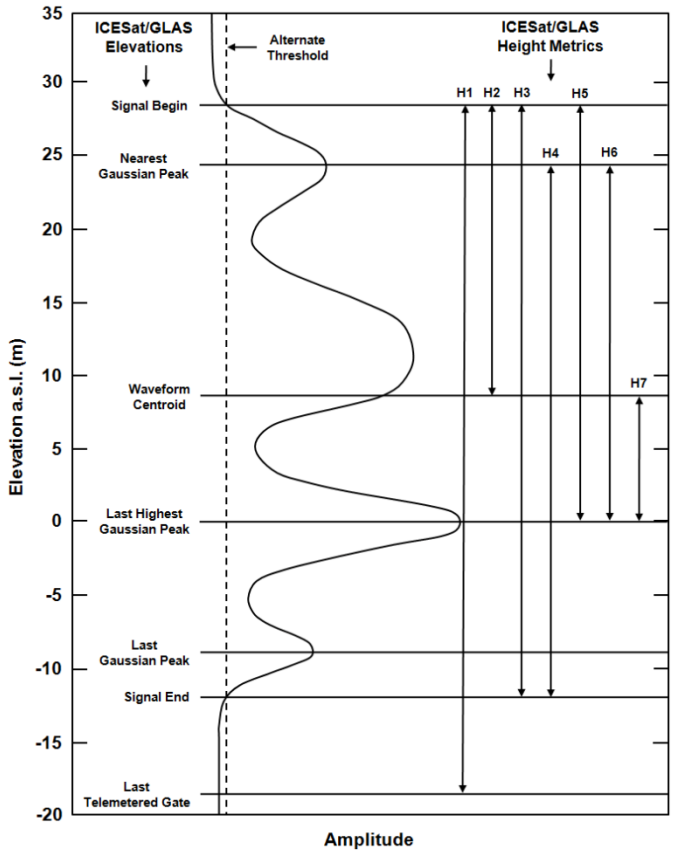

Figure IV-2: Simplified ICESat/GLAS waveform with four Gaussian peaks. On the left, the location of the different ICESat/GLAS elevations is depicted and, on the right, the varying ICESat/GLAS height metrics derived from them are shown. The Signal Begin and the Signal End of the waveform are defined by the crossing of an Alternate Threshold (dashed line).

2.2.2 Airborne LiDAR data

Airborne LiDAR data was acquired during a flight campaign conducted between 5 and 10 August 2007 (Ballhorn *et al.*, 2009). A Riegl LMS-Q560 Airborne Laser Scanner was mounted to a Bell 206 helicopter. Small-footprint full-waveform LiDAR data was collected from a flight altitude of 500m above ground over a scan angle of ±30° (swath width ±500m). The laser sensor had a pulse rate of up to 100,000 pulses per second with a footprint of 0.25m and a wavelength of 1.5µm (near infrared). Due to the accurate time stamping (10^9 samples per second), the three dimensional coordinates of the laser beam reflections (x, y, and z), the intensity, and the pulse width can be extracted by a waveform decomposition, which fits a series of Gaussian pulses to the waveform. This resulted in an average of 1.4 echoes per square meter. The Riegl LMS-Q560 Airborne Laser Scanner system allows height measurements of ±0.02m. Single beam measurements have an absolute horizontal accuracy of

±0.50m and vertical accuracy of ±0.15m Root Mean Square Error (RMSE). 13,626ha of LiDAR data was available for this study of which 9,702ha of LiDAR transects were intersected by ICESat/GLAS data (Figure IV-1(B)).

2.2.3 SRTM data

The Shuttle Radar Topography Mission (SRTM), a joint mission conducted by the National Aeronautics and Space Administration (NASA) and the National Imagery and Mapping Agency (NIMA), was flown from 11 to 22 February 2000 and collected single-pass radar interferometry data covering 119.51 million km^2 of the earth's surface including over 99.9% of the land area between 60°N and 56°S latitude. The C-band InSAR acquired data in 225km swaths and was provided by the Jet Propulsion Laboratory (JPL). For Southeast Asia digital elevation models with a pixel spacing of three arcseconds (about 90m) were produced. The absolute horizontal and vertical accuracy of the data are better than 20 and 16m respectively (Lillesand *et al.*, 2008).

2.2.4 MODIS data

To determine potential vegetation cover change between the acquisition of the SRTM data (11–22 February 2000) and the ICESat/GLAS data (February 2003 to October 2003) the area proportional estimate of woody vegetation, provided in the 500m resolution Vegetation Continuous Fields (VCF) product from the Moderate Resolution Imaging Spectroradiometer (MODIS) was used, which is referred to as the percent tree cover layer (Hansen *et al.*, 2003). Hansen *et al.* (2003) used global training data derived from high resolution imagery to extract VCF woody vegetation, herbaceous vegetation, and bare cover estimates from cloud-corrected, monthly composites of MODIS surface reflectance.

2.2.5 Field inventory data

Field inventory data in Central Kalimantan was collected from May to August 2008. 9 Clusters each with four sample plots were selected depending on representativeness of forest, sub forest and land use type, and accessibility. The cluster positions were

set in advance to assure that they lie within the swath of the aerial LiDAR data set. A GPS device (Garmin GPS map60CSx, accuracy of 3 to 10m) was used to locate the position of the clusters, as well as to mark the center of each sample plot. The four sample plots of one cluster build the corners of a 50×50m square. In each sample plot trees were measured using the nested plot method which is based on circular fixed-area plots (Pearson *et al.*, 2005b). Three nests of circular shape with radii of 4, 14 and 20m were used. Trees with a Diameter at Breast Height (DBH) smaller than 7cm were excluded. In each nest, trees of a certain DBH range were measured: 7 to 20cm (4m radius), 20 to 50cm (14m radius), and greater than 50cm (20m radius). For each tree following parameters were recorded: local species name, DBH in cm, and tree height in m. Local names were translated to corresponding Latin names through information provided by the experts of a local herbarium at the Centre for International Co-operation in Management of Tropical Peatland (CIMTROP) in Palangka Raya and tropical timber databases provided by Chudnoff (1984) and the World Agroforestry Centre (2011). Species specific wood densities were also derived from these databases as well as from IPCC (2006). Some local names could not be translated and some trees could not be identified in the field. In these cases an average specific wood density for Asian tropical trees, 0.57Mg m^{-3}, was applied (Brown, 1997). AGB was calculated using an allometric model of Chave *et al*. (2005) for moist tropical forests which includes DBH and wood density but not tree height. We decided to use a model which excludes tree height as accurate tree height measurements in this tropical ecosystem are almost impossible due to the dense and tall forest canopy. 36 sample plots, located in peat swamp forest, were used to compare AGB calculated in the field to airborne LiDAR 3D point cloud height statistics.

2.3 Data analysis

2.3.1 Airborne LiDAR data processing and correlation with field inventory data

A filtering algorithm based on Kraus & Pfeifer (1998) was applied to differentiate between ground and vegetation points within the airborne LiDAR 3D point clouds. Every track was examined further in small subsets to validate the results and

manually delete outliers. Digital Terrain Models (DTMs) were then generated by interpolating the filtered ground points. Kriging interpolation was applied (cell size 1m) as it showed the best results.

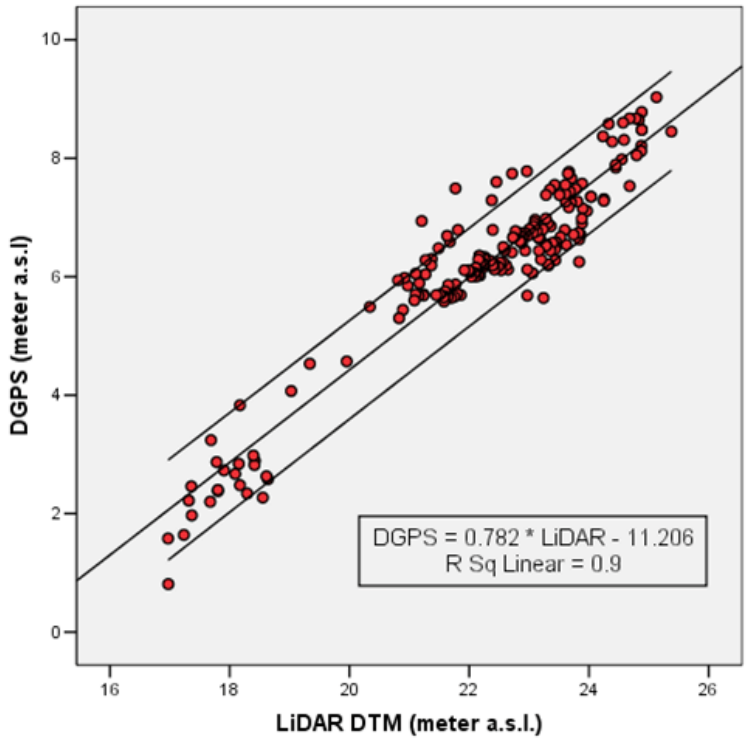

Figure IV-3: Correlation of the airborne LiDAR derived DTMs and the Differential Global Positions System (DGPS) points collected in the field (R^2 = 0.9, n = 201). Also shown are the 95% confidence intervals.

In order to assure the quality of the generated LiDAR DTMs, 201 field points measured with a Differential Global Positioning System (DGPS) were correlated to the interpolated LiDAR DTMs. A high correlation coefficient (R^2 = 0.9) between both data sets was observed (Figure IV-3). This proves the quality of the LiDAR derived DTMs. The altitude differences observed are due to the use of different height reference systems. Also small deviations are expected, since the LiDAR point clouds are from August 2007 and the DGPS measurements from August 2010, and this time shift can lead to discrepancies, mainly near to canals, due to new fires and peat subsidence.

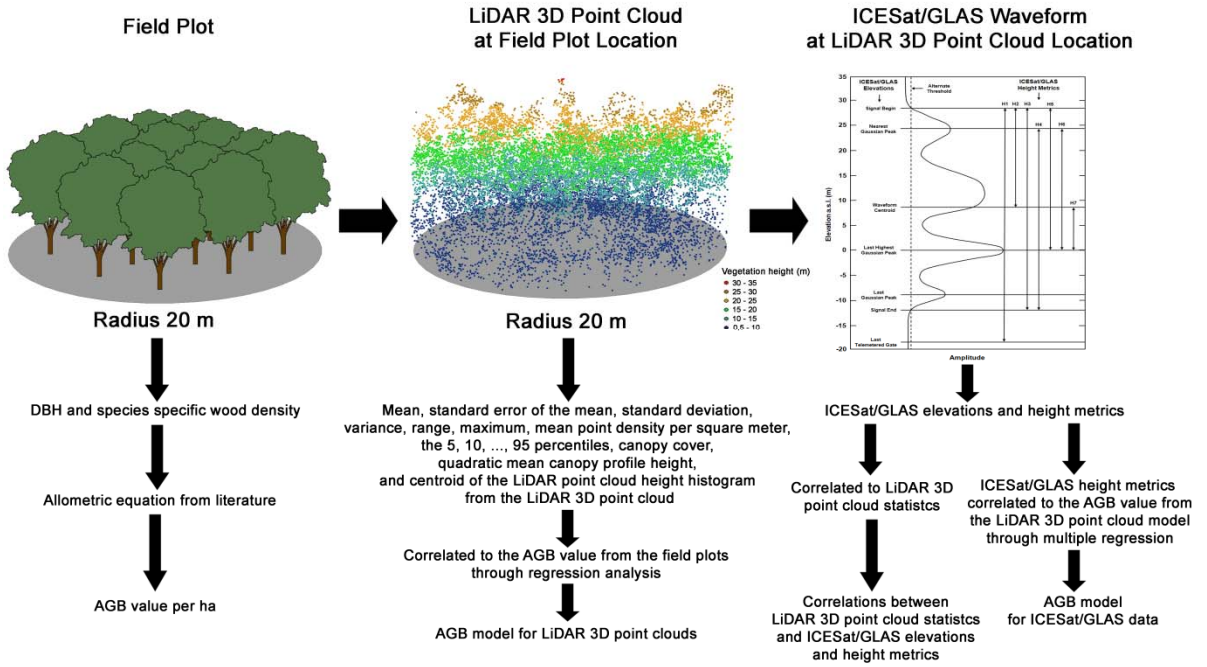

Figure IV-4: Overview of the methodology to derive Above Ground Biomass (AGB) values from the field plots (left), the development of AGB models by correlating AGB from the field to airborne LiDAR 3D point clouds statistics (middle), and the correlation of ICESat/GLAS elevations and height metrics to LiDAR 3D point cloud statistics and the development of a AGB model by correlating AGB results from the airborne LiDAR AGB model to ICESat/GLAS height metrics (right).

The LiDAR 3D point cloud statistics within a defined polygon were correlated to the corresponding ground-based AGB value. Linear and multiple linear regression analysis were applied to identify the best AGB estimation model. 36 sample plot centers were expanded by a circle with a radius of 20m. These areas were used to clip the LiDAR 3D point clouds. The height above the terrain (absolute vegetation heights) for each point within the cloud was determined by subtracting the corresponding pixel value of the DTM. Only points with a value higher than 0.5m were included in the analysis. LiDAR point height distributions of each sample plot were analyzed statistically and following metrics were derived and used as predictors: mean, Standard Error of the Mean (*SEM*), standard deviation, variance, range, maximum, mean point density per square meter, and the quantiles corresponding to the 5, 10, ..., 95 percentiles of the distributions. As further potential predictors Canopy Cover (CC), the Quadratic Mean Canopy profile Height (QMCH) (Lefsky *et al.*, 2002a) and the centroid of the LiDAR point cloud height histogram (CL) were determined. For every pixel of a certain size (5m), CC was calculated by dividing the number of points above a certain height threshold (10m) by the number

of points below the threshold. A schematic overview of this approach is shown in Figure IV-4. For final model validation, the coefficient of determination (R^2), the corrected coefficient of determination (R^2_{corr}), and the Standard Error of the Estimate (*SEE*) were used.

2.3.2 ICESat/GLAS data processing and analysis

The original GLA14 data product was converted to the ESRI point Shape file format using an in house Java script. GLA14 data contains elevations with respect to the TOPEX/Poseidon-Jason Ellipsoid (Schutz *et al.*, 2005). For the reason of comparison GLA14 data was converted to the WGS84 ellipsoid and orthometric elevations were obtained by applying the EGM96 geoid. In ArcGis 9.3 the elliptical footprints for the individual shots were extracted. Only footprints located completely on peatland were selected (Wetlands International, 2004; Figure IV-1(A)).

The SRTM data, three 3D peatland elevation models in Central Kalimantan (Figure IV-1(B)), and MODIS VCF product for the years 2000 and 2003 were resampled to 5m with the nearest neighbor interpolation method. Additionally the slope in degrees was calculated from the SRTM data by using a 3×3 moving window which then was also resampled to 5m. From these layers for each ICESat/GLAS footprint zonal statistics were extracted.

Furthermore a number of different ICESat/GLAS elevations and height metrics were calculated (Figure IV-2).

A range of different filters were generated. To avoid terrain slope and heterogeneous effects the SLOPE filter indicates whether the slope, derived from the interpolated SRTM slope layer, in a footprint is less than 10 degrees or not. The SATURATION filter shows whether an ICESat/GLAS waveform suffers from saturation. To define this filter the *i_satCorrFlg* flag from the GLA14 records was utilized. If there is a thin cloud cover ICESat/GLAS data is returned from the earth's surface, but a thick cloud layer may prevent the laser pulse from reaching the ground and either no return is detected or the return is from the cloud top (Carabajal & Harding, 2006). To prevent this outlier occurrence the OUTLIER filter was implemented. This filter indicates whether the ICESat/GLAS elevation is more than 100m above the SRTM elevation as these records are associated with laser returns from cloud tops (Carabajal &

Harding, 2006). Additionally the ATMOSPHERE filter was established, defined by the *i_FRir_qaFlag* flag of the GLA14 data product, which indicates the presence of clouds. All waveforms ≤60m are indicated by the WAVEFORM EXTENT filter. The ELEVATION filter indicates whether the elevation information of a footprint can be considered as valid and is defined by the *i_ElvuseFlg* flag. With the help of the GLA14 *i_rng_UQF* flag the RANGE filter is determined which indicates the quality of the range increments. The filters VCF CHANGE 0% to VCF CHANGE 25% show the woody vegetation change in percent between the years 2000 and 2003 defined by the MODIS VCF product. Through visual comparison of the ICESat/GLAS footprints and Landsat imagery the vegetation change between the acquisition of the ICESat/GLAS data and the acquisition of the airborne LiDAR data was assessed and the footprints were classified into 8 vegetation change classes (no change, forest–degraded forest, forest–deforested area, degraded forest–deforested area, degraded forest–forest, deforested area–forest, deforested area–degraded forest, water). This VEGETATION CHANGE filter could then be used to exclude ICESat/GLAS footprints with a vegetation change from the statistical comparison.

2.3.3 Comparison ICESat/GLAS and airborne LiDAR data

ICESat/GLAS footprints located completely within airborne LiDAR point clouds were selected. For these footprints, on average about 65m in diameter, different statistics from the airborne LiDAR point clouds and the DTMs were calculated and then correlated to the corresponding ICESat/GLAS elevations. Statistics included: minimum, maximum, mean of the z values from the airborne LiDAR points and DTMs within the ICESat/GLAS footprints. Furthermore different statistics from the normalized airborne LiDAR point clouds (z values of the airborne LiDAR points minus the corresponding DTM values) were correlated to ICESat/GLAS height metrics H1–H7 (Figure IV-2). Statistics included: minimum, maximum, mean, and the 5, 10, ..., 95 percentiles. Additionally the Quadratic Mean Canopy profile Height (QMCH) and the centroid of the LiDAR point cloud height histogram (CL) were compared to these ICESat/GLAS height metrics. A schematic overview of this approach is shown in Figure IV-4.

2.3.4 Development of above ground biomass prediction models from ICESat/GLAS data

Again ICESat/GLAS footprints located completely within airborne LiDAR point clouds were selected. For these footprints the airborne LiDAR point statistics of the 20m circular buffers at footprint center (representing the 20 m field plots with a size of 0.13ha) were used to calculate AGB derived from the airborne LiDAR regression models (see section IV-2.3.1, Figure IV-4). These AGB values at ICESat/GLAS footprint location were then correlated to different ICESat/GLAS height metrics. Multiple linear regression analysis was applied to create ICESat/GLAS AGB estimation models.

Following ICESat/GLAS height metrics were used as predictors: last telemetered gate–signal begin (H1), waveform centroid–signal begin (H2), signal end–signal begin (H3), signal end–nearest Gaussian peak (H4), last highest Gaussian peak–signal begin (H5), last highest Gaussian peak–nearest Gaussian peak (H6), and last highest Gaussian peak–waveform centroid (H7) (Figure IV-2).

Stepwise and backward selection was performed to determine which independent variables should be included in the final models. For final model validation, the coefficient of determination (R^2), the corrected coefficient of determination (R^2_{corr}), and the Standard Error of the Estimate (*SEE*) were used. Figure IV-4 shows a simplified overview of this approach.

2.3.5 Conceptual overview

Figure IV-5 gives a conceptual overview of the methodology described above.

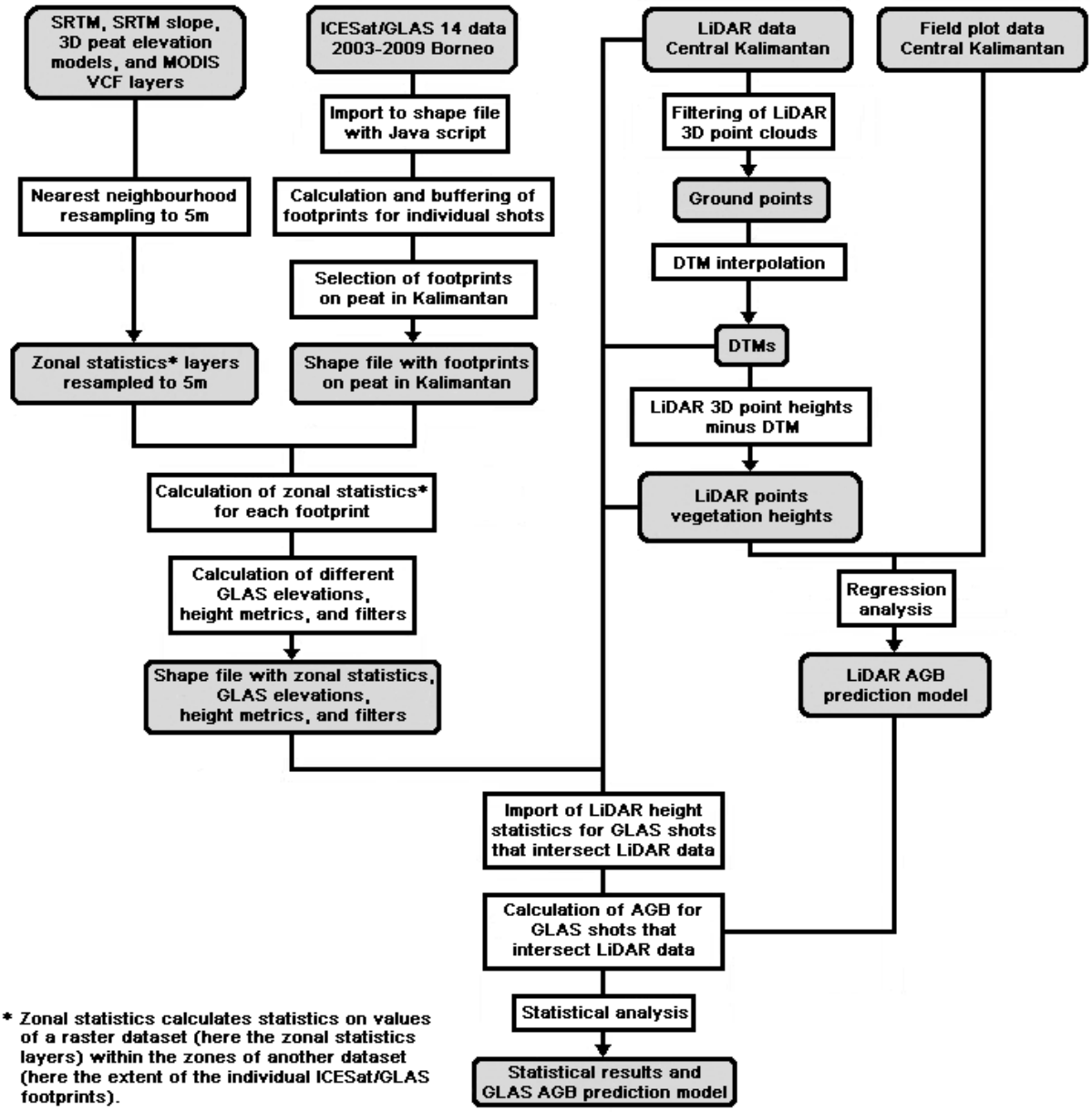

Figure IV-5. Conceptual overview of the methodology used in this study.

3 Results

3.1 Comparison ICESat/GLAS, SRTM data, and SRTM 3D peatland elevation models

The ICESat/GLAS data is referenced to a consistent geodetic reference frame, so that its horizontal and vertical geolocation accuracy and its ability to resolve the height distribution of elevations within the laser footprint, provides a set of accurate control points which can be used to investigate the vertical accuracy of the SRTM digital elevation model (Carabajal & Harding, 2006). ICESat/GLAS's capability to measure the vertical distribution of forests and the underlying surface is useful to assess especially the SRTM C-band microwave penetration depth into these forested areas (Carabajal & Harding, 2006). First we established correlations between SRTM mean elevation at footprint location and ICESat/GLAS elevations of signal begin, waveform centroid, and signal end on peatlands for the whole of Kalimantan. In 2003 9,849 ICESat/GLAS footprints were recorded on peatlands in Kalimantan. This ICESat/GLAS data were quality filtered to incorporate valid and usable footprints for further analyses. Only footprints with a slope of less than 10 degrees and with an ICESat/GLAS elevation not more than 100m above the SRTM elevation, indicated by the SLOPE and OUTLIER filters respectively, were used. Waveforms that suffer from saturation or that indicate the presence of clouds were excluded using the SATURATION and ATMOSPHERE filters. Furthermore footprints with a waveform >60 m, without valid elevation information, and without sufficient quality of the range increments, indicated by the WAVEFORM EXTENT, the ELEVATION, and the RANGE filters respectively, were also excluded. Finally for the statistical analysis we only used footprints that show a vegetation cover change of less than 15% between the years 2000 and 2003 (derived from the MODIS VCF product and represented by the VCF CHANGE 15% filter). The ICEsat/GLAS elevations of the signal begin, waveform centroid, and the signal end of the remaining 4,186 shots were correlated to the corresponding mean SRTM elevation. The R^2 values are 0.88, 0.92, and 0.60 respectively, where waveform centroid shows the highest correlation. Figure IV-6 displays the results of this correlation in three scatter plots. The mean ICESat/GLAS and SRTM elevation differences are 8.7m (±6.1m) for signal begin, −4.9m (±3.8m) for waveform centroid, and −16.1m (±8.4m) for signal end. This result also indicates that the SRTM C-band phase is not reflected by the top of the peat swamp forest canopy

but somewhere within the 3D forest structure. Figure IV-7(B) suggests that on average the C-band penetrates approximately 10–15m into the forest cover.

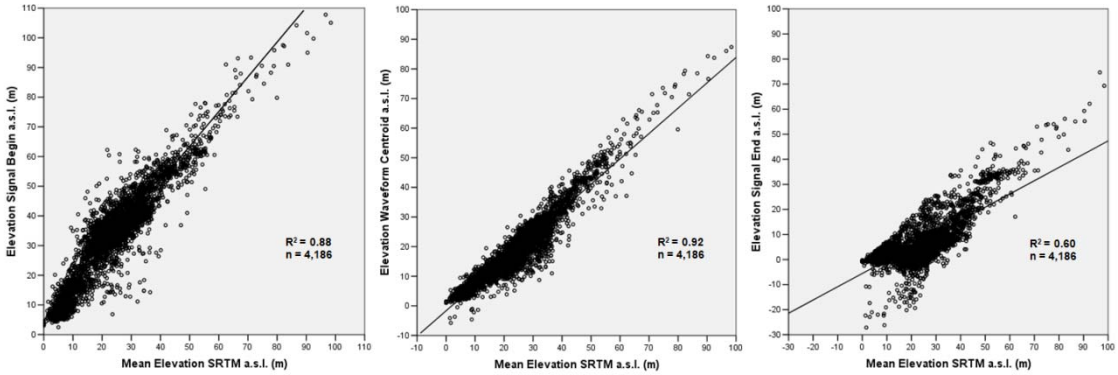

Figure IV-6: Scatter plots displaying the correlation between ICESat/GLAS signal begin, waveform centroid, and signal end elevations a.s.l. (m) to the mean elevation a.s.l. (m) of the corresponding SRTM data. All ICESat/GLAS footprints are from the year 2003 and located on peatlands. The elevation of the waveform centroid with a coefficient of determination (R^2) of 0.92 shows the highest correlation to the SRTM data.

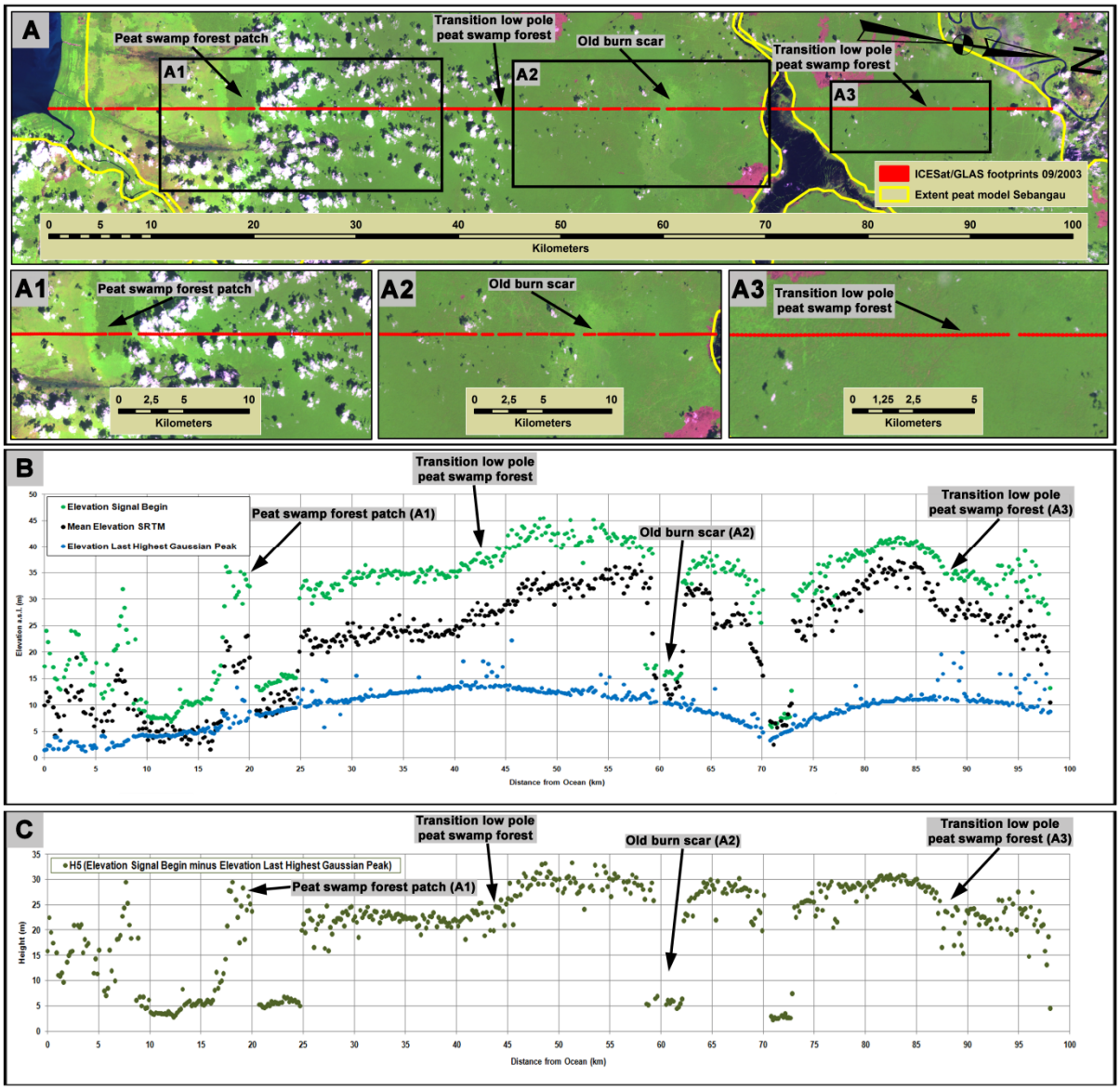

Figure IV-7: ICESat/GLAS transect covering the Sebangau peatland area from south to north. The transect of 98km length starts at the ocean in the south then transects heavily degraded forest, logged peat swamp forest, an old burn scar, and further north a lake, and peat swamp forest again. (**A**): ICESat/GLAS transect superimposed on a Landsat ETM+ image (22-05-2003, bands 5, 4, 3). Bright green represents degraded forest, dark green peat swamp forest. **A1–A3**: Three enlarged areas within this ICESat/GLAS footprint transect. The locations of these areas are indicated by the three black rectangles in A; (**B**): Elevation profile of the ICESat/GLAS transect. Shown are the ICESat/GLAS elevations for the forest canopy (green) and the peat surface (blue). Note the curvature of the peat dome. Also displayed is the mean elevation at footprint location from the SRTM data (black). The locations of a peat swamp forest fragment, two low pole peat swamp forest transition zones, and an old burn scar are indicated by black arrows; (**C**): Measurement of absolute vegetation height by subtracting ICESat/GLAS peat surface elevation from ICESat/GLAS forest canopy signals (ICESat/GLAS height metric H5).

Based on the results above, it is reasonable to use ICESat/GLAS data as a tool to validate 3D peatland elevation models which were derived from SRTM data. 14,312 footprints acquired between 2003 and 2009 were located on the three investigated 3D peatland elevation models (see location in Figure IV-1). For these footprints we applied the same filters as described above with exception of the VCF CHANGE 15% filter as this was not necessary. After filtering 4,045 footprints remained, of which 1,116 were located on the peat model Sebangau, 1,244 on the peat model Block B, and 1,685 on the peat model Block C. As the elevation from the last highest Gaussian peak is known to correspond best with the actual surface elevation (Boudreau *et al.*, 2008; Rosette *et al.*, 2008) this parameter was correlated to the mean elevation of the three 3D peatland elevation models. The R^2 value for this correlation is 0.90. Although some of the elevations of the 3D peatland elevation models differ from the corresponding elevations of the last highest Gaussian peak the mean difference between the two elevation parameters was only −1.0m (±3.2m).

Furthermore we investigated specific ICESat/GLAS footprint transects in more detail for several well investigated peat domes in Central Kalimantan. Figure IV-7 shows one transect that extends 98km from south to north over the Sebangau peat dome. The transect starts at the coastline in the south and first covers heavily degraded peat swamp forest with some remaining tall forest fragments, then more or less disturbed tall peat swamp forest, an old burn scar, a lake with adjacent wetland scrubs and further north again peat swamp forest which has been logged 20 years ago. From the elevation of the ICESat/GLAS signal begin, which corresponds to the top of the forest canopy, these different vegetation types are clearly discernible (Figure IV-7(B)). Also apparent is a variation in the forest canopy height of the peat swamp forest which is related to different subtypes of peat swamp forests (low pole, medium, and tall). This is clearly visible in Figure IV-7(B,C) at km 42 and 87. In Figure IV-7(C) the elevation of the last highest Gaussian peak is subtracted from the elevation of the signal begin (ICESat/GLAS height metric H5) and so showing the absolute vegetation height. Also shown in Figure IV-7(B) is the corresponding mean SRTM elevation. The penetration depth of the SRTM C-band phase center into the forest canopy can be assessed. On deforested sites the SRTM C-band phase center and the last highest Gaussian peak match to each other and represent the surface elevation. The blue line in Figure IV-7(B) indicates the peat surface topography

across a vast distance with high accuracy using ICESat/GLAS. Over a distance of 30km the peat surface increases from 5 to 15m and forms a convex shape which is typical for peat swamp ecosystems.

3.2 Comparison ICESat/GLAS and airborne LiDAR data

In order to compare ICESat/GLAS derived elevations with those of airborne LiDAR measurements ICESat/GLAS footprints located completely within airborne LiDAR point clouds were selected. After filtering 104 valid footprints remained.

We correlated the minimum, maximum, and mean z values from the airborne LiDAR points and DTMs to the signal begin, nearest Gaussian peak, waveform centroid, last highest Gaussian peak, last Gaussian peak, and signal end from the ICESat/GLAS data. The results of these correlations are displayed in Table IV-1. The highest correlation, with a R^2 value of 0.91, was observed when comparing the mean z value of the airborne LiDAR points to the waveform centroid of the ICESat/GLAS data. Also high correlations are evident for the comparison of the maximum and mean z values of the LiDAR points to the signal begin of the ICESat/GLAS data and the maximum z values of the airborne LiDAR points to the waveform centroid of the ICESat/GLAS data (Table IV-1). The mean elevation difference between these two data sets was −0.5m (±1.9m) for waveform centroid and the mean z value, 2.3m (±3.3m) for the last highest Gaussian Peak and the minimum z value, and 3.2m (±3.2m) for signal begin and the maximum z value.

Table IV-1: Coefficients of determination (R^2) for the correlation of the minimum, maximum, and mean of the z values from the airborne LiDAR points and DTMs with different ICESat/GLAS elevation parameters. Where n is the number of ICESat/GLAS footprints used for the comparison. The highest coefficients of determination (R^2) are bold.

Airborne LiDAR statistics	ICESat/GLAS elevations						
	n	Signal begin	Nearest Gaussian peak	Waveform centroid	Last highest Gaussian peak	Last Gaussian peak	Signal end
Minimum z	103[a]	0.50	0.48	0.61	0.63	0.68	0.66
Maximum z	103[b]	**0.86**	0.76	**0.81**	0.48	0.43	0.42
Mean z	104	**0.84**	0.77	**0.91**	0.60	0.60	0.59
Minimum DTM	104	0.57	0.54	0.67	0.63	0.71	0.67
Maximum DTM	104	0.57	0.54	0.67	0.62	0.70	0.67
Mean DTM	104	0.57	0.54	0.67	0.62	0.71	0.67

[a] Footprints with a minimum z value < 0m were considered as outliers and removed; [b] Footprints with a maximum z value > 100m were considered as outliers and removed

Statistics from the normalized airborne LiDAR point clouds (z values of the airborne LiDAR points minus the corresponding DTM values) were then compared to ICESat/GLAS height metrics H1–H7 (Figure IV-2). Statistics included: minimum, maximum, mean, the 5, 10, …, 95 percentiles, Quadratic Mean Canopy profile Height (QMCH), and the centroid of the LiDAR point cloud height histogram (CL). The results are shown in Table IV-2. The highest R^2 values were found when correlating percentile 95 with the ICESat/GLAS height metrics with exception of H7 where 80% had the highest R^2. The overall highest correlation was between percentile 95 and ICESat/GLAS height metric H3.

Table IV-2: Coefficients of determination (R^2) for minimum, maximum, mean, the 5, 10, ..., 95%, Quadratic Mean Canopy profile Height (QMCH), and the centroid of the LiDAR point cloud height histogram (CL) from the normalized airborne LiDAR point clouds (z values of the airborne LiDAR points minus the corresponding DTM values) correlated to ICESat/GLAS height metrics H1–H7 (Figure IV-2). Where n is the number of ICESat/GLAS footprints used for the comparison. The highest coefficients of determination (R^2) are bold.

Airborne LiDAR statistics	**ICESat/GLAS height metrics**							
	N	**H1**	**H2**	**H3**	**H4**	**H5**	**H6**	**H7**
Minimum	102[a]	0.01	0.00	0.00	0.01	0.00	0.00	0.00
Maximum	103[b]	0.40	0.46	0.54	0.42	0.49	0.33	0.28
Mean	104	0.26	0.22	0.36	0.30	0.34	0.25	0.29
Percentile 5	104	0.00	0.00	0.00	0.00	0.00	0.01	0.01
Percentile 10	104	0.00	0.01	0.01	0.00	0.00	0.00	0.00
Percentile 15	104	0.00	0.01	0.02	0.01	0.00	0.00	0.00
Percentile 20	104	0.00	0.01	0.03	0.02	0.01	0.01	0.01
Percentile 25	104	0.01	0.02	0.05	0.04	0.04	0.02	0.04
Percentile 30	104	0.03	0.03	0.09	0.07	0.07	0.04	0.08
Percentile 35	104	0.09	0.06	0.16	0.13	0.15	0.10	0.17
Percentile 40	104	0.14	0.09	0.22	0.17	0.22	0.15	0.25
Percentile 45	104	0.18	0.11	0.25	0.19	0.24	0.16	0.26
Percentile 50	104	0.21	0.13	0.28	0.22	0.28	0.18	0.29
Percentile 55	104	0.26	0.17	0.34	0.26	0.34	0.23	0.34
Percentile 60	104	0.29	0.20	0.38	0.30	0.38	0.26	0.36
Percentile 65	104	0.33	0.24	0.43	0.36	0.42	0.31	0.39
Percentile 70	104	0.37	0.29	0.48	0.40	0.47	0.36	0.41
Percentile 75	104	0.40	0.33	0.51	0.44	0.51	0.40	0.42
Percentile 80	104	0.42	0.36	0.53	0.47	0.53	0.43	**0.43**
Percentile 85	104	0.43	0.39	0.53	0.48	0.54	0.44	0.41
Percentile 90	104	0.42	0.41	0.53	0.49	0.53	0.44	0.38
Percentile 95	104	**0.45**	**0.47**	**0.57**	**0.50**	**0.56**	**0.45**	0.37
Percentile 100	103[b]	0.40	0.46	0.54	0.42	0.49	0.33	0.28
QMCH	102[c]	0.27	0.23	0.40	0.35	0.39	0.34	0.31
CL	104	0.28	0.21	0.38	0.32	0.37	0.35	0.28

[a] Footprints with a minimum z value > 5m were considered as outliers and removed; [b] Footprints with a maximum z value > 100m were considered as outliers and removed; [c] Footprints where QMCH could not be calculated were excluded

3.3 Above ground biomass predictions models from airborne LiDAR data and ICESat/GLAS data

To derive an AGB prediction model from ICESat/GLAS we used the model derived from airborne LiDAR and forest inventory data. In a first step 36 forest sample plots were used to correlate AGB values calculated in the field to airborne LiDAR 3D point clouds. The best overall predictor of AGB was the centroid of the airborne LiDAR point cloud height histogram (CL). The model could further be enhanced through incorporating the average LiDAR point density per square meter per sample plot of all LiDAR points. Sample plots with a higher average LiDAR point density per square meter were weighted higher during the computation of the final model (Figure IV-8). The average LiDAR point densities per square meter for these 36 sample plots were between 0.2 and 3.6. The R^2 value of this model is 0.75, the corrected coefficient of determination (R^2_{corr}) is 0.73, and the Standard Error of the Estimate (*SEE*) is 2.66 ton 0.13ha^{-1}.

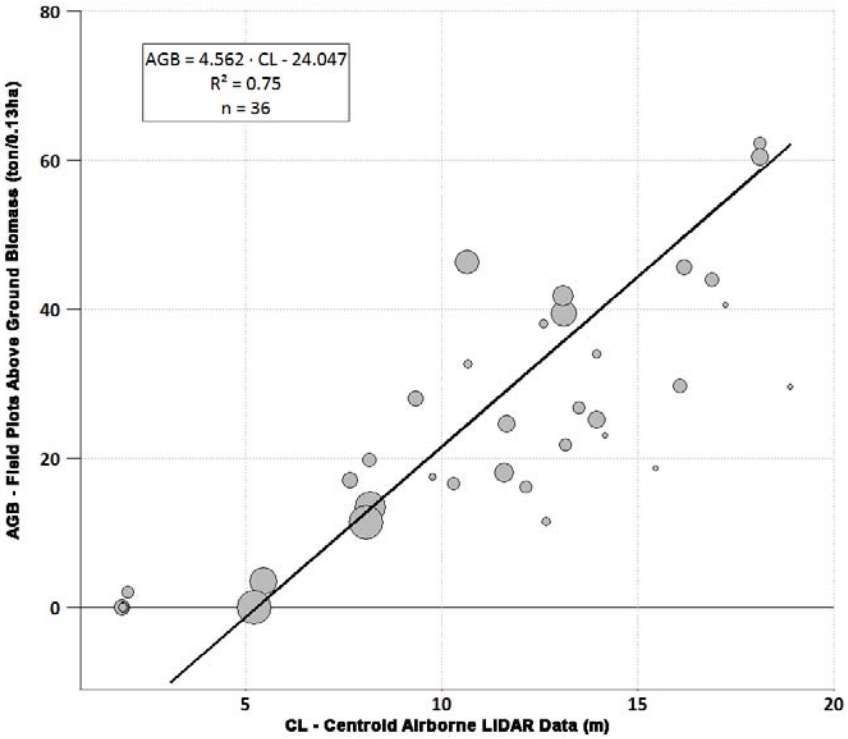

Figure IV-8: Scatter plot displaying the correlation between the Above Ground Biomass (AGB), calculated from field plots, to the centroid of the airborne LiDAR point cloud height histogram (CL). The sizes of the circles represent the average LiDAR point density per square meter (small = lower average LiDAR point density per square meter; big = higher average LiDAR point density per square meter).

To analyze biomass estimates from ICESat/GLAS we selected only footprints, where the 20m radius circular buffers at footprint center (representing the field plot size of 0.13ha) were completely located within the airborne LiDAR point clouds. After filtering 104 valid footprints remained.

The centroid of the airborne LiDAR point cloud height histogram (CL) at these footprints was correlated to the ICESat/GLAS height metrics H1–H7 (Figure IV-2) depending on the average LiDAR point density per square meter per 20m radius circular buffer. The corresponding R^2 values are shown in Table IV-3. The highest R^2 values were found for H5 with average LiDAR point densities per square meter ≥0.7 and ≥0.8.

Stepwise and backward multiple regression approaches, incorporating all 7 ICESat/GLAS height metrics (H1–H7), were applied to determine which independent variables should be included in the final models. The highest R^2 value of 0.61 (n = 35) was reached through a backward multiple regression approach with H1, H2, H4, H6, and H7 as independent variables and where the average LiDAR point density per square meter was ≥0.8 points. The corrected coefficient of determination (R^2_{corr}) was 0.54 and the Standard Error of the Estimate (*SEE*) 9.76 ton 0.13ha^{-1}. The mean difference between the ICESat/GLAS AGB estimation and the airborne LiDAR AGB estimation was −2.62 ton 0.13ha^{-1} (±10.78 ton 0.13ha^{-1}, n = 104).

Table IV-3: Coefficients of determination (R^2) for the ICESat/GLAS height metrics (H1–H7; Figure IV-2) correlated to the centroid of the airborne LiDAR point cloud height histogram (CL) at the 20m radius circular buffers at footprint center (representing the field plot size) dependent on the average LiDAR point density per square meter. Where n is the number of ICESat/GLAS footprints used for the comparison. The highest coefficients of determination (R^2) are bold.

Average LiDAR point densitiy per square m	n	ICESat/GLAS height metrics						
		H1	H2	H3	H4	H5	H6	H7
all	104	0.32	0.25	0.43	0.37	0.44	0.33	0.40
≥ 0.1	93	0.40	0.31	0.51	0.43	0.52	0.40	0.46
≥ 0.2	72	0.45	0.34	0.54	0.49	0.59	0.53	0.56
≥ 0.3	54	0.55	0.45	0.63	0.60	0.67	0.62	0.63
≥ 0.4	47	0.65	0.55	0.69	0.66	0.70	0.63	0.67
≥ 0.5	46	0.68	0.57	0.73	0.68	0.75	0.65	0.71
≥ 0.6	43	0.70	0.60	0.74	0.69	0.75	0.67	0.70
≥ 0.7	41	0.72	0.62	0.75	0.71	**0.77**	0.70	0.70
≥ 0.8	39	0.72	0.62	0.74	0.71	**0.77**	**0.71**	**0.72**
≥ 0.9	35	0.70	0.61	0.75	0.73	0.76	**0.71**	0.70
≥ 1	32	**0.73**	**0.63**	**0.76**	**0.74**	0.76	0.70	0.68

4 Discussion and conclusions

Since most peatlands in Indonesia are highly inaccessible, very few field measurements have been made to date to assess these carbon pools. Especially the potential spatial variation is unknown because up-to-date no systematic large scale sampling has been undertaken. ICESat/GLAS data have been demonstrated to accurately estimate forest structural properties especially well in topographically even areas (Harding & Carajabal, 2005; Lefsky *et al.*, 2007; Baccini *et al.*, 2008; Boudreau *et al.*, 2008; Rosette *et al.*, 2008; Sun *et al.*, 2008; Goetz *et al.*, 2010; Lefsky, 2010; Dolan *et al.*, 2011). As peatlands have an especially smooth topography (Page *et al.*, 1999; Rieley & Page, 2005) we assessed the applicability of ICESat/GLAS data to measure peatland topography, peat swamp forest vertical structure, and peat swamp forest AGB in Central Kalimantan, Indonesia. ICESat/GLAS data was compared to different other data (SRTM data, 3D peatland elevation models derived from SRTM data, and airborne LiDAR data).

Jaenicke *et al.* (2008) demonstrated that SRTM data can be used to determine the extent and topography of the dome shaped surface and a correlation was obtained between the convex peat dome surface and the depth of the underlying mineral ground, which was then used to calculate the peat volume and carbon store. The main problem of this approach was the determination of the vegetation height growing on top of the peat domes as the SRTM C-band sensor does not completely penetrate the forest cover. To get a high number of quality filtered footprints we investigated ICESat/GLAS data on peatlands for the whole of Kalimantan. The comparison of ICESat/GLAS elevations to the mean SRTM elevation showed a very high correlation of the waveform centroid (R^2 = 0.92). The mean ICESat/GLAS and SRTM elevation difference of −4.9m (±3.8m) also showed that the SRTM C-band phase center penetration depth is dependent on forest structural parameters such as canopy closure. These results comply well with a study by Carabajal and Harding (2006) and indicate that even for densely forested peat swamp areas the error is well below the 16m at 90% confidence vertical accuracy specifications for the SRTM mission. These findings demonstrate that with the help of ICEsat/GLAS data the penetration depth of the SRTM C-band phase center into different peat swamp forest canopy closures and consequently the height of the SRTM elevation above the actual peat surface can be measured. Based on this it is reasonable to use

ICESat/GLAS data as a tool to validate 3D peatland elevation models which were derived from SRTM data for selected regions in Central Kalimantan. Because the elevation from ICESat/GLAS last highest Gaussian peak is known to correspond best with the actual peat surface (Boudreau *et al.*, 2008; Rosette *et al.*, 2008) we correlated it to the mean elevation of the three 3D peatland elevation models. Transects covering entire peat domes, clearly show the convex curvature of the peat domes (Figure IV-7(B)). The difference between the last highest Gaussian peak from the ICESat/GLAS data, referring to the estimated peat surface within the ICESat/GLAS waveform, and the 3D peatland elevation models, in which the forest canopy height was eliminated from the SRTM terrain model, was with −1.0m (±3.2m) low. These results indicate that ICESat/GLAS data can be used to validate and enhance SRTM derived 3D peatland elevation models.

Furthermore, ICESat/GLAS data can be used as a sampling tool to screen for peatland areas in remote areas, such as West Papua. A systematic sampling with ICESat/GLAS could help to improve the knowledge on the spatial extent and curvature variation of peat domes and also consequently lead to better estimates of the carbon pools.

Considering peat swamp forest vertical structure we investigated specific ICESat/GLAS footprint transects in more detail that covered peat domes and adjacent areas where the land cover was known from optical satellite imagery and field surveys. Figure IV-7 shows one of these transects. From the elevation of the ICESat/GLAS signal begin, which corresponds to the top of the forest canopy, new and old burn scars, peat swamp forest fragments, logged and unlogged peat swamp forests are clearly discernible. Also apparent is a variation in the tree canopy height of the peat swamp forest which corresponds to different growth conditions in relation to hydrology. This leads to the conclusion that through combing optical data with ICESat/GLAS data it would be possible to obtain transect samples on the state and structure of peat swamp forests not only across the Indonesia archipelago but also in other regions where tropical peatlands occur.

Our field derived AGB values for tropical peat swamp forest lie in the range of existing literature values (Waldes & Page, 2001). Different degradation levels between unlogged, logged and burned forests could be quantified. Most problematic were *in situ* tree height measurements as a multi-layered and dense canopy made it

almost impossible to clearly sight tree tops. Especially in logged forest, dense undergrowth prevented from moving to a point where the tree top could be identified. Therefore we decided to use an allometric model for AGB calculation, which includes DBH and wood density but not tree height. The resulting correlation between field derived AGB values and airborne LiDAR data is comparable to other previously published values (Means *et al.*, 1999; Drake *et al.*, 2002a; Lefsky *et al.*, 2002a; Lucas *et al.*, 2006; Asner *et al.*, 2009; Asner *et al.*, 2010). However, possible errors and limitations must be considered. For example errors might occur due to the use of a navigation GPS (C/A code only) for the forest sample plot locations, which had an accuracy of 3 to 10m. Also effects like multi-path of the GPS signal in dense forested environments can lead to inaccurate location of the field plots. Due to these error sources the correlation might be influenced if the field plot location does not accurately match the location within the LiDAR 3D point cloud, which was measured more accurately by differential GPS. Also the filtering for ground points plays a key role. Peat swamp forests grow on very flat terrain covered by tall forests with sometimes dense, scrubby undergrowth, which may impede the detection of the real soil surface. The error produced hereby and by the interpolation process could not be quantified because of a lack of reliable fine scale elevation data from the field. The resulting R^2 value of 0.75 (n = 36), where the average LiDAR point density per square meter was used as weighting factor in the linear regression, indicates that the established model should be valid, but the R^2 value is slightly lower than those reported for other biomes. LVIS (Laser Vegetation Imaging Sensor) data was successfully analyzed for forests in Costa Rica with a R^2 value of 0.89 (Drake *et al.*, 2002a). Asner *et al.* (2009) quantified AGB of a rain forest reserve on Hawaii Island using vertical profiles of a full waveform LiDAR system and showed that field-measured AGB was best predicted by the mean canopy height (R^2 = 0.78). Applying this approach in the Peruvian Amazon improved the resulting model (R^2 = 0.85) (Asner *et al.*, 2010). Analyzing discrete LiDAR data from a range of forest structural types in Australia Lucas *et al.* (2006) derived a R^2 value of 0.92. A possible explanation for the lower R^2 value in our study could be that filtering for ground points is more erroneous in peat swamp forests. Preliminary results, where we investigated the same LiDAR data set in a lowland dipterocarp forest in Central Kalimantan resulted in a R^2 value higher than 0.90.

When correlating ICESat/GLAS elevations to airborne LiDAR 3D clouds and DTMs derived from these the signal begin and waveform centroid compared to the maximum z and mean z value all had R^2 values higher than 0.8, with the highest correlation between the waveform centroid and the mean z value (R^2 = 0.91, n = 104) (Table IV-1). The mean elevation difference between these two data sets was −0.5m (±1.9m) for waveform centroid and the mean z value, 2.3m (±3.3m) for the last highest Gaussian Peak and the minimum z value, and 3.2m (±3.2m) for signal begin and the maximum z value. These results indicate that ICESat GLAS data and airborne LiDAR data comply well regarding elevation and that ICESat/GLAS data can be used as a tool to measure different elevations in these dense tropical peat swamp forest ecosystems. On the other hand when comparing ICESat/GLAS height metrics H1–H7 (Figure IV-2) to statistics from the normalized airborne LiDAR point clouds (z values of the airborne LiDAR points minus the corresponding DTM values) R^2 values were lower than 0.58 (Table IV-2). The highest R^2 were found when correlating percentile 95 with the ICESat/GLAS height metrics with exception of H7 (Figure IV-2) where percentile 80 had the highest R^2 value. The overall highest correlation (R^2 = 0.57, n = 104) was between 95% and ICESat/GLAS height metric H3 (Figure IV-2).

The best ICESat/GLAS AGB prediction model was achieved through a backward multiple regression approach with H1, H2, H4, H6, and H7 (Figure IV-2) as independent variables where the average LiDAR point density per square meter was ≥0.8 points (R^2 = 0.61, n = 35). The mean difference between the ICESat/GLAS AGB estimation and the airborne LiDAR AGB estimation was −2.62 ton 0.13ha^{-1} (±10.78 ton 0.13ha^{-1}, n = 104). For future studies it would be beneficial to have a higher number of ICESat/GLAS footprints intersecting with LiDAR point clouds with high average point densities. It has to also be considered that having multiple waveform derived variables (in our case 5) in the same equation may lead to collinearity problems. Comparing the model with other studies the R^2 value is in the lower range. Baccini *et al.* (2008) found a strong positive correlation (R^2 = 0.90) between ICESat/GLAS height metrics and AGB values predicted from MODIS data across tropical Africa. Lefsky *et al.* (2005) combined ICESat/GLAS waveforms and SRTM data to estimate maximum forest height in three ecosystems (tropical broadleaf forests in Brazil, temperate broadleaf forests in Tennessee, and temperate

needleleaf forests in Oregon). Additionally ICESat/GLAS derived heights for the Brazilian plots were correlated to AGB estimates from the field (R^2 = 0.73).

The results of our study demonstrate the usefulness and robustness of ICESat/GLAS data as a sampling tool to extract information on peatlands, which can be used as a proxy for peat volume and consequently carbon storage, state and structure of peat swamp forests, and peat swamp forest AGB for large inaccessible areas at low costs where no systematic sampling has been conducted yet. When combined with other data sources (optical satellite imagery, SRTM, and airborne LiDAR) ICESat/GLAS data can help to better understand carbon pools in tropical peatlands and their spatial distribution across Indonesia and other regions.

Acknowledgments

The authors would like to thank the National Snow and Ice Data Center for providing the ICESat/GLAS data. We would like to thank Suwido Limin and his team from the Centre for International Co-operation in Management of Tropical Peatland (CIMTROP) in Palangka Raya for the logistic support during the field inventory and Sampang Gaman (CIMTROP) and Simon Husson (Orangutan Tropical Peatland Project, OUTROP) for providing their tree species lists. Furthermore we would like to thank the Forest Restoration and Rehabilitation in Southeast Asia (FORRSA) project of the EU-funded Asia Link programme for financially supporting the field trip to Indonesia. The LiDAR data set was acquired by Kalteng Consultants.

CHAPTER V:
Above ground biomass estimation across forest types at different degradation levels in Central Kalimantan using LiDAR data

International Journal of Applied Earth Observations and Geoinformation, **18**, 37-48

Karin Kronseder[a,b], Uwe Ballhorn[a,b], Victor Böhm[c], Florian Siegert[a,b]

[a]Biology Department II, GeoBio Center, Ludwig-Maximilians-University, Grosshaderner Strasse 2, D-82152 Planegg-Martinsried, Germany

[b]Remote Sensing Solutions GmbH, Isarstrasse 3, D-82065 Baierbrunn, Germany

[c]Kalteng Consultans, Kirchstockacher Weg 2, D-85635 Hoehenkirchen, Germany

doi: 10.1016/j.jag.2012.01.010
Received 10th February 2011
Accepted 3rd January2012

Abstract

The quantification of tropical forest carbon stocks is a key challenge in creating a basic methodology for REDD (Reducing Emissions from Deforestation and Degradation in developing countries) projects. Small-footprint LiDAR (Light Detection And Ranging) systems have proven to successfully correlate to Above Ground Biomass (AGB) estimates in boreal and temperate forests. Their applicability to two different tropical rainforest types (lowland dipterocarp and peat swamp forest) in Central Kalimantan, Indonesia, was tested by developing multiple regression models at plot level using full waveform LiDAR point cloud characteristics. Forest inventory data is barely available for Central Kalimantan's forests. In order to sample a high number of field plots the angle count method was applied which allows fast sampling. More laborious fixed-area plots (three nests of circular shape) were used as a control and approved the use of the angle count method. AGB values, calculated by using existing allometric models, were in the range of 15 to 547Mg ha^{-1} depending on forest type, degradation level and the model used for calculation. As expected, logging resulted in significant AGB losses in all forest types. AGB-prediction models were established for each forest type using statistical values of the LiDAR point clouds and the forest inventory plots. These regression models were then applied to six LiDAR tracks (altogether with a size of 5,241ha) covering unlogged, logged and burned lowland dipterocarp and peat swamp forest. The regression analysis showed that the 45th and 65th percentiles and the standard error of the mean explain 83% of the variation in lowland dipterocarp forest plots (*RMSE* = 21.37%). The best model for peat swamp forest could only explain 32% of the AGB variation (*RMSE* = 41.02%). Taking both forest types together explained 71% (*RMSE* = 33.85%). Calculating AGB for whole LiDAR tracks demonstrated the ability of this approach to quantify not only deforestation but especially forest degradation and its spatial variability in terms of biomass change in different forest ecosystems using LiDAR transects. Concluding it can be stated that the combined approach of extensive field sampling and LiDAR point cloud analysis have high potential to significantly improve current estimates of carbon stocks across different forest types and degradation levels and its spatial variation in highly inaccessible tropical rainforests in the framework of REDD.

Keywords: LiDAR; tropical forest; above ground biomass; reduced emissions from deforestation and forest degradation; forest inventory; Indonesia

1 Introduction

Between 1990 and 2005 about 13 million hectares (Mha) of mostly tropical forest were destroyed annually (FAO, 2006) and with 1.3% per year insular Southeast Asia had the highest rate of deforestation (FAO, 2001; Archad et al., 2002; FWI/GWI, 2002). In Kalimantan, Indonesia, forest cover was reduced by about 78% between 1973 and 2003 (Page *et al.*, 2009). Deforestation and forest degradation in Borneo are almost exclusively caused by human economic activities such as shifting cultivation, illegal logging, and the establishment of industrial timber estates and large-scale oil palm plantations (Boehm & Siegert, 2004; Curran et al, 2004; Rieley & Page, 2005; Sandker *et al.*, 2007; Hansen *et al.*, 2009; Sheil *et al.*, 2009). During extended droughts caused by the periodic El Niño phenomenon vast areas of the Indonesian forests have been destroyed by fire (Langner & Siegert, 2009). Fire serves as the principal tool for land clearing and its impacts and severity increases in degraded forests (Siegert *et al.*, 2001). It is estimated that in 2008, worldwide deforestation and forest degradation emissions contributed about 6 to 17% of the total anthropogenic carbon dioxide (CO_2) emissions (Van der Werf *et al.*, 2009). In Indonesia increased Green House Gas (GHG) emissions are particularly evident in the coastal lowlands of Sumatra and Kalimantan, where peat fires and peat oxidation, due to peatland drainage, result in the release of huge amounts of CO_2 (Page *et al.*, 2002; Ballhorn *et al.*, 2009; Hooijer *et al.*, 2010). The planned programme on Reduced Emissions from Deforestation and Degradation in developing countries (REDD) is involving the private sector of industrialized countries in the protection of the remaining tropical forests. Conservation and the involved emission reduction allow for a compensation of their GHGs emission quota exceeding. REDD projects require an exact quantification and monitoring of forest carbon stocks which remains a big challenge in tropical forests (Gibbs *et al.*, 2007). The main carbon pool of tropical forest ecosystems is typically the Above Ground Biomass (AGB) (Gibbs *et al.*, 2007), but the soil carbon has to be critically considered for tropical peat swamp forests, where massive amounts of carbon are stored within the peat layer (Jaenicke *et al.*, 2008; Page *et al.*, 2010).

AGB at a landscape scale can be estimated by extrapolating results measured in the field or from remote sensing instruments (Brown, 1997; Chave *et al.*, 2005). For Central Kalimantan and most other regions in Indonesia forest inventory data and specific allometric formulas from destructive sampling barely exist. Non-destructive forest inventory methods are based on the statistical relation of field measurements to destructive harvest measurements, and the conversion to biomass estimates using allometric equations (Brown, 1997; Chave *et al.*, 2005; Basuki *et al.*, 2009). According to Brown (2002), grouping all species together and establishing generalized equations for broad forest types turned out to be highly effective for the tropics. However, the structural and biotic complexity of tropical forest causes difficulties for the inventory: the generic relationships are not appropriate for all regions, inventories can be expensive and time-consuming, and it is challenging to produce globally consistent results (Chave *et al.*, 2005; Gibbs *et al.*, 2007). Since remote sensing instruments estimate biomass indirect they are depending on additional in-situ data (Roesenqvist *et al.*, 2003). The estimation of tropical forest biomass by the means of optical remote sensing methods is generally challenging and has not yet been satisfactorily resolved due to dense canopies, heterogeneous, complex, tall structure, and the low saturation level of spectral bands and derived indices (Gibbs *et al.*, 2007). Frequent cloud cover in the inner tropics further hampers the data analysis (Foody & Curran, 1994). Spaceborne synthetic aperture radar (SAR) sensors have the advantage to be weather and daylight independent. In tropical regions, longer wavelengths have proven to be more useful because of an increasing backscatter range with changing biomass (Dobson et al., 1992; Luckman et al., 1997; Castro et al., 2003; Lu, 2006), but again, there is a problem of saturation at high AGB values (e.g. Imhoff, 1995; Luckman *et al.*, 1997; Kuplich *et al.*, 2005; Lucas *et al.*, 2007; Mitchard *et al.*, 2009). Nevertheless, optical remote sensors and SAR are potential tools to upscale AGB estimates from a smaller scale.

Airborne Light Detection and Ranging (LiDAR), or laser altimetry, provides three-dimensional information of forest structure and represents a potential technique for biomass quantification and monitoring. LiDAR is based on the transmission of laser pulses from the aircraft toward the ground surface and the recording of the return signal. By analyzing the time delay for each pulse back to the sensor, relative and absolute surface heights can be determined with an accuracy of several centimeters.

LiDAR systems have certain advantageous characteristics, such as high sampling intensity, direct measurements of heights, precise geolocation, and automated processing (Mallet & Bretar, 2009). These properties make LiDAR systems useful for direct assessment of vegetation characteristics and deriving forest biomass at multiple scales from individual trees (e.g. Popescu, 2007; Zhao *et al.*, 2009) to regional extents (e.g. Lefsky et al., 1999a; 1999b; 2002a; 2005; Means et al., 1999). The correlation of laser height metrics to the field-measured AGB of a certain plot, known as the quantile estimator method (Magnussen & Boudewyn, 1998), was successfully applied in temperate (e.g. Lim & Treitz, 2004, Patenaude *et al.*, 2004; Hollaus *et al.*, 2007) and boreal forest (e.g. Naesset, 2002; 2004). LiDAR data analysis in tropical forest holds difficulties due to forest structure complexity (Nelson *et al.*, 1997). Drake *et al.* (2002a; 2002b; 2003) estimated AGB in Panama and Costa Rica using the full waveform system Laser Vegetation Imaging Sensor (LVIS) and Asner *et al.* (2009; 2010) succeeded in relating small-footprint LiDAR metrics to above ground carbon densities of tropical forests in Hawaii and the Peruvian Amazon.

The main goal of this study was the estimation of AGB values for two different forest types (lowland dipterocarp and peat swamp forest) in study sites located in Central Kalimantan by LiDAR data analysis, making use of an extensive forest inventory database collected in the field. The approach was tested for its applicability as input to a basic methodology for future REDD projects. The study was divided into the following subtasks:

(1) In-situ data of forest parameters was collected within two different forest types (lowland dipterocarp and peat swamp forest) at various degradation levels using the angle count method which allows fast sampling. To test this method on its feasibility for biomass estimates in the tropics several plots were also recorded with the nested plot method.

(2) LiDAR three-dimensional point clouds were analyzed and correlated to field AGB estimates on plot level to establish robust biomass estimation models. The feasibility, effectiveness, advantages and disadvantages of the plot level approach were assessed and the resulting models were compared to literature.

(3) Finally the biomass estimation models were applied to different LiDAR tracks covering unlogged, logged and burned lowland dipterocarp and peat swamp forest. Results were compared to a land cover classification based on Landsat imagery.

2 Materials and methods

2.1 Study area

In this study two forest types within Central Kalimantan, Borneo, were targeted: Lowland dipterocarp forest and peat swamp forest. Both forest types can usually be well discriminated in the field by means of species composition, average tree height, tree crown diameter, and canopy closure, with lowland dipterocarp forest being more diverse with taller trees and a more closed canopy (MacKinnon *et al.*, 1996). All forest ecosystems in Central Kalimantan have been severely impacted by more than three decades of extensive logging (Moeliono *et al.*, 2009). The Mega Rice Project, a transmigration project of the Indonesian government and the Worldbank established during the 1990s (Rieley & Page, 2005) led to severe peat drainage through the building of a channel system and recurrent fire disasters with huge CO_2 emissions (Page *et al*., 2002; Ballhorn *et al.*, 2009; Langner & Siegert, 2009).

Field inventory data was collected in six study sites from September to October 2007 and from May to August 2008. The first study site was located in the Sebangau peat swamp catchment. The Sebangau forests had been selectively logged for 20 years until 1997 (Waldes & Page, 2001). Nine field inventory clusters (see section V-2.2) were located in each of four sub peat swamp forest types described by Sheperd *et al.* (1997) (Figure V-1). Study sites 2 and 3 were located within Block C and B of the former Mega Rice Project. These blocks consist of peat swamp forest and large burned peatland areas. Most peat swamp forests are severely degraded due to logging, peatland drainage, and fire. Fires occurred in 1997/98, 2002, 2006 and 2009 on different sites. Nine clusters were located in logged forest and three clusters in burned areas (Figure V-1, LiDAR tracks 2a, 2d and 3b). Lowland dipterocarp forest was studied at three study sites (Figure V-1, study sites 4-6). Ten clusters of nearly unlogged forest were recorded near the village Tumbang Danau (study site four). Within study site five, near Tewaibaru, four clusters were measured in regrown

lowland dipterocarp forest within a shifting cultivation area and five clusters in logged lowland dipterocarp forest further east. In Bawan (study site six), five clusters each were located in unlogged and logged lowland dipterocarp forest.

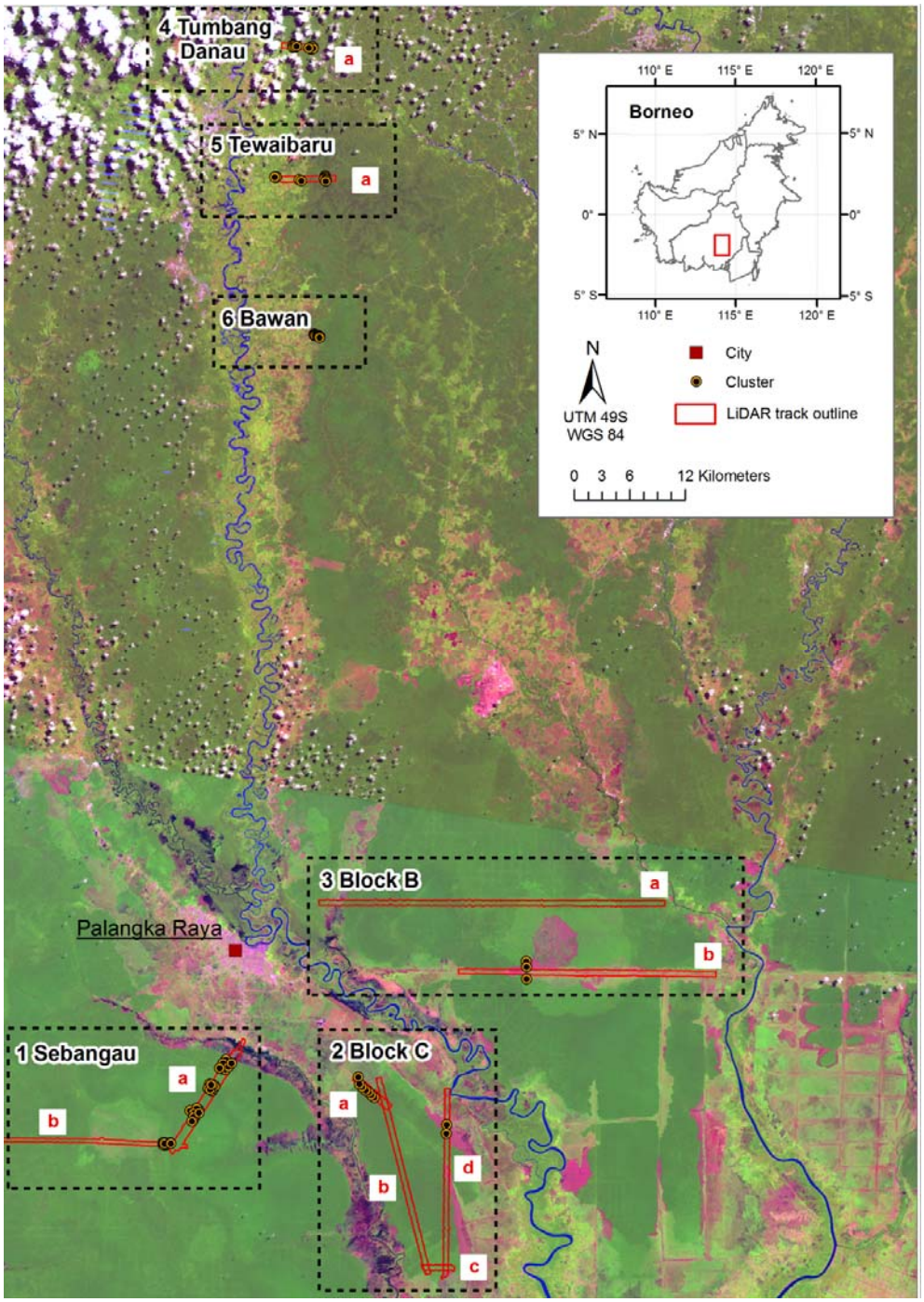

Figure V-1: Overview of field inventory locations, LiDAR tracks and cluster distribution (Landsat scenes: ETM+ 118-61, 2009-05-22 and ETM+ 118-62, 2007-08-05; bands 5-4-3 and both scenes are gap filled)

2.2 Field inventory

Altogether 77 clusters (see section V-2.1) each with four sample plots were selected depending on representativeness of forest type (lowland dipterocarp or peat swamp forest), degradation level (unlogged/little logging, logged and burned), and on accessibility. It has to be considered that unlogged forest is virtually not present in the lowlands of Central Kalimantan (own observations). The cluster positions were set in advance to assure that they lie within the swath of the LiDAR data set. A Global Positioning System (GPS) device (Garmin GPSmap60CSx) was used to locate and mark each sample plot. The four sample plots of one cluster build the corners of a 50×50m square. In each sample plot the angle count method (Bitterlich, 1947) was conducted. A Bitterlich Spiegel Relascope with a wide scale was used to select the trees to be measured. Trees of DBH smaller than 7cm were excluded. To validate the accuracy of the angle count method in tropical forests the nested plot method with circular design was conducted additionally in one to two clusters per forest, sub forest and land use type. The nested plot method is based on fixed-area plots (Pearson *et al.*, 2005a; Pearson *et al.*, 2005b). In each of the three circular nests trees of a certain DBH range were measured: 7 to 20cm (4m radius), 20 to50 cm (14m radius), and greater than 50cm (20m radius). The sum of DBH, tree height, basal area, and biomass per nest was multiplied by an expansion factor in order to get the values per ha. Expansion factors were 198.9 for the small, 16.2 for the intermediate and 8.0 for the large nest, respectively. To test the applicability of the angle count method for biomass estimates in the tropics results were statistically compared to results from the nested plot method. Correlation analysis was carried out applying bivariate correlation tests with the correlation coefficient of Pearson, Kendall's tau b, Spearman's rho, and a two-tailed test of significance. Comparing the means of the two different sampling methods models the Paired Samples T-test for two dependent variables was applied.

For each tree selected by either the angle count or the nested plot method the following parameters were recorded: Local species name, DBH in cm (at 1.3m above the ground), and tree height in m. A HAGA tree height measuring device was used for tree height determination. Local names were translated to corresponding Latin names using information provided by a local herbarium at the Centre for International Co-operation in Management of Tropical Peatland (CIMTROP) in Palangka Raya,

local expert knowledge, and tropical timber databases provided by Chudnoff (1984) and the World Agroforestry Centre (http://www.worldagroforestrycentre.org/Sea/Products/AFDbases/WD/Index.htm (last visited: 07.10.2011). Species specific wood densities were also derived from these databases as well as from IPCC (2006). In case of lacking identification or translation an average specific wood density for Asian tropical forests, 0.57Mg m^{-3}, was applied (Brown, 1997).

AGB was calculated using an allometric model for tropical forest stands from Chave *et al.* (2005). Two models are proposed for moist forest, one of which includes tree height, DBH and wood density, the other includes DBH and wood density, but no tree height. It was decided to use the second model excluding tree height as accurate tree height measurements in the field were impossible due to the dense and tall forest canopy.

Significant differences of the means of DBH, tree height, basal area, number of stems per ha, and AGB between the different forest types and degradation levels (namely more than two independent groups) were determined using One-Way-ANOVA (Analysis of Variance). A subsequent Post-Hoc-Test was applied in order to analyse the differences between two classes individually.

2.3 LiDAR data

2.3.1 Acquisition and processing of airborne laser scanner data

The airborne LiDAR data set was acquired in a flight campaign by Milan Geoservice GmbH and Kalteng Consultants from the 5th to 10th August 2007. During the campaign 13,626ha were scanned. A Riegl LMS-Q560 Airborne Laser Scanner was mounted to a Bell 206 helicopter. Small-footprint full-waveform LiDAR data was collected from a flight altitude of ±500m above ground over a scan angle of ±30 degrees (swath width ±500m). The laser sensor had a pulse rate of up to 100,000 pulses per second with a footprint of 0.25m and a wavelength of 1.5µm (near Infrared). To avoid noise and outliers only echoes with intensity higher than 9 were used in this study. This resulted in an average of 1.4 echoes per square meter. The corresponding GPS ground station for differential geo-correction was located at Palangka Raya airport at an elevation of 25m above sea level (a.s.l.). Position and

orientation of the aircraft and LiDAR measurement system were measured in-flight by GPS and an Inertial Measurement Unit (IMU). The Riegl LMS-Q560 Airborne Laser Scanner system allows height measurements of ±0.02m. Single beam measurements have an absolute horizontal accuracy of ±0.50m and vertical accuracy of ±0.15m Root Mean Square Error (*RMSE*).

A filtering algorithm based on Kraus & Pfeifer (1998) was applied to differentiate between ground and vegetation points. The algorithm is based on linear prediction with an individual accuracy for each measurement. Digital Terrain Models (DTMs) and Canopy Surface Models (CSMs) were generated by interpolating the filtered ground and vegetation points respectively. Ordinary Kriging interpolation method was selected to generate the DTM (cell size 1m). It showed the best results with fewest artefacts. CSMs were generated using the Inverse Distance weighted interpolation (cell size 1m) as point clouds exceeded feasible data size for Kriging. Subtracting the DTM from the CSM resulted in the Canopy Height Model (CHM) which provides an estimate of vegetation height.

2.3.2 Generation of multiple regression models: Plot level approach

The plot level approach of biomass estimation focuses on the direct correlation of the LiDAR 3D point cloud statistics within a defined polygon with the corresponding ground-based AGB value. Multiple regression analysis was applied to create AGB estimation models. Our analysis follows the principles of Magnussen & Boudewyn (1998) and its application follows Lim & Treitz (2004), Patenaude (2004), and Lucas (2006). As the angle count method is designed to extrapolate measurements to 1ha values, a circle of 1ha (56.42m radius around the sample plot center) was used to clip the LiDAR point cloud. The height above the terrain (absolute vegetation heights) for each point within the cloud was determined by subtracting the corresponding pixel value of the DTM. Only points with a value greater than 0.5m were included in the analysis (Lucas *et al.*, 2006). LiDAR point height distributions of each sample plot were analyzed statistically and following metrics were derived and used as predictors: (1) mean h_{mean}, (2) measures of dispersion including the Standard Error of the Mean (*SEM*) h_{SEM}, standard deviation (σ) h_{σ}, variance h_{var}, range h_{range} and

maximum h_{max}, and (3) the quantiles corresponding to the 5, 10, ..., 95 percentiles of the distributions ($h_{5,...,95}$). As a further potential predictor, Canopy Cover (*CC*) was determined. For every pixel of a certain size (5m), *CC* was calculated by dividing the number of points above a certain height threshold (10m) by the number of points below the threshold. The 10-meter-threshold was assumed to be appropriate for getting significant differences between the plots. A small cell size of 5m was used in order to avoid large errors at the borders of the plot circle, since the cut pixels along the border are either counted completely or not.

All above variables within the sampling area of the angle count method were correlated to the corresponding estimated AGB values per ha. Multiple linear regression analysis was conducted for all sample plots as well as for different forest and land use types. Stepwise selection was performed to determine which independent variables should be included in the final models. Further, a log-transformation of the predictors and an exponential regression were tested. For final model validation, the coefficient of determination (R^2), the adjusted coefficient of determination (R^2_{adj}), the Standard Error of the Estimate (*SEE*), and absolute as well as relative Root Mean Square Error (*RMSE*) were used.

2.3.3 Application of the regression models

Fitted regression models were applied to six selected LiDAR tracks which together have a size of 5,241ha (adding up to 93,221m length and on average 562m wide). In lowland dipterocarp forest area, tracks 4a (236ha, Tumbang Danau) and 5a (462ha, Tewaibaru) were analysed. The other four tracks cover peat swamp forest within the Sebangau National Park (parts of track 1a, 556ha and 2, 472ha), Block C (track 2b, 1,280ha) and Block B (track 3a, 2,234ha) (Figure V-1). Each track was overlaid by a grid with a cell size of 100m representing forest inventory plot size (1ha). The point cloud statistics for each grid cell including mean height, canopy cover, standard error of the mean, standard deviation, variance, range, maximum height, percentiles, and standard error of the mean was calculated. Based on these statistics and the regression models developed (see section V-2.3.2) the AGB values for each 1ha grid cell were calculated.

For comparison, a Landsat image (ETM+ 118-62, 2007-08-05) was classified. Prior to the classification the Landsat imagery was geometrically corrected by automated image to image matching techniques. Afterwards a radiometric correction was applied in order to compensate atmospheric distortions, resulting from water vapour, viewing geometry, and other physical parameters. The land cover classification of the imagery was implemented using an object oriented approach, applying a segmentation algorithm prior to the classification. Classification itself corresponds in fact a database query by formulating rule bases on how the objects should be evaluated. The AGB values of the different land cover types were based on standard values of the IPCC (2006) for insular Asia: tropical rain forest (350Mg ha^{-1}, here: pristine peat swamp forest) and tropical shrubland (70Mg ha^{-1}, here: bushland, shrub, regrowth). The class ‘open peat swamp forest’ was assumed to be 75% of the pristine class based on the canopy closure maximum of this class.

2.4 Conceptual overview

Figure V-2 gives a conceptual overview of the methodology described above.

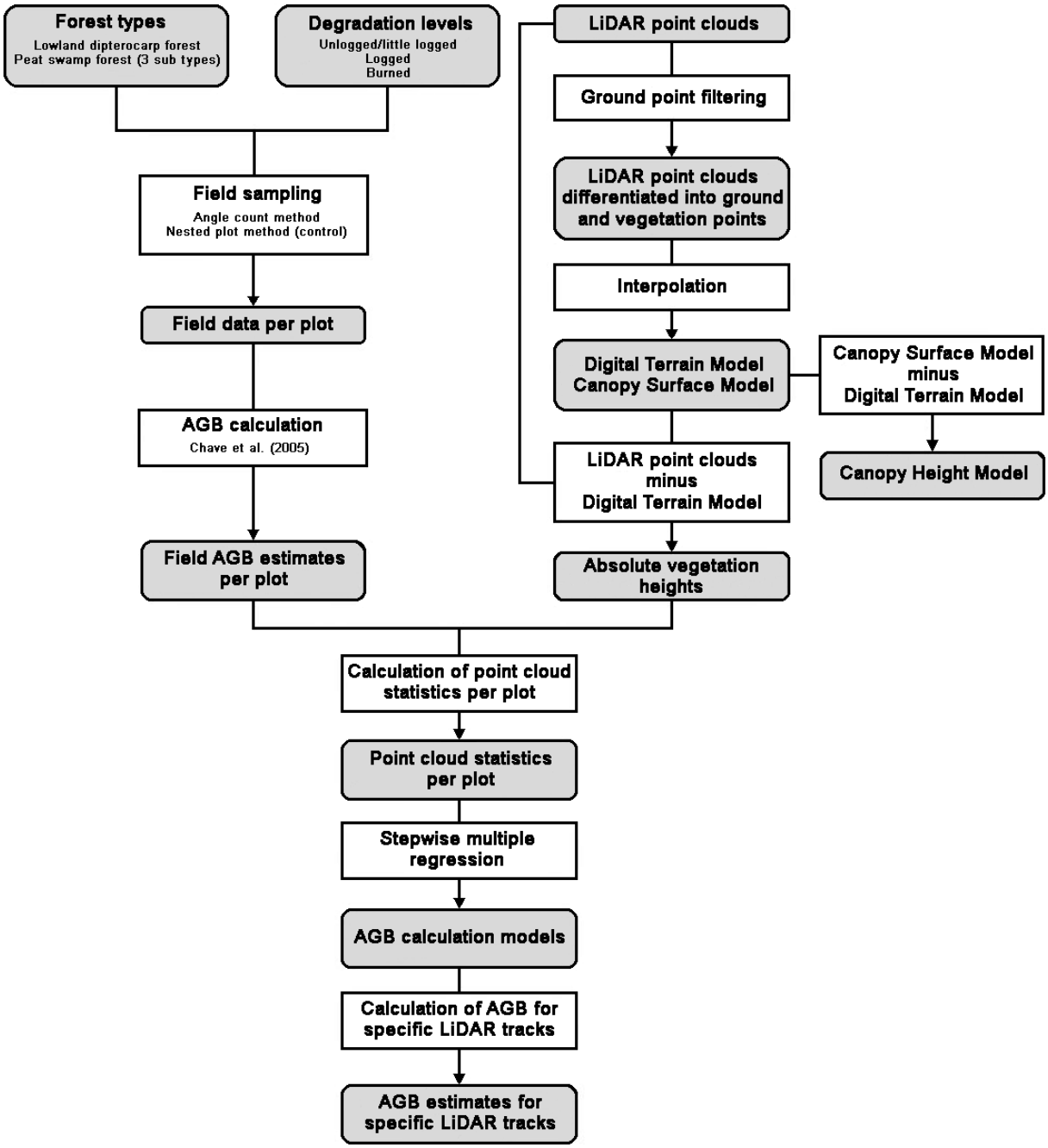

Figure V-2: Conceptual overview methodology (AGB = Above Ground Biomass)

3 Results

3.1 Field inventory analysis

3.1.1 Angle count versus nested plot method

A total of 64 sample plots were measured with both sampling methods. Mean DBH measurements per plot and AGB estimates per ha of angle count and nested plot method were analyzed. DBH showed a significant Pearson correlation of 0.744** (significant at the 0.01-level), so did AGB estimates (0.873**). Both rank correlation coefficients also indicated significant correlations: Kendall's tau b (DBH: 0.654**; AGB: 0.738**), and Spearman's rho (DBH: 0.810**; AGB: 0.889**). Plotting the parameters of the angle count against those of the nested plot method showed linear relationships with a R^2 of 0.55 (DBH) and 0.76 (AGB). The mean, range, and standard deviation of DBH and AGB are clearly higher when applying the angle count method (Table V-1). The latter also produced more outlier and extreme cases of AGB estimates than the nested plot method. The Paired Samples T-Test showed a difference in mean DBH but no significant difference was found between derived AGB. The mean difference between the two sampling design values was 3.3cm and 3.1Mg ha^{-1} respectively. Due to this analysis the remaining field work analysis is based on the angle count method only.

Table V-1: Descriptive statistics and paired differences of DBH measurements and AGB estimates per ha of the two sampling methods (n = 64). (*SEM*: Standard error of the mean; *σ*: standard deviation; Sig. 2-tailed: two-tailed test of significance)

	Sampling method	Mean	*SEM*	σ	Range	Paired difference		
						Mean	*SEM*	Sig. 2-tailed
DBH (cm)	Angle Count	19.77	1.42	11.32	46.47	**3.34**	0.96	0.001
	Nested Plot	16.42	1.21	9.65	38.83			
AGB (Mg)	Angle Count	228.01	26.90	215.20	910.05	**3.13**	13.15	0.813
	Nested Plot	224.89	22.66	181.26	822.69			

3.1.2 Comparison of forest types at different degradation levels

In total 2,788 trees were measured during the two field inventories. The means of DBH, tree height, basal area, number of stems per ha, and AGB per category forest

type/ degradation level are listed in Table V-2. For all parameters, One-Way-ANOVA analysis showed that the mean values of the categories are significantly different. In all categories, the Tamhane Post-Hoc test was used as the variances were tested to be not homogeneous (Levène-Test). The main findings of the Post-Hoc analysis can be summarized as the following:

(1) Mean AGB values per ha are lower in peat swamp forest than in lowland dipterocarp forest. For the mean number of stems per ha this trend is the opposite. Comparing unlogged lowland dipterocarp forest to unlogged peat swamp forest all differences are significant except for the mean number of stems per ha. Differences between logged lowland dipterocarp forest and logged peat swamp forest are all significant except for basal area.

(2) Higher values were measured in unlogged forest. All parameters are significantly higher in unlogged lowland dipterocarp forest than in logged lowland dipterocarp forest. Comparing unlogged to logged peat swamp forest, significant differences are only found for DBH and AGB, none are found for tree height, basal area and number of stems per ha. The latter is higher in logged peat swamp forest.

(3) In burned peat swamp forest, average values of number of stems per ha, basal area, volume, and AGB were significantly lower than all other classes. One-Way-ANOVA and Post-Hoc test results for the class burned peat swamp forest have to be taken with certain care as sample sizes were comparatively small.

Table V-2: Means per ha (in bold) and their respective standard deviation (in italic, below mean) of angle count method field parameters and calculated values (PSF: Peat Swamp Forest; LDF: Lowland Dipterocarp Forest).

	Forest-/ land use type				
	PSF unlogged-little logging	**PSF logged**	**PSF burned**	**LDF unlogged-Little logging**	**LDF logged**
DBH (cm)	**21.6**	**14.7**	**12.7**	**41.2**	**28.6**
	5.3	*4.6*	*16.9*	*13.1*	*10.2*
Basal area (m²)	**30.7**	**25.1**	**1.9**	**51.6**	**25.3**
	12.4	*9.6*	*2.6*	*17.5*	*11.0*
Number of stems	**1,956**	**2,429**	**143**	**1,612**	**1,074**
	1,151	*983*	*282*	*850*	*819*
Tree height (m)	**19.8**	**18.3**	**10.7**	**33.1**	**24.6**
	4.3	*4.6*	*15.1*	*7.2*	*8.0*
AGB (Mg)	**228.1**	**159.9**	**14.6**	**547.1**	**230.8**
	98.1	*88.2*	*22.4*	*193.8*	*104.2*

3.2 LiDAR data analysis

Figure 3 shows examples of the 3D view of a lowland dipterocarp and peat swamp forest DTM and CHM. The DTM of peat swamp forest is very flat in elevation. In contrary, the DTM of lowland dipterocarp forest clearly shows a hilly landscape. The canopy is higher and the crowns appear larger in the CHM of the lowland dipterocarp forest compared to the peat swamp forest. Figure V-3 also shows the frazzled structure of the peat swamp forest canopy. The forest types further differed in laser point distribution (Figure V-4). In peat swamp forest, the vertical distribution is quite even, thus, more laser pulses were able to penetrate the less dense upper canopy layer and reach lower canopies and understorey vegetation. In lowland dipterocarp forest most laser pulses concentrate around the upper canopy layer.

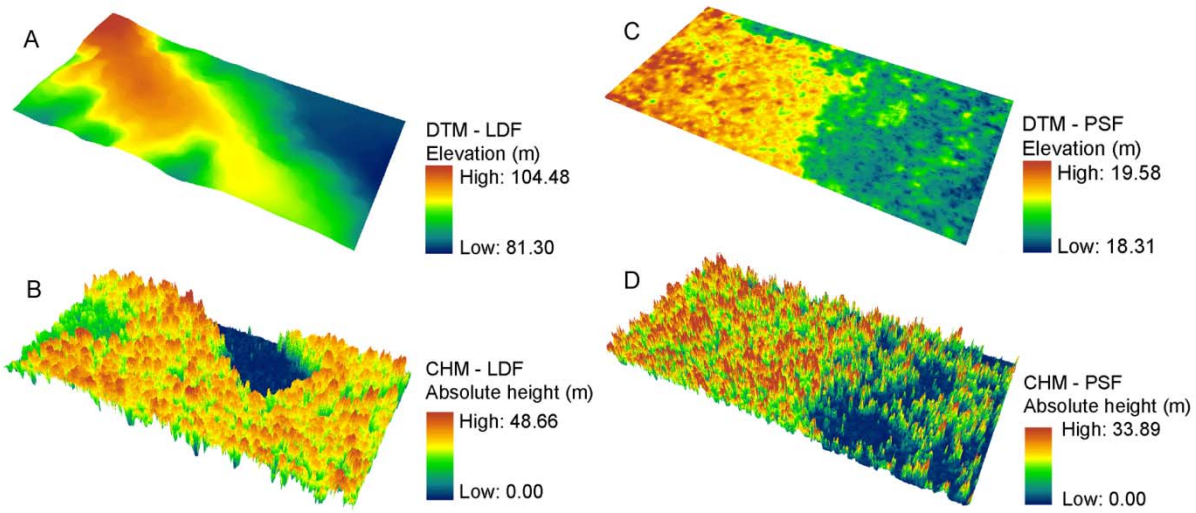

Figure V-3: 3D view of Lowland Dipterocarp Forest (LDF) (left) and Peat Swamp Forest (PSF) (right) surface models: (A, C) DTM, and (B, D) CHM. The 12.5ha subsets of the lowland dipterocarp forest show primary and secondary forest and a just recently abandoned rice field. The peat swamp forest subsets show a transition zone from burned to forested (logged) area. Note the lower tree height compared to those of lowland dipterocarp forest.

3.2.1 Multiple regression analysis: Plot level approach

142 sample plots within unlogged and logged forest could be evaluated and compared. 70 were located in lowland dipterocarp forest and 72 in peat swamp forest. Figure V-4 shows the height distributions of plot point clouds. In unlogged

lowland dipterocarp forest the height range and peak position is clearly higher than in peat swamp forest.

Mean tree height from field measurements and from the sample plot point clouds showed a good relationship in lowland dipterocarp forests (R^2 = 0.71), but no relationship was found in peat swamp forests. The same trend could be observed when plotting the average plot values of the 5th and 85th percentile, and the canopy cover percentage against field AGB. In lowland dipterocarp forest, the best linear relationships were found for the higher percentiles like the 85th (R^2 = 0.73). The parameter *CC* could explain 42% of variation in AGB. The results for peat swamp forest were less significant.

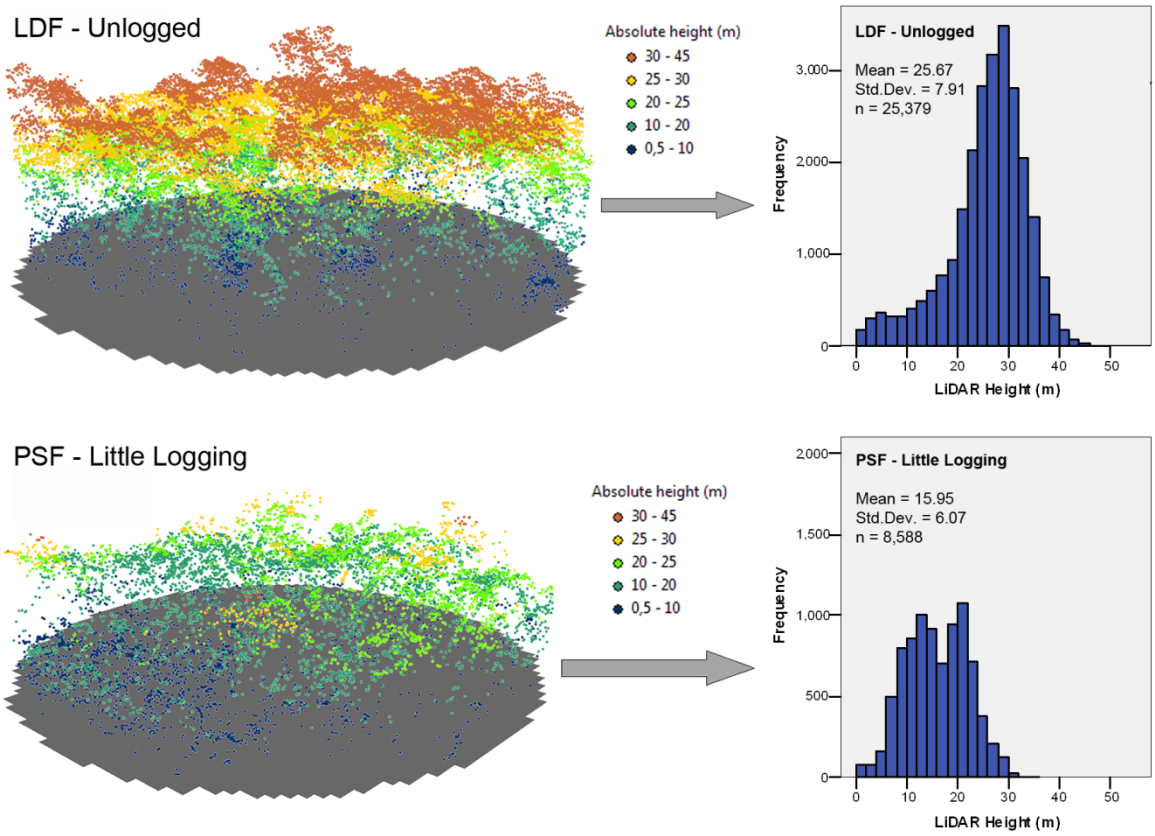

Figure V-4: Distribution of LiDAR point heights within 1ha plots: comparison of lowland dipterocarp forest and mixed peat swamp forest (LDF: Lowland Dipterocarp Forest; PSF: Peat Swamp Forest). Mean tree height, its standard deviation (Std. Dev.) and the total number of points higher than 0.5m (n) is given in the histograms.

Results of multiple regression analysis of the angle count plots are presented in Table V-3 and Figure V-5. Burned sample plots were excluded because too few

samples for different fire impact scenarios had been measured. A linear multiple regression models showed best results. Log-transformation of predictor did not improve the models. Best R^2 values were derived for lowland dipterocarp forests (R^2 = 0.83). The 45th, 65th percentile and the *SEM* were selected (stepwise) as predictor variables with a *RMSE* of 21.37 %. In contrast, the model for peat swamp forest had a very low R^2 of 0.32. Here, only a single variable (50th percentile) was sufficient for biomass prediction. When all sample plots were put together, R^2 is accordingly lower (0.71) than that of lowland dipterocarp forest due to the low results for peat swamp forest.

Table V-3: Results of multiple regression analysis of angle count plots for both forest types (All), for Lowland Dipterocarp Forest (LDF) and for Peat Swamp Forest (PSF) Where No. is model numbers 1 to 3 and *n* (SP) is number of sample plots. Models are validated by the coefficient of determination (R^2), adjusted R^2 (R^2_{adj}), Standard Error of the Estimate (*SEE*), and Root Mean Square Error (*RMSE*).

Forest type	No.	*n* (SP)	Model	R^2	R^2_{adj}	*SEE* (Mg ha^{-1})	*RMSE* (Mg ha^{-1})	*RMSE* (%)
All	1	142	-386.84+ 23.59 * h_{70}+6.52* h_{Range}	**0.71**	0.70	116.44	115.20	33.85
LDF	2	70	-378.07 + 67.99 * h_{65} – 5090.94 * *SEM* – 27.39 * h_{45}	**0.83**	0.82	99.63	96.74	21.37
PSF	3	72	-8.87 + 19.35 * h_{50}	**0.32**	0.31	96.11	94.77	41.02

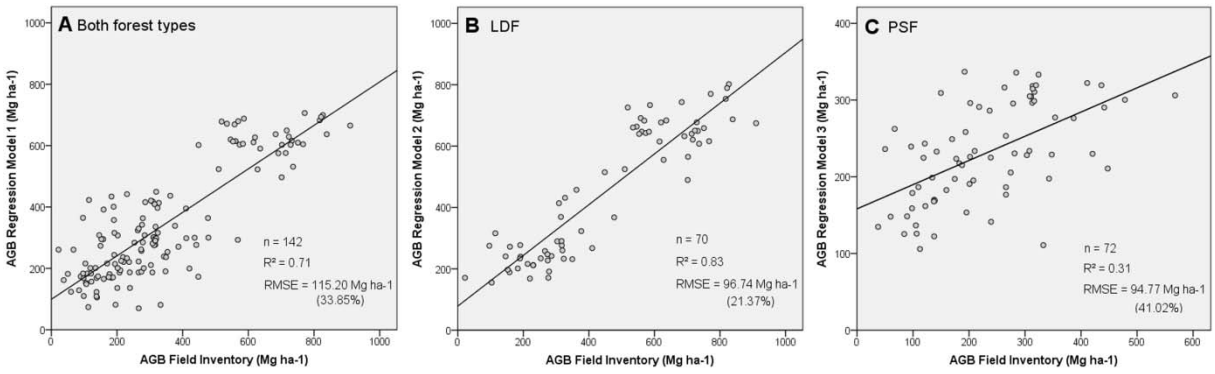

Figure V-5: Comparison of AGB values (Mg ha-1) per sample plot measured in the field and those derived from the established regression models. **A**: Both forest types (model 1). **B**: Lowland Dipterocarp Forest (model 2). **C**: Peat Swamp Forest (model 3).

3.2.2 Application of the regression models

Results of the multiple regression model application are presented in Table V-4. As can be seen the mean AGB values for the intensively logged Tewaibaru lowland dipterocarp forest site (track 5a) are considerably lower than for the less intensively

logged Tumbang Danau lowland dipteropcarp forest site (track 4a). The Sebangau LiDAR track 1b covers a burned scar so that here also the mean AGB value is considerably lower than in the three other peat swamp forest sites (1a, 2b and 3a).

Table V-4: Results of the multiple regression model application for angle count plots (models 2 and 3) for both forest types (LDF: Lowland Dipterocarp Forest; PSF: Peat Swamp Forest; Size: size of LiDAR track in ha; Size appli.: size in ha within the LiDAR track for which AGB was calculated; σ: standard deviation; Sum: sum AGB in Mg for Size appli.).

Track	Size (ha)	Size appli. (ha)	Forest type	Regression model	Mean (Mg ha^{-1})	σ (Mg ha^{-1})	Sum (Mg)
4a (Tumbang Danau)	236	165	LDF	**2**	511.36	189.27	84,374.21
5a (Tewaibaru)	463	352	LDF	**2**	114.40	277,76	40,269.17
1a (Sebangau)	556	320	PSF	**3**	258.47	74.69	82,710.95
1b (Sebangau)	472	295	PSF	**3**	98.41	140.82	29,032.03
2b (Block C)	1280	908	PSF	**3**	251.83	73.69	228,666.04
3a (Block B)	2234	1636	PSF	**3**	214.90	91.86	351,572.63

Figure V-6 shows an example of the AGB estimates calculated for a subset of the LiDAR track 3a (multiple regression model 3). In Figure V-6 A, B, and C1-C3 the LiDAR track and AGB estimates are superimposed on two RapidEye satellite images (West: satellite image taken 2010-02-11, bands: 4, 5, 3; east: satellite image taken 2010-02-10, bands: 4, 5, 3). This subset covers intensively logged and less intensively logged peat swamp forest in the west and two burned scars in the east (burned in 1997/98). Clearly visible is that the AGB values are lower in degraded forests and very low in regrowing forest on a fire scar (Figure V-6 B and C1-C3). This variation is also apparent in the AGB histogram of Figure V-6 E. The two profiles of Figure V-6 D (from the interpolated LiDAR DTM and CSM) show the ground surface, in this case the curvature of the peat dome with an elevation of 13 meters from the edge to the center of the dome and the tree canopy height which also clearly reflects degradation levels.

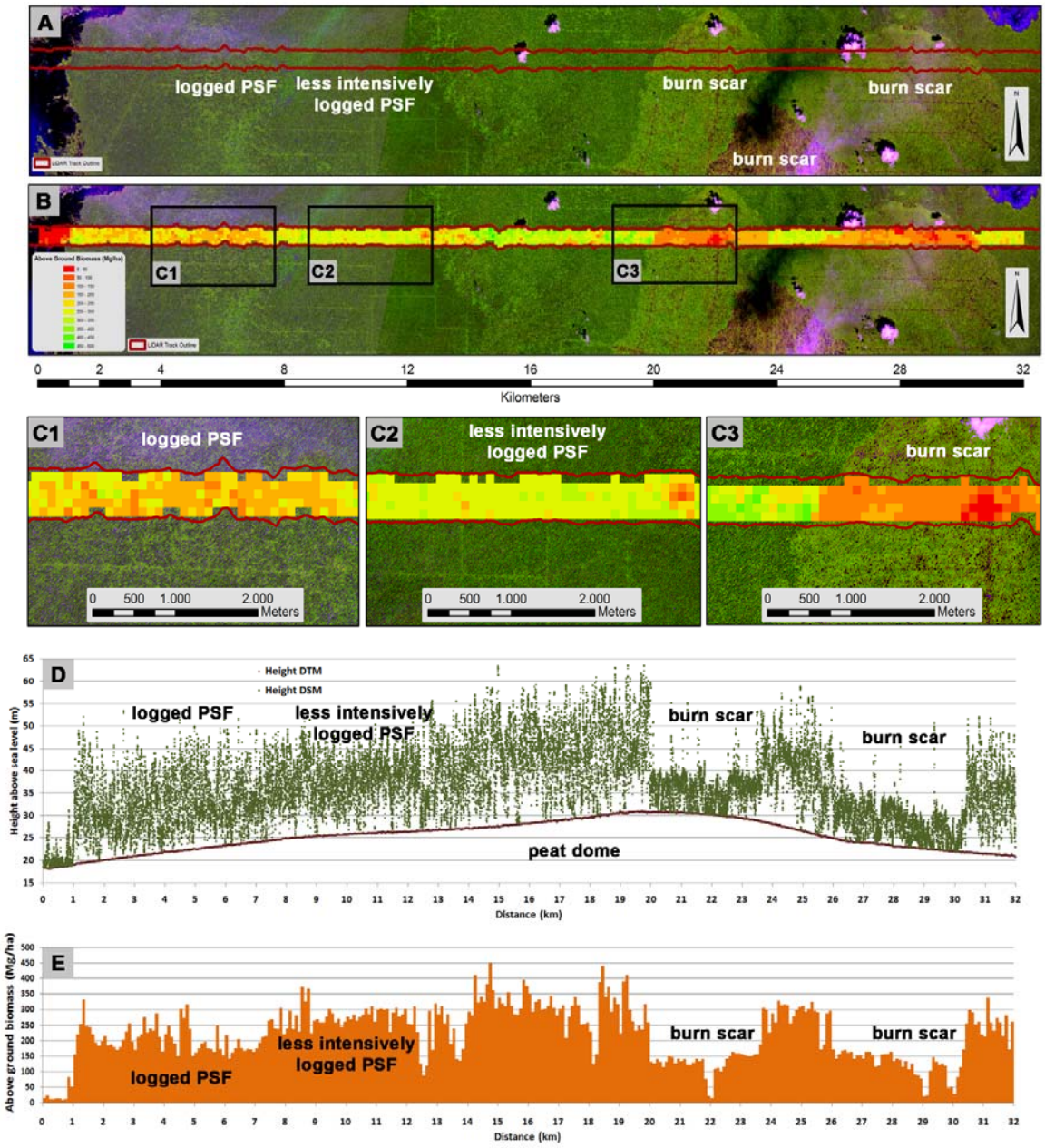

Figure V-6: Results of the multiple regression application for a subset of the LiDAR track 3a (1ha plots and regression model 3). **A**: Outline of a subset of the LiDAR track 3a superimposed on two RapidEye satellite images (West: satellite image taken 2010-02-11, bands: 4, 5, 3; east: satellite image taken 2010-02-10, bands: 4, 5, 3), logged and less intensively logged Peat Swamp Forest (PSF) in the west (logged in the 1990ies) and two burned scars in the east (burned 1997/98). **B**: LiDAR subset of the calculated AGB values from regression model 3 superimposed on two RapidEye satellite images; clearly visible is the AGB variability of the different land cover types. **C1 - C3**: Three subsets from A and B representing logged peat swamp forest (C1), less intensively logged peat swamp forest (C2), and an burned scar (C3); the three black rectangles in B indicate the locations of C1 – C3. **D**: Two height profiles (from the interpolated LiDAR DTM and CSM) representing the center of the LiDAR track. **E**: Histogram of the calculated AGB values along the profile represented by Figure V-6 D.

Figure V-7 illustrates logging impact in Block C of the years 1991 and 2007, and its differing consequence on Landsat classification and LiDAR estimated biomass. Logging activities in peat swamp forest are clearly visible in 1991 (Figure V-7 A). In 2007, this impact can still be recognized visually (Figure V-7 B) but in the Landsat classification these areas are not assigned to open or secondary, but uniformly to pristine peat swamp forest. The calculated AGB estimates of LiDAR track 2b (Block C) clearly show a variation and lower values within the former logging area (Figure V-7 D, E). Comparing mean AGB within the borders of the land cover classes, the mean IPCC value (350Mg ha^{-1}) for pristine forest clearly exceeds the corresponding mean LiDAR estimate (286.46Mg ha^{-1}). The IPCC standard for bushland (70Mg ha^{-1}) is also much higher than the LiDAR estimate (27.88Mg ha^{-1}). The values of open forest are comparable (IPCC: 262.50Mg ha^{-1}; LiDAR mean: 257.58Mg ha^{-1}).

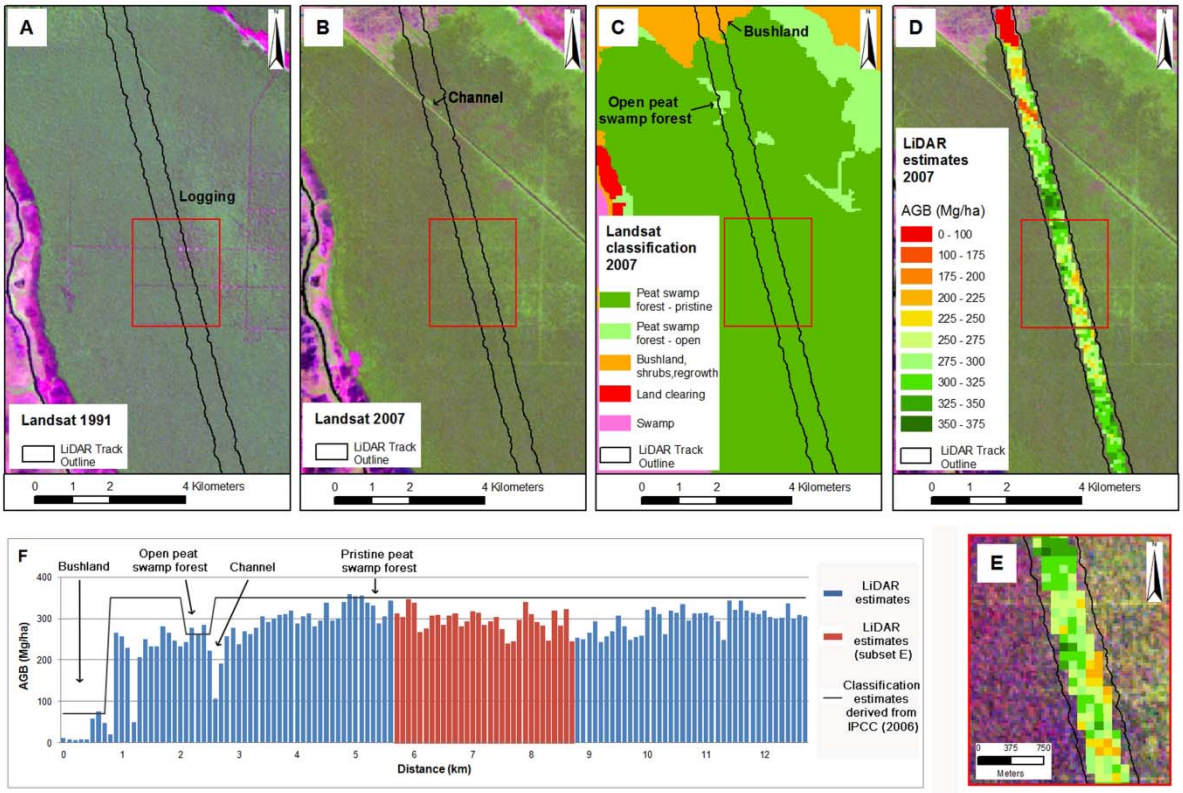

Figure V-7 Illustration of logging impact in Block C at two point of times (1997, 2007), and its differing consequence on Landsat classification and LiDAR estimated Above Ground Biomass (AGB). **A**: Logging activities in peat swamp forest in 1991 (Landsat scene: ETM+ 118-62, 1991-06-30, bands: 5-4-3). **B**: The same extent 16 years later (Landsat scene: ETM+ 118-62, 2007-08-05, bands 5-4-3). **C**: Classification based on Landsat scene 2007. **D**: Subsets of LiDAR track 2b (Block C) showing the calculated AGB values from regression model 3 (background: Landsat scene 2007). **E**: A small subset of the LiDAR track highlighting the former logging area (the extent is shown as a red rectangle in A to D). **F**: Histogram of the calculated AGB values of a profile along the centre of the LiDAR track subset. Mean AGB derived from Landsat classification is shown by the dark grey line (source: IPCC).

4 Discussion and conclusions

Kalimantan's forests serve as an important carbon sink, as does the immense peat layer underlying the peat swamp forests, so that the estimation of the carbon stored within them is of global interest (Gibbs *et al.*, 2007). These forests are also not only a hotspot of biodiversity with numerous valuable timber species (MacKinnon *et al.*, 1996), they are also the home to endangered species like the orangutan (*Pongo pygmaeus*), and the basis of life for indigenous people.

REDD projects, as a tool to stop rapid deforestation, urgently need precise information on AGB storage and on levels of forest degradation over larger areas. This study succeeded in deriving larger scale AGB estimates and showing its spatial variability for Central Kalimantan's peat swamp and lowland dipterocarp forests correlating field estimates with LiDAR point cloud metrics. It provides a possible approach as input to future REDD projects. Further, this study adds new in-situ AGB estimates of forest ecosystems that were barely inventoried in the past. Especially information on biomass in peat swamp forests is limited.

The field inventory derived AGB values are considered to be reliable as they reflect the estimates from the literature and therefore present a robust basis for the correlation to LiDAR data. In the following comparison the respective equations and methods used, and their bias have to be considered. The biome average values for tropical rain forest of IPCC (2006) for insular Southeast Asia agree quite well with the numbers of this study. AGB estimates of unlogged and logged lowland dipterocarp forest (547.08 and 230.84Mg ha^{-1}) are comparable to results from previous studies. No reference was found for lowland dipterocarp forests in Central Kalimantan. In East Kalimantan, Yamakura *et al.* (1986) and Toma *et al.* (2005) reported AGB values of 500Mg ha^{-1} and greater than 400Mg ha^{-1} for original mixed and lowland dipterocarp forest. Ashton & Hall (1992), MacKinnon *et al.* (1996), and Brown (1997) measured AGB in mixed dipterocarp forest in Sarawak, one of the two Malaysian districts on Borneo. Their values lie between 325 and 1,115Mg ha^{-1}. The logged lowland dipterocarp forest biomass value of this study is in the range of the values of fire-degraded lowland dipterocarp forest in East Kalimantan estimated by Toma *et al.* (2005) (117 to 315Mg ha^{-1}). It is slightly below the average estimate of 300Mg ha^{-1} for commercially logged forest in Indonesia reported by Hairiah *et al.* (2001), as well as the biomass values of Brown (1997) measured in medium stocking mixed dipterocarp forest in Sarawak, and logged lowland dipterocarp forests on the Philippines (Brown, 1997) and in Papua (Indonesia) (Stanley, 2009). Secondary dipterocarp forest, selectively logged in the 1940s, reached a biomass value of 547Mg ha^{-1} (Lasco *et al.*, 2004). Waldes & Page (2001) measured AGB of different sup types within the Sebangau peat swamp forests with a range from 249 to 312Mg ha^{-1}. One single plot was measured within the sub type tall interior forest showing a very high AGB value (643Mg ha^{-1}). In this study, the results from Sebangau show relatively homogenous

AGB values for all subtypes (mean of 228.06Mg ha^{-1}, Table V-2). Sebangau forest was logged for more than 20 years. Field plots of this study might have been located closer to a former logging road than those of Waldes & Page (2001). For peat swamp forests in Southern Thailand Kaneko (1992) reported AGB values ranging from 287 to 491Mg ha^{-1} which are slightly higher than the study's estimates. Apart from the difference in geographical location, the extent of logging activities within all peat swamp study areas can be the reason for lower values.

Field derived mean DBH and tree height reflected the expected differences between lowland dipterocarp forest and peat swamp forest described by MacKinnon *et al.* (1996), and between unlogged, logged and burned forest areas. The extreme conditions in peatlands, like acid soil and water logging, lead to an abundance of lower and thinner trees at a higher number. In unlogged lowland dipterocarp forest, the canopy is higher and multi-layered and consequently denser than in peat swamp forest thus hampering the growth of a high number of saplings and understorey trees. In logged lowland dipterocarp forest more sunlight penetrates the canopy and more saplings can grow on the clearances.

The field inventory data was collected under very difficult conditions. Dense vegetation, long walking distances and waterlogged swamps complicated access and measurements. In the following, sources of error are addressed which are possible explanations for differences to literature results or contradicting phenomena. Tree height values were assumed to be relatively inaccurate. A multi-layered and dense canopy made it almost impossible to clearly sight tree tops. Especially in logged forest, dense undergrowth prevented from moving to a point where the tree top could eventually be seen. If different individuals measured tree height an error due to subjectivity was introduced. This error was considered to be higher than an error produced by an AGB prediction model leaving out height as an input variable, supporting the choice of the Chave *et al.* (2005) model excluding tree height. Another source of error is the selection of trees to be measured. Especially in stands with dense undergrowth, the risk of missing trees is high (Köhl *et al.*, 2006). This is more serious when using the angle count method, but cases of extremely dense undergrowth, trees can also be missed when applying the nested plot method as moving around is limited. The correct translation from local to scientific tree species names was not possible for about 24% of the measured trees. These trees were

attributed with a standard wood density of Brown (1997).The use of an average introduces a bias in the biomass estimates as this constant might not represent the actual density value of a plot.

The angle count method could be shown to be an adequate sampling method for the purpose of fast, quantitative sampling. The comparison of mean DBH and AGB estimates from plots where angle count and nested plot method were used showed positive correlations. Despite the higher risk of missing trees in dense stands (Köhl *et al.*, 2006), the angle count method was assumed to be applicable in all forest types. Nevertheless, strong correlations do not provide for a small bias. Since a high number of sample plots are necessary for the correlation of the field data to LiDAR measurement, the time-saving of the angle count method outweighs this loss in accuracy.

This study shows that decomposed full-waveform, small-footprint LiDAR data can be used for AGB estimation in Central Kalimantan. The multiple regression analysis on plot level brought good results for lowland dipterocarp forest with model validation being comparable to literature values. The approach showed some weakness when applying it to peat swamp forests and further study is necessary to confirm current results. However, the subsequent application of the regression models to complete LiDAR tracks demonstrated the ability of this approach to monitor not only deforestation but especially forest degradation and its variability at high spatial resolution.

The derived coefficient of determination of lowland dipterocarp forest (model 2: R^2 = 0.83, *RSE* = 99.63Mg ha^{-1}, *RMSE* = 96.74Mg ha^{-1} or 21.37%) is comparable with those reported in studies throughout different biomes. LVIS data was successfully analyzed for forests in Costa Rica (Drake *et al.*, 2002a) with slightly higher R^2 of 0.89 (*RMSE* = 22.54Mg ha^{-1}). Asner *et al.* (2009) quantified AGB of a 5,016ha rain forest reserve on Hawaii Island using vertical profiles of a full waveform LiDAR system. Field-measured AGB of 59 plots (24 and 30m radius) was predicted by the mean canopy height (R^2 = 0.78), one of the vegetation LiDAR metrics developed by Lefsky *et al.* (1999a). Applying this approach in the Peruvian Amazon improved the coefficient of determination (R^2 = 0.85) (Asner *et al.*, 2010). Analyzing discrete return data from a range of forest communities and structural types in Injune (Australia), Lucas *et al.* (2006) derived a R^2 of 0.92 (*SEE* = 12.06Mg ha^{-1}). Only 32 sample plots

(50x50m grids) were evaluated which had ground-measured AGB values ranging from about 2 to 160Mg ha^{-1}. The resulting equation was comprised of seven predictors (percentiles 5, 10, 20, 40, 75, 85 and *CC*), whereas in this study only three variables (percentile 45, 65 and the *SEM*) predict the AGB of lowland dipterocarp forest best.

Also using the concept of Magnussen & Boudewyn (1998), but log-transformed, Naesset (2004) reported coefficients of determination of 0.83 to 0.97 for volume estimation in boreal forests of Norway. Nearly 1,400 plots of 200 to 400m² were analyzed and produced a model with a *RMSE* of 32.9 to 67.8m³ ha^{-1} (17.5 to 22.5%). Stands mainly containing *Picea abies* (96%) in Vorarlberg (Austria) were estimated by Hollaus *et al.* (2007) like in Naesset (2002, 2004). Volume data of plots of 10m radius (n = 103) ranging from 15.7 to 1,137.7m³ ha^{-1} were used for regression analysis (R^2 = 0.85, *RMSE* = 90.9m³ ha^{-1} or 21.4%). Lim & Treitz (2004), analyzing hardwood forest in Ontario, reported a R^2 from 0.82 to 0.90 (*RMSE* of 48.07 to 66.65Mg ha^{-1}) for logarithmic models each with one quartile as predictor. The 75th quartile has the lowest *RMSE*. 36 sample plots of 400m² were used as reference. Using large-footprint full-waveform data derived from SLICER, Means *et al.* (1999) could establish an AGB model with a very high R^2 of 0.96 (*RMSE* = 88Mg ha^{-1}) for a douglas-fir stand in Oregon. The single equation of Lefsky *et al.* (2002a, 2005) could explain 84% of variation in three biomes within North America.

All studies employing the quantile-estimator approach have correlated AGB values and height characteristics, etc. obtained from relatively small areas compared to the 1-ha-plots used in this study. Inaccuracy of plot location produced by GPS devices is more an issue for smaller plots, but they have the advantage that the biomass is determined for exactly this area. In the 1-ha-plots, the accuracy problem is minimized, but the extrapolated biomass value does not necessarily match to the whole area. The GPS accuracy range of 3 to 10m in the field inventory of 2008, and only 8 to 20m in 2007, supports the choice of 1-ha-plots in this study. Smaller plots of different size, also using AGB estimates from the nested plot method will be tested in future.

The difference between regression results of the forest types is considerable. In peat swamp forests, all height characteristics plotted against AGB field measures showed a poor relationship compared to those of lowland dipterocarp forests. Therefore,

height characteristics do not seem to be very strong predictors of AGB in peat swamp forests. The occurrence of *CC* in most peat swamp forest regression models generated during this study further indicates that biomass of peat swamp forests might be better predicted by different density metrics. This should be tested in further studies. In contrary, AGB of lowland dipterocarp forest seems to be highly dependent on height. *CC* does not occur in the lowland dipterocarp forest model.

Another possible explanation could be that filtering for ground points was more difficult in peat swamp forest LiDAR tracks. Filtering for ground points plays a key role in LiDAR data analysis. Peat swamp forest grows on very flat and even terrain usually covered by dense, scrubby undergrowth like *Pandanus spp*. Signals from the true soil surface and signals from scrubs and low growing leaves are not easy to differentiate. The error produced here and by the interpolation process could not be quantified because of a lack of reliable fine scale elevation data from the field. In addition, peat swamp forests are not as multi-layered as lowland dipterocarp forest. The tree crowns are quite small and in degraded forest they appear frazzled (Figure V-3). One canopy layer might be more or less missing due to logging operations. This fact may also contribute to the poor relationship of height distributions.

When applying the regression models to different LiDAR tracks covering unlogged, logged and burned lowland dipterocarp and peat forest it is possible to quantify natural biomass variability and forest degradation by logging and fire with high spatial resolution (Figures V-6 and V-7). This clearly is an advantage to indirect AGB estimations where AGB values are attributed to land cover types not considering the spatial variability within these land covers. As shown by the comparison of Landsat and LiDAR analysis (Figure V-7), Landsat classification tends to overestimate biomass as it neither detects degraded forest from smaller scale logging activities and selective logging, nor from logging in past decades. By analyzing spectral information, large areas of forest are assigned to be one class. Thereby, the negative impact of named logging activities on AGB or carbon content is neglected. The plot level analysis of LiDAR data makes it possible to detect these former logging activities.

Since our approach is almost completely automated, extensive LiDAR tracks can be assessed in very short periods of time. LiDAR-derived values can be extrapolated to large-scale vegetation maps (Asner *et al.*, 2010; Englhart *et al.*, 2011). Englhart *et al.*

(2011) succeeded to directly estimate AGB combining two spaceborne SAR-instruments (TerraSAR-X and ALOS PALSAR). The model was calibrated using field data and the peat swamp forest model of our study. The model does not saturate until 300Mg ha^{-1}.

For the future, the generation of allometric models from destructive sampling is of high importance, especially for peat swamp forest. Bias from generic models could be decreased. Concerning the plot level analysis further study should focus on the inclusion of density metrics into regression analysis. Laser pulse intensity might also be a helpful parameter, implementing it as a weight for each laser point. Generally, the analysis of leaf area index- and crown cover photos from the field might be a valuable complement to the current findings. More sample plots in low biomass stands are currently established to optimize the multiple regressions models because most models had problems calculating AGB values for grid cells with obviously low biomass. Different plot/ grid cell sizes should also be tested. Generating new parameters at varying plot sizes, variable selection, variable transformation, and model formulation have to be considered anew.

Concluding, it can be stated that the combined approach of extensive field sampling and LiDAR point cloud analysis have high potential to significantly improve current estimates of carbon stocks across different forest types and degradation levels and its spatial variation in the highly inaccessible tropical rainforests of Kalimantan. A basis for AGB estimation in the framework of REDD projects has been created but, of course, further work is needed to reach more precise prediction models and to create a final tool to predict AGB for larger areas in a relatively short time.

Acknowledgements

We gratefully acknowledge JP Morgan for the financial support considering the LiDAR data. We would like to thank Suwido Limin and his team from CIMTROP for the logistic support during the field inventory and Sampang Gaman (CIMTROP) and Simon Husson (Orang Utan Tropical Peatland Project, OUTROP) for providing their tree species lists. Further we would like to thank FORRSA (Forest Restoration and Rehabilitation in Southeast Asia) project of the EU-funded Asia Link programme for financially supporting the field trips to Indonesia.

CHAPTER VI:
Deriving forest above ground biomass in Central Kalimantan (Indonesia) using airborne LiDAR

Manuscript in preparation for *Nature Climate Change*

Juilson Jubanski[a], Uwe Ballhorn[a,b], Karin Kronseder[a,b], Florian Siegert[a,b]

[a]Remote Sensing Solutions GmbH, Isarstrasse 3, D-82065 Baierbrunn, Germany

[b]Biology Department II, GeoBio Center, Ludwig-Maximilians-University, Grosshaderner Strasse 2, D-82152 Planegg-Martinsried, Germany

Abstract

The quantification of tropical forest carbon stocks over large geographic areas is a key challenge in creating a basic methodology for Reduced Emissions from Deforestation and forest Degradation in developing countries (REDD+) projects. As the main carbon pool of tropical forests is typically the Above Ground Biomass (AGB) (Brown, 1997; Chave *et al.*, 2005; Gibbs *et al.*, 2007) we estimated AGB of different tropical forests in the Indonesian province of Central Kalimantan through correlating airborne Light Detection and Ranging (LiDAR) data to forest inventory data. Two metrics, the Quadratic Mean Canopy profile Height (QMCH) and the Centroid Height (CH) from the LiDAR height histogram, which was developed for this study, were analysed. The regression models could be improved through the use of the LiDAR point densities as weight. The highest coefficient of determination was achieved for CH (R^2 = 0.88, n = 52). Rigorous covariance propagation analysis showed that surveying with a LiDAR point density between 2 and 4 points per square meter (pt/m^2) results in the best cost-benefit relation. A Landsat based classification approach resulted in an overestimation of 60.8% compared to the LiDAR derived AGB estimates for a 2,987,726ha study area. This AGB overestimation can lead to significantly wrong emission estimates and compensation payments. The best solution to monitor tropical forest carbon stocks would be the continuous mapping with airborne LiDAR data, which is not feasible for large-scale use due to the relatively high cost of operation. The combination of satellite data, LiDAR, and field plots, however, would be a cost effective alternative and reduces uncertainty in estimating carbon densities for REDD+ projects. Further the new approach presented here, through using CH and the LiDAR point densities as weight, has a high potential to improve current estimates of carbon stocks in these highly inaccessible tropical rainforests.

1 Summary and conclusions

It is estimated that in 2008, worldwide deforestation and forest degradation emissions contributed about 6% to 17% of the total anthropogenic carbon dioxide (CO_2) emissions (Van der Werf *et al.*, 2009). Between 1990 and 2005 about 13 million hectares (ha) of tropical forest were deforested annually and with 0.98% South and Southeast Asia had one of the highest annual deforestation rates for the time period of 2000 to 2005 (FAO, 2006). Deforestation and forest degradation in this region are almost exclusively caused by human economic activities such as shifting cultivation, illegal logging, and the establishment of industrial timber estates and large-scale oil palm plantations (Siegert *et al.*, 2001; Rieley & Page, 2005; Langner *et al.*, 2007; Hansen *et al.*, 2009; Langner *et al.*, 2009). In Indonesia increased Green House Gas (GHG) emissions are particularly evident in the coastal lowlands of Sumatra and Kalimantan, where peat fires and peat decomposition, due to peatland drainage, result in the release of huge amounts of CO_2 (Page *et al.*, 2002; Ballhorn *et al.*, 2009; Hooijer *et al.*, 2010).

One important measure of the United Nations Framework Convention on Climate Change (UNFCCC) to curb GHG emissions from this sector is the REDD+ programme which involves the private sector of industrialized countries in the protection of the remaining tropical forests to compensate the exceeding of their GHG emission quota. To estimate GHG emissions from deforestation and forest degradation information on both the area of forest loss and/or degradation and the corresponding carbon stock of the land that is cleared and/or degraded is needed which remains a big challenge in tropical forests (Gibbs *et al.*, 2007). Especially GHG emission from forest degradation is difficult to monitor, particularly considering that degraded and regrowing forests are predicted to include increasingly large portions of the tropics (Gibbs *et al.*, 2007). The main carbon pool of tropical forest ecosystems is typically the AGB (Brown, 1997; Chave *et al.*, 2005; Gibbs *et al.*, 2007). However, the structural and biotic complexity of tropical forest causes difficulties for the inventory: the generic relationships are not appropriate for all regions, inventories can be expensive and time-consuming, and it is challenging to produce regionally and globally consistent results (Chave *et al.*, 2005; Gibbs *et al.*, 2007). AGB can also be estimated by remote sensing, but no remote sensing instrument can detect AGB

values directly, so that additional in situ data collection is necessary (Drake *et al.*, 2003; Rosenqvist *et al.*, 2003).

Airborne LiDAR provides three-dimensional information of forest structure and represents a potential technique for biomass quantification and monitoring. LiDAR systems have certain advantageous characteristics, such as high sampling intensity, direct measurements of heights, precise positioning, and highly automated processing (Mallet & Bretar, 2009). These properties make airborne LiDAR systems an efficient tool for direct assessment of vegetation characteristics and deriving forest biomass at multiple scales from individual trees (e.g. Popescu, 2007; Zhao *et al.*, 2009) to large contiguous forest stands (e.g. Means *et al.*, 1999; Lefsky *et al.*, 1999a; 1999b; 2002a; 2005; Asner *et al.*, 2009; 2010).

The main goal of this study was the estimation of AGB values for different tropical forests in the Indonesian province of Central Kalimantan through small-footprint full-waveform LiDAR data analysis (Figure VI-1). Central Kalimantan comprises a peat dominated landscape where large-scale peatland drainage systems and resulting repeating severe wildfires destroyed large tracts of these peatland ecosystems (Rieley & Page, 2005). The LiDAR point clouds were analysed using two techniques: the Quadratic Mean Canopy profile Height (QMCH) (Asner *et al.*, 2010); and the Centroid Height (CH), which was developed for this study (see methods). These parameters were correlated to the field-measured AGB on plot level (0.13ha) in order to establish robust non-linear biomass estimation models (see methods). As additional parameter to improve the robustness of the models, the LiDAR point density per square meter (pt/m^2) at each plot was treated as weight during the regression (see methods). The biomass estimation models were applied to 33,178ha of LiDAR tracks covering diverse forest types in Central Kalimantan (Figure VI-1). Further the LiDAR AGB estimates were quantitatively compared to results obtained by an object-oriented land cover classification based on Landsat imagery for a 2,987,726ha study area (see methods). Finally the developed approach was tested for its applicability as input to a basic methodology for future REDD+ projects.

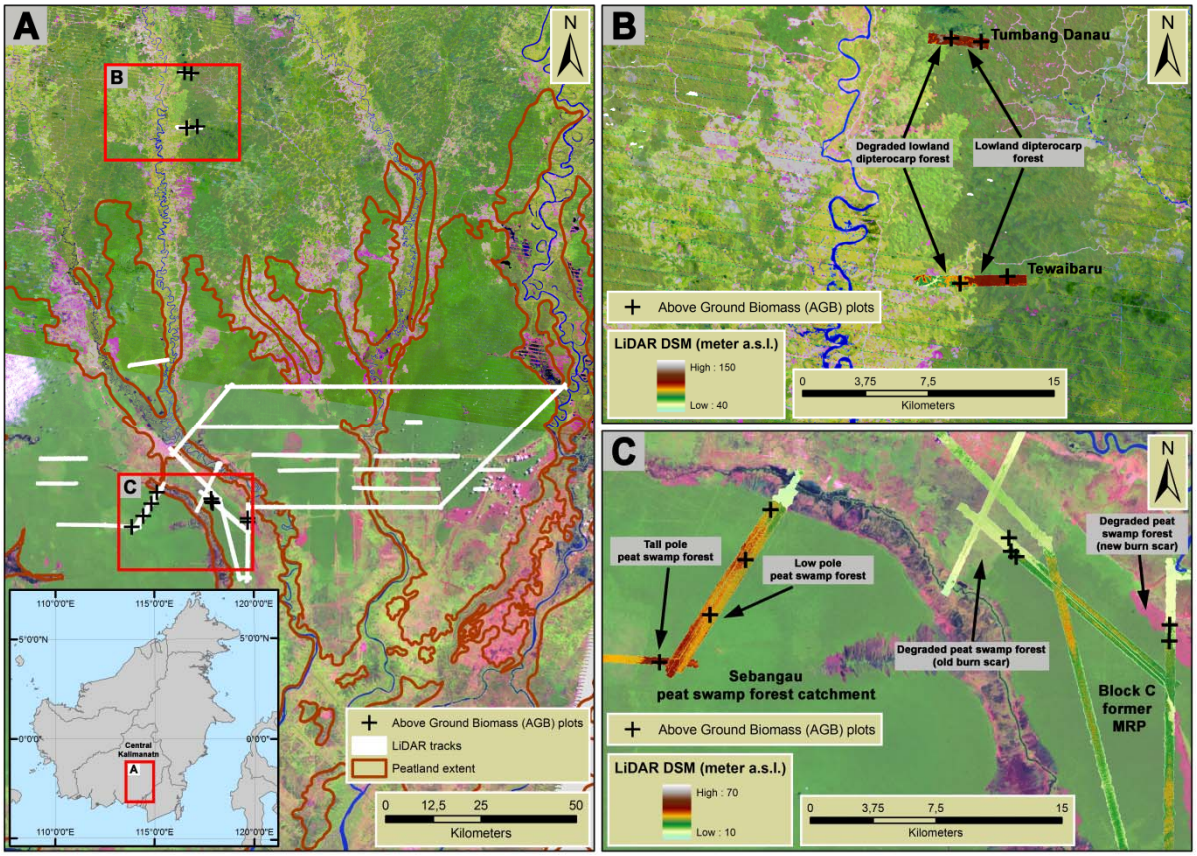

Figure VI-1: Location of the LiDAR tracks and Above Ground Biomass (AGB) plots (0.13ha) within Central Kalimantan, Indonesia, superimposed on Landsat imagery (ETM+ 118-61, 2009-05-22 and ETM+ 118-62, 2007-08-05; bands 5-4-3 and both scenes were gap filled). The red rectangles show the location of A, B, and C. In B and C also the LiDAR derived Digital Surface Models (DSM) are shown.

Four main forest types - tall peat swamp forest, low pole peat swamp forest, degraded forest (logged or burned) and lowland dipterocarp forest - were analysed. Figure VI-2 shows four typical field plots, one for each of the analysed forest types, their LiDAR height profiles with absolute vegetation heights, and the derived LiDAR height histograms. These LiDAR height histograms illustrate the clear structural differences between the different forest types.

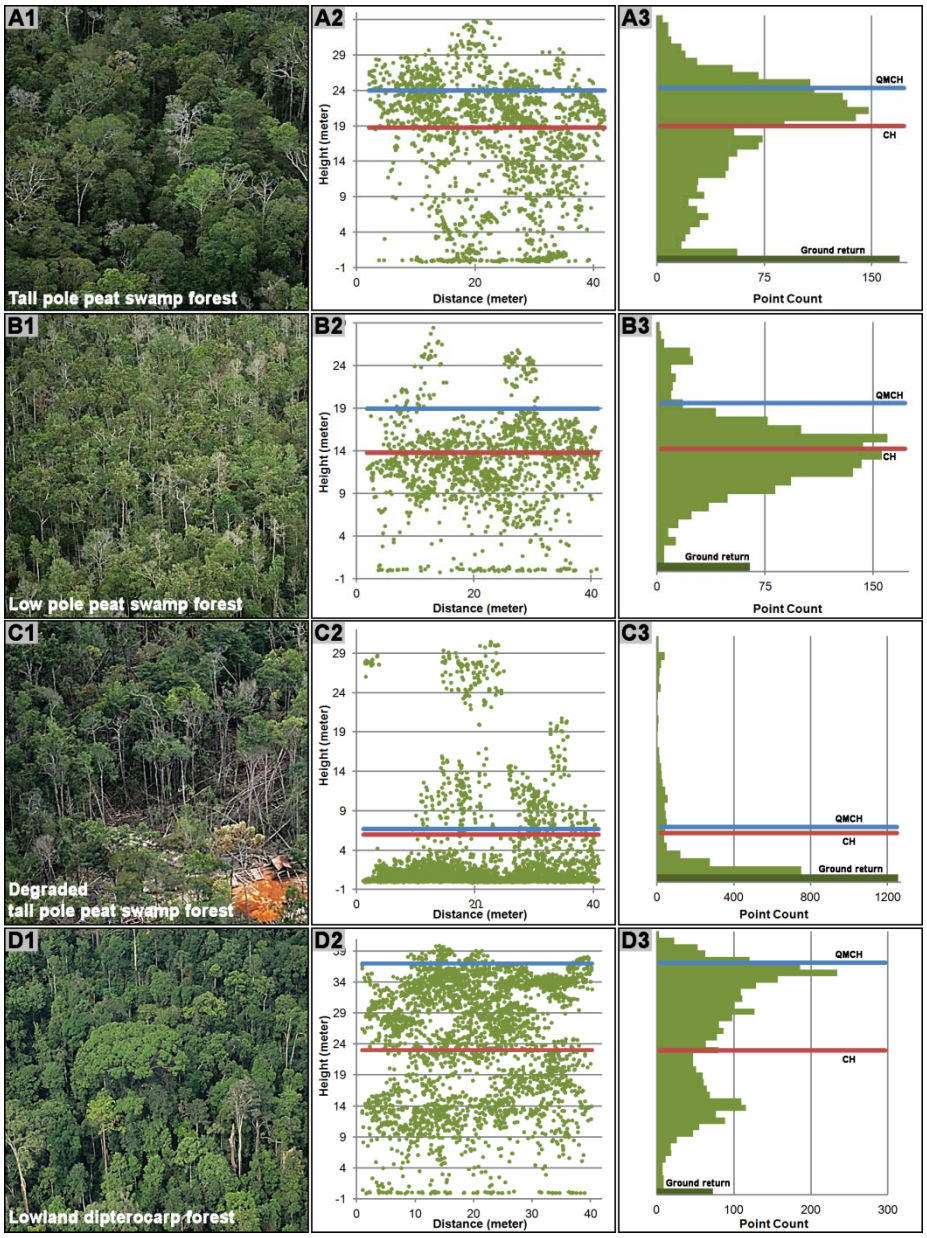

Figure VI-2: (A) shows a plot within tall pole peat swamp forest (AGB = 57.61t/0.13ha, LiDAR point density = 1.5pt/m^2, Centroid Height (CH) = 18.7m, Quadratic Mean Canopy profile Height (QMCH) = 24.0m). Observe in A2 and A3 that the CH and the QMCH are located in high levels of the forest. (B) shows a low pole peat swamp forest (AGB = 19.12t/0.13ha, LiDAR point density = 1.1pt/m^2, CH = 13.7m, QMCH = 18.9m) with emergent trees. In B3 the forest structure can be clearly observed (a small peak at about 24m representing the emergent trees and a large peak at about 14m representing the main canopy layer). (C) shows a degraded tall pole peat swamp forest (AGB = 5.05t/0.13ha, point density = 2.9 pt/m^2, CH = 5.8m, QMCH = 6.2m). The small peak in C2 at about 26m height indicates remaining high trees. C3 shows clearly the dominant ground return. Note also that the CH and the QMCH are located in similar heights. (D) shows a lowland dipterocarp forest (AGB = 108.20t/0.13ha, LiDAR point density = 2.3pt/m^2, CH = 25.3m, QMCH = 35.3m). The two main peaks in D3 (at about 14m and 34m) indicate a higher and more complex structured canopy.

Figure VI-3A shows the results for the regression using the CH as input. A high correlation coefficient (R^2 = 0.88) was obtained when the LiDAR point densities per square meter (pt/m^2) were treated as weight during the regression. The derived coefficient of determination is comparable with those reported in studies throughout various tropical biomes (Drake *et al.*, 2002a; Asner *et al.*, 2009; 2010). Also for the QMCH a high correlation was obtained (R^2 = 0.84) when applying the LiDAR point density weighting (Figure VI- 3B). In both cases, the use of the LiDAR point densities as weight improved the regression models (9% and 8% for the CH and QMCH respectively). As the presented approach is easy to reproduce it would be of interest whether these improved results are also observed for other tropical forest ecosystems around the world.

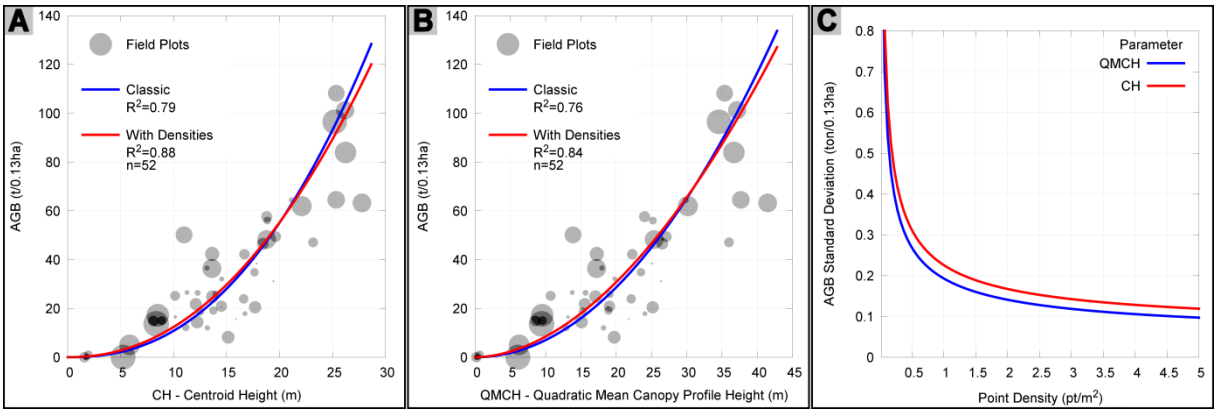

Figure VI-3: (A) In red the Centroid Height (CH) based regression model with LiDAR point density weighting (AGB = 0.0865 x CH$^{2.1564}$; R^2 = 0.88) and in blue without weighting (AGB = 0.0484 x CH$^{2.3494}$; R^2 = 0.79). (B) In red the Quadratic Mean Canopy profile Height (QMCH) based regression model with LiDAR point density weighting (AGB = 0.1150 x QMCH$^{1.8656}$; R^2 = 0.84) and in blue without weighting (AGB = 0.0660 x QMCH$^{2.0277}$; R^2 = 0.76). The circle sizes represent the point densities (the smallest about 0.2pt/m^2 and the biggest about 3.5pt/m^2). (C) Standard deviation behaviour estimation curves for CH and QMCH based regression models (derived from the covariance propagation analysis).

Next the AGB estimates for 15,950ha of LiDAR tracks were compared to the Landsat land cover classification (Table VI-1, see methods). Through applying the CH based regression model it was possible to quantify natural AGB variability (linked to soil properties and water availability) and the impact of previous logging operation and fire with high spatial resolution. Variability could also be detected in low AGB ranges. These disturbances cannot be identified unambiguously in Landsat imagery. By

analysing spectral information, large areas of forest are assigned to be one class (e.g. pristine peat swamp forest). Thereby, the negative impact of named degradation activities on AGB or carbon content is neglected. In our study this leads to a serious overestimation of the AGB by the indirect method, while with LiDAR it is possible to detect these previous disturbances. Table VI-1 shows that 43.1% of the LiDAR track area has been classified as pristine peat swamp forest constituting approximately 80% of the total AGB. The LiDAR estimate for this class is 52.3% lower than the literature value. Similar relations were found in all other classes and therefore the direct LiDAR based AGB estimate is 56.3% lower than the indirect method via optical remote sensing considering the intersected area, and 60.8% lower considering a 2,987,726ha study area (Table VI-1, Figure VI-4). These results are in accordance with a study by Asner *et al.* (2010) who observed a 33% lower regional carbon estimate than by a default estimation approach based on average Intergovernmental Panel on Climate Change (IPCC, 2006) carbon values assigned to biomes in the Peruvian Amazon. These AGB overestimations can lead to significantly wrong emission estimates and compensation payments.

Table VI-1: Above Ground Biomass (AGB) comparison between the LiDAR based estimation model and the object-oriented land cover classification based on Landsat in which each class was linked to a single AGB value determined from a regional biomass database.

Class		Averaged AGB (t/0.13ha)		Total AGB (t)				Difference (%)
Name	% Area	Landsat	LiDAR	Landsat	%	LiDAR	%	
Peat swamp forest - pristine	43.1	40.56	19.13 ± 9.91	2,146,981	79.3	1,012,852	85.6	-52.8
Bushland, secondary forest, shrubs	33.5	3.90	0.81 ± 3.18	160,066	5.9	33,626	2.8	-78.9
Land clearing for plantation	8.3	9.49	0.30 ± 1.10	96,742	3.5	3,129	0.3	-96.7
Peat swamp forest - open, canopy closure < 75%	5.7	30.42	15.49 ± 14.72	215,195	7.9	109,634	9.2	-49.0
Peat swamp forest - fragmented, burned	8.2	8.11	2.34 ± 4.12	80,900	2.9	23,435	1.9	-71.0
Swamp	1.2	5.72	0.46 ± 1.31	8,432	0.3	692	>0.1	-91.7
		TOTAL (Intersection)		**2.71Mt**		**1.18Mt**		**-56.3**
		TOTAL (whole study area)		**398.23Mt**		**156.25Mt (±139.25Mt)**		**-60.8**

Figure VI- 4 shows the results for both up-scaling approaches (Figures VI-4C and VI-4D), as well as a LiDAR track (888ha) covering three main land cover classes (Figures VI-4E and 4F): burned peat swamp forest (fire scar from 1997), open peat swamp forest (logged), and pristine peat swamp forest. Figure VI-4E shows the LiDAR AGB estimates superimposed on the Landsat based land cover classification. Figure VI-4F shows the AGB profile (along the black line indicated in Figure VI-4E) for the direct LiDAR AGB estimate and the indirect AGB estimate based on the Landsat land cover classification. The profile clearly shows the ability of airborne LiDAR to describe AGB variations with high resolution. The Landsat based AGB estimates only determine variations between the three land cover classes.

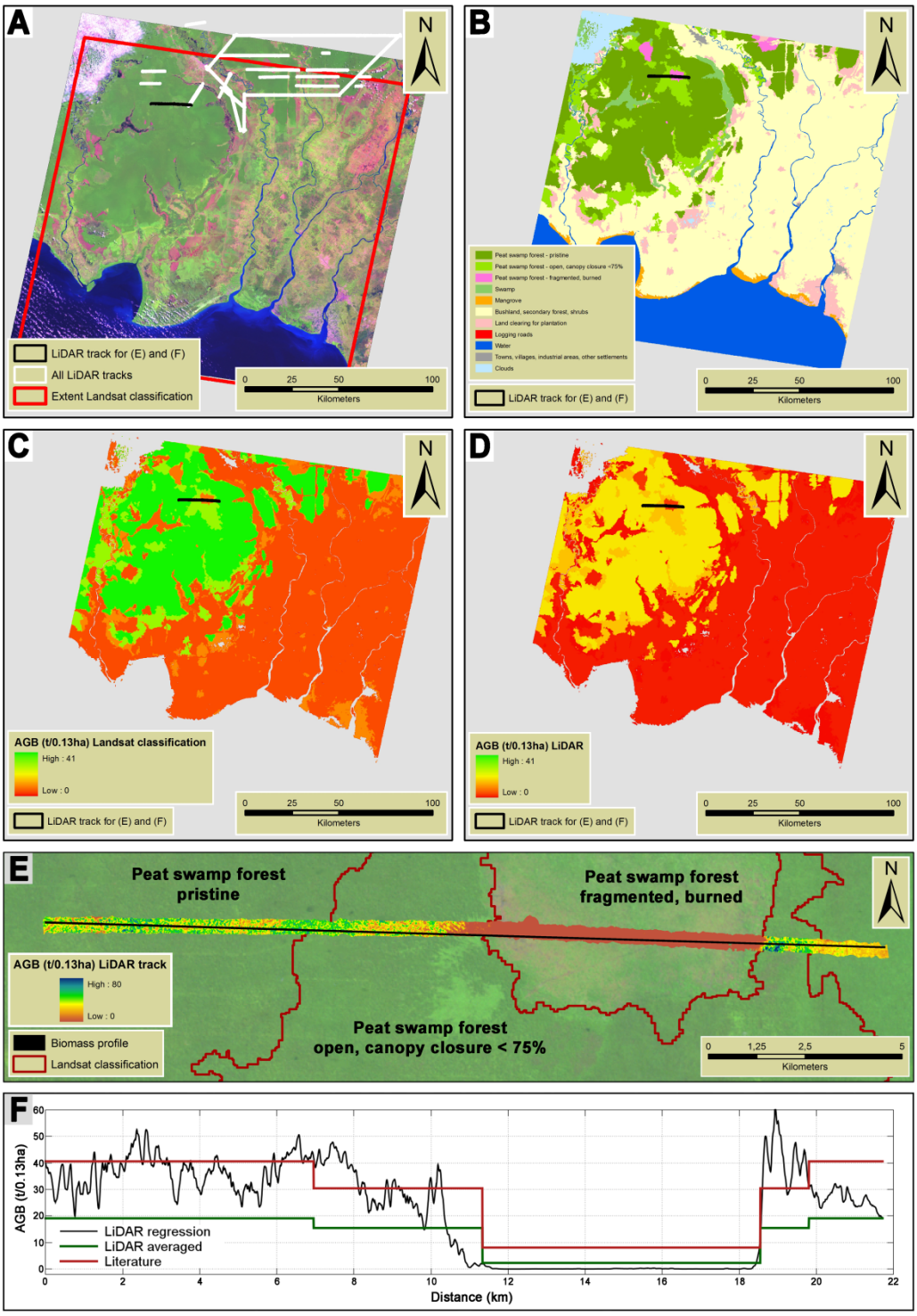

Figure VI-4: AGB estimation for a Landsat scene classification based on literature values and LiDAR regression model (CH with LiDAR point density weighting). (A) Landsat Scene (ETM+ 118-62, 2007-08-05; bands 5-4-3; gap filled). (B) Landsat Classification. (C) Literature based AGB estimation. (D) LiDAR average AGB estimation. (E) Subset of the of the LiDAR AGB regression results covering a track with about 22km length in the Sebangau peat swamp forest catchment superimposed on the Landsat image. The red outlines indicate the borders of the Landsat classification. (F) AGB variability captured by LiDAR (black), the averaged LiDAR values for all tracks (green), and the Landsat classification (red) along the profile indicated by the black lines in A-E.

The costs of LiDAR surveying are decreasing, but still relatively high, and are strongly related to the desired point density. To assess the influence of the LiDAR point density on the estimation of the AGB, a rigorous covariance propagation analysis was performed (see methods). The results of this analysis show that the AGB standard deviation decreases significantly with increasing LiDAR point density until approximately 2pt/m^2 and for LiDAR point densities higher than 4pt/m^2 no significant standard deviation improvement could be observed (Figure VI-3C). These results suggest that expensive LiDAR surveying with more than 4pt/m^2 are not necessary to achieve reasonable AGB regression models but on the other hand surveying with less than 1pt/m^2 can lead to significant inaccuracies, so that surveying with a point density between 2 and 4pt/m^2 shows the best cost-benefit relation. The QMCH tends to perform better than the CH in terms of standard deviation.

Up to date the best solution to monitor tropical forest carbon stocks, at the high resolution monitoring agencies and investors demand, would be the continuous mapping of the REDD+ project areas with LiDAR data. This approach produces the most accurate estimates of forest carbon stocks and their spatial variability, but is not feasible for large-scale use due to the relatively high cost of operation. However, in combination with satellite data (optical and/or RADAR) LiDAR could be a cost effective approach to derive more accurate maps on forest carbon densities (Asner *et al.*, 2010, Englhardt *et al.*, 2011). Asner *et al.* (2010) for example successfully up-scaled LiDAR derived AGB estimates to 4.3 million ha of tropical lowland forest in Peru with the help of optical satellite data (Landsat). The new approach presented here through using the CH and incorporating LiDAR point densities as weight has a high potential to improve current estimates of AGB and carbon stocks across different forest types and degradation levels and its spatial variation in these highly inaccessible tropical rainforests. Further it could assist the efforts in up-scaling LiDAR derived AGB estimates to large-scale geographic areas as it will be necessary for future REDD+ projects.

2 Methods

2.1 Field inventory

Field inventory data was collected in 3 study sites from May to August 2008 (Figure VI-1). The first study site was located in the Sebangau peat swamp forest catchment (Fig VI-1C), with 16 field inventory plots covering tall and low pole peat swamp forests. The second study site was located within Block C of the former Mega Rice Project (MRP), with 20 field inventory plots covering diverse degradation stages of peat swamp forest (Figure VI-1C). The third study site was located in Tumbang Danau and Tewaibaru, with 16 field plots covering logged and unlogged lowland dipterocarp forests (Figure VI-1B). The location of the nested plots were selected depending on forest type representativeness and set in advance to assure that they lie within the swath of the LiDAR point clouds. Trees with a Diameter at Brest Height (DBH) smaller than 7cm were excluded. The nested plot method is based on fixed-area plots (Pearson *et al.*, 2005b). In each of the three circular nests trees of a certain DBH range were measured: 7 to 20cm (4m radius), 20 to 50cm (14m radius), and greater than 50cm (20m radius). The sum of DBH, tree height, basal area, and biomass of the two smaller nests was multiplied by an expansion factor in order to get the values for the 20m radius inventory plot (0.13ha). Local species name and DBH were recorded. Local names were translated to corresponding Latin names using information provided by a local herbarium at the Centre for International Co-operation in Management of Tropical Peatland (CIMTROP) in Palangka Raya, local expert knowledge, and tropical timber databases provided by Chudnoff (1984) and the World Agroforestry Centre (http://www.worldagroforestrycentre.org/Sea/Products/AFDbases/WD/Index.htm (last visited: 21.11.2011). Species specific wood densities were also derived from these databases as well as from IPCC (2006). Some local names, especially of various dipterocarp species, could not be translated. In these cases an average specific wood density for Asian tropical forests, 0.57t/m^3, was applied (Brown, 1997). Finally, the AGB values were calculated using the allometric model for tropical forest stands from Chave *et al.* (2005) excluding tree height.

2.2 Acquisition and processing of airborne laser scanner data

The airborne LiDAR data set was acquired in a flight campaign by Milan Geoservice GmbH and Kalteng Consultants from the 5th to 10th August 2007. A Riegl LMS-Q560 Airborne Laser Scanner was mounted on a Bell 206 helicopter. Small-footprint full-waveform LiDAR data was collected from a flight altitude of approximately 500m above ground over a scan angle of ±30 degrees (swath width ±500m). The laser sensor had a pulse rate of up to 100,000 pulses per second with a footprint of 0.25m and a wavelength of 1.5µm (near Infrared). This survey configuration resulted in a nominal point density of 1.4pt/m^2. The Riegl LMS-Q560 Airborne Laser Scanner system allows height measurements of up ±0.02m under laboratory conditions. The acquired data set has an absolute horizontal accuracy of ±0.50m and vertical accuracy of ±0.15m Root Mean Square Error (*RMSE*). Next step was the filtering of the LiDAR point clouds. This is a crucial step, since the DTM is directly derived from the filtered point clouds. In this work, the filtering was a simple separation between ground and off-ground LiDAR points, since within the study area all off-ground points consist of vegetation. The applied filtering approach was the hierarchic robust filtering, and the method used to generate the DTMs (1m resolution) the linear adaptable prediction interpolation. Both solutions are implemented within the Inpho software package (DTMaster and SCOP++).

2.3 Generation of the regression models

The first step for the generation of the regression models was the creation of a height histogram for every field plot. In order to achieve this, all points within each plot area were normalized to the ground using the DTM as reference. After that, given a pre-defined height interval (or bin size), the number of points within the given intervals was stored in the form of a histogram. In order to correlate the AGB field observations with the LiDAR metrics, two parameters derived from the height histograms were used. The first one correlates the AGB with the Quadratic Mean Canopy profile Height (QMCH) (Asner *et al.*, 2010). The second is based on Centroid Height (CH) of the histogram. The first bin of each plot was considered ground return and therefore eliminated from the further processing. Figure VI-2 shows four typical field plots, their point cloud profile, and the derived histogram.

One important parameter in LiDAR surveying is the point density. The acquisition of high point densities is expensive, because it requires most recent equipment and a slow and low flying aircraft. The real point density can strongly vary across the surveyed area mainly due to stripe overlapping, flight velocity, height variation, return quality variation caused by smoke or water vapour in the atmosphere, and target reflectance. In order to account for these factors within the regression models, the point density was used for each plot as a weighting factor. Since the point density affects directly the quality of the height histogram, this also affects the metrics derived from it (i.e. the CH and QMCH). Usually, the regression models applied for AGB estimations use the AGB as dependent variable and the LiDAR metrics as independent. In this study, this order was changed because the least-squares solution chosen permitted only weighting the dependent variable, which are treated as observations with known weights - the point densities. For both studied metrics (CH and QMCH) the regression models were derived using the classic approach and the weighted adjustment. After the regression processing, the obtained parameters were transformed in order to obtain an equation that directly determines the AGB based on the LiDAR metrics. Their variances and co-variances were calculated through covariance propagation. In order to verify the influence of point density in the AGB accuracy, a further rigorous covariance analysis was performed.

2.4 Covariance propagation analysis

The basic regression model used in this work correlates the AGB with de LiDAR Metrics (LM) though a power function:

$$AGB = a \cdot LM^b \qquad \text{(eq. VI-1)}$$

Although, in order to permit LiDAR metrics weighting, it is necessary to rewrite eq. VI-1 with LM as dependent variable:

$$LM = k \cdot AGB^w \qquad \text{(eq. VI-2)}$$

In this form, the LiDAR metrics can be treated as observations and weighted with the correspondent LiDAR point density within a non-linear least-squares solution. After the regression processing, the residuals of the observations can be determined as well as the covariance matrix of the parameters k and w (Σ_{kw}). Now it is necessary to transform the parameters k and w into a and b, which actually correlate the LiDAR metrics with the AGB:

$$a = \left({}^{1}/_{k}\right)^{{}^{1}/_{w}} \quad \text{(eq. VI-3)}$$

$$b = {}^{1}/_{w} \quad \text{(eq. VI-4)}$$

In order to perform a rigorous AGB accuracy estimation, it is necessary to determine the covariance matrix of the parameters a and b (Σ_{ab}) though a covariance propagation:

$$\Sigma_{ab} = G \cdot \Sigma_{kw} \cdot G^T \quad \text{(eq. VI-5)}$$

Where:

$$G = \begin{bmatrix} {}^{\partial a}/_{\partial k} & {}^{\partial a}/_{\partial w} \\ {}^{\partial b}/_{\partial k} & {}^{\partial b}/_{\partial w} \end{bmatrix} = \begin{bmatrix} {}^{-1}/_{k^{\frac{w+1}{w}} \cdot w} & {}^{\ln(k)}/_{k^{\frac{1}{w}} \cdot w^2} \\ 0 & {}^{-1}/_{w^2} \end{bmatrix} \quad \text{(eq. VI-6)}$$

Returning to eq. VI-1, one can write a new covariance propagation equation:

$$\Sigma_{AGB} = \sigma_{AGB}^2 = D \cdot \Sigma_{LM,ab} \cdot D^T \quad \text{(eq. VI-7)}$$

Considering all terms on the right side of the eq. VI-1 as parameters, one comes to:

$$D = \begin{bmatrix} {}^{\partial_{AGB}}/_{\partial_{LM}} & {}^{\partial_{AGB}}/_{\partial a} & {}^{\partial_{AGB}}/_{\partial b} \end{bmatrix} = [a \cdot b \cdot LM^{b-1} \quad LM^b \quad a \cdot LM^b \cdot \ln(LM)] \quad \text{(eq. VI-8)}$$

Take $\Sigma_{LM,ab}$ as the extended covariance matrix:

$$\Sigma_{LM,ab} = \begin{bmatrix} \sigma_{LM}^2 & 0 & 0 \\ 0 & \sigma_a^2 & \sigma_{ab} \\ 0 & \sigma_{ab} & \sigma_b^2 \end{bmatrix} \quad \text{(eq. VI-9)}$$

Solving eq. VI-7 with eq. VI-8 and eq. VI-9 and denoting the point density ρ, one comes to the final AGB standard deviation (σ_{AGB}) estimation model:

$$\sigma_{AGB} = \sqrt{{}^{A}/_{\sqrt{\rho}} + B + C} \quad \text{(eq. VI-10)}$$

With:

$A = (a \cdot b \cdot LM^{b-1})^2$

$B = LM^b \cdot \left(LM^b \cdot \sigma_a^2 + \sigma_{ab} \cdot \left(a \cdot LM^b \cdot \ln(LM)\right)\right)$

$C = \left(a \cdot LM^b \cdot \ln(LM)\right) \cdot \left(\sigma_{ab} \cdot LM^b + \sigma_b^2\left(a \cdot LM^b \cdot \ln(LM)\right)\right)$

Eq. VI-4, eq. VI-5, and eq. VI-10 were applied to the CH and QMCH models derived in this work.

2.5 Comparison between optical remote sensing and LiDAR approach for AGB estimation

The obtained AGB estimation parameters were applied to 33,178ha of LiDAR tracks. The chosen regression model was the CH due to its higher correlation coefficient, lower *RMSE* and better computational performance. In order to avoid artefacts caused by filtering problems, 20m of the LiDAR track borders were excluded from the processing.

Prior to the classification the Landsat imagery (ETM+ 118-62, 2007-08-05) was geometrically corrected by automated image to image matching techniques. Afterwards a radiometric correction was applied in order to compensate atmospheric distortions, resulting from water vapour, viewing geometry, and other physical parameters. The land cover classification of the imagery (2,987,726ha) was implemented using an object-oriented approach, applying a segmentation algorithm prior to the classification. The segmentation generates objects and evaluates spectral reflectance, as well as texture information and additional thematic information such as altitude. Classification itself corresponds in fact a database query by formulating rule bases on how the objects should be evaluated. The AGB values of the different land cover types were based on results of a literature survey and assigned to the different land cover types classified in the satellite imagery.

Acknowledgements

We would like to thank Suwido Limin and his team from CIMTROP for the logistic support during the field inventory and Sampang Gaman (CIMTROP) and Simon Husson (Orang Utan Tropical Peatland Project, OUTROP) for providing tree species lists. Further we would like to thank FORRSA (Forest Restoration and Rehabilitation in Southeast Asia) project of the EU-funded Asia Link programme for financially supporting the field trips to Indonesia. The LiDAR data set was acquired by Kalteng Consultants.

CHAPTER VII:
Synthesis

1 Summary and main conclusions

During the last decade the global carbon dioxide concentration growth rate was 1.9ppm per year on average, resulting mainly from the emission of 7.2Gt of carbon per year due to the use of fossil fuels and proximately 1.6Gt of carbon per year due to land use change (IPCC, 2007). It is estimated that in 2008, worldwide deforestation and forest degradation emissions contributed about 6% to 17% of the total anthropogenic CO_2 emissions (Van der Werf *et al.*, 2009). About 13 million ha of tropical forest were deforested annually between 1990 and 2005 and with 0.98% South and Southeast Asia had one of the highest annual deforestation rates for the time period of 2000 to 2005 (FAO, 2006). Deforestation and forest degradation in this region are almost exclusively caused by human economic activities such as shifting cultivation, illegal logging, and the establishment of industrial timber estates and large-scale oil palm plantations (Hansen *et al.*, 2009; Rieley & Page, 2005). During extended droughts caused by the periodic El Niño phenomenon vast areas of the Indonesian forests have been destroyed by fire (Langner & Siegert, 2009). Fire serves as the principal tool for land clearing and its impacts and severity increases in degraded forests (Siegert *et al.*, 2001). In Indonesia increased GHG emissions are particularly evident in the coastal lowlands of Sumatra and Kalimantan, where peat fires and peat decomposition, due to peatland drainage, result in the release of huge amounts of CO_2 (Ballhorn *et al.*, 2009; Hooijer *et al.*, 2010; Page *et al.*, 2002). With Indonesia's ranking as one of the world's biggest emitters of carbon (Hooijer *et al.*, 2006) and with a peat carbon store of about 57 ±11Gt (Jaenicke *et al.*, 2008; Wetlands International, 2003; 2004; 2006;), it has enormous potential to negatively influence the global climate it its peatlands are burned and drained at rates currently observed. One important measure of the UNFCCC to curb GHG emissions from this sector is the REDD+ program which involves the private sector of industrialized countries in the protection of the remaining tropical forests to compensate the exceeding of their GHG emission quota. To estimate GHG emissions from deforestation and forest degradation information on both the area of forest loss and/or degradation and the corresponding carbon stock of the land that is cleared and/or degraded is needed which remains a big challenge in tropical forests (Gibbs *et al.*, 2007). Especially GHG emissions from forest degradation is difficult to monitor, particularly considering that degraded and regrowing forests are predicted to include

increasingly large portions of the tropics (Gibbs *et al.*, 2007). The quantification of tropical forest carbon stocks is a key challenge in creating a basic methodology for REDD+ projects. Since most peatlands in Indonesia are highly inaccessible, very few field measurements have been made to date. One way to overcome this problem may be the use of LiDAR data. Airborne LiDAR systems (discrete-return and full-waveform), compared to other remote sensing technologies, have been shown to yield the most accurate estimates for land topography, forest structural properties, and forest AGB.

The main goal of this thesis was *the assessment of the potential and accuracy of airborne and spaceborne LiDAR data in measuring peatland topography, peat fire burn depth, peat fire carbon emissions, and forest AGB in Central Kalimantan, Indonesia*.

The focus of our investigation was on a peat dominated landscape in Central Kalimantan, Borneo, where almost all peat swamp forest ecosystems have been severely impacted by extensive logging and drainage for more than two decades (Rieley & Page, 2005; Figure I-9). The area also covers the former Mage Rice Project (MRP), an ill-fated transmigrasi resettlement project initiated in 1995 by the Indonesian government, which resulted in the serious degradation of more than one million ha of peat swamp forest (Rieley & Page, 2005).

Following five specific objectives were analyzed in this thesis:

Objective (1): Assessment of the potential and accuracy of airborne LiDAR data to measure peat burn depth for single and multiple fire events.

The results of CHAPTERS II and III demonstrate that airborne LiDAR has the ability to collect sufficiently accurate and spatially representative measurements of peat burn scar depths over large areas in this very inaccessible terrain. In CHAPETR II, through using an airborne LiDAR data set acquired in Central Kalimantan, in 2007, one year after the severe peatland fires of 2006, an average peat burn scar depth of 0.33 ±0.18m was determined. The peat burn depth for this single fire event was calculated through determining the elevation difference of the LiDAR derived DTMs at the border between burn and adjacent unburned peatlands. The determined average burn depth correlated well with field measurements recorded in the same year at locations near the LiDAR transects. The relatively invariable burn depth and

the low standard deviation indicated restrictions in fire behavior and impact. Fires never burned considerably deeper than 0.5m although sometimes extreme burn depths of up to 1.1m were observed. These extremes were small in scale and originated most probably from places where ignited tree trunks and roots facilitated oxygen supply and thus allowed the fire to propagate deeper into the peat layer. The consistent burn depth relates to the water table in the peat layer. Additional factors may be important in regulating burn depth, for example, as fire progresses deeper a build-up of char and ash makes the peat less flammable and impedes the flow of oxygen. The results also suggest that peat fires burning several meters below the surface (Goldammer, 1993), like fires observed in coal deposits, are extremely unlikely. In CHAPTER III, based on the same LiDAR data set, a different and advanced approach to estimate peat loss after fire, not only for single but also for multiple fire events, was introduced. Through 3D modeling a pre-fire peat surface was reconstructed from which the peat loss was then derived. The pre-fire peat surface was modelled using anchor points to the left and right of each of the recorded fire scars, either in undisturbed reference areas or in areas which had burned once, twice and so forth. The peat loss after single and multiple fire events was calculated by comparing the LiDAR derived DTM with the modelled pre-fire peat surface. The small mean elevation differences of -0.01-0.02 ±0.07-0.19m between the modelled pre-fire surface and the LiDAR derived DTMs in unburned areas demonstrated that the applied modelling approach accurately estimated the pre-fire peat surface elevation. The results of the average peat loss calculations showed that peat loss after the first fire event with 0.37 ±0.22m was the highest, after the second fire event with 0.30 ±0.17m lesser, and after the third fire event with 0.11 ±0.25m the lowest, so that no linear relationship was observed. This result agrees with evidence from aerial and field surveys suggesting that fires in peat swamp forests burn deeper into the peat layer than fires on areas previously affected by fire. When comparing the average peat loss results separately for the years they originated from (1997 = 0.57 ±0.09m; 2002 = 0.35 ±0.17m; 2006 = 0.33 ±0.23m) it is obvious that the year 1997 had by far the highest peat loss. If the duration of the dry season for these three years is additionally compared the year 1997 with 184 days also had the longest dry season. This result indicates that there is a relation between duration of the dry season and the average peat loss after fire.

Objective (2): *Estimation of carbon emissions from peat fires for single and multiple fire events at different spatial scales from the sub district level to the national level based on the peat depth calculations.*

To estimate Indonesia's contribution to global carbon emissions through peatland fires the results of the average peat burn depths was set in relation to burned peatland area determined from satellite data. In CHAPTER II, based on burned peatland area derived from Landsat imagery, it was estimated that within the 2.79 million hectare study area 49.15 ±26.81Mt of carbon were released during the 2006 El Niño episode. This represents 10-33% of all carbon emissions from transport for the European Community in the year 2006 (http://unfccc.int/di/DetailedByParty/Event.do;jsessionid_4B56CEF8097A1587450FBB5AC8451F87.diprod02?event_go). These emissions, originating from a comparatively small area (approximately 13% of the Indonesian peatland area), underline the importance of peat fires in the context of GHG emissions and global warming. Further the approximate carbon emissions from peatland fires for Indonesia in 2006 were estimated based on (a) active fire recordings of the MODIS (Davies *et al.*, 2009), (b) a correction factor for the MODIS burned area determined from a correlation with Landsat-derived burned areas, (c) peatland maps of Indonesia (Wetlands International, 2003, 2004, 2006), and (d) the results of the LiDAR-derived burn depth calculations. There is considerable uncertainty in this estimate due to a range of factors (e.g. MODIS burned area, extent of the peatland, burn depth in relation to water table, moisture conditions, and emission factors), but this calculation may provide a reasonable estimate of the order of magnitude of this event. Peat fires in 2006 released about 0.25 ±0.14Gt of carbon which is equal to 7-24% of all global emissions by land use change in that year (IPCC, 2007). Van der Werf *et al.* (2008) estimated that in 2006 0.30 ±0.12Gt of carbon were released by fires in Indonesia and Papua New Guinea, however, this estimate also includes non-peat fires and AGB burning. In CHAPTER III based on historical Landsat fire scar classifications and the results of the average peat loss calculations is was estimated that 61.361Mt of carbon were emitted within the Kapuas district (1,489,325ha), Central Kalimantan, between the years 1990-2009. This is equal to about 25% of all carbon emissions from transport (civil aviation, road transportation, railways, navigation, and other transportation) for the European Community in the year 2009 (http://unfccc.int/di/DetailedByParty/Event.do;jsessionid_4B56CEF8097A1587450FB

B5AC8451F87.diprod02?event_go). In the past 15 years, severe peat fires have occurred almost every second year during El Niño induced droughts in 1997, 2002, 2004, 2006, and 2009. This is a new phenomenon and has not been observed in this frequency and spatial extent before. Currently, this important source of carbon emissions is not yet included in the IPCC estimate for land cover change (IPCC, 2008) or in most regional and global cycling models. As most studies on tropical land conversion and climate change consider only AGB this study shows that in the future, emissions from tropical peat combustion should be included in the emissions estimates. The carbon content of the peat layer depends on its thickness and can be up to 19 times higher than that of a pristine peat swamp forest growing on top of the peat (Jaenicke *et al.*, 2008). In addition, deforested and drained peatlands release considerable amounts of carbon due to bacterial oxidation (Hooijer *et al.*, 2009). These emissions are persistent for many years and add to the estimates given here.

Objective (3): Assessment of the potential and accuracy of spaceborne LiDAR to measure peatland topography.

As already mentioned most peatlands in Indonesia are highly inaccessible so that very few field measurements have been made to assess these carbon pools. Especially the potential spatial variation is unknown because up-to-date no systematic large scale sampling has been undertaken. ICESat/GLAS data have been demonstrated to accurately estimate topography especially well in even areas. As peatlands have and especially smooth topography (Page *et al.*, 1999; Rieley & Page, 2005) this spaceborn LiDAR data set was assessed for its applicability to measure peatland topography in Central Kalimantan. In CHAPTER IV ICESat/GLAS data was compared to other elevation data. (SRTM data, 3D peatland elevation models derived from SRTM data, and elevation data derived from airborne LiDAR). Jaenicke *et al.* (2008) demonstrated that SRTM data can be used to determine the extent and topography of the dome shaped surface and a correlation was obtained between the convex peat dome surface and the depth of the underlying mineral ground, which was then used to calculate peat volume and carbon store. The main problem of this approach was the determination of the vegetation height growing on top of the peat domes as the SRTM C-band sensor does not completely penetrate the forest cover. To get a high number of quality filtered footprints ICESat/GLAS data on peatlands for the whole of Kalimantan was investigated. The comparison of the ICESat/GLAS

elevations to the mean SRTM elevation showed a very high correlation of the waveform centroid (R^2 = 9.92). The mean ICESat/GLAS and SRTM elevation difference of -4.9 ±3.8m also showed that the SRTM C-band phase center penetration depth is dependent on forest structural parameters such as canopy closure. These results complied well with a study by Carabajal and Harding (2006) and indicate that even for densely forested peat swamp areas the error is well below the 16m at 90% confidence vertical accuracy specifications for the SRTM mission. These findings demonstrated that with the help of ICESat/GLAS data the penetration depth of the SRTM C-band phase center into different peat swamp forest canopy closures and consequently the height of the SRTM elevation above the actual peat surface can be measured. Based on this it is reasonable to use ICESat/GLAS data as a tool to validate peatland elevation models derived from SRTM data for selected areas in Central Kalimantan. Because the elevation from the ICESat/GLAS last highest Gaussian peak is known to correspond best with the actual peat surface (Boudreau *et al.*, 2008; Rosette *et al.*, 2008) it was correlated to the mean elevation of three 3D peatland elevation models derived from SRTM data. ICESat/GLAS transects covering entire peat domes, clearly showed the convex curvature of them. The difference between the last highest Gaussian peak from the ICESat/GLAS data, referring to the estimated peat surface within the ICESat/GLAS waveform, and the 3D peatland elevation models, in which the forest canopy height was eliminated from the SRTM terrain model, was with −1.0 ±3.2m low. These results indicate that ICESat/GLAS data can be used to validate and enhance SRTM derived 3D peatland elevation models. When correlating ICESat/GLAS elevations to airborne LiDAR 3D point clouds and DTMs derived from these the signal begin and waveform centroid compared to the maximum z and mean z value all had R^2 values higher than 0.8, with the highest correlation between the waveform centroid and the mean z value (R^2 = 0.91, n = 104). The mean elevation difference between these two data sets was -0.5 ±1.9m for waveform centroid and the mean z value, and 3.2 ±3.2m for signal begin and the maximum z value. These results indicated that ICESat/GLAS data and airborne LiDAR data comply well regarding elevation and that ICESat/GLAS data can be used as a tool to measure different elevations in these dense tropical peat swamp forest ecosystems. The findings show that ICESat/GLAS data can be used as a sampling tool to screen for peatlands in remote areas, such as West Papua. A systematic sampling with ICESat/GLAS could help to improve the knowledge on the

spatial extent and curvature variation of peat domes and also consequently lead to better estimates of the carbon pools.

Objective (4): Collection of forest in-situ data at various degradation levels.

For the analyses in CHAPTERS IV, V, and VI forest in-situ data at different degradation levels within Central Kalimantan was collected. Altogether 77 clusters each with four sample plots were selected depending on representativeness of forest type (lowland dipterocarp or peat swamp forest), degradation level (unlogged/little logging, logged and burned), and on accessibility. The four sample plots of one cluster build the corners of a 50x50m square. In each sample plot the angle count method (Bitterlich, 1947) was conducted. Trees with a Diameter at Breast Height (DBH) smaller than 7cm were excluded. Additionally the nested plot method with circular design was conducted in one to two clusters per forest, sub forest, and land use type. The nested plot method is based on fixed-area plots (Pearson *et al.*, 2005a; Pearson *et al.*, 2005b). In each of the three circular nests trees of a certain DBH range were measured: 7 to 20cm (4m radius), 20 to 50 cm (14m radius), and greater than 50cm (20m radius). The applicability of the angle count method for AGB estimates in the tropics was tested through statistically comparing its results with them from the nested plot method. For each tree selected by either the angle count or the nested plot method following parameters were recorded: Local species name, DBH in cm (at 1.3m above the ground), and tree height in m. AGB was calculated using an allometric model for tropical forest stands from Chave *et al.* (2005). Two models are proposed for moist forest, one which includes tree height, DBH and wood density, the other includes DBH and wood density, but no tree height. It was decided to use the second model excluding tree height as accurate tree height measurements in the field were impossible due to the dense and tall forest canopy. The field inventory derived AGB values were considered to be reliable as they reflected the estimates from the literature. The derived mean DBH and tree height reflected the expected differences between lowland dipterocarp forest and peat swamp forest and between unlogged, logged and burned forest areas. The angle count method could be shown to be an adequate sampling method for the purpose of fast, quantitative sampling. A comparison of mean DBH and AGB estimates from plots where angle count and nested plot method were used showed positive correlations. Despite the

higher risk of missing trees in dense stands (Köhl *et al.*, 2006), the angle count method was assumed to be applicable in all forest types.

Objective (5): Assessment of the potential and accuracy of airborne and spaceborn LiDAR data to calculate forest AGB through correlation with the collected forest in-situ data.

In CHAPTERS IV-VI the airborne LiDAR 3D point cloud statistics within a defined polygon were correlated to the corresponding ground-based AGB value. In CHPATER V multiple regression analysis was applied to create AGB estimation models. This analysis followed the principles of Magnussen & Boudewyn (1998) and its application followed Lim & Treitz (2004), Patenaude (2004), and Lucas (2006). As the angle count method is designed to extrapolate measurements to 1ha values, a circle of 1ha area was used to clip the LiDAR point clouds. The height above the terrain (absolute vegetation heights) for each point within the cloud was determined by subtracting the corresponding pixel value of the LiDAR derived DTM. LiDAR point height distributions of each sample plot were analyzed statistically and following metrics were derived and used as predictors: (a) mean h_{mean}, (b) measures of dispersion including the Standard Error of the Mean (*SEM*) h_{SEM}, standard deviation (σ) h_{σ}, variance h_{var}, range h_{range} and maximum h_{max}, and (c) the quantiles corresponding to the 5, 10, ..., 95 percentiles of the distributions ($h_{5,..,.95}$). As a further potential predictor, Canopy Cover (*CC*) was determined. All above variables within the sampling area of the angle count method were correlated to the corresponding estimated AGB values per ha. Multiple linear regression analysis was conducted for all sample plots as well as for different forest and land use types. Best R^2 value was derived for lowland dipterocarp forests (R^2 = 0.83) and was comparable to literature values. The 45th, 65th percentile and the *SEM* were selected (stepwise) as predictor variables with a *RMSE* of 21.37%. In contrast, the model for peat swamp forest had a very low R^2 of 0.32. Here, only a single variable (50th percentile) was sufficient for biomass prediction. When all sample plots were put together, R^2 is accordingly lower (0.71) than that of lowland dipterocarp forest due to the low results for peat swamp forest. The subsequent application of the regression models to complete LiDAR tracks demonstrated the ability of this approach to monitor not only deforestation but especially forest degradation and its variability at high spatial resolution. This clearly is an advantage to indirect AGB estimations where AGB values are attributed to land

cover types not considering spatial variability within these land covers. As shown by the comparison of Landsat and LIDAR analysis, Landsat classification tends to overestimate biomass as it neither detects degraded forest from small-scale logging activities and selective logging, nor from logging in past decades. By only analyzing spectral information, large areas of forest are assigned to be one class. Thereby, the negative impact of named logging activities an AGB or carbon content is neglected. In CHAPTER IV the LIDAR 3D point clouds statistics were correlated to the corresponding ground-based AGB from the nested plot samples. 36 sample plot centers were expanded by a circle with a radius of 20m. These areas were used to clip the LiDAR 3D point clouds. Additionally to the metrics mentioned above the Quadratic Mean Canopy profile Height (QMCH) (Lefsky *et al.*, 2002a) and the Centroid of the LiDAR point cloud height histogram (CL) were used as predictors. The best overall predictor of AGB was the CL. The model could further be enhanced through incorporating the average LiDAR point density per square meter per sample plot of all LiDAR points. Sample plots with a higher average LiDAR point density per square meter were weighted higher during the computation of the final model. The R^2 value of this model was 0.75 (R^2_{corr} = 0.73, *SEE* = 2.66t/0.13ha). In CHAPTER VI the coefficient of determination could even be improved (R^2 = 0.88, *RMSE* = 13.8t/0.13ha, n = 52) and was comparable with those reported in studies throughout various tropical biomes. Here also the regression models could be further improved, for both of the LiDAR canopy vertical profile metrics (9% and 8% for CL and QMCH respectively) through the use of the LiDAR point densities as weight. In terms of correlation coefficient the CL showed a better performance than the QMCH. The costs of LiDAR surveying are decreasing, but still relatively high, and are strongly related to the desired point density. To assess the influence of the LiDAR point density on the estimation of AGB, a rigorous covariance propagation analysis was performed. The results of this analysis show that the AGB standard deviation decreases significantly with increasing LiDAR point density until approximately 2pt/m^2 and for LiDAR point densities higher than 4pt/m^2 no significant standard deviation improvement could be observed. These results suggest that expensive LiDAR surveying with more than 4pt/m^2 are not necessary to achieve reasonable AGB regression models but on the other hand surveying with less than 1pt/m^2 can lead to significant inaccuracies, so that surveying with a point density between 2 and 4pt/m^2 shows the best cost-benefit relation. The CL based regression model was also

applied to different LiDAR tracks and showed that it was possible to quantify natural AGB variability (linked to soil properties and the duration of water logging) and the impact of previous logging operation and fire with high spatial resolution. Variability could be also be detected in low AGB ranges. Further the results of the LiDAR AGB estimates were compared with an indirect Landsat based classification approach, in which each class was linked to a single biomass value, determined from a regional biomass database. Here the Landsat classification showed an overestimation of 60.8% for a 2,987,726ha study area. This can again be explained due to the fact that the Landsat classification neither detects degraded forest from small-scale logging activities and selective logging, nor from logging in past decades. These AGB overestimations can lead to significantly wrong emission estimates and compensation payments. In CHAPTER IV a multiple linear regression analysis was applied to create ICESat/GLAS AGB estimation models through correlating ICESat/GLAS height metrics to AGB estimates derived from the airborne LiDAR regression models. Following ICESat/GLAS height metrics were used as predictors: last telemetered gate–signal begin (H1), waveform centroid–signal begin (H2), signal end–signal begin (H3), signal end–nearest Gaussian peak (H4), last highest Gaussian peak–signal begin (H5), last highest Gaussian peak–nearest Gaussian peak (H6), and last highest Gaussian peak–waveform centroid (H7). The highest R^2 value of 0.61 (R^2_{corr} = 0.54, *SEE* = 9.76t/0.13ha, n = 35) was reached through a backward multiple regression approach with H1, H2, H4, H6, and H7 as independent variables and where the average LiDAR point density per square meter was ≥0.8 points. The mean difference between the ICESat/GLAS AGB estimation and the airborne LiDAR AGB estimation was −2.62t/0.13ha (±10.78t/0.13ha, n = 104). However it has to be considered that having multiple waveform derived variables (in our case 5) in the same equation may lead to collinearity problems.

Concluding, it can be stated that the application of airborne LiDAR data succeeded in deriving estimates on peat loss for single and multiple fire events in Central Kalimantan. Based on this estimates peat fire carbon emissions could be extrapolated to the sub district, district, and national level in Indonesia. The findings of these analyses resulted in a deeper understanding on the dimension and impact of these peat fires on the global carbon cycle and their ecological dynamics.

It was also possible to derive large scale AGB estimates and show its spatial variability for Central Kalimantan's peat swamp and lowland diperocarp forests through correlating field estimates with airborne LiDAR point cloud metrics, which then provides a possible approach as input to future REDD+ projects. Up to date the best solution to monitor tropical carbon stocks, at the high resolution monitoring agencies and investors demand, would be the continuous mapping of the REDD+ project areas with airborne LiDAR data. This approach produces the most accurate estimates of forest carbon stocks and their spatial variability, but is not feasible for large-scale use due to the relatively high cost of operation. However, in combination with satellite data (optical and/or RADAR) airborne LiDAR could be a cost effective approach to derive more accurate estimates on carbon densities of these tropical forests (Asner *et al.*, 2010; Englhardt *et al.*, 2011).

Further the results of this study demonstrated the usefulness and robustness of ICESat/GLAS data as a sampling tool to extract information on peatlands, which can be used as a proxy for peat volume and consequently carbon storage, state and structure of peat swamp forests, and peat swamp forest AGB for large inaccessible areas at low costs where no systematic sampling has been conducted yet. When combined with other data sources (optical satellite imagery, SRTM, and airborne LiDAR) ICESat/GLAS data could help to better understand carbon pools in tropical peatlands and their spatial distribution across Indonesia and other regions.

2 Future research

During the course of this thesis several interesting research issues for future research beyond the scope of this work evolved.

Since there were no historical burn depth measurements and only mono-temporal airborne LiDAR data available it should be realized that there might be uncertainties due to unknown variables such as non-fire subsidence of the peat. In future uncertainties could be better estimated and reduced once multi-temporal airborne LiDAR will be available (currently a new airborne LiDAR campaign is conducted within the investigated area). By comparing the new airborne LiDAR data set to the on analyzed here, the results of this study could be re-evaluated and subsidence rates across the peatland and within different land covers or in proximity to drainage

canals could be spatially estimated in more detail. Due to the geo-statistically (size and spatial distribution) not sufficient occurrence of areas that burned more than three times no mean peat loss calculations were carried out for these areas. For future research it would be of interest how peat loss changes after the third fire event. Does the mean peat loss stabilize at a certain depth or does it become less and less after every successive fire event? How important is the fuel load on top of the peatlands for peat loss after fire? In future these research questions could be answered in more detail once multi-temporal airborne LiDAR data will be available. When correlating peat loss after different fire events to water table measurements all R^2 values were lower than 0.29. This shows that no statistical significant correlation could be identified here. One explanation for this unexpected weak correlation could be that the water table measurements were collected at sites far away from the investigated fire scars, so that they might not be a good enough representation of the hydrological conditions at the fire scars during the specific fire events. To investigate the relation between peat loss and water table level more accurately it would be necessary to collect water table measurements near burning peat fires.

Considering the estimation of AGB values from airborne LiDAR data it would be of high importance for the future to generate allometric models from destructive sampling, especially for peat swamp forests, so that bias from generic models could be decreased. Also the inclusion of the laser pulse intensity might be a helpful parameter, implementing it as a weight for each laser point. More sample plots in low biomass stands should be established to optimize the regression models because most models had problems calculating AGB values for grid cells with obviously low biomass. The approach presented in CHAPTER VI through using the CL and incorporating LiDAR point densities as weight has a high potential to improve current estimates of AGB and carbon stocks across different forest types and degradation levels and its spatial variation in these highly inaccessible tropical rainforests. As the presented approach is easy to reproduce it would be of interest whether the improved results are also observed for other tropical forest ecosystems.

For future studies it would be beneficial to have a higher number of ICESat/GLAS footprints intersecting with LiDAR point clouds with high average point densities. Further it would be of interest whether ICESat/GLAS data can be used as a sampling tool to screen for peatland in other remote areas, such as the Amazon region or

tropical Africa. A systematic sampling with ICESat/GLAS could help to improve the knowledge on the spatial extent of peatlands and consequently lead to better estimates of this carbon pool

REFERENCES

Aaby B, Tauber H (1975) Rates of peat formation in relation to humification and local environment, as shown by studies of a raised bog in Denmark. *Boreas*, **4**, 1-17.

Adams JB, Smith MO, Johnson PE (1986) Spectral mixture modelling: a new analysis of rock and soil types at the Viking Lander 1 site. *Journal of Geophysical Research*, **91**, 8090-8112.

ADB (Asian Development Bank) / BAPPENAS (National Development Planning Agency) (1999) Causes, Extent, Impact and Costs of 1997/98 Fires and Drought. Final Report, Asian Development Bank TA 2999-INO, Jakarta, Indonesia.

Anderson JAR (1964) The structure and development of the peat swamps of Sarawak and Brunei. *Journal of Tropical Geography*, **18**, 7-16.

Anderson JAR (1983) In: *Ecosystems of the World 4b—Mires: Swamp, Bog, Fen and Moor*, (ed Gore AJP), pp. 181-199. Elsevier, Amsterdam.

Archad F, Eva HD, Stibig HJ, Mayaux P, Gallego J, Richards T, Malingreau JP (2002) Determination of deforestation rates of the World's humid tropical forests. *Science*, **297**, 999-1002.

Ashton PS, Hall P (1992) Comparisons of Structure among Mixed Dipterocarp Forests of North-Western Borneo. *Journal of Ecology*, **80**, 459-481.

Asner GP, Hughes RF, Varga TA, Knapp DE, Kennedy-Bowdoin T (2009) Environmental and biotic controls over aboveground biomass throughout a tropical rain forest. *Ecosystems*, **12**, 261-278.

Asner GP, Powell GVN, Mascaro J *et al.* (2010) High-resolution forest carbon stocks and emissions in the Amazon. *Proceedings of the National Academy of Sciences of the United States of America*, **107**, 16738-16742.

Assmus E (1975) Extension of Stuttgart Contour Program to treating terrain break lines. In: *Proceedings of the symposium of the ISP, Commision III, Stuttgart 2.-6.9.1974*, pp. 171-178. DGK, Reihe B, vol. 214.

Bae S, Schutz BE (2002) *Geoscience Laser Altimeter System (GLAS), Precision attitude determination (PAD)*. Algorithm Theoretical Basis Documents (ATBD), Version 2.2, Center for Space Research, The University of Texas at Austin, USA.

Baccini A, Laporte N, Goetz SJ, Sun M, Dong H (2008) A first map of tropical Africa's above-ground biomass derived from satellite imagery. *Environmental Research Letters*, **3**, 045011.

Ballhorn U, Siegert F, Mason M, Limin S (2009) Derivation of burn scar depths and estimation of carbon emissions with LIDAR in Indonesian peatlands. *Proceedings of the National Academy of Sciences of the United States of America*, **106**, 21213-21218.

Basuki TM, van Laake PE, Skidmore AK, Hussin YA (2009) Allometric equations for estimating the above-ground biomass in tropical lowland Dipterocarp forests. *Forest Ecology and Management*, **257**, 1684-1694.

Bitterlich W (1947) The angle count method. *Allgemeine Forst und Jagdzeitung*, **58**, 94-96.

Boardman JW (1998) Leveraging the high dimensionality of AVIRIS data for improved sub-pixel target unmixing and rejection of false positives: mixture tuned matched filtering. In: *Summaries of the 7th JPL Airborne Earth Science Workshop*, (ed Jet Propulsion Laboratory), pp. 55-56. Jet Propulsion Laboratory, Pasadena.

Boehm HDV, Siegert F (2004) The impact of logging on land use change in Central Kalimantan, Indonesia. *International Peat Journal*, **12**, 3-10.

Bompard JM, Guizol P (1999) *Land Management in South Sumatra Province, Indonesia. Fanning the Flames: the Institutional Cause of Vegetation Fires.* European Union Forest Fire Prevention and Control Project and Indonesian Ministry of Forestry and Estate Crops, Jakarta, Indonesia.

Boudreau J, Nelson RF, Margolis HA, Beaudoin A, Guindon L, Kimes DS (2008) Regional aboveground forest biomass using airborne and spaceborne LiDAR in Quebec. *Remote Sensing of Environment*, **112**, 3876-3890.

Bowen MR, Bompard JM, Anderson IP, Guizol P, Gouvon A (2000) In: *Forest Fires and Regional Haze in Southeast Asia*, (eds Eaton P, Radojevic M), pp. 52-66, Nova Science, New York.

Brenner AC, Zwally HJ, Bentley CR, Csatho BM, Harding DJ, Hofton MA, Minster JB, Roberts LA, Saba JL, Thomas RH, Yi D (2003) *Geoscience Laser Altimeter*

System (GLAS), Derivation of Range and Range Distributions from Laser Pulse Waveform Analysis for Surface Elevations, Roughness, Slope, and Vegetations Heights. Algorithm Theoretical Basis Documents (ATBD), Version 4.1, Center for Space Research, The University of Texas at Austin, USA.

Brown S (1997) *Estimating biomass and biomass change of tropical forests: A primer*. FAO Forestry Paper, 134, 1-84.

Brown S (2002) Measuring carbon in forests: current status and future challenges. *Environmental Pollution*, **116**, 363-372.

Brown S, Gillespie A, Lugo AE (1989) Biomass estimation methods for tropical forests with applications to forest inventory data. *Forest Science*, **35**, 881–902.

Brown S, Iverson LR, Prasad A, Liu D (1993) Geographic distribution of carbon in biomass and soils of tropical Asian forests. *Geocarto International*, **8**, 45–59.

Carabajal CC, Harding DJ (2006) SRTM C-band and ICESat laser altimetry elevation comparisons as a function of tree cover and relief. *Photogrammetric Engineering & Remote Sensing*, **72**, 287-298.

Castro K, Sanchez-Azofeifa G, Rivard B (2003) Monitoring secondary tropical forests using space-borne data: Implications for Central America. *International Journal of Remote Sensing*, **24**, 1853-1894.

Chave J, Andalo C, Brown S *et al.* (2005) Tree allometry and improved estimation of carbon stocks and balance in tropical forests. *Oecologica*, **145**, 87-99.

Chomitz KM, Brenes E, Costantino L (1999) Financing Environmental Services: The Costa Rican Experience and Its Implications. *Science of the Total Environment*, **240**, 157-169.

Cochrane MA (2003) Fire science for rainforests. *Nature*, **421**, 913-919.

Chudnoff M (1984) *Tropical Timbers of the World*. Agriculture Handbook 607, US Department of Agriculture, Forest Service, Forest Products Laboratory: Madison, WI, USA.

Curran LM, Trigg SN, McDonald AK *et al.* (2004) Lowland Forest Loss in Protected Areas of Indonesian Borneo. *Science*, **303**, 1000-1003.

Davies DK, Ilavajhala S, Wong MM, Justice CO (2009) Fire information for resource management system: Archiving and distributing MODIS active fire data. *IEEE Transactions on Geoscience Remote Sensing*, **47**, 72-79.

Dobson MC, Pierce L, McDonald KC, Sharik T (1991) Seasonal change in radar backscatter from mixed conifer and hardwood forests in northern Michigan. In: *Proceedings if the International Geoscience and Remote Sensing Symposium*, pp. 1121-1124.

Dolan KA, Hurtt GC, Chambers JQ, Dubayah RO, Frolking S, Masek JG (2011) Using ICESat's Geoscience Laser Altimeter System (GLAS) to assess large-scale forest disturbance caused by hurricane Katrina. *Remote Sensing of Environment*, **115**, 86-96.

Drake JB, Dubayah RO, Clark DB *et al.* (2002a) Estimation of tropical forest structural characteristics using large-footprint lidar. *Remote Sensing of Environment*, **79**, 305-319.

Drake JB, Dubayah RO, Knox RG, Clark DB, Blair JB (2002b) Sensitivity of large-footprint lidar to canopy structure and biomass in a neotropical rainforest. *Remote Sensing of Environment*, **81**, 378-392.

Drake JB, Knox RG, Dubayah RO, Clark DB, Condit R, Blair JB, Hofton M (2003) Above-ground biomass estimation in closed canopy Neotropical forests using lidar remote sensing: factors affecting the generality of relationships. *Global Ecology and Biogeography*, **12**, 147-159.

Dubayah RO, Drake JB (2000) Lidar remote sensing for forestry. *Journal of Forestry*, **98**, 44-46.

Englhart S, Keuck V, Siegert F (2011) Aboveground biomass retrieval in tropical forests – The potential of combined X- and L-band SAR data use. *Remote Sening of Environment*, **115**, 1260-1271.

Engels HA (1986) Least Squares Method for Estimation of Bezier Curves and Surfaces and its Applicability to Multivariate Analysis. *Mathematical Biosciences*, **79**,155-170.

FAO (2001) *Global Forest Resources Assessment Report 2000*. Food and Agriculture Organization, Rome, Italy.

FAO (2006) *Global Forest Resources Assessment Reprot 2005.* Food and Agriculture Organization, Rome, Italy.

Field RD, van der Werf GR, Shen SSP (2009) Human amplification of drought-induced biomass burning in Indonesia since 1960. *Nature Geoscience*, **2**, 185-188.

Foody GM, Curran PJ (1994) Estimation of tropical forest extent and regenerative stage using remotely sensed data. *Journal of Biogeography*, **21**, 223-244.

FWI/GWI (2002) *The State of the Forest: Indonesia*. Forest Watch Indonesia / Global Forest Watch, Bogor, Indonesia / Washington, DC.

Gibbs HK, Brown S, Niles JO, Foley JA (2007) Monitoring and estimating tropical forest carbon stocks: making REDD a reality. *Environmental Research Letters*, **2**, 045023.

Goetz SJ, Sun M, Baccini A, Beck PSA (2010) Synergistic use of spaceborne lidar and optical imagery for assessing forest disturbance: An Alaska case study. *Journal of Geophysical Research*, **115**, G00E07

Goldammer JG (1993) *Feuer in Waldökosystemen der Tropen und Subtropen*. Birkhaeuser Verlag, Basel-Boston.

Gorham E (1991) Northern peatlands: role in the carbon cycle and probable responses to global warming. *Ecological Applications*, **1**, 182-195.

Hairiah K, Sitompul SM, van Noordwijk M, Palm C (2001) *Carbon stocks of tropical land use systems as part of the global C balance: effects of forest conversion and options for 'clean development' activities*. International Centre for Research in Agroforestry, Southeast Asian Regional Research Programme, Bogor, Indonesia.

Hansen MC, DeFries RS, Townshend JRG, Carroll M, Dimiceli C, Sohlberg RA (2003) Global percent tree cover at a spatial resolution of 500 meters: First results of the MODIS Vegetation Continuous Fields Algorithm. *Earth Interactions*, **7**, 1-15.

Hansen MC, Stehman SV, Potapov PV, Arunarwati B, Stolle F, Pittman K (2009) Quantifying changes in the rates of forest clearing in Indonesia from 1990 to

2005 using remotely sensed data sets. *Environmental Research Letters*, **4**, 034001.

Harding DJ, Carajabal CC (2005) ICESat waveform measurements of within footprint topographic relief and vegetation vertical structure. *Geophysical Research Letters*, **32**, L21S10.

Hollaus M, Wagner W, Maier B, Schadauer K (2007) Airborne laser scanning of forest stem volume in a mountainous Environment. *Sensors*, **7**, 1559-1577.

Holling CS (1996) The Resilience of Terrestrial Ecosystems: Local Surprise and Blobal Change. In: *Sustainable Development of the Biosphere*, (eds Clark WC, Munn RE), pp. 107-132. Cambridge University Press.

Hooijer A, Page S, Canadell JG, Silvius M, Kwadijk J, Wösten H, Jauhianien J (2009) Currnet and future CO_2 emissions from drained peatlands in Southeast Asia. *Biogeosciences Discussions*, **6**, 7207-7230.

Hooijer A, Page S, Canadell JG, Silvius M, Kwadijk J, Wösten H, Jauhiainen J (2010) Current and future CO2 emissions from drained peatlands in Southeast Asia. *Biogeosciences*, **7**, 1505-1514.

Hooijer A, Page S, Jauhiainen J, Lee WA, Lu X (2011) Recent findings on subsidence and carbon loss in tropical peatlands: reducing uncertainties. In: *Workshop on "Tropical Wetland Ecosystems of Indonesia: Science Needs to Address Climate Change Adaptation and Mitigation"*. Bali, 11-14 April 2010.

Hooijer A, Silvius M, Wösten H, Page S E (2006) *PEAT-CO2, Assessment of CO2 emissions from drained peatlands in SE Asia*. Delft Hydraulics report Q3943, Delft, Netherlands.

Huffman GJ, Adler RF, Morrissey M *et al.* (2001) Global Precipitation at One-Degree Daily Resolution from Multi-Satellite Observations. *Journal of Hydrometeorology*, **2**, 36-50.

Imhoff ML (1995) Radar backscatter and biomass saturation — Ramifications for global biomass inventory. *IEEE Transactions on Geoscience and Remote Sensing*, **33**, 511-518.

Immirzi CP, Maltby E, Clymo RS (1992) *The global status of peatlands and their role in carbon cycling*. Report No.11, Wetlands Research Group. London, Friends of the Earth.

Intergovernmental Panel on Climate Change (2006) In: *IPCC Guidelines for National Greenhouse Gas Inventories*, (eds Eggleston HS, Buendia L, Miwa K, Ngara T, Tanabe K). Prepared by the National Greenhouse Gas Inventories Programme, IGES, Hayama, Japan.

Intergovernmental Panel on Climate Change (2007) In: *Climate Change 2007: The Physical Science Basis. Contribution of Working Group I to the Fourth Assessment Report of the Intergovernmental Panel on Climate Change*, (eds Solomon S, Qin D, Manning M *et al.*). Cambridge University Press, Cambridge.

Jaenicke J, Rieley J O, Mott C, Kimman P, Siegert F (2008) Determination of the amount of carbon stored in Indonesian peatlands. *Geoderma*, **147**, 151-158.

Jauhiainen J, Heikkinen JEP, Martikainen PJ, Vasander H (2001) CO_2 and CH_4 fluxes in pristine peat swamp forest and peatland converted to agriculture in Central Kalimantan, Indonesia. *International Peat Journal*, **11**, 43-49.

Jauhiainen J, Jaya A, Inoue T, Heikkinen J, Martikainen P, Vasander H (2004) Carbon Balance in Managed Tropical Peat in Central Kalimantan. In: *Proceedings of the 12th International Peat Congress, Tampere 6 - 11.6.2004*, (ed Päivänen J), pp. 653-659.

Jauhiainen J, Silvennoinen H, Hämäläinen R, Kusin K, Limin S, Raison RJ, Vasander H (2011) Nitrous oxide fluxes from tropical peat with different disturbance history and management. *Biogeosciences Discussions*, **8**, 5423-5450.

Jauhiainen J, Takahashi H, Heikkinen JEP, Martikainen PJ, Vasander H (2005) Carbon fluxes from a tropical peat swamp forest floor. *Global Change Biology*, **11**, 1788-1797.

Kaneko N (1992) Comparison of forest structure of tropical peat swamp forests in Southern Thailand and Malaysia. In: *Coastal Lowland Ecosystems in Southern Thailand and Malaysia* (eds Kyuma K, Vijarnsorn P, Zakaria A), pp. 152-163. Kyoto, Japan.

Köhl M, Magnussen S, Marchetti M (2006) *Sampling Methods, Remote sensing and GIS Multisource Inventory*. Springer-Verlag, Berlin Heidelberg, Germany.

Kraus K (1998) Interpolation nach kleinsten Quadraten versus Kriege-Schätzer. *Österreichische Zeitschrift für Vermessung und Geoinformation*, **86**, 45-48.

Kraus K, Pfeifer N (1998) Determination of terrain models in wooded areas with airborne laser scanner data. *ISPRS Journal of Photogrammetry and Remote sensing*, **53**, 193-203.

Kuplich TM, Curran PJ, Atkinson PM (2005) Relating SAR image texture to the biomass of regenerating tropical forests. *International Journal of Remote Sensing*, **26**, 4829-4854.

Langner A, Miettinen J, Siegert F (2007) Land cover change 2002–2005 in Borneo and the role of fire derived from MODIS imagery. *Global Change Biology*, **13**, 1-12.

Langner A, Siegert F (2009) Spatiotemporal fire occurrence in Borneo over a period of 10 years. *Global Change Biology*, **15**, 48-62.

Lasco RD, Guillermo IQ, Cruz RVO, Bantayan NC, Pulhin FB (2004) Carbon stocks assessment of a secondary forest in Mount Makiling Forest Reserve, Philippines. *Journal of Tropical Science*, **16**, 35-45.

Lefsky MA (2010) A global forest canopy height map from the Moderate Resolution Imaging Spectroradiometer and the Geoscience Laser Altimeter System. *Geophysical Research Letters*, **37**, L15401.

Lefsky MA, Cohen WB, Acker SA, Parker GG, Spies TA, Harding D (1999a) Lidar remote sensing of the canopy structure and biophysical properties of Douglas-fir western hemlock forests. *Remote Sensing of Environment*, **70**, 339-361.

Lefsky MA, Cohen WB, Harding DJ, Parker GG, Acker SA, Gower ST (2002a) Lidar remote sensing of above-ground biomass in three biomes. *Global Ecology and Biogeography*, **11**, 393-399.

Lefsky MA, Cohen WB, Parker GG, Harding DJ (2002b) Lidar Remote Sensing for Ecosystem Studies. *BioScience*, **52**, 19-30.

Lefsky MA, Harding D, Cohen WB, Parker G, Shugart HH (1999b) Surface Lidar Remote Sensing of Basal Area and Biomass in Deciduous Forests of Eastern Maryland, USA. *Remote Sensing of Environment*, **67**, 83-98.

Lefsky MA, Harding DJ, Keller M, Cohen WB, Carabajal CC, Del Bom Espirito-Santo F, Hunter MO, de Oliveira R Jr (2005) Estimates of forest canopy height and aboveground biomass using ICESat. *Geophysical Research Letters*, **32**, L22S02.

Lefsky MA, Keller M, Pang Y, de Camargo PB, Hunter MO (2007) Revised method for forest canopy height estimation from Geoscience Laser Altimeter System waveforms. *Journal of Applied Remote Sensing*, **1**, 013537.

Lillesand TM, Kiefer RW, Chipman JW (2008) *Remote Sensing and Image Interpretation*. John Wiley & Sons Inc.: Hoboken, NJ, USA.

Lim KS, Treitz PM (2004) Estimation of above ground forest biomass from airborne discrete return laser scanner data using canopy-based quantile estimators. *Scandinavian Journal of Forest Research*, **19**, 558-570.

Longley PA, Goodchild MF, Maguire DJ, Rhind DW (2005) *Geographic Information Systems and Science*. John Wiley & Sons Inc.: Hoboken, NJ, USA.

Lu DS (2006) The potential and challenge of remote sensing-based biomass estimation. *International Journal of Remote Sensing*, **27**, 1297-1328.

Lucas RM, Cronin N, Lee A, Moghaddam M, Witte C, Tickle P (2006) Empirical relationships between AIRSAR backscatter and LiDAR-derived forest biomass, Queensland, Australia. *Remote Sensing of Environment*, **100**, 407-425.

Lucas RM, Mitchell AL, Rosenqvist A, Proisy C, Melius A, Ticehurst C (2007) The potential of L-band SAR for quantifying mangrove characteristics and change: Case studies from the tropics. *Aquatic Conservation: Marine and Freshwater Ecosystems*, **17**, 245-264.

Luckman A, Baker J, Kuplich TM, Yanasse CDF, Frery AC (1997) A study of the relationship between radar backscatter and regenerating tropical forest biomass for spaceborne SAR instruments. *Remote Sensing of Environment*, **60**, 1-13.

MacKinnon K, Hatta G, Halim H, Mangalik A (1996) *The Ecology of Kalimantan - Indonesian Borneo*. Periplus Editions (HK) Ltd., Dalhousie University.

Magnussen S, Boudewyn P (1998) Derivations of stand heights from airborne laser scanner data with canopy-based quantile estimators. *Canadian Journal of Forest Research – Revue Canadienne de recherché Forestiere*, **28**, 1016-1031.

Mallet C, Bretar F (2009) Full-waveform topographic lidar: State-of-the-art. *ISPRS Journal of Photogrammetry and Remote Sensing*, **64**, 1-16.

Means JE, Acker SA, Harding DJ, Blair JB, Lefsky MA, Cohen WB, Harmon ME, McKee WA (1999) Use of large-footprint scanning airborne lidar to estimate forest stand characteristics in the Western Cascades of Oregon. *Remote Sensing of Environment*, **67**, 298-308.

Miettinen J, Langner A, Siegert F (2007) Burnt area estimation for the year 2005 in Borneo using multi-resolution satellite imagery. *International Journal of Wildland Fire*, **16**, 45-53.

Mitchard ETA, Saatchi SS, Woodhouse IH *et al.* (2009) Using satellite radar backscatter to predict above-ground woody biomass: A consistent relationship across four different African landscapes. *Geophysical Research Letters*, **36**, L23401.

Moeliono M, Wollenberg E, Limberg G (2009) *The Decentralizaton of Forest Governance: Politics, Economics and the Fight for Control*. Earthscan, London.

Muraleedharan TR, Radojevic M, Waugh A, Caruana A (2000) Emissions from the combustion of peat: An experimental study. *Atmospheric Environment*, **34**, 3033-3035.

Naesset E (2002) Predicting forest stand characteristics with airborne scanning laser using a practical two-stage procedure and field data. *Remote Sensing of Environment*, **80**, 88-99.

Naesset E (2004) Effects of different flying altitudes on biophysical stand properties estimated from canopy height and density measured with a small-footprint airborne scanning laser. *Remote Sensing of Environment*, **91**, 243-255.

Nelson R, Oderwald R, Gregoire TG (1997) Separating the ground and airborne laser sampling phases to estimate tropical forest basal area, volume, and biomass. *Remote Sensing of Environment*, **60**, 311-326.

Neuzil SG (1997) Onset and rate of peat and carbon accumulation in four domed ombrogenous peat deposits, Indonesia. In: *Biodiversity and Sustainability of Tropical Peatlands*, (eds Rieley JO, Page SE), pp. 55-72. Samara Publishing Limited, Cardigan, United Kingdom.

Page SE, Banks C (2007) Tropical Peatlands: Distribution, Extent and Carbon Storage - Uncertainties and Knowledge Gaps. *Peatlands International*, **2**, 26-27.

Page S, Hoscilo A, Wösten H *et al.* (2009) Restoration Ecology of Lowland Tropical Peatlands in Southeast Asia: Current Knowledge and Future Research Directions. *Ecosystems*, **12**, 888-905.

Page SE, Rieley JO (1998) Tropical peatlands: A review of their natural resource functions with particular reference to Southeast Asia. *International Peat Journal*, **8**, 95-106.

Page SE, Rieley JO, Banks CJ (2010) Global and regional importance of the tropical peatland carbon pool. *Global Change Biology*, ***17***, 798-818, doi: 10.1111/j.1365-2486.2010.02279.x.

Page SE, Rieley JO, Shotyk ØW, Weiss D (1999) Interdependence of peat and vegetation in a tropical peat swamp forest. *Philosophical Transactions of the Royal Society London B*, **354**, 1885-1897.

Page SE, Siegert F, Rieley JO, Böhm HDV, Jaya A, Limin S (2002) The amount of carbon released from peat and forest fires in Indonesia during 1997. *Nature*, **420**, 61-65.

Page SE, Wüst RA, Weiss D, Rieley JO, Shotyk W, Limin SH (2004) A record of Late Pleistocene and Holocene carbon accumulation and climate change from an equatorial peat bog (Kalimantan, Indonesia): Implications for past, present and future carbon dynamics. *Journal of Quaternary Science*, **19**, 625-635.

Patenaude G, Hill RA, Milne R, Gaveau DLA, Briggs BBJ, Dawson TP (2004) Quantifying forest above ground carbon content using LiDAR remote sensing. *Remote Sensing of Environment*, **93**, 368-380.

Pearson T, Brown S, Ravindranath NH (2005a) *Intergrating Carbon Benefit Estimates into GEF Projects - Guidelines*. UNDP, GEF.

Pearson T, Walker S, Brown S (2005b) *Sourcebook for Land Use, Land-Use Change and Forestry Projects*. Winrock International: Little Rock, AR, USA.

Pfeifer N, Stadler P, Briese C (2001) Derivation of digital terrain models in SCOP++ environment. In: *OEEPE Workshop on Airborne Laserscanning and Interferometric SAR for Detailed Digital Elevation Models*. Stockholm.

Popescu SC (2007) Estimating biomass of individual pine trees using airborne lidar. *Biomass and Energy*, **31**, 646-655.

Portela R, Wendland KL, Pennypacker LL (2008) The Idea of Market-Based Mechanisms for Forest Conservation and Climate Change. In: *Climate Change and Forests: Emerging Policy and Market Opportunities*, (eds Streck C, O'Sullivan R, Janson-Smith T, Tarasofsky), pp. 11-29. Chatham House, London, United Kingdom, Brookings Institution Press, Washington DC, USA.

Ranson KJ, Kimes D, Sun G, Nelson R, Kharuk V, Montesano P (2007) Using MODIS and GLAS Data to Develop Timber Volume Estimates in Central Siberia. In: *Proceedings of the IEEE International Geoscience and Remote Sensing Symposium, IGARSS 2007*, pp. 2306-2309. Barcelona, Spain.

Ranson KJ, Sun G, Kovacs K, Kharuk VI (2004a) Landcover Attributes from ICESat GLAS Data in Central Siberia. In: *Proceedings of the IEEE International Geoscience and Remote Sensing Symposium, IGARSS 2004*, Volume 2, pp. 753-756. Anchorage, AK, USA.

Ranson KJ, Sun G, Kovacs K, Kharuk VI (2004b) Use of ICESat GLAS Data for Forest Disturbance Studies in Central Siberia. In: *Proceedings of the IEEE International Geoscience and Remote Sensing Symposium, IGARSS 2004*, Volume 3, pp. 1936-1939. Anchorage, AK, USA.

Rashed T, Weeks JR, Roberts DA, Rogan J, Powell RL (2003) Measuring the physical composition of urban morphology using multiple endmember spectral mixture models. *Photogrammetric Engineering and Remote Sensing*, **69**, 1011-1020.

Rieley JO, Ahmad-Shah A (1996) The vegetation of tropical peat swamp forests. In: *Tropical Lowland Peatlands of Southeast Asia. Proceedings of a Workshop on Integrated Planning and Management of Tropical Lowland Peatlands* (eds

Maltby E, Immirzi CP, Safford RJ), pp. 55-74. Cisrua, Indonesia, IUCN, Gland, Switzerland.

Rieley JO, Ahmad-Shah AA, Brady MA (1996) The extent and nature of tropical peat swamps. In: *Tropical Lowland Peatlands of Southeast Asia. Proceedings of a Workshop on Integrated Planning and Management of Tropical Lowland Peatlands* (eds Maltby E, Immirzi CP, Safford RJ), pp. 17-54. Cisarua, Indonesia, IUCN, Gland, Switzerland.

Rieley JO, Page SE (2005) In: *Wise Use of Tropical Peatlands: Focus on Southeast Asia* (eds Rieley JO, Page SE). ALTERRA, Wageningen, Netherlands.

Rim HJ, Schutz BE (2002) *Geoscience Laser Altimeter System (GLAS), Precision orbit determination (POD)*. Algorithm Theoretical Basis Documents (ATBD), Version 2.2, Center for Space Research, The University of Texas at Austin, USA.

Rosenqvist A, Milne A, Lucas R, Imhoff M, Dobson C (2003) A review of remote sensing technology in support of the Kyoto Protocol. *Environmental Science & Policy*, **6**, 441-455.

Rosette JAB, North PRJ, Suarez JC (2008) Vegetation height estimates for a mixed temperate forest using satellite laser altimetry. *International Journal of Remote Sensing*, **29**, 1475-1493.

Saatchi SS, Houghton RA, Dos Santos Alvala RC, Soares JV, Yu Y (2007) Distribution of aboveground live biomass in the Amazon Basin. *Global Change Biology*. **13**, 816-37.

Salomon D (2006) Chapter 6 Bezier Appromination. In: *Curves and Surfaces for Computer Graphics*, pp. 175-250. Springer Science+Business Media, Inc.

Sandker M, Suwarno A, Campbell BM (2007) Will forests remain in the face of oil palm expansion? Simulating change in Malinau, Indonesia. *Ecology and Society*, **12**, 37.

Schutz BE (2002) *Geoscience Laser Altimeter System (GLAS), Laser footprint location (geolocation) and surface profiles*. Algorithm Theoretical Basis Documents (ATBD), Version 3.0, Center for Space Research, The University of Texas at Austin, USA.

Schutz BE, Zwally HJ, Shuman CA, Hancock D, DiMarzio JP (2005) Overview of the ICESat Mission. *Geophysical Research Letters*, **32**, L21S01.

Sheil D, Casson A, Meijaard E *et al.* (2009) *The impacts and opportunities of oil palm in Southeast Asia: What do we need to know?* Occasional paper no. 51. CIFOR, Bogor, Indonesia.

Sheperd PA, Rieley JO, Page SE (1997) The Relationship Between Forest Vegetation and Peat Characteristics in the Upper Catchment of Sungai Sebangau, Central Kalimantan. In: *Biodiversity and Sustainability of Tropical Peatlands* (eds Rieley JO, Page SE), pp. 191-210. Samara Publishing Limited, Cardigan.

Sieffermann RG, Fournier M, Triutomo S, Sadelman MT, Semah AM (1988) Velocity of tropical forest peat accumulation in Central Kalimantan Province, Indonesia (Borneo). In: *Proceedings of the 8th International Peat Congress, Leningrad, August 1988*, pp. 90-98. International Peat Society, Jyväskylä.

Siegert F, Rücker G, Hinrichs A, Hoffmann A (2001) Increased fire impacts in logged over forests during El Niño driven fires. *Nature*, **414**, 437-440.

Siegert F, Zhukov B, Oertel D, Limin S, Page SE, Rieley JO (2004) Peat fires detected by the BIRD satellite. *International Journal of Remote Sensing*, **25**, 3221-3230.

Sorensen KW (1993) Indonesian peat swamp forests and their role as a carbon sink. *Chemosphere*, **27**, 1065-1082.

Stanley SA (2009) *Preliminary biomass estimate in PT Mamberamo Alas Mandiri concession, Papua, Indonesia.* Final Report for Conservation International. Forest Carbon.

Staub JR, Esterle JS (1994) Peat-accumulating depositional systems of Sarawak, East Malaysia. *Sedimentary Geology*, **89**, 91-106.

Sun G, Ranson KJ, Kimes DS, Blair JB, Kovacs K (2008) Forest vertical structure from GLAS: An evaluation using LVIS and SRTM data. *Remote Sensing of Environment*, **112**, 107-117.

Tansey K, Beston J, Page SE, Paredes Hernández CU (2008) Relationship between MODIS fire hot spot count and burned area in a degraded tropical peat swamp

forest in Central Kalimantan, Indonesia. *Journal of Geophysical Research*, **113**, D23112.

The National Snow and Ice Data Center, University of Colorado Boulder, Boulder, CO, USA, 2011a. Available online: http://nsidc.org/data/icesat/data.html (accessed on 30 March 2011).

The National Snow and Ice Data Center *NSIDC*, *Distributed ICESat GLAS Laser Operations Periods: Latest release*. University of Colorado Boulder, Boulder, CO, USA, 2011b. Available online: http://nsidc.org/data/icesat/pdf/glas_laser_ops_attrib.pdf (accessed on 18 August 2011).

Toma T, Ishida A, Matius P (2005) Long-term monitoring of post-fire aboveground biomass recovery in a lowland dipterocarp forest in East Kalimantan, Indonesia. *Nutrient Cycling in Agroecosystems*, **71**, 63-72.

Tompkins S, Mustard JF, Pieters CM, Forsyth DW (1997) Optimization of endmembers for spectral mixture analysis. *Remote Sensing of Environment*, **59**, 472-489.

Usup A, Hashimoto Y, Takahashi H, Hayasaka H (2004) Combustion and thermal characteristics of peat fire in tropical peatland in Central Kalimantan, Indonesia. *Tropics*, **14**, 1-19.

Van der Werf GR, Dempewolf J, Trigg SN *et al.* (2008) Climate regulation of fire emissions and deforestation in equatorial Asia. *Proceedings of the National Academy of Sciences of the United States of America*, **105**, 20350-20355.

Van der Werf GR, Morton DC, DeFries RS, Olivier JGJ, Kasibhatla PS, Jackson RB, Collatz GJ, Randerson JT (2009) CO_2 emissions from forest loss. *Nature Geoscience*, **2**, 737-738.

Van der Werf GR, Randerson JT, Giglio L *et al.* (2010) Global fire emissions and the contribution of deforestation, savanna, forest, agricultural, and peat fires (1997-2009). *Atmospheric Chemistry and Physics Discussions*, **10**, 16153-16230.

Waldes NJL, Page SE (2001) Forest Structure and Tree Diversity of A Peat Swamp Forest in Central Kalimantan, Indonesia. In: *Proceedings of the International Symposium on Tropical Peatlands*, pp. 16-22. Jakarta, Indonesia.

Waring RH *et al.* (1995) Imaging radar for ecosystem studies. *BioScience*, **45**, 715-23.

Wetlands International (2003) *Map of Peatland Distribution Area and Carbon Content in Sumatera 1990-2002*. Wetlands International - Indonesia Programme & Wildlife Habitat Canada, Bogor, Indonesia.

Wetlands International (2004) *Map of Peatland Distribution Area and Carbon Content in Kalimantan 2000-2002*. Wetlands International - Indonesia Programme & Wildlife Habitat Canada, Bogor, Indonesia.

Wetlands International (2006) *Cadangan Karbon Bawah Permukaan di Papua (Below ground carbon content in Papua)*. Wetlands International - Indonesia Programme & Wildlife Habitat Canada, Bogor, Indonesia.

Wild E (1983) Die Prädiktion mit Gewichtsfunktionen und deren Anwendung zur Beschreibung von Geländeflächen bei topographischen Geländeaufnahmen. *In: DGK, Reihe C, vol. 277*. Dissertation, Universität Stuttgart.

Williams AM, Hunt Jr ER (2002) Estimation of leafy spurge from hyperspectral imagery using mixture tuned matched filtering. *Remote Sensing of Environment*, **82**, 446-456.

World Agroforestry Centre, *Wood Density Database*; World Agroforestry Centre: Nairobi, Kenya, 2011. Available online: http://www.worldagroforestrycentre.org/Sea/Products/AFDbases/WD/Index.htm (accessed on 30 March 2011).

World Resources Institute (2005) *Ecosystems and Human Well-being: Biodiversity Synthesis*. Millennium Ecosystem Assessment, World Resources Institute, Washington DC, USA.

World Wide Fund for Nature (2009) *Die Torfmoorwälder von Sebangau: Besondere Kohlenstoffspeicher und Lebensräume*. Project Information Brochure, World Wide Fund for Nature, Frankfurt, Germany.

Wösten JHM, Ismail AB, van Wijk ALM (1997) Peat subsidence and its practical implications: A case study in Malaysia. *Geoderma*, **78**, 25-36.

Yamakura A, Hagihara A, Sukardjo S, Ogawa H (1986) Above ground biomass of tropical rain forest stands in Indonesian Borneo. *Vegetatio*, **68**, 71-82.

Zhao KG, Popescu S, Nelson R (2009) Lidar remote sensing of forest biomass: A scale-invariant estimation approach using airborne lasers. *Remote Sensing of Environment*, **113**, 182-196.

CURRICULUM VITAE

Personal Information

Name	Uwe Franz Ballhorn
Date of Birth	April 14, 1974
Place of Birth	Mayen, Germany

Education

10/2008 – present **PhD remote sensing of tropical ecosystems at the Ludwig Maximilians University Munich, Germany**

Focal areas
- LiDAR data processing
- Retrieval of biophysical forest parameters from air- and spaceborne discrete-return and full-waveform LiDAR data
- Analysis of tropical peat surfaces after fire and possible carbon emissions with the help of air- and spaceborne discrete-return and full-waveform LiDAR data
- Processing of optical remote sensing data
- Land cover classification
- Accuracy assessment
- GIS modeling
- Statistics
- Forest inventory in the tropics
- Ground truthing
- Carbon baseline assessment and monitoring of Clean Development Mechanism (CDM) and Reduced Emissions from Deforestation and forest Degradation in developing countries (REDD) projects
- Development of Monitoring, Reporting, and Verification (MRV) methodologies for CDM and REDD projects
- Assistance in the preparation of Project Design Documents (PDDs) for CDM and REDD projects

10/2004 – 03/2007 **International MSc program 'Sustainable Resource Management' at the Technical University of Munich, Germany (course language: English)**

Focal areas
- Remote sensing
- GIS
- Environmental economics
- International environmental law and politics
- Soil science and soils of the world
- Climate science
- Hydrology and hydrological modeling
- Wildlife management
- Protected area management
- System analyses and modeling
- Agroforestry

Topic master thesis
Assessment of the Changes in the Distribution of Mount Kenya's Indigenous pure Bamboo Vegetation (*Yushania alpina*), between 1975 - 2005, with Pixel based and Object Oriented Classification Methods

10/1998 – 04/2004 **Study of Forestry at the University of Applied Sciences Weihenstephan, Germany**

Focal areas
- Sustainable forest management
- Economics
- Wildlife management
- GIS
- Statistics
- Conflict management
- Practical forest work

Topic diploma thesis
Luchsübergriffe auf landwirtschaftliche Wildgehege - Bedeutung, Ursachen und Lösungsansätze am Beispiel des Naturpark Bayerischer Wald

Employment History

10/2008 – present **Remote Sensing Solutions GmbH, Munich, Germany**
- Research associate and consultant for environmental remote sensing
- Permanent staff

04/2007 – 09/2008 **Ludwig Maximilians University, Munich, Germany**
- Research associate and consultant for environmental remote sensing
- Permanent staff

02/2006 – 03/2007 **Remote Sensing Solutions GmbH, Munich, Germany**
- Research associate and consultant for environmental remote sensing
- Freelancer

10/2005 – 01/2006 **World Agroforestry Centre (ICRAF), Nairobi, Kenya**
- Research fellowship: Project leader for a remote sensing study of Mount Kenya's indigenous pure bamboo vegetation (*Yushania alpina*)

07/2004 – 09/2004 **Bund Naturschutz e.V., Munich, Germany**
- Public relations associate for the petition for a referendum against the privatization of the Bavarian forest

03/2002 – 06/2002 **Internship at the forestry office Bodenmais, Germany**
- Planning of forest roads and skid tracks
- Management and planning of logging operations
- Wildlife management

10/2000 – 02/2000 **Internship at the forestry office Altötting, Germany**
- Handling of all necessary practical forestry activities

Work Abroad

08/2010 – 09/2010 **Australian Agency for International Development (AUSAID), Central Kalimantan, Indonesia**
- Differential GPS measurements
- Forest inventory
- Ground truthing

01/2008 – 02/2008 **Forest Restoration and Rehabilitation in Southeast Asia (FORRSA), Northern Thailand**
- Lecturer on remote sensing and GIS
- Field trip assistance

08/2007 – 11/2007 **LiDAR Study, Central Kalimantan, Indonesia**
- Forest inventory
- Ground truthing

07/2007 – 07/2007 **Forest Restoration and Rehabilitation in Southeast Asia (FORRSA), Bogor, Indonesia**
- Lecturer on remote sensing and GIS
- Field trip assistance

05/2007 – 06/2007 **South Sumatra Forest Fire Management Project (SSFFMP), Palembang, Indonesia**
- International short term expert on remote sensing and GIS

06/2006 – 07/2006 **Forest Restoration and Rehabilitation in Southeast Asia (FORRSA), West Java, Indonesia**
- Remote sensing and GIS land cover study

10/2005 – 01/2006 **World Agroforestry Centre (ICRAF), Nairobi, Kenya**
- Research fellowship: Project leader for a remote sensing study of Mount Kenya's indigenous pure bamboo vegetation (*Yushania alpina*)

Lectures

05/2007 – present **Remote Sensing and GIS course, GeoBio Center of the Ludwig Maximilians University Munich, Germany**
- Supervisor

01/2008 – 02/2008 **Forest Restoration and Rehabilitation in Southeast Asia (FORRSA), Northern Thailand**
- Lecturer on remote sensing and GIS

07/2007 – 07/2007 **Forest Restoration and Rehabilitation in Southeast Asia (FORRSA), Bogor, Indonesia**
- Lecturer on remote sensing and GIS

Publications in peer-reviewed journals

Kronseder K, **Ballhorn U**, Böhm V, Siegert F (2012) Above ground biomass estimation across forest types at different degradation levels in Central Kalimantan using LiDAR data. *International Journal of Applied Earth Observations and Geoinformation*, **18**, 37-48.

Ballhorn U, Jubanski J, Siegert F (2011) ICESat/GLAS Data as a Measurement Tool for Peatland Topography and Peat Swamp Forest Biomass in Kalimantan, Indonesia. *Remote Sensing*, **3**, 1957-1982.

Ballhorn U, Siegert F, Mason M, Limin S (2009) Derivation of burn scar depths and estimation of carbon emissions with LiDAR in Indonesian peatlands. *Proceedings of the National Academy of Sciences of the United States of America*, **106**, 21213-21218.

Publications in preparation for peer-reviewed journals

Ballhorn U, Jubanski J, Siegert F Pre-fire surface 3D modeling of tropical peatland burn scars based on airborne LiDAR in Central Kalimantan, Indonesia. Manuscript in preparation for *Global Change Biology*.

Jubanski J, **Ballhorn U**, Kronseder K, Siegert F A new method to estimate tropical forest above ground biomass in Central Kalimantan, Indonesia, using airborne LiDAR data. Manuscript in preparation for *Nature Climate Change*.

Conference presentations

Kronseder K, **Ballhorn U**, Siegert F (2010) Estimation of Aboveground Biomass Across Forest Types at Different Degradation Levels in Central Kalimantan (Borneo) using LiDAR and Field Inventory Data. Presentation at the conference *Tropentag 2010*, Zürich, Switzerland, 14^{th}-16^{th} September 2010. Poster presentation.

Kronseder K, **Ballhorn U**, Siegert F (2010) Estimation of above ground biomass across forest types at different degradation levels in Central Kalimantan (Borneo) using LiDAR and field inventory data. Presentation at the conference *ForestSAT 2010*, Lugo, Spain, 7^{th}-10^{th} September 2010. Oral presentation.

Uryu Y, Mott C, **Ballhorn U**, Jaenicke J, Budiman A, Siegert F (2009) CO_2 Emissions from Land Use, Land Use Change, and Forestry (LULUCF) in the Province of Riau, Indonesia, from 1990 – 2007. Presentation at the *8th International Carbon Dioxide Conference*. Jena, Germany, 13th-19th September 2009. Poster presentation.

Ruecker G, Moder F, Siegert F, **Ballhorn U**, Solichin, Sidiq M (2009) Reducing emissions from deforestation and degradation in South Sumatra, Indonesia: a remote sensing supported feasibility study. Presentation at the *33rd International Symposium on Remote Sensing of Environment*. Stresa, Italy, 4th-8th May 2009. Oral Presentation.

Ballhorn U, Siegert F (2009) Derivation of Burn Scar Depths with Airborne Light Detection and Ranging (LIDAR) in Indonesian Peatlands. Presentation at Conference *European Geosciences Union General Assembly 2009*. Vienna, Austriy, 19th-24th April 2009. Poster presentation.

Other publications

Ballhorn U, Mott C, Siegert F (2007) *Peat Dome Mapping & Analysis*. Report for the South Sumatra Forest Fire Management Project (SSFFMP) (Delegation of the European Commission to Indonesia, Singapore and Brunei Darussalam), Palembang, Indonesia.

Ballhorn U (2007) *Assessment of the Changes in the Distribution of Mount Kenya's Indigenous pure Bamboo Vegetation (Yushania alpina), between 1975 - 2005, with Pixel based and Object Oriented Classification Methods*. Master thesis, Technical University of Munich, Germany.

Ballhorn U, Brück-Dyckhoff C (2004) *Luchsübergriffe auf landwirtschaftliche Wildgehege - Bedeutung, Ursachen und Lösungsansätze am Beispiel des Naturpark Bayerischer Wald*. Diploma thesis, University of Applied Sciences Weihenstephan, Germany.